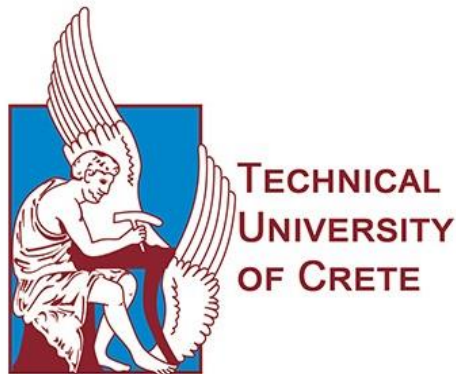


**SCHOOL OF ELECTRICAL AND COMPUTER
ENGINEERING (ECE)**

***Study Of Concentrating Solar Power
(CSP) Station And Simulation Using
Software***



***A Diploma Thesis in Partial Fulfillment of the
Requirements for the Degree Diploma***

***Polomarkaki Sofia
Registration Number 2010030131***

***Prof. Kalaitzakis Konstantinos (Supervisor)
Prof. Stavrakakis George (Member)
Dr. Eleftheria Sergaki (Co-supervisor)
Chania 2019***

Acknowledgements

This diploma thesis was held at Technical University of Crete, under the supervision of Dr Eleftheria Sergaki and is my first in-depth work as a student electrical engineer.

I would like to thank and express my gratitude to Dr Eleftheria Sergaki for the opportunity she gave me to deal with this contemporary subject, but also for the trust that has shown to my face, the really pleasant climate of cooperation, the tips, ideas and the valuable suggestions, help and guidance for solving various issues. Thanks for the time she spent, the patience she showed during the implementation of this work. Without her contribution, the completion of my diploma would be much more difficult.

I would like to thank my very beloved and remarkable people, my friends I made during my studies, and are still next to me. These people who, with their daily support, patience and positive thinking, support me in every pleasant or difficult times and contribute to the fulfillment of the goals I have set.

Finally, I would like to express my gratitude to my family, for the support and confidence that has shown me throughout my years of studies with their unrelenting spiritual but also material support in every area of my life until today. These people were beside me and supported me all the time from the very beginning of my life, and continue to believe in me even at times when even I did not believe in myself, without whom nothing I have accomplished so far would be a reality. In spite of this valuable support, they have given me all the necessary supplies to become a right Person and that is something that is not learned but transmitted.

My father when I entered the university said "do not enjoy the swimmer when he comes in but enjoy him when he comes out" so that the swimmer finally came out. And along with the diploma-that coveted paper which seemed to give me a long way to say-diabetes will come to close the most splendid circle of my life that will encircle my family that so long supported you, two or three real friends, dreams for the future and memories capable of making me smile a whole life .

All these years of studying I had nightmares, I was seeing in my sleep that degree was at the top of a mountain and I was trying to climb with my hands and did not do it, I never reached, it was very high and I was unable to reach it. From now on I will see that I am on the top of this mountain and I have it in my hands.

Thanks

Polomarkaki Sofia

Contents

<i>Abstract</i>	1
<i>Περίληψη</i>	3
<i>Chapter 1. Energy Problem</i>	5
1.1 <i>World Energy Problem</i>	5
1.2 <i>Energy Problem In Greece</i>	7
1.3 <i>Solution of the Environmental Problem - Renewable Energy</i>	9
1.4 <i>Thesis Objectives and Methods</i>	10
1.5 <i>Thesis Structure</i>	11
<i>Chapter 2. Renewable Energy</i>	15
2.1 <i>Renewable Energy Sources - Basic Fundamentals</i>	15
2.2 <i>Categories of Renewable Energy Sources</i>	16
2.2.1 <i>Biogas</i>	16
2.2.2 <i>Solar Energy</i>	17
2.2.3 <i>Wind Energy</i>	23
2.2.4 <i>Geothermal Energy</i>	24
2.2.5 <i>Hydrodynamic Energy (Water Energy)</i>	25
2.2.6 <i>Biomass</i>	26
2.2.7 <i>Osmotic effect</i>	27
2.3 <i>Concentrated Solar Systems</i>	27
<i>Chapter 3. Solar Energy</i>	29
3.1 <i>Solar Energy Exploitation- Basic Fundamentals</i>	29
3.2 <i>Thermodynamic Cycles</i>	32
3.2.1 <i>Stirling Cycle</i>	33
3.2.2 <i>Brayton Cycle</i>	35
3.2.3 <i>Rankine Cycle</i>	37
3.3 <i>Types of Concentrated Solar Systems</i>	38
3.3.1 <i>Parabolic Through Collectors</i>	41

3.3.2 Dish System.....	42
3.3.3 Linear Fresnel Reflector (CLFR).....	44
3.3.4 Solar Power Tower.....	46
3.3.5 Choice of the Appropriate System.....	47
Chapter 4. Historical Return – Existing Installations of Solar Power Towers.....	49
4.1 Experimental CSPs of Little Power/Force.....	51
4.2 Large Scale CSPs.....	53
4.2.1 Ivanpah Solar Electric Generating System.....	53
4.2.2 Solar Energy Generating Systems (SEGS).....	55
4.2.3 Mojave Solar Project.....	56
4.2.4 Solana Generating Station.....	58
4.2.5 Genesis Solar Energy Project.....	59
4.2.6 List of Solar Thermal Power Stations.....	60
4.3 Solar Power Tower Installation Under Construction.....	65
4.4 Solar Power Tower Installation Announced.....	66
4.5 Solar Power Tower In Greece.....	67
Chapter 5.....	73
5.1 Solar Power Tower Operation Principle.....	73
5.2 Solar Power Tower Subsystems.....	75
5.2.1 Solar Field.....	75
5.2.2 Solar Receiver.....	83
5.2.3 Electricity Production System.....	89
5.2.3.1 Water – Steam Systems.....	90
5.2.3.2 Molten Salt Systems.....	92
5.2.3.3 Atmospheric Air Systems.....	93
5.2.3.4 Compressed Air Systems.....	93
5.2.3.4.1 Tank Design.....	93
5.2.3.4.2 Startup.....	94
5.2.4 Thermal Energy Storage System.....	95

5.2.5	<i>Refugee Fuel Systems</i>	100
5.2.6	<i>Details of Subsystems</i>	101
5.2.6.1	<i>Master Control</i>	101
5.2.6.2	<i>Water Consumption Requirements</i>	102
5.2.6.3	<i>Heliostat Control</i>	102
5.2.6.4	<i>Heat Transport and Exchange Subsystem</i>	103
5.2.6.5	<i>Heat Exchangers</i>	104
5.2.6.6	<i>Insulation</i>	104
5.2.6.7	<i>Instrumentation</i>	104
5.2.6.8	<i>Tower</i>	105
5.3	<i>Performance and Losses</i>	106
5.3.1	<i>Evaluation</i>	106
5.3.2	<i>Solstice Field Losses</i>	107
5.3.2.1	<i>Atmospheric Attenuation</i>	107
5.3.2.2	<i>Spillage Losses</i>	108
5.3.2.3	<i>Reflectivity Losses</i>	108
5.3.2.4	<i>Cosine Losses</i>	109
5.3.2.5	<i>Shadowing and Blocking Losses</i>	110
5.3.3	<i>Solar Receiver Losses</i>	110
5.3.3.1	<i>Absorption Losses</i>	112
5.3.3.2	<i>Convection Losses</i>	112
5.3.3.3	<i>Radiation Losses</i>	114
5.3.3.4	<i>Conduction Losses</i>	114
5.3.4	<i>Other Losses</i>	115
+	5.3.5 <i>Performance of a Power Generation System</i>	116
<i>Chapter 6. Methodology of Designing the Solar Power Station</i>		117
6.1	<i>Design of Energy Collection system Localization - Dimension Procedure</i>	117
6.1.1	<i>Ground inclination</i>	118
6.1.2	<i>Power Block</i>	119
6.1.3	<i>Design Point</i>	119
6.1.4	<i>Heat and Storage Heat Transfer</i>	120
6.1.5	<i>Capacity Factor</i>	120
6.1.6	<i>Geographical Width</i>	121
6.2	<i>Design of the Energy Collection System</i>	122

6.2.1 Solar Field.....	122
6.2.1.1 Number of Heliostats.....	123
6.2.1.2 Solar Field Layout	124
6.2.1.3 Area and shape of reflective surface of Heliostats....	126
6.2.1.4 Solar Field.....	127
6.2.1.5 Optimization Codes.....	131
6.2.2 Solar Multiple Ratio.....	132
6.2.3.Solar Receiver.....	133
6.2.4 Tower height.....	135
6.3 Use of Energy - Design of Thermal Energy Storage System Size.....	136
6.4 Annual Electricity Production Assessment.....	137
6.5 Energy Cost.....	138
6.6 Energy Balance Sheet.....	138
6.6.1 Solar Energy.....	138
6.6.2 Thermal Energy.....	139
6.6.3 Production of Electricity.....	140
6.6.4 Gross to Net Conversion.....	140
6.6.5 Reflecting Surface Calculation - Energy Balance.....	141
6.7 Theoretical Approach.....	144
6.7.1 Theoretical Modeling.....	144
6.7.2 Theoretical Optimization.....	146
6.7.3 Theoretical Installation at the Design Point.....	148
6.8 Software for Solar Power Tower Modeling.....	149
6.9 Software Used in the Present Thesis.....	155

Chapter 7

7.1 The Proposed Modeling in SAM.....	159
7.1.1 Starting the Program.....	160
7.1.2 Data Used in the Proposed Modeling in SAM.....	170
7.1.3 Optimization Procedure of Solar Power Tower in SAM.....	177
7.1.4 Optimization Procedure of Storage system of Solar Power Tower in SAM.....	178
7.1.5 Financial - Cost Analysis Procedure in SAM.....	184
7.2 Scenarios Simulation and Results in SAM.....	189
7.2.1 Tower Height Scenarios.....	192
7.2.2 Solar Multiple Scenarios.....	210
7.2.3 Design Point DNI Scenarios.....	229
7.3 Scenarios Results.....	245

7.3.1 Tower Height Scenarios.....	245
7.3.2 Solar Multiple Scenarios.....	247
7.3.3 Design Point DNI Scenarios.....	249
7.4 Solar Field Geometry.....	252
7.4.1 Tower Height	252
7.4.2 Solar Multiple.....	257
7.4.3 Design Point DNI	261
7.5 Scenario 4 - Optimal Scenario.....	264
Conclusions.....	273
Bibliography.....	275

Abstract

The technology of CSP (Concentrated Solar Power systems) has become very popular in the recent years. The purpose of the present thesis is to study modeling, optimal sizing and LC-cycle analysis of a Concentrated Solar Power Tower (CSP) station. A Literature overview is done about the available programs (software) for modeling and simulation of Concentrated Solar Power Tower (CSP) plants. The aim of this thesis is to propose an optimization study how to optimal design the size of a solar tower power system, as also to minimize the capitalization cost and to maximize the energy dispatch capacity.

In this thesis modeling of a CSP and its optimization of all parameters is implemented, using the free program SAM by National Renewable Energy Laboratory (NREL). Parametric studies are performed for the same localization of a CSP, focusing on 3 factors that affect the performance of the CSP system, the tower height, the solar multiple and the design point DNI, in order to understand how they affect the overall power output of the plant and the LCOE. A detailed presentation of the plant data used is presented, analyzing the values of the variables and then the optimization procedure of CSP system in SAM follows, resulting in the layout of the solar field and basic features of the optimized CSP station. The optimization of the CSP's sizing is done, analyzing the inserted data. After that the LC-cycle-analysis procedure for 25 years in SAM is explained, explaining the used priced due to national laws in Greece and energy trade. Scenarios simulation and results in SAM are implemented for 22 scenarios. For every scenario one factor remains constant on an optimal empirical value, scaling the rest. SAM gives results, tables and diagrams that enabled us understand the behavior of the CSP system through changes. Comparing these results and especially focusing on energy cost and energy production, our conclusions are made. The solar field geometry for every scenario is examined in order to see how the solar field geometry changed, affected by scenarios. The final optimal scenario with the best values of the CSP factors is presented and the results are compared. The results are positive and CSP seems to be sustainable projects.

Key Words: CSP, SAM, Minos CSP Greek plant.

Περίληψη

Η τεχνολογία του CSP (Συγκεντρωτικό σύστημα ηλιακής ενέργειας) έχει γίνει πολύ δημοφιλής τα τελευταία χρόνια. Σκοπός της παρούσας διπλωματικής είναι η μελέτη μεθοδολογίας για την εύκολη μοντελοποίηση και διαστασιολόγηση ενός CSP, λαμβάνοντας υπόψη και της τεχνοοικονομικής ανάλυσης, προκειμένου να βελτιστοποιηθεί η διαστασιολόγηση των κύριων παραμέτρων που επηρεάζουν την απόδοση του σταθμού, ώστε να ελαχιστοποιηθεί το κόστος κεφαλαιοποίησης και να μεγιστοποιηθεί η δυναμικότητα αποστολής ενέργειας καθώς και η βέλτιστη λειτουργία και το μέγεθος της αποθήκευσης ενός ηλιακού πύργου. Μια επισκόπηση της σχετικά με τα διαθέσιμα προγράμματα διεξάγεται για τη μοντελοποίηση και την προσομοίωση των σταθμών CSP.

Στην παρούσα διπλωματική γίνεται μοντελοποίηση ενός CSP και βελτιστοποίηση σημαντικών παραμέτρων του, προσομοιώνοντας τον σταθμό στο πρόγραμμα SAM από το Εθνικό Εργαστήριο Ανανεώσιμων Πηγών Ενέργειας (NREL). Εκπονούνται παραμετρικές μελέτες για τον ίδιο τόπο εγκατάστασης, εξετάζοντας 3 παράγοντες που επηρεάζουν την ισχύ εξόδου του CSP και το LCOE του: το ύψος του πύργου, το ηλιακό πολλαπλό (solar multiple) και την ηλιακή ακτινοβολία στο σημείο σχεδιασμού. Παρουσιάζονται λεπτομερώς τα δεδομένα που χρησιμοποιούνται, αναλύοντας τις τιμές των μεταβλητών και με την χρήση του SAM πετυχαίνεται βελτιστοποίηση του συστήματος CSP στο SAM, όσον αφορά την διάταξη - γεωμετρία του ηλιακού πεδίου και τα βασικά χαρακτηριστικά του βελτιστοποιημένου σταθμού CSP. Η βελτιστοποίηση του συστήματος αποθήκευσης του CSP γίνεται με ανάλυση των εισαγόμενων δεδομένων. Η τεχνοοικονομική ανάλυση (ανάλυση κύκλου LC) υπολογίζεται για 25 χρόνια μέσω του SAM. Για τις τρεις παραμέτρους μελετιούνται 22 σενάρια, διατηρώντας πάντα μια σταθερή σε τιμή που εμπειρικά έχει αποδειχθεί βέλτιστη και μεταβάλλοντας τις υπόλοιπες, λαμβάνοντας την τρέχουσα νομοθεσία net metering και CO2 καθώς και τις δυνατότητες επιδότησης. Για κάθε σενάριο, το SAM δίνει αποτελέσματα, πίνακες και διαγράμματα που μας επιτρέπουν να κατανοήσουμε τη συμπεριφορά του συστήματος CSP μέσω αυτών των αλλαγών. Συγκρίνοντας αυτά τα αποτελέσματα και ειδικά εστιάζοντας στο ενεργειακό κόστος και στην παραγωγή ενέργειας, βγάζουμε τα συμπεράσματά μας. Η γεωμετρία του ηλιακού πεδίου για κάθε σενάριο εξετάζεται για γίνει αντιληπτό πώς η γεωμετρία του ηλιακού πεδίου άλλαξε, επηρεασμένη από τα σενάρια και στο τέλος παρουσιάζεται το τελικό βέλτιστο σενάριο με τις καλύτερες τιμές των μεταβλητών και τα αποτελέσματα συγκρίνονται. Τα αποτελέσματα είναι ελπιδοφόρα και το CSP φαίνεται να είναι βιώσιμα έργα.

Λέξεις Κλειδιά: Συγκεντρωτικό σύστημα ηλιακής ενέργειας CSP, SAM, Minos CSP

Chapter 1

Energy Problem

1.1 World Energy Problem

When energy is scarce or expensive, people can suffer material deprivation and economic hardship. When it is obtained in ways that fail to minimize environmental and political costs, human wellbeing can be threatened in fundamental and pervasive ways.

The energy problem today combines these syndromes: much of the world's population has too little energy to meet basic human needs; the monetary costs of energy are rising nearly everywhere; the environmental impacts of energy supply are growing and already dominant contributors to local, regional, and global environmental problems (including air pollution, water pollution, ocean pollution, and climate change); and the sociopolitical risks of energy supply (above all the danger of conflict over oil and the links between nuclear energy and nuclear weapons) are growing too.

This predicament has many causes, but predominant among them are the nearly 20-fold increase in world energy use since 1850 and the cumulative depletion of the most convenient oil and gas deposits that this growth has entailed, resulting in increasing resort to costlier and/or environmentally more disruptive energy sources. The growth of world population in this period was responsible for 52% of the energy growth, while growth in per capita energy use was responsible for 48% (excluding causal connections between population and energy use per capita).

In the United States in the same period, population growth accounted for 66% of the 36-fold increase in energy use. In the late 1980s, population growth was still accounting for a third of energy growth both in the United States and worldwide.

Dealing with global energy problems will require greatly increased investment in improving the efficiency of energy and in reducing the environmental impacts of contemporary energy technologies, and it will require financing a transition over the next

several decades to a set of more sustainable (but probably also more expensive) energy sources. The difficulty of implementing these measures will be greatest by far in the developing countries, not least because of their high rates of population growth and the attendant extra pressures on economic and managerial resources.

If efficiency improvements permit delivering the high standard of living to these that the world aspires based on a per capita rate of energy use as low as 3 kilowatts—about a quarter of the current U.S. figure—then a world population stabilized at 10 billion people would be using energy at a rate of 30 terawatts, and a population of 14 billion would imply 42 terawatts (compare 13.2 terawatts in 1990). Delivering even the lower figure at tolerable monetary and environmental costs will be difficult; each additional billion people added to the world population will compound these difficulties and increase energy's costs, making everyone poorer.

As we understand human life depends on energy. Since the industrial revolution of the 19th century until today, energy industry was developed and therefore all the sectors around it. The main source of energy for this development was fossil fuels (coal, hydrocarbons, fissionable nuclear materials), but oil was the most widespread of all.

The dependence of the industry and the production of fossil fuel energy was extended, resulting in even geopolitical strategies being implemented to manage the stocks. In the past, this dependence has led humanity to economic crises (such as the oil crisis in 1973), but also in wars.

The world population is growing very rapidly and with the constant rise in living standards, the demand for energy is greater than that we can produce with the use of minerals fuel. Fossil fuels are not an inexhaustible source of energy so unfortunately there are serious environmental impacts.

Fossil emissions from fossil fuels affect the environment and the atmosphere of the earth, resulting in global warming. In the recent decades, there have been changes in the global climate, which are due to the phenomenon of the Greenhouse, which is created by the excessive use of fossil fuels.

The consequences from global warming will be catastrophic in the future. Ice on the Earth's poles tend to melt, resulting in increasing the sea level, anhydrous areas will become deserts, and serious health effects for people due to the resistance of microbes to the higher temperatures. [1],[2],[3],[64],[85],[128]

1.2 Energy Problem In Greece

The Greek energy sector is still largely dependent on fossil fuels, most of which are imported. About 54% of its energy requirements are covered by petroleum products alone, compared to an average of 33.4% at the EU level. These petroleum products are not only used in the transport sector, but they are also converted in relevant amounts into electricity. In particular, the non-interconnected Greek islands obtain their electricity primarily from inefficient and expensive diesel generators. In total, the extra cost that had to be recovered in 2016 through a public service obligation was 720 m€ to subsidize the electricity tariffs in those areas. Natural gas, which also has to be imported at a significant cost, plays a growing role in meeting energy requirements.

Domestic energy sources include lignite which accounts for around 50% of electricity generation as well as renewable energy sources (RES) such as hydro-power, wind, solar energy and biomass. Almost 61% of Greece's primary energy needs are fulfilled through imports with the remaining 39% being covered through domestic energy sources, mainly lignite (77%) and RES (22%). Imported energy sources are mainly petroleum products that account for 44% of total energy consumption and natural gas with a share of around 13%.

A national target of a 20% RES share in gross final energy consumption by 2020 has been defined under Law 3851/2010, exceeding the national target of 18% according to the EU Directive 2009/28/EC. The specific trajectory for achieving this target is presented in the National Renewable Energy Action Plan (NREAP) of 2010. Specific targets for RES electricity share (40%), RES heating and cooling share (20%), and RES transport share (10%) have been defined in order to achieve the national RES target until 2020.

The overall target is therefore supposed to be achieved through a combination of measures for energy efficiency and the large-scale penetration of RES technologies in electricity production, heat supply and transport sector. The variables and assumptions which have been used for the elaboration of the NREAP are currently being revised in the context of the national energy planning, taking into consideration the lower than expected levels of energy consumption due to the economic crisis and the adjusted macroeconomic values, as well as the differences between the NREAP projections and

the actual development and share of the different RES technologies in terms of installed capacities and electricity generation.

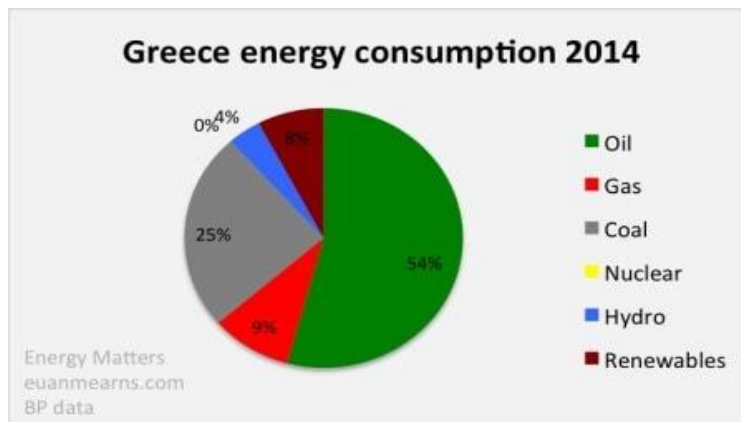


Figure 1.1 Total Consumption of Greece[102]

A number of significant reforms aiming at a further liberalization of the electricity and gas sector, the reform of the various energy markets, as well as a number of strategic grid infrastructure works are currently being implemented. In addition, the Greek support scheme for electricity production from RES is currently undergoing a major transition in order to improve the cost-efficiency of the support scheme, to facilitate the integration of RES in electricity market and to ensure conformity with requirements under EU state aid regulations.

Around 61% of Greece's energy needs are covered through imports with the remaining 39% being covered through national energy sources, mainly lignite (77%) and RES (22%). Imported energy sources are mainly petroleum products that account for 44% of total energy consumption and natural gas with a share of around 13%.

According to the Greek Electricity Market Operator (LAGIE), the total installed capacity in the Greek interconnected system at the end of 2016 accounted for almost 16,615 MW, including 3,912 MW lignite, 4,658 MW natural gas, 3,173 MW large hydro-power and 4,873 MW RES. The total electricity generation in the Greek interconnected system for the year 2016 amounted to almost 41.6 TWh. An additional 10.7 TWh of electricity was imported and 2.2 TWh were exported. Lignite accounted for 23.55% of the installed capacity in the interconnected system, natural gas for 28.4%, hydro-power for 19.10% and RES for 29.33%.

According to the Hellenic Electricity Distribution Network Operator (HEDNO), on the non-interconnected islands (NIIs), the diesel-driven generators' production was 3,604 GWh by December 2016. The renewable energy share in the electricity mix of the NII was 21.8%, corresponding to a production of 1,003 GWh and an installed capacity of 482.3 MW.

Gross national electricity consumption in 2016 was roughly 50.1 TWh, including transmission and distribution losses of about 2.9%. The annual peak load in the interconnected system currently stands at around 9,082 MW.

The average cost of RES electricity production in 2016 accounted for 161.5 €/MWh compared to the value of 162.7 €/MWh in 2015 and it was down from 200 €/MWh in 2014. This has been mainly due to the adjustment of feed-in tariffs (FIT) in April 2014 that have been implemented in the context of Law 4254/2014. The RES cost compares to an average electricity system marginal price (SMP) of 42.83 €/MWh in 2016 (51.94 €/MWh in 2015). The highest value has been recorded in December 2016 at 51.09 €/MWh. As reported by Eurostat, electricity tariffs in 2016 for final consumers in Greece were on average 176 €/MWh for medium-size households (including taxes and levies) and 92 €/MWh for medium-size industrial companies (including levies but excluding taxes). [4],[5],[57],[64],[85],[102]

1.3 Solution of the Environmental Problem - Renewable Energy

The ever-increasing demand for energy and the impact of use fossil fuels have created the need for penetration alternative forms of energy in electricity generation worldwide. Realizing this need and recognizing the environmental impact, the Kyoto Protocol was signed, which has goal to reduce greenhouse gas emissions .

The European Union, wanting to achieve emission reductions and improving energy efficiency, has set new and more ambitious targets in the Copenhagen Accord which was signed. The EU has also seen the growing dependence on imports (mainly oil and gas). All this shows the way to Renewable Energy Sources, understanding that this is the solution to the environmental problems.

Renewable energy is a practical, affordable solution to our electricity needs. By ramping up renewable energy, we can reduce air pollution, cut global warming emissions , create new jobs and industries ,diversify our power supply and decrease dependence on coal and other fossil fuels.

We have the technologies and resources to reliably produce at least 40 percent of our electricity from renewable energy sources within the next 20 years, and 80 percent by 2050. [6],[7],[8],[9],[122],[125]

1.4 Thesis Objectives and Methods

In this thesis we are going to make:

- A technology study including modeling, optimal sizing and LC-cycle analysis about Renewable Energy Source of a Concentrated Solar Power Tower (CSP) station.*
- Literature overview about the available programs (software) for modeling and simulation of Concentrated Solar Power Tower (CSP)plants.*
- Use available software in order to model a CSP and optimize the dimension procedure. The optimization consists various parameters, such as tower geometry, solar field, etc.*
- A techno - economical analysis of our system is studied. In order to achieve these goals, several scenarios related to CSP are taken. E.g. changing the system 's variables every time, in order to find the best scenario taken for the CSP system, taking into account the financial factors and the energy production of the system.*
- An Optimization study in order to minimize the capitalization cost and to maximize the energy dispatch capacity, as also to make Optimal sizing of a solar tower power system.*

The method employed in developing the SAM for the 52 MW CSP plant located in Greece. SAM was used because it is free software, and it can analyze different renewable energy systems. It also includes financial analyses models, which help to determine the profitability of a given renewable energy project. The approach used to develop the SAM generally follows the guidelines as suggested by Wagner (Wagner, 2014 Wagner, M. 2014. "Modelling parabolic trough systems." 2014 Webinars. Retrieved from <https://sam.nrel.gov/webinars> [Google Scholar]). Because there are various fields that need to be specified, Wagner recommended the following approach:

- *Configure receiver and collector components*
- *Specify HTF and operating temperatures*
- *Determine transport operation limits*
- *Configure the loop*
- *Specify power cycle design point*
- *Specify thermal storage parameters*
- *Update costs and financials*
- *Optimize uncertain parameters*
- *Optimize solar multiple and TES capacity*

1.5 Thesis Structure

At the 1st chapter of this thesis, the energy problem is analyzed, starting from world energy problem, continuing with the energy problem in Greece, ending up with finding the solution to that important problem, which is renewable energy.

The 2nd chapter analyzes the renewable energy sources, presents the renewable energy categories, and the subject of this thesis, which is the Concentrated Solar Power Tower system (CSP).

Chapter 3 concerns basic knowledge fundamentals of solar energy exploitation, thermodynamic cycles (Stirling cycle, Brayton cycle and Rankine cycle), the types of concentrated solar system are presented (parabolic trough collectors, dish systems, linear fresnel reflectors (CLFR) and solar power tower), and in the end we come to the conclusion that solar power tower technology is rapidly developing over the last decade and is expected to outperform the other systems in the coming years, so it is interest to

deal with it to see what exactly that system is, and its possibilities, so we finally in Chapter 3 come up to Solar Power Tower Systems.

Chapter 4 includes an historical return about CSP systems, presents the existing installations of such systems, as also the experimental CSP systems of little power, continuing with the large scale CSP systems, and a presentation of the 5 biggest system in the world is made (Ivan Solar Electric Generating Systems, Solar Energy Generating Systems (SEGS), Mojave Solar Project, Solana Generating Station, Genesis Solar Energy Project). A list of the existing solar thermal power station is presented, the solar power tower installations under construction is presented, but also the solar power tower installations announced are presented. In the end of chapter 4, the situation concerning CSP system in Greece is presented, with the 2 main installations, Maximus and Minos.

Chapter 5 refers to an analytic theoretical background for CSPs. Starts with solar power tower operating principle, analyzing how the systems works and of what subsystems it consists. The basic subsystems are the solar field, the solar receiver, the electricity production system, the thermal energy storage system and the refugee fuel system. Chapter 5 ends up with the performance and losses of the CSP systems, analyzing the parameters and factors that affect them.

Chapter 6 includes the methodology of designing the solar power tower system - factors of localization, separated in the energy collection area (solar field, solar receiver, tower and piping) and the energy recovery area (steam generator, power system, thermal energy storage system and conventional system). The energy collection system localization factors include the ground inclination, the power block, the design point, the heat and storage heat transfer, the capacity factor and the geographical width. The design of energy collection system factors include solar field, numbers of heliostats, solar field layout, area and shape of reflective surface, solar multiple ratio, solar receiver and tower height. After that Chapter 6 deals with use of energy, design of thermal energy storage system size, annual electricity production assessment, energy cost, energy balance sheet, solar energy, thermal energy, production of energy, gross to net conversion, reflecting surface calculation - energy balance and a theoretical approach of designing of the CSP system, theoretical modeling, theoretical optimization and theoretical installation at the design point. Chapter 6 continues with the presentation of the available software in market that enables the dimensioning and optimization of renewable energy systems and ends up with the software that is used in the present

thesis, which is SAM - System Advisor Model by National Renewable Energy Laboratory (NREL).

Chapter 7 includes the implementation of modeling of a CSP and its optimization using the free software SAM, so that safer conclusions about such systems can be made. A presentation of the basic frames of SAM is made, in order to see what SAM is, and then modeling is started. A detailed presentation of the data used in this thesis is made, analyzing the prices of the variables used and then the optimization procedure of CSP system in SAM, resulting in the layout of the solar field and basic features of the optimized CSP station (receiver height, receiver diameter, tower height and heliostat count). The optimization of the CSP 's storage system follows, by analyzing the inserted data of this thesis. After that the financial and cost analysis procedure in SAM is explained, explaining the used priced due to laws and energy trade. Chapter 7 ends up with scenarios simulation and results in SAM. In this thesis we examined 3 factors that affect the performance of the CSP system, the tower height, the solar multiple and the design point DNI. For that purpose 22 scenarios were made, every time only one variable was changed. The scenarios made in this thesis are:

Scenario 1 (Tower Height Scenario)

Scenario 1.1 :Tower Height = 127 m, Solar Multiple = 2.1, Design Point DNI = 950 (scenario 1.1 is the basic scenario made that was changed afterwards to make all the other scenario so it is taken into account for all the comparisons between scenarios as it is a case for every examined factor in this thesis)

Scenario1.2 :Tower Height = 63.5 m,

Scenario1.3 :Tower Height =190.5 m,

Scenario1.4 :Tower Height =254 m,

Scenario1.5 :Tower Height =317.5 m,

Scenario1.6 :Tower Height =400 m,

Scenario1.7 :Tower Height =450 m,

Scenario1.8 :Tower Height =480 m

Scenario 2 (Solar Multiple Scenario)

Scenario2.1 : Solar Multiple = 1.05,

Scenario2.2 : Solar Multiple = 1.6,

Scenario2.3 : Solar Multiple = 2.6,

Scenario2.4 : Solar Multiple = 4.2,

Scenario2.5 : Solar Multiple = 8.4,

Scenario2.6 : Solar Multiple = 16.8,

Scenario2.7 : Solar Multiple = 21

Scenario 3 (Design Point DNI Scenario)

Scenario3.1 : Design Point DNI = $475W / m^2$,

Scenario3.2 : Design Point DNI = $700W / m^2$,

Scenario3.3 : Design Point DNI = $800W / m^2$,

Scenario3.4 : Design Point DNI = $1000W / m^2$,

Scenario3.5 : Design Point DNI = $1100W / m^2$,

Scenario3.6 : Design Point DNI = $1475W / m^2$

Scenario 4 - The optimal Scenario

For every scenario SAM gives results, tables and diagrams that enabled us understand the behavior of the CSP system through these changes. Comparing these results and especially focusing on energy cost and production, our conclusions were made. Chapter 7 also presents the solar field geometry for every scenario made in order to see how the solar field geometry changed, affected by tower height, solar multiple and design point DNI scenarios and at the end of this Chapter the final optimal scenario (scenario 4) with the best prices of the changed variables is presented.

Chapter 2

Renewable Energy

2.1 Renewable Energy Sources - Basic Fundamentals

Renewable Energy Sources are called the energy derived from nature. The categories of the renewable energy sources are: wind, solar, geothermal, hydrothermal, water energy, hydropower, biomass, energy from gases which are straight-in landfill, gas energy from sewage treatment plants, osmotic energy (or blue energy) and energy from biogas.

Procedures such as mining, extraction or burning are not needed for the exploitation of renewable energy sources, because an exploitation of existing energy flow in nature takes place. Renewable energy is "clean" energy, "friendly" to the environment, it does not emit pollutants into the environment, hydrocarbons, carbon dioxide or toxic and radioactive waste, as they would do other energy sources. For these reasons the Renewable Energy Sources are a solution to environmental problems facing the environment, and a solution to the problem of a future depletion of fossil fuel reserves.

Most of these forms of energy are based on solar radiation, except from geothermal energy which is energy flow from the interior of the earth. Geothermal energy is not renewable, and geothermal fields sometime are exhausted. So it is obvious that since they are based on solar radiation they are renewable, since it does not run out as long as the sun exists.

Biomass is solar energy bound in plants (in the tissues) through photosynthesis, wind energy is based on wind, and energy-related categories based on water evaporation-condensation cycle of water and release. Renewable Energy Sources are

used either directly (mainly for heating) or they are converted into other forms of energy (electricity or mechanical energy).

The exploitation of renewable energy came from the oil crisis (1970), and due to environmental pollution. Initially they were costly and they started as a pilot program. Today they have a high position in the official plans of developed countries for energy, although even if they are not for the time being a large percentage of energy production, the future is very optimistic about their development and their cost constantly drops. The wind energy, hydropower, biomass, are the most competing energy sources such as coal and nuclear energy.

The Benefits of Renewable Energy Sources are that they are environmentally friendly because they have almost zero waste, and will never be exhausted, unlike fossil fuels. They help energy self-sufficiency of small and developing countries, they are flexible applications that can generate power commensurate with the needs of the population on the ground, eliminating the need for huge power plants (in principle for the countryside). The equipment is simple, easy maintenance and a very long life-time.

Renewable Energy Sources have disadvantages such as they have a small coefficient of performance (about 30%), requiring fairly large initial cost of implementing a large area of land, that is why they are used as supplementary energy sources, and cannot be used to meet the needs large urban centers. The performance of wind, hydro and solar energy depends on the time of year, but also on latitude and climate of the area in which they are established, so according to these criteria is sometimes more efficient and sometimes less.[10],[64],[101],[122],[129]

2.2 Categories of Renewable Energy Sources

2.2.1 Biogas

Biogas is a fuel more environmentally friendly than the ordinary. An energy source with many features and applications that will be used widely in the future. Biogas

typically refers to a mixture of different gases that are produced by the breakdown of organic matter in the absence of oxygen. It can be produced from raw materials such as agricultural waste, manure, municipal waste, plant material, sewage or food waste. Biogas is a renewable energy source and in many cases exerts a very small carbon footprint.

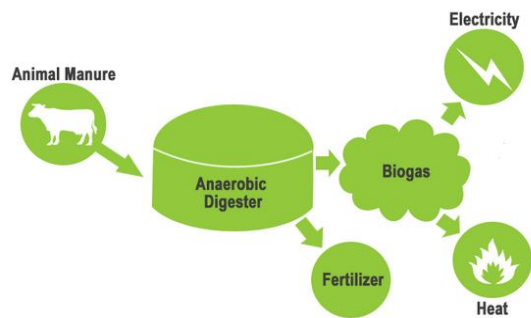


Figure 2.1 Biogas production [2]

It can be produced by anaerobic digestion with anaerobic organisms, which digest material inside a closed system, or fermentation of biodegradable materials. Biogas is primarily methane (CH_4) and carbon dioxide (CO_2) and it may have small amounts of hydrogen sulfide (H_2S), moisture and siloxanes. The gases methane, hydrogen, and carbon monoxide (CO) can be combusted or oxidized with oxygen. This energy release allows biogas to be used as a fuel; it can be used for any heating purpose. It can also be used in a gas engine to convert the energy in the gas into electricity and heat. Biogas is produced as landfill gas, which is produced by the breakdown of Biodegradable waste inside a landfill due to chemical reactions and microbes, or as digested gas, produced inside an anaerobic digester.[10],[129]

2.2.2 Solar Energy

Solar energy is more used for thermal applications (solar water heaters and ovens) and for electricity production. Solar energy is radiant light and heat from the sun that is harnessed using a range of ever-evolving technologies such as solar heating,

photovoltaic, solar thermal energy, solar architecture, molten salt power plants and photosynthesis. It is an important source of renewable energy and its technologies are broadly characterized as either passive solar or active solar depending on how they capture and distribute solar energy or convert it into solar power.

Active solar techniques include the use of photovoltaic systems, concentrated solar power and solar water heating to harness the energy. Passive solar techniques include orienting a building to the sun, selecting materials with favorable thermal mass or light-dispersing properties, and designing spaces that naturally circulate air. [10],[11],[129]

❖ Solar Thermal Systems:

Solar Thermal Systems are the systems with thermally context that is holding the heat of solar radiation (mainly for water heating). Solar Thermal collectors are classified by the United States Energy Information Administration as low-, medium-, or high-temperature collectors. Low-temperature collectors are flat plates generally used to heat swimming pools. Medium-temperature collectors are also usually flat plates but are used for heating water or air for residential and commercial use. High-temperature collectors concentrate sunlight using mirrors or lenses and are generally used for fulfilling heat requirements up to 300 deg C / 20 bar pressure in industries, and for electric power production. Solar thermal systems include Concentrated Solar Thermal (CST) for fulfilling heat requirements in industries, and Concentrated Solar Power (CSP) when the heat collected is used for power generation.

❖ Photovoltaic Systems:

Photovoltaic Systems are the systems where the conversion of solar energy into electricity is achieved using frames because of the photovoltaic effect. A photovoltaic system, also solar PV power system, or PV system, is a power system designed to supply usable solar power by means of photovoltaics. It consists of an arrangement of several components, including solar panels to absorb and convert sunlight into electricity, a solar inverter to change the electric current from DC to AC, as well as

mounting, cabling and other electrical accessories to set up a working system. It may also use a solar tracking system to improve the system's overall performance and include an integrated battery solution, as prices for storage devices are expected to decline.



Figure 2.2 Photovoltaic System [11]

Moreover, PV systems convert light directly into electricity and should not be confused with other technologies, such as concentrated solar power or solar thermal, used for heating and cooling. PV systems range from small, rooftop-mounted or building-integrated systems with capacities from a few to several tens of kilowatts, to large utility-scale power stations of hundreds of megawatts. Operating silently and without any moving parts or environmental emissions, PV systems have developed from being niche market applications into a mature technology used for mainstream electricity generation.[10],[11],[129]

❖ The photovoltaic effect

Photovoltaic effect is not applied in Solar Towers, analyzed in this paper, but it is interesting to know some things about it. The photovoltaic effect is described as the polarization of electrical charges that occurs in specific materials when they are exposed to light. This is observed in the physical elements belonging to the semiconductor group as well as in the semiconductor devices. The polarization of electrical charges is translated as the creation of a potential difference between the generated poles, so we have a rudimentary electric generator.

The production of electricity in PV is due to the photovoltaic phenomenon. Solar energy is converted into electrical because of the properties of semiconductor materials. The material that is used to create PV modules is silicon (Si). Silicon has an indirect energy gap with a low value of 1.1 eV. These features, we would say that they do not make it the ideal semiconductor for the conversion of solar radiation, but instead it has a leading position in the construction of PV elements because: it is easily found in nature, it is the second most abundant material on the planet after oxygen. It is in the form of silicon dioxide (SiO₂), so we need to process it to make use of it. After processing it, the silicon has purity and perfection of crystalline structure. Thus it easily melts and forms, it is converted into its monocrystalline form. Electrical properties of silicon are maintained up to 125 °C, so it can be used in particularly difficult environmental conditions. This is why the silicon PV modules are working satisfactorily in a wide range of temperatures.

The silicon atom has 14 electrons. These are structured with such a way that the 4 outer electrons (valence electrons) can be given, accepted or shared with another person. A large number of people, through valence electrons, can interconnect with bonds and then form a crystalline grid, creating a solid.

When solar radiation falls on crystalline silica, it reflects, or it penetrates the crystal absorbed, and if the solar radiation is low energy the silicon atoms oscillate around their position without loosening the bonds between them while the electrons of the bonds get more energy and go up to higher energy levels that are not stable, so they soon return to their original energy levels, yielding heat in the form of heat, the energy they have gained. On the other hand, if the solar radiation has enough energy, it is possible to change the electrical properties of the crystal. Thus, the electron of a bond can be separated from its position in the crystal and can move to the conduction zone leaving behind a bond from the missing zone of an electron, called a hole.

The valence holes and the electrons in the conduction zone are free to move through the crystal, defining the electrical behavior of the solar cells. The electron-hole pairs created with the help of sunlight are the basic process of the photovoltaic effect, but they are not able to generate current. For power generation, the potential barrier is necessary. Each solar cell contains a potential barrier that separates the produced electron-hole pairs, sending more electrons to one side of the cell and more holes in the other, so there is little chance of reconnection between them. This separation of loads

creates a potential difference at both ends of the cell, which can give current to one external circuit.

The silicon atom has 4 valence electrons, as we said, each of which forms a bond with another silicon atom. If a blending silicon crystal is introduced into a pure silicon crystal by replacing a silicon atom with an atom from the fifth group of the periodic system, e.g. Phosphorus, having 5 valence electrons. The atom - impurity will replace a silicon atom by providing 4 electrons for each of the 4 bonds with 4 other silicon atoms and will leave an electron that will not be bonded. This will be at an intermediate level very close to the conduction zone where at room temperature there is enough thermal energy in the crystal to move this electron to the conduction zone without fear of reconnected with a hole because it has not created a hole behind it but a positive phosphorus ion and it is always ready to contribute to some electricity. So, a silicon crystal in which a large number of atoms are replaced by phosphorus atoms, will have many free electrons in conductivity band and a corresponding number of positive ions in the crystal structure.

Thus the electrical properties change, while as a whole it remains electrically neutral. Impurities of this type having an extra valence electron are called donors and the crystal is called -n (n-TYPE). By replacing a silicon atom with an atom from the third group of the periodic system e.g. Boron, with 3 outer electrons, the atom-impurity will give these three electrons in 3 bonds with 3 silicon atoms, but the fourth bond will lack an electron, so a hole will be created. This hole is at an intermediate level very close to the valence zone, so with heat energy, it will be moved to the valence zone.

Thus, a silicon crystal with many boron atoms has many holes that are considered as free positive charges and are moved through the crystal lattice. Such admixtures are called receivers, because their holes receive electrons (bond electrons or electrons conductivity) and the crystal is called -p (p-TYPE).

In an n-type material, electrons (negative charges) are the majority bodies while the holes are the minority bodies. In one p-type material, holes (positive charges) are the majority carriers, while electrons are the minority carriers. If we contact a n-type material and a p-type material, the dividing line called contact is the focal point of creating the dynamic dam, which, as we have seen, is essential condition for the operation of the solar cell. When the two materials come in contact, free electrons from the n-type

material jump (through the diffusion process) through contact in the p-type material and are connected to corresponding holes, since the material has a large number of holes.

If n is the density of electrons, is the one-dimensional concentration of electron concentration. It is obvious that the electron flow is proportional to the negative fundraising of the concentration. Because the current is proportional to the flow of the charged particles, the above phenomenon consists of a diffusion current whose density is given by the relation:

$$J_e = qD_e \left(\frac{dn}{dx} \right) \quad (2.1)$$

$$q = 1.6 \cdot 10^{(-19)} \text{ Cb} \quad (2.2)$$

where D_e = electron diffusion constant, is the one-dimensional concentration of electron concentration.

The apertures (holes) of the p-type material jump (through diffusion) into the n-type material (i.e., valence electron from the n-type material jump into the p-type material and are connected with holes) that constitute a diffusion current. So we have a load imbalance on the two sides of the contact: negative charges (plus electrons) on the p-type side and positive loads (ions) on the n-type side. This process, of course, does not go unlimited. The charged carriers carried on the two sides of the contact create an electric field that acts as a barrier and opposes the further flow of the vectors.

In other words, in a narrow area around the contact, space loads are generated, creating the potential barrier, which opposes the further diffusion of the majority bodies through contact. Minority entities are not blocked by the potential barrier. On the contrary, when the cell is not illuminated, there is a small number of minority carriers, such as free electrons in the p-type material, which are driven by the electric field of the contact on the opposite side (n-type material) and constitute the slip stream (current). That is the photovoltaic effect.[10],[129]

❖ Solar Towers (will be described and analyzed extensively in the next chapters)

2.2.3 Wind Energy

Windmills (wind machines) are used, which exploit wind energy, for various uses (pumping water, grinding grain, etc.). Wind energy is used to rotate the shaft of a generator to produce electricity. Previously used for pumping water from wells and for applications such as grinding windmills. Often we meet and wind farms.

Wind energy is a form of solar energy. Wind energy (or wind power) describes the process by which wind is used to generate electricity. Wind turbines convert the kinetic energy in the wind into mechanical power. A generator can convert mechanical power into electricity. Mechanical power can also be utilized directly for specific tasks such as pumping water. A rooftop system recoups the invested energy for its manufacturing and installation within 0.7 to 2 years and produces about 95 % of net clean renewable energy over a 30-year service lifetime. Wind is caused by the uneven heating of the atmosphere by the sun, variations in the earth's surface, and rotation of the earth. Mountains, bodies of water, and vegetation all influence wind flow patterns.



Figure 2.3 Wind farms [12]

Wind turbines convert the energy in wind to electricity by rotating propeller-like blades around a rotor. The rotor turns the drive shaft, which turns an electric generator. Three key factors affect the amount of energy a turbine can harness from the wind: wind speed, air density, and swept area.[10],[12],[104],[129]

2.2.4 Geothermal energy

Geothermal energy is the thermal energy from the earth, namely from the inside (by the radioactive decay of the earth rocks). It relies on heat transfer by conduction, and exploitation depends on the temperature. It is usable where the heat that rises naturally to the surface, e.g. the geysers or hot springs. It can be used either directly for thermal applications or to generate electricity.



Figure 2.4 Geothermal energy [13]

The geothermal energy of the Earth's crust originates from the original formation of the planet and from radioactive decay of materials. The geothermal gradient, which is the difference in temperature between the core of the planet and its surface, drives a continuous conduction of thermal energy in the form of heat from the core to the surface. Earth's internal heat is thermal energy generated from radioactive decay and continual heat loss from Earth's formation. Temperatures at the core–mantle boundary may reach over 4000 °C (7,200 °F). The high temperature and pressure in Earth's interior cause some rock to melt and solid mantle to behave plastically, resulting in portions of mantle convecting upward since it is lighter than the surrounding rock. Rock and water is heated in the crust, sometimes up to 370 °C (700 °F).

- ❖ *Water infiltration: the percentage of precipitation that penetrates the surface of the ground reaching the underground aquifers. The replenishment rate of the groundwater reserves through infiltration is a very important component of the hydrological cycle and is determined by the permeability of the soil and subsoil,*

the stone composition as well as the slope of the terrain, vegetation, altitude, distribution and intensity of precipitation etc.[10],[13],[129]

2.2.5 Hydrodynamic Energy (Water Energy)

The Hydropower is energy which is based on exploitation and conversion of the potential energy of the water of the lakes and the kinetic energy of the water of rivers into electricity.



Figure 2.5 Dams on river - Hydrodynamic Energy [14]

This conversion takes place in two stages. In the first step, by means of the impeller of the turbine, we have the conversion of the kinetic energy of the water into mechanical energy in the form of rotation of the impeller shaft and at the second stage, through the generator, we achieve the conversion of mechanical energy into electricity. All works and equipment through which the transformation of hydraulic energy is transferred into electricity, is called Hydroelectric Project (HEP). The planned release of these amounts of water and their expansion in turbines leads to controlled electricity production. Given that adequate water resources and their adequate supply of the necessary rainfall, it becomes an important alternative source of renewable energy.

a)The water flow can initiate one impeller which rotates the shaft of a generator and thus electricity is generated. This is done by dams on rivers where the water flow is great. Renewable energy source are considered small-scale hydropower.

b)Energy from tides. Exploits the gravity of the Sun and the Moon, causing elevation of the water level. The water is stored as rising and to be downloaded again it has to pass through a turbine to produce electricity.

c)Energy from waves exploits the kinetic energy of sea waves.

d)Energy from the oceans. Exploits the temperature difference between the layers of the ocean, using thermal cycling, but this kind of action is still under investigation.[10],[14],[129]

2.2.6 Biomass

Biomass is any material which is produced by living organisms (plants, animal waste and derivatives etc.). The biomass can be met in various forms, and the energy generated by this, is used in many applications. Biomass uses carbohydrates of plants (mainly waste wood industry, food, feed and the sugar industry) in order to release the energy bound by the plant through photosynthesis. Even municipal waste and waste can be used. Woods considered biomass and by burning thermal energy can be produced. It is capable of producing bioethanol and biogas that can be used as fuel. It is possible diesel production (biodiesel) from vegetable oils and animal fats. Biomass is considered renewable energy source.

Biomass is an industry term for getting energy by burning wood, and other organic matter. Burning biomass releases carbon emissions, around a quarter higher than burning coal, but has been classed as a "renewable" energy source, because plants can regrow. It has become popular among coal power stations, which switch from coal to biomass to comply with the law. Biomass most often refers to plants or plant-based materials that are not used for food or feed, and are specifically called lignocellulosic biomass. As an energy source, biomass can either be used directly via combustion to produce heat, or indirectly after converting it to various forms of biofuel. Conversion of biomass to biofuel can be achieved by different methods which are broadly classified into: thermal, chemical, and biochemical methods.[10],[105],[129]

2.2.7 Osmotic Effect

The mixing of fresh and salt water releases large amounts of energy, as happens when a river flows into the ocean. This action is called osmotic energy (or blue energy) and is recovered when the water of the river and the sea water is separated by a semi-permeable membrane and the fresh water passes through it.

Osmotic pressure is the minimum pressure which needs to be applied as a solution to prevent the inward flow of water across a semi permeable membrane. It is also defined as the measure of the tendency taken in water by osmosis. Potential osmotic pressure is the maximum osmotic pressure that could develop in a solution if it were separated from distilled water by a selectively permeable membrane. The phenomenon of osmosis arises from the propensity of a pure solvent to move through a semi-permeable membrane and into a solution containing to which the membrane is impermeable. This process is of vital importance in biology as the cell's membrane is semi permeable.[10],[129]

2.3 Concentrated Solar Systems

There are many types of fuel in the world energy market, but few ways of exploiting them. The most common way of producing energy is using steam power stations. The fuel heats the working mean which performs a thermodynamic cycle so that the difference of the temperature produces mechanic work.

In practice, the heating of the working mean is achieved by burning minerals fuels such as coal or lignite, hydrocarbons, nuclear energy, or geothermal energy. The working mean is converted into high pressure steam, it enters a steam turbine and then

rotates one generator.



Figure 2.6 Concentrated Solar System [15]

It is perceived that the main issue of energy production with this way, is the thermal energy produced by combustion. However, this thermal energy can also be produced by the radiation of the sun. So, research has been centered over the past decades in finding more efficient methods for solar thermal systems, resulting in concentrated solar systems. Gathering the solar radiation at one point, we can heat the working mean. Concentrated Solar Systems will be described and analyzed extensively in the next chapter.

Concentrating solar power is the second most popular solar harvesting technology available on the market. What is unique about this technology is that it can be combined with thermal energy storage (TES) or possibly hybridized with another fuel, so that not only can it generate clean energy but also energy that is dispatchable, along with other operational capabilities that support the electricity grid. The main reason CSP is behind PV is because of the high cost attached to the electricity production. However, CSP is a well proven technology, and with the addition of cost effective TES, it is set to increase its share of the solar market. That being said, incentives are currently needed for this technology to be cost competitive with other traditional forms of energy generation.[15],[125],[130]

Chapter 3

Solar Energy

3.1 Solar Energy Exploitation-Basic Fundamentals

The Sun is the star at the center of the Solar System. It is a nearly perfect sphere of hot plasma, with internal convective motion that generates a magnetic field via a dynamo process. It is by far the most important source of energy for life on Earth. Its diameter is about 1.39 million kilometers, which is 109 times that of Earth, and its mass is about 330,000 times that of Earth, accounting for about 99.86% of the total mass of the Solar System. About three quarters of the Sun's mass consists of hydrogen (~73%); the rest is mostly helium (~25%), with much smaller quantities of heavier elements, including oxygen, carbon, neon, and iron.

Sun is a naturally occurring nuclear reactor. It releases tiny packets of energy called photons, which travel the 93 million miles from the sun to Earth in about eight-and-a-half minutes. Every hour, enough photons impact our planet to theoretically satisfy global energy needs for an entire year. Solar technology is improving and costs are dropping rapidly, though, so our ability to harness the sun's abundance of energy is on the rise.

Solar energy is the energy that is in sunlight. It has been used for thousands of years in many different ways by people all over the world. As well as its traditional human uses in heating, cooking, and drying, it is used today to make electricity where other power supplies are absent, such as in remote places and in space. It is becoming cheaper to make electricity from solar energy and in many situations it is now competitive with energy from coal or oil.

After passing through the Earth's atmosphere, most of the Sun's energy is in the form of visible light and infrared light radiation. Plants convert the energy in sunlight into

chemical energy (sugars and starches) through the process of photosynthesis. Humans regularly use this store of energy in various ways, as when they burn wood or fossil fuels, or when simply eating plants, fish and animals.

Solar radiation reaches the Earth's upper atmosphere with the power of 1366 watts per square meter (W/m^2). Since the Earth is round, the surface nearer its poles is angled away from the Sun and receives much less solar energy than the surface nearer the equator.

Many technologies have been developed to make use of solar radiation. Some of these technologies make direct use of the solar energy (e.g. to provide light, heat, etc.), while others produce electricity. Solar irradiance is the power per unit area received from the Sun in the form of electromagnetic radiation in the wavelength range of the measuring instrument. Irradiance may be measured in space or at the Earth's surface after atmospheric absorption and scattering. It is measured perpendicular to the incoming sunlight. Total solar irradiance, is a measure of the solar power over all wavelengths per unit area incident on the Earth's upper atmosphere.

The solar constant is a conventional measure of mean total solar irradiance at a distance of one Astronomical Unit (AU). Irradiance is a function of distance from the Sun, the solar cycle, and cross-cycle changes. Irradiance on Earth is also measured perpendicular to the incoming sunlight. Isolation is the power received on Earth per unit area on a horizontal surface. It depends on the height of the Sun above the horizon and atmospheric conditions.

The solar irradiance integrated over time is called solar irradiation, solar exposure, or isolation. However, isolation is often used interchangeably with irradiance in practice. The SI unit of irradiance is watt per square meter (W/m^2).

An alternate unit of measure is the Langley (1 thermo chemical calorie per square centimeter or $41,840 J/m^2$) per unit time. The solar energy industry uses watt-hour per square meter (Wh/m^2) per unit time. The relation to the SI unit is thus: $1 kW/m^2 = 24 kWh/m^2/day = 8760 kWh/m^2/year$.

Part of the radiation reaching an object is absorbed and the remainder reflected. Usually the absorbed radiation is converted to thermal energy, increasing the object's temperature. Manmade or natural systems, however, can convert part of the absorbed radiation into another form such as electricity or chemical bonds, as in the case of

photovoltaic cells or plants. The proportion of reflected radiation is the object's reflectivity or albedo.

At a lower angle the light must also travel through more atmosphere. This attenuates it (by absorption and scattering) further reducing isolation at the surface. Attenuation is governed by the Beer-Lambert Law, namely that the transmittance or fraction of isolation reaching the surface decreases exponentially in the optical depth or absorbance (the two notions differing only by a constant factor of $\ln(10) = 2.303$) of the path of isolation through the atmosphere. For any given short length of the path the optical depth is proportional to the quantity of absorbers and scatterers along that length, typically increasing with decreasing altitude. The optical depth of the whole path is then the integral (sum) of those optical depths along the path.

Direct isolation is measured at a given location with a surface element perpendicular to the Sun. It excludes diffuse isolation (radiation that is scattered or reflected by atmospheric components). Direct isolation is equal to the irradiance above the atmosphere minus the atmospheric losses due to absorption and scattering. While the irradiance above the atmosphere varies with time of year (because the distance to the sun varies), losses depend on time of day (length of light's path through the atmosphere depending on the Solar elevation angle), cloud cover, moisture content and other contents.

Average annual solar radiation arriving at the top of the Earth's atmosphere is roughly 1361 W/m^2 . The radiation is distributed across the electromagnetic spectrum. About half is infrared light. The Sun's rays are attenuated as they pass through the atmosphere, leaving maximum normal surface irradiance at approximately 1000 W/m^2 at sea level on a clear day. When 1361 W/m^2 is arriving above the atmosphere (when the sun is at the zenith in a cloudless sky), direct sun is about 1050 W/m^2 , and global radiation on a horizontal surface at ground level is about 1120 W/m^2 . The latter figure includes radiation scattered or reemitted by atmosphere and surroundings. The actual figure varies with the Sun's angle and atmospheric circumstances. Ignoring clouds, the daily average isolation for the Earth is approximately $6 \text{ kWh/m}^2 = 21.6 \text{ MJ/m}^2$. [131],[132],[133],[134]

3.2 Thermodynamic Cycles

A thermodynamic cycle consists of a linked sequence of thermodynamic processes that involve transfer of heat and work into and out of the system, also varying pressure, temperature, and other state variables within the system, that eventually returns the system to its initial state. In the process of passing through a cycle, the working fluid (system) may convert heat from a warm source into useful work, and dispose of the remaining heat to a cold sink, thereby acting as a heat engine. Conversely, the cycle may be reversed and use work to move heat from a cold source and transfer it to a warm sink thereby acting as a heat pump.

During a closed cycle, the system returns to its original thermodynamic state of temperature and pressure. Process quantities (or path quantities), such as heat and work are dependent process. For a cycle for which the system returns to its initial state the first law of thermodynamics applies by

$$\Delta E = E_{out} - E_{in} = 0 \quad (3.1)$$

The above states that there is no change of the energy of the system over the cycle. E_{in} might be the work and heat input during the cycle and E_{out} would be the work and heat output during the cycle. The first law of thermodynamics also dictates that the net heat input is equal to the net work output over a cycle. The repeating nature of the process path allows for continuous operation, making the cycle an important concept in thermodynamics. Thermodynamic cycles are often represented mathematically as stochastic processes in the modeling of the workings of an actual device.

For the production of projects in which heat is used, thermodynamic cycles are necessary. Circles can be used in solar thermal power plants. They receive heat from an external source. The selection of a thermodynamic cycle varies if the fluid that transfers heat is also used as a working mean. Consequently, the cycles used in systems using Solar energy are three, the Stirling cycle, the Brayton cycle and the Rankine cycle.[16],[17],[130],[134]

3.2.1 Stirling Cycle

The Stirling cycle is a thermodynamic cycle that describes the general class of Stirling devices. This includes the original Stirling engine that was invented, developed and patented in 1816 by Robert Stirling.

The cycle is reversible, meaning that if it is supplied with mechanical power, it can function as a heat pump for heating or cooling, and even for cryogenic cooling. The cycle is defined as a closed regenerative cycle with a gaseous working fluid. It is a "closed cycle" that means that the working fluid is permanently contained within the thermodynamic system. This also categorizes the engine device as an external heat engine.

The cycle is the same as most other heat cycles in that there are four main processes: compression, heat addition, expansion, and heat removal. However, these processes are not discrete, but rather the transitions overlap.

The idealized Stirling cycle consists of four thermodynamic processes acting on the working fluid :

1. *Isothermal expansion: The expansion space is heated externally, and the gas undergoes near.*
2. *Constant-volume (known as iso volumetric or isochoric) heat removal: The gas is passed through the regenerator, thus cooling the gas, and transferring heat to the regenerator for use in the next cycle.*
3. *Isothermal compression: The compression space is intercooled, so the gas undergoes near.*
4. *Constant-volume heat addition: The compressed air flows back through the regenerator and picks up heat on the way to the heated expansion space.*

In the ideal thermodynamic Stirling cycle, the change 1->2 requires work for compression of the fluid resulting by

$$W_{1-2} = \int_1^2 P dV = mT \ln \frac{R}{M} \ln \left(\frac{V_2}{V_1} \right) [\text{Joule}] \quad (3.2)$$

where P is the pressure ,

V is the total volume ,

T_{min} is the low temperature of the circle ,

R is the gas constant ,

M is the molecular weight and

m is the fluid mass.

The change 3->4 work produced is equal to

$$W_{3-4} = mT_{max} \frac{R}{M} \ln\left(\frac{V_4}{V_3}\right) [\text{Joule}] \quad (3.3)$$

where T_{max} is the highest cycle temperature.

Also, during change 3->4 heat enters the system, and force $Q_{3-4} = W_{3-4}$ (positive values) as $Q_{1-2} = W_{1-2}$ (negative values).

Therefore, the produced work is $W_{net} = W_{1-2} + W_{3-4}$ [Joule]. Combining these equations, we find the performance of the cycle

$$ne = \frac{T_{max} - T_{min}}{T_{max}} \quad (3.4)$$

and it is identical to the efficiency of the Carnot cycle.[16],[17],[134]

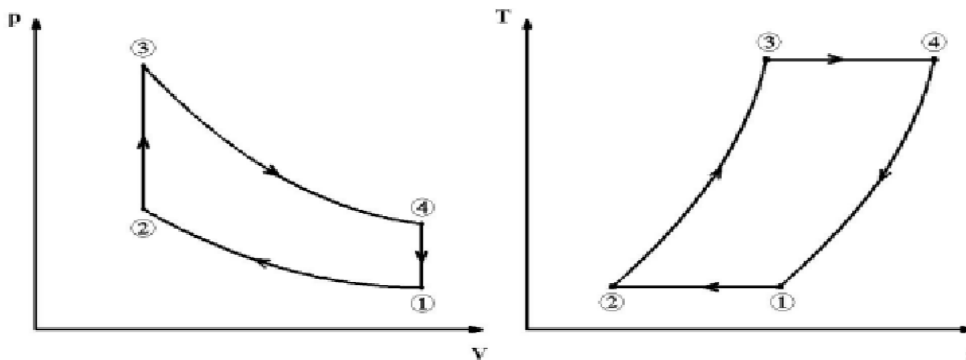


Figure 3.1 P-V and T-S diagrams of the Ideal Stirling Cycle [16]

3.2.2 Brayton Cycle

The Brayton cycle is a thermodynamic cycle that uses gas turbines. Brayton cycle is suitable for use in small and large scale applications. The main advantage is the ability for low operating costs and maintenance. The Brayton cycle is a thermodynamic cycle named after George Bailey Brayton that describes the workings of a constant pressure heat engine. The original Brayton engines used a piston compressor and piston expander, but more modern gas turbine engines and airbreathing jet engines also follow the Brayton cycle. Although the cycle is usually run as an open system, it is conventionally assumed for the purposes of thermodynamic analysis that the exhaust gases are reused in the intake, enabling analysis as a closed system. It is also sometimes known as the Joule cycle. There are two types of Brayton cycles, open to the atmosphere and using internal combustion chamber or closed and using a heat exchanger.

A Brayton-type engine consists of three components: a compressor, a mixing chamber and an expander. Modern Brayton engines are almost always a turbine type although Brayton only made piston engines. The compressed air runs through a mixing chamber where fuel is added, an isobaric process. The pressurized air and fuel mixture is then ignited in an expansion cylinder and energy is released, causing the heated air and combustion products to expand through a piston/cylinder; another ideally isentropic process.

Ideal Brayton cycle's processes:

- 1. Isentropic process : Ambient air is drawn into the compressor, where it is pressurized.(adiabatic process – compression)*
- 2. Isobaric process : The compressed air then runs through a combustion chamber, where fuel is burned, heating that air—a constant-pressure process, since the chamber is open to flow in and out (heat addition).*
- 3. Isentropic process : The heated, pressurized air then gives up its energy, expanding through a turbine (or series of turbines). Some of the work extracted by the turbine is used to drive the compressor.*
- 4. Isobaric process : Heat rejection (in the atmosphere).*

Initially, during the change 1->2 air enters the compressor and gets compressed. Then, the change 2->3 compressed air enters the combustion chamber where it is heated at constant pressure. During the change 3->4 the hot compressed air is expanded through one or more turbines so they produce work, part of which is utilized for the compressor. Finally, when the change 4->1 heat is rejected to the environment. The four processes of the Brayton cycle performed on devices steady flow.

Since neither the compression nor the expansion can be truly isentropic, losses through the compressor and the expander represent sources of inescapable working inefficiencies. In general, increasing the compression ratio is the most direct way to increase the overall power output of a Brayton system.

The highest temperature in the cycle occurs at the end of the combustion process, and it is limited by the maximum temperature that the turbine blades can withstand. This also limits the pressure ratios that can be used in the cycle. For a fixed turbine inlet temperature, the net work output per cycle increases with the pressure ratio (thus the thermal efficiency) and the net work output. With less work output per cycle, a larger mass flow rate (thus a larger system) is needed to maintain the same power output, which may not be economical.

In solar thermal systems, the use of the Brayton engine suitable for disc systems - machine, placing a small engine focal point, but also solar power tower systems heat compressed air in the solar receiver. [9],[16],[17],[134],[135]

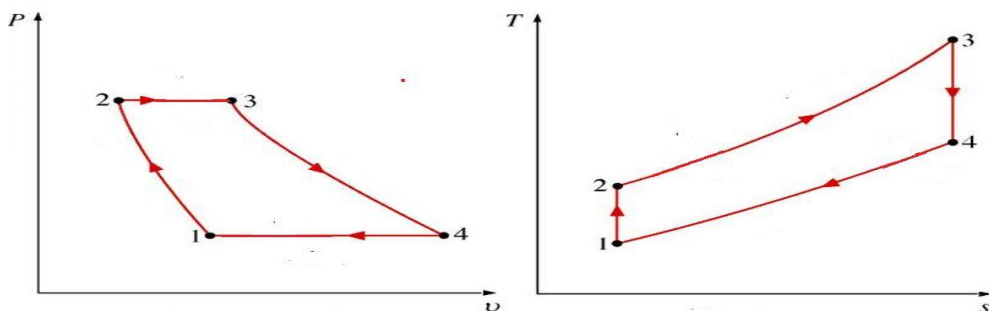


Figure 3.2 P-V and T-S diagrams of the Ideal Brayton Cycle [9]

3.2.3 Rankine cycle

The most common thermodynamic cycle in all conversion systems heat into work is the Rankine cycle. This cycle combines isobaric changes and adding heat elimination by adiabatic reversible compression and expansion changes.

The Rankine cycle is a model that is used to predict the performance of steam turbine systems. The Rankine cycle is an idealized thermodynamic cycle of a heat engine that converts heat into mechanical work. The heat is supplied externally to a closed loop, which usually uses water as the working fluid. It is named after William John Macquorn Rankine, a Scottish polymath and Glasgow University professor.

The Rankine cycle closely describes the process by which steam-operated heat engines commonly found in thermal power generation plants generate power. The heat sources used in these power plants are usually nuclear fission or the combustion of fossil fuels such as coal, natural gas, and oil. The efficiency of the Rankine cycle is limited by the high heat of vaporization of the working fluid.

There are four processes in the Rankine cycle:

- 1. Compression (adiabatic – isentropiki) : The working fluid is pumped from low to high pressure. As the fluid is a liquid at this stage, the pump requires little input energy.*
- 2. Isobaric impart heat : The high pressure liquid enters a boiler where it is heated at constant pressure by an external heat source to become a dry saturated steam.*
- 3. Relief : The dry saturated steam expands through a turbine, generating power. This decreases the temperature and pressure of the steam, and some condensation may occur.*
- 4. Isothermal - Isobaric heat elimination : The wet steam then enters a condenser where it is condensed at a constant pressure to become a saturated liquid.*

In an ideal Rankine cycle the pump and turbine would be isentropic, the pump and turbine would generate no entropy and hence maximize the net work output.

The actual vapor power cycle differs from the ideal Rankine cycle because of irreversibilities in the inherent components caused by fluid friction and heat loss to the

surroundings; fluid friction causes pressure drops in the boiler, the condenser, and the piping between the components, and as a result the steam leaves the boiler at a lower pressure; heat loss reduces the net work output, thus heat addition to the steam in the boiler is required to maintain the same level of net work output.[16],[17],[18],[134],[136]

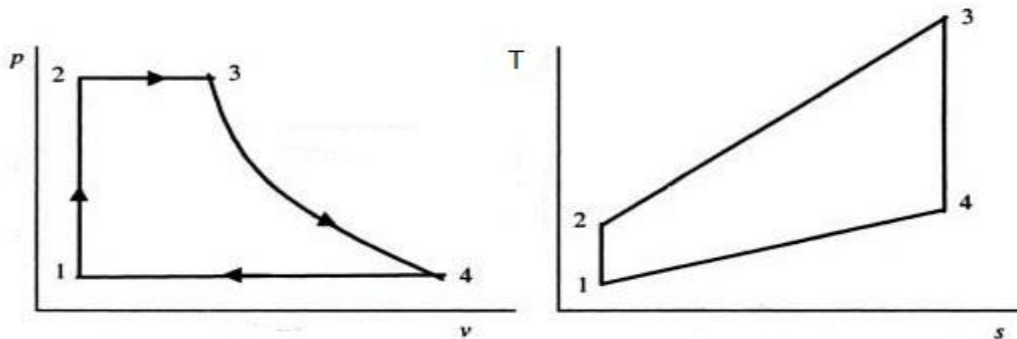


Figure 3.3 P-V and T-S diagrams of the Ideal Rankine cycle [18]

3.3 Types of Concentrated Solar Systems

Concentrated solar power (also called concentrating solar power, concentrated solar thermal, and CSP) systems generate solar power by using mirrors or lenses to concentrate a large area of sunlight, or solar thermal energy, onto a small area. Electricity is generated when the concentrated light is converted to heat, which drives a heat engine (usually a steam turbine) connected to an electrical power generator or powers a thermo chemical reaction. Heat storage in molten salts allows some solar thermal plants to continue to generate after sunset and adds value to such systems when compared to photovoltaic panels.

CSP is being commercialized and the CSP market saw about 740 MW of generating capacity added between 2007 and the end of 2010. More than half of this (about 478 MW) was installed during 2010, bringing the global total to 1095 MW. Spain added 400 MW in 2010, taking the global lead with a total of 632 MW, while the US ended the year with 509 MW after adding 78 MW, including two fossil-CSP hybrid plants. The Middle East is also ramping up their plans to install CSP based projects.

Shams-I has been installed in Abu Dhabi, by Masdar. The largest CSP projects in the world is Ivanpah Solar Power Facility in the United States (which uses solar power tower technology) and Mojave Solar Project (which uses parabolic troughs).

In January 2014, Spain had a total capacity of 2,300 MW making this country the world leader in CSP. United States follows with 1,740 MW. Interest is also notable in North Africa and the Middle East, as well as India and China. In Italy, companies are trying to get authorization for 14 plants, total 392 MW, despite a strong local and political opposition. The global market has been dominated by parabolic-trough plants, which account for 90% of CSP plants.

In most cases, CSP technologies currently cannot compete on price with photovoltaic (solar panels), which have experienced huge growth in recent years due to falling prices of the panels and much smaller operating costs. However, the Chile Copiano reached €6.3/kWh.

In 2015, CSP represented less than 2% of worldwide installed capacity of solar electricity plants. CSP is not to be confused with concentrator photovoltaics (CPV). In CPV, the concentrated sunlight is converted directly to electricity via the photovoltaic effect, as we have already analyzed that in another chapter.

In 1866, Auguste Mouchout used a parabolic trough to produce steam for the first solar steam engine. The first patent for a solar collector was obtained by the Italian Alessandro Battaglia in Genoa, Italy, in 1886. Over the following years, inventors such as John Ericsson and Frank Shuman developed concentrating solar-powered devices for irrigation, refrigeration, and locomotion. In 1913 Shuman finished a 55 HP parabolic solar thermal energy station in Maadi, Egypt for irrigation. The first solar-power system using a mirror dish was built by Dr. R.H. Goddard, who was already well known for his research on liquid-fueled rockets and wrote an article in 1929 in which he asserted that all the previous obstacles had been addressed.

Professor Giovanni Francia (1911–1980) designed and built the first concentrated-solar plant, which entered into operation in Sant'Ilario, near Genoa, Italy in 1968. This plant had the architecture of today's concentrated-solar plants with a solar receiver in the center of a field of solar collectors. The plant was able to produce 1 MW with superheated steam at 100 bar and 500 °C. The 10 MW Solar One power tower was developed in Southern California in 1981, but the parabolic-trough technology of the

nearby Solar Energy Generating Systems (SEGS), begun in 1984, was more workable. The 354 MW SEGS is another large solar power plant, and especially one of the largest until the 390 MW Ivanpah power tower project reaches full power.

CSP is used to produce electricity (sometimes called solar thermoelectricity, usually generated through steam). Concentrated-solar technology systems use mirrors or lenses with tracking systems to focus a large area of sunlight onto a small area. The concentrated light is then used as heat or as a heat source for a conventional power plant (solar thermoelectricity). The solar concentrators used in CSP systems can often also be used to provide industrial process heating or cooling, such as in solar air conditioning.

Concentrating technologies exist in four optical types, namely parabolic trough, dish, concentrating linear Fresnel reflector, and solar power tower. Although simple, these solar concentrators are quite far from the theoretical maximum concentration. For example, the parabolic-through concentration gives about 1/3 of the theoretical maximum for the design acceptance angle, that is, for the same overall tolerances for the system. Approaching the theoretical maximum may be achieved by using more elaborate concentrators based on non imaging optics.

Different types of concentrators produce different peak temperatures and correspondingly varying thermodynamic efficiencies, due to differences in the way that they track the sun and focus light. New innovations in CSP technology are leading systems to become more and more cost-effective.

The basic concept of centralized solar systems is the concentration of solar radiation at a focal point for heating a fluid at high temperatures through one Thermodynamic cycle in order to produce work. A common feature of all of these systems, is the fact that they are made up of specific parts. These are the solar collectors, the solar receiver, the system transfer of the working mean, the thermal storage system of energy and energy conversion system.

The degree of efficiency of the concentrated solar systems depends mainly on the temperature developed in the solar receiver. A size that determines the temperature of the receiver is the ratio of concentration of solar radiation, which is defined as its ratio of the surface of the solar collector that receives the solar radiation to the surface of the solar receiver that absorbs it. Also important role for the efficiency of the concentrated

solar systems is also the focal distance, which is defined as the distance from the optical center of the mirror to the point where the light rays converge.[137]

3.3.1 Parabolic Through Collectors

A parabolic trough is a type of solar thermal collector that is straight in one dimension and curved as a parabola in the other two, lined with a polished metal mirror. The energy of sunlight which enters the mirror parallel to its plane of symmetry is focused along the focal line, where objects are positioned that are intended to be heated.

For other purposes, there is often a tube, frequently a Dewar tube, which runs the length of the trough at its focal line. The mirror is oriented so that sunlight which it reflects is concentrated on the tube, which contains a fluid which is heated to a high temperature by the energy of the sunlight. The hot fluid can be used for many purposes. Often, it is piped to a heat engine, which uses the heat energy to drive machinery or to generate electricity. This solar energy collector is the most common and best known type of parabolic trough.

The trough is usually aligned on a north-south axis, and rotated to track the sun as it moves across the sky each day. Alternatively, the trough can be aligned on an east-west axis; this reduces the overall efficiency of the collector due to cosine loss but only requires the trough to be aligned with the change in seasons, avoiding the need for tracking motors. Parabolic trough concentrators have a simple geometry, but their concentration is about 1/3 of the theoretical maximum for the same acceptance angle, that is, for the same overall tolerances of the system to all kinds of errors, including those referenced above.

Heat transfer fluid (usually thermal oil) runs through the tube to absorb the concentrated sunlight. This increases the temperature of the fluid to some 400 °C. The heat transfer fluid is then used to heat steam in a standard turbine generator. The process is economical and, for heating the pipe, thermal efficiency ranges from 60%-80%. The overall efficiency from collector to grid, $(\text{Electrical Output Power})/(\text{Total Impinging Solar Power})$ is about 15%, similar to PV but less than Stirling dish

concentrators. These systems are two-dimensional and revolve about an axis along the north - south direction following the course of the sun from sunrise to sunset. Also, systems parabolic hollow panels are capable operate at full power using only sunlight, especially during the summer months, which operate at nominal power typically 10 to 12 hours per day. Nevertheless, all existing plants are hybrid, having a back-up boiler operate with fossil fuels for heating water in periods low solar radiation. It is also possible to use for thermo cline storing the thermal energy.[41],[137],[139]

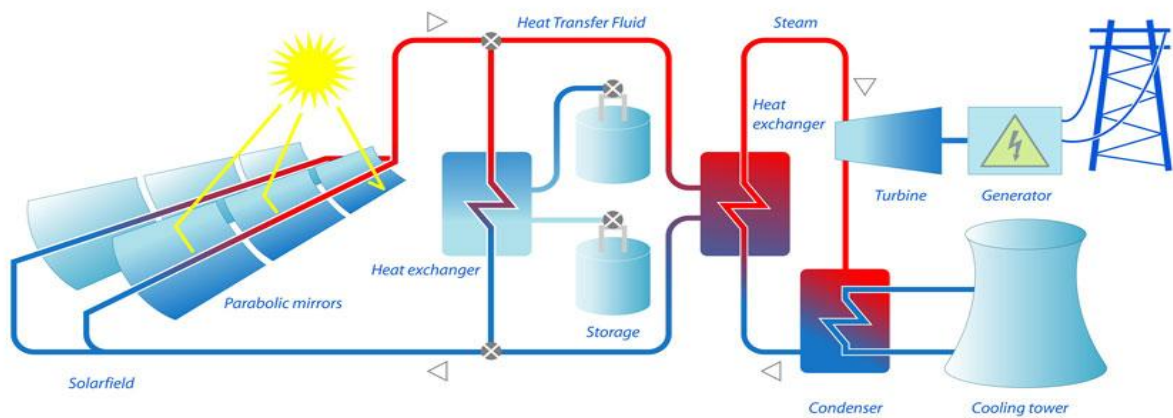


Figure 3.4 Parabolic Through Collector[41]

3.3.2 Dish systems

Dish/engine systems use a parabolic dish of mirrors to direct and concentrate sunlight onto a central engine that produces electricity. The dish/engine system is a concentrating solar power (CSP) technology that produces smaller amounts of electricity than other CSP technologies—typically in the range of 3 to 25 kilowatts. The two major parts of the system are the solar concentrator and the power conversion unit.

The solar concentrator, or dish, gathers the solar energy coming directly from the sun. The resulting beam of concentrated sunlight is reflected onto a thermal receiver that collects the solar heat. The dish is mounted on a structure that tracks the sun

continuously throughout the day to reflect the highest percentage of sunlight possible onto the thermal receiver. A very important factor is the construction of which can comprise multiple mirrors and that makes such systems capable of autonomous remote applications and clustering them for use in remote parts of the network. Also, there is possibility hybrid operation using conventional fuels.

The power conversion unit includes the thermal receiver and the engine/generator. The thermal receiver is the interface between the dish and the engine/generator. It absorbs the concentrated beams of solar energy, converts the energy to heat, and transfers the heat to the engine/generator. A thermal receiver can be a bank of tubes with a cooling fluid—usually hydrogen or helium—that typically is the heat-transfer medium and also the working fluid for an engine. Alternate thermal receivers are heat pipes, where the boiling and condensing of an intermediate fluid transfers the heat to the engine.

The engine/generator system is the subsystem that takes the heat from the thermal receiver and uses it to produce thermal to electric energy conversion. The most common type of heat engine used in dish/engine systems is the Stirling engine. A Stirling engine uses the heated fluid to move pistons and create mechanical power. The mechanical work, in the form of the rotation of the engine's crankshaft, drives a generator and produces electrical power.

Although these, their use is very limited for energy production (25kW). This technology is still in a developmental stage, as the cost is prohibitive for their mass production.[42],[106],[137],[138]

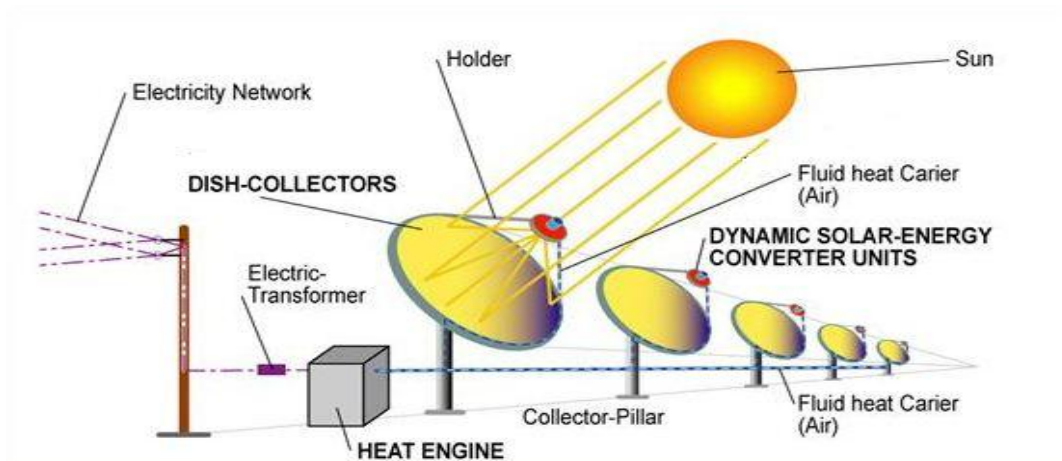


Figure 3.5 Dish system [42]

3.3.3. Linear Fresnel Reflector (CLFR)

A compact linear Fresnel reflector (CLFR) – also referred to as a concentrating linear Fresnel reflector – is a specific type of linear Fresnel reflector (LFR) technology. Linear Fresnel reflectors use long, thin segments of mirrors to focus sunlight onto a fixed absorber located at a common focal point of the reflectors. These mirrors are capable of concentrating the sun's energy to approximately 30 times its normal intensity. This concentrated energy is transferred through the absorber into some thermal fluid (this is typically oil capable of maintaining liquid state at very high temperatures). The fluid then goes through a heat exchanger to power a steam generator. The first linear Fresnel reflector was developed in Italy in 1961 by Giovanni Francia of the University of Genoa.

The reflectors are located at the base of the system and converge the sun's rays into the absorber. A key component that makes all LFR's more advantageous than traditional parabolic trough mirror systems is the use of "Fresnel reflectors". These reflectors make use of the Fresnel lens effect, which allows for a concentrating mirror with a large aperture and short focal length while simultaneously reducing the volume of material required for the reflector. This greatly reduces the system's cost since sagged-glass parabolic reflectors are typically very expensive.

The absorber is located at the focal line of the mirrors. It runs parallel to and above the reflector segments to transport radiation into some working thermal fluid. The

basic design of the absorber for the CLFR system is an inverted air cavity with a glass cover enclosing insulated steam tubes. This design has been demonstrated to be simple and cost effective with good optical and thermal performance.

Despite the similarities with Parabolic trough collectors, there are technical differences that distinguish the one system from another. Linear Fresnel reflectors consist of several parallel series linear Fresnel reflectors which are located so as to concentrate solar radiation onto a receiver that is arranged along the rows but at a greater height. One of the main advantages of this system is its lower cost of construction and of the system tracking the sun, since the mirrors are positioned in a way that allows lines to be coupled and driven by a single engine. However, the most essential difference is in operation. Fluid heat transfer to the receiver is water, since the steam production made directly to the absorber tube. This is great advantage because the system does not require a steam generator. Therefore, the linear Fresnel reflector systems considered an economical solution but with questionable reliability due to lower efficiency levels and failure in high power output.[43],[107],[140]

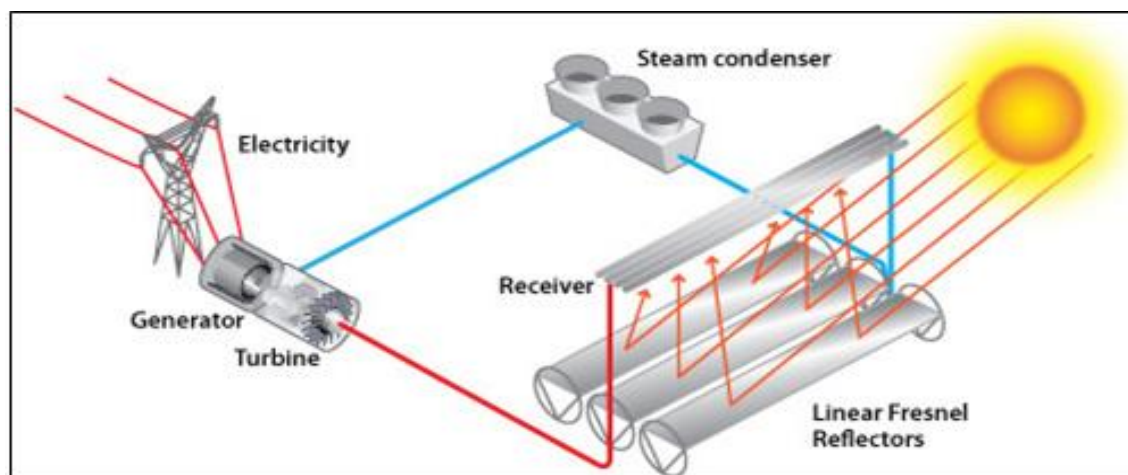


Figure 3.6 Linear Fresnel Reflector [43]

3.3.4 Solar Power Tower

Concentrated solar power or Solar concentrator or simply CSP are called systems that produce solar energy using mirrors or lenses for high sunlight concentration, or solar thermal energy in a small area. The electricity is produced when the light is converted to heat, which leads to a heat engine (usually a steam turbine) which is connected to an electric power generator by making a thermo chemical reaction. Solar panels that are used in CSP systems, can be used for industrial heating or cooling, such as solar air conditioning.

Solar power tower is the most complicated system of centralized solar systems and it consists of a series dual-axis tracking reflectors (heliostats) that concentrate sunlight on a central receiver at the top of a tower. The heliostat field is around or north of the tower and it consists of hundreds or even thousands of flat mirrors (heliostats) that move independently (in three dimensions) to collect and channel the solar energy. The receiver includes a liquid, which may contain salt. The working fluid in the receiver is heated to 500°C - $1,000^{\circ}\text{C}$ ($(773^{\circ}\text{C}$ - $1,273^{\circ}\text{C})$) (932°F - $1,832^{\circ}\text{F}$) and then it is used as a heat source after entering a steam turbine which drives a generator and produces electrical power by performing a thermodynamic cycle (usually conventional Rankine cycle). CSP is widely available commercially and their capacity has now reached approximately 740 MW. It must not to be confused with photovoltaic concentration (CPV), because the CPV, sunlight is converted directly into electricity through the photovoltaic effect.

An advantage in solar towers are the reflectors that can be adapted instead of adapting the whole tower. CSP is less advanced than enclosed trough systems but they offer higher performance and better energy storage capability. Many solar power tower systems use energy storage systems and backup fossil fuel combustion systems. The choice of such systems depends on the location and on the use of the facility. In cases where the solar radiation has low prices for a long period of time either because of position or due to weather conditions, it is necessary to use such systems for the smooth operation of the plant.[44],[141]

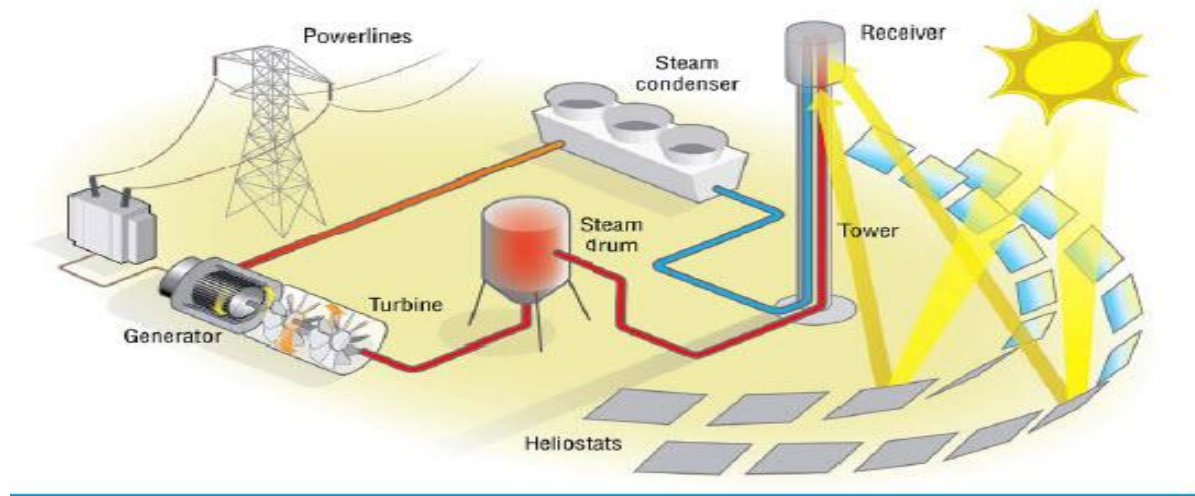


Figure 3.7 Solar Power Tower [44]

3.3.5 Choice of the Appropriate System

The process of selecting a suitable system is complex and depends on many parameters. By studying the energy demand, the available space for the installation, the required time of the operation and finally the cost, we come to the choice of the appropriate system that meets the needs of the situation.

Until today, the more mature and more widespread technology of concentrated solar systems around the world are systems Parabolic through collectors, their installed power worldwide exceeds 8,500 MW and is expected to have a total power station that exceeds the 4,000 MW.

The technology of dish/engine systems is now at an early stage, while Fresnel linear reflector systems are spreading and we already have commercial stations of such technology the high power/force or other are manufactured all over the world.

Solar power tower technology is rapidly developing over the last decade and is expected to outperform the parabolic through collectors technology in the coming years.[125],[126],[137]

Chapter 4

Historical Return - Existing Installations of Solar Power Towers

The early development of solar technologies starting in the 1860's was driven by an expectation that coal would soon become scarce. Charles Fritts installed the world's first rooftop photovoltaic solar array, using 1%-efficient selenium cells, on a New York City roof in 1884. However, development of solar technologies stagnated in the early 20th century in the face of the increasing availability, economy, and utility of coal and petroleum. In 1974 it was estimated that only six private homes in all of North America were entirely heated or cooled by functional solar power systems. The 1973 oil embargo and 1979 energy crisis caused a reorganization of energy policies around the world and brought renewed attention to developing solar technologies. Deployment strategies focused on incentive programs such as the Sunshine Program in Japan. Other efforts included the formation of research facilities in the United States (SERI, now NREL), Japan (NEDO), and Germany (Fraunhofer-ISE). Between 1970 and 1983 installations of photovoltaic systems grew rapidly, but falling oil prices in the early 1980's moderated the growth of photovoltaic from 1984 to 1996.

In the mid-1990's, development of both, residential and commercial rooftop solar as well as utility-scale photovoltaic power stations, began to accelerate again due to supply issues with oil and natural gas, global warming concerns, and the improving economic position of PV relative to other energy technologies. In the early 2000's, the adoption of feed-in tariffs—a policy mechanism, that gives renewable priority on the grid and defines a fixed price for the generated electricity—lead to a high level of investment security and to a soaring number of PV deployments in Europe.

For several years, worldwide growth of solar PV was driven by European deployment, but has since shifted to Asia, especially China and Japan, and to a growing number of countries and regions all over the world, including, Australia, Canada, Chile, India, Israel, Mexico, South Africa, South Korea, Thailand, and the United States.

Worldwide growth of photovoltaic has averaged 40% per year from 2000 to 2013 and total installed capacity reached 303 GW at the end of 2016 with China having the most cumulative installations (78 GW) and Honduras having the highest theoretical percentage of annual electricity usage which could be generated by solar PV (12.5%). The largest manufacturers are located in China.

Concentrated solar power (CSP) also started to grow rapidly, increasing its capacity nearly tenfold from 2004 to 2013, albeit from a lower level and involving fewer countries than solar PV. As of the end of 2013, worldwide cumulative CSP-capacity reached 3,425 MW.

The first documented use of concentrated solar power technology was in 1866 where Auguste Mouchout used parabolic troughs to heat water and produce steam to run the first solar steam engine. A series of inventors applied the technology in the following years. In 1912 in Meadi, Egypt, parabolic solar collectors were established in a small farming community by Frank Schuman, a Philadelphia inventor, solar visionary and business entrepreneur. The parabolic troughs were used for producing steam, which drove large water pumps, pumping 6,000 gallons of water per minute to vast areas of arid desert land.

The first operational concentrated solar power plant was built in Sant'Ilario, Italy in 1968 by Professor Giovanni Francia. This plant has architectural similarities to modern plants with its central receiver surrounded by a field of solar collectors. In 1982 the U.S. Department of Energy, along with an industry consortium began operating Solar One, a 10MW central-receiver demonstration project. The project established the feasibility of power tower systems. Four years later, in 1986, the world's largest solar thermal facility, located in Kramer Junction, California, was commissioned. The solar field contained rows of mirrors that concentrated the sun's energy onto a system of pipes circulating a heat transfer fluid. The heat transfer fluid was used to produce steam, which powered a conventional turbine to produce electricity. In 1996 the U.S. Department of Energy, along with an industry consortium, began operating Solar Two - an upgrade of its Solar One concentrating solar power tower project. Operated till 1999, Solar Two demonstrated how solar energy can be stored efficiently and economically so that power can be produced even when the sun isn't shining. It also fostered commercial interest in power towers.

In June 2010, there were 34 CSP plants installed worldwide, totaling 880.45MW. The country with most plants is the USA with 16 plants installed. Moreover, the USA is currently planning 36 new projects. Spain is the most active country with 12 new plants installed since 2007. Furthermore, Spain has 33 CSP plants under construction and additionally 17 planned projects. Countries like Algeria, Australia, Egypt, France, India, Italy, Mexico and Morocco are also constructing concentrated solar power plants and joining the future of renewable energy.

In 2010, the International Energy Agency predicted that global solar PV capacity could reach 3,000 GW or 11% of projected global electricity generation by 2050—enough to generate 4,500 TWh of electricity. Four years later, in 2014, the agency projected that, under its "high renewable" scenario, solar power could supply 27% of global electricity generation by 2050 (16% from PV and 11% from CSP).
[144],[145],[146],[147],[148],[149]

4.1 Experimental CSPs of Little Power / Force

Although energy towers are commercially less mature than systems parabolic troughs, a number of different experimental systems have been tested around the world over the past 24 years, demonstrating the mechanical realization and economic feasibility of the technology. Since the early 1980s, energy towers have been placed in Russia, Italy, Spain, Japan, France, and the United States. Below the experimental facilities are presented along with some of their most important features. These experimental installations were built to demonstrate that solar energy towers can generate electricity and improve on individual parts of the systems.

The beginning was in Europe, where in 1976 it was decided by the European Commission to carry out an initial feasibility study of one solar power tower solar power station. The result of this study was the specification of the technical specifications, the acquisition experience in designing, operating and solving problems sustainability of solar thermal plants. In most experimental tower solar thermal stations solar power built

over the last decade, it seems that research focuses mainly on thermal energy storage technology, using various means.

It is perceived that if there were not so many experimental stations, the solar power tower technology would not have evolved to the extent that is present today. Also, the future is very optimistic in construction of experimental stations to improve all which contribute to more efficient stations.[144],[145],[146],[147],[148],[149]

Programm	Country	Power	Heat Tranfer Fluid	Way of Storage	Start
1.Solar One	U.S.A	10	Steam		1982
2.Solar Two	U.S.A	10	Molten Salt of Nitrates	Nitrate / Water	1996
3.SPP-5	Russia	5	Steam	Water / Steam	1986
4.Eurelius	Italy	1	Steam	Nitrate / Water	1981
5.Sunshine	Japan	1	Steam	Nitrate / Water	1981
6.CESA-1	Spain	1	Steam	Nitrate / Water	1983
7.MSEE/Cat B	U.S.A	1	Molten nitrate	Nitrate / Water	1984
8.THEMIS	France		High-Tec Salt	High-Tec Salt	1984
9.TSA	Spain	1	Air	Ceramics	1993
10. SSDS	Spain	0.5	Liquid sodium	Sodium	1981

Table 4.1 Experimental Solar Power Tower Stations



Figure 4.1 Solar One Project (U.S.A) [11]

4.2 Large Scale CSPs

The principal advantage of CSP is the ability to efficiently add thermal storage, allowing the dispatching of electricity over up to a 24-hour period. Since peak electricity demand typically occurs at about 5 pm, many CSP power plants use 3 to 5 hours of thermal storage.[116],[117]

4.2.1 Ivanpah Solar Electric Generating System

The Ivanpah Solar Electric Generating System is a concentrated solar thermal plant in the Mojave Desert. It is located at the base of Clark Mountain in California, a short way over the state line from Primm, Nevada. The plant has a gross capacity of 392 megawatts (MW). It deploys 173,500 heliostats, each with two mirrors focusing solar energy on boilers located on three centralized solar power towers. The first unit of the system was connected to the electrical grid in September 2013 for an initial synchronization test. The facility formally opened on February 13, 2014. In 2014, it was the world's largest solar thermal power station.



Figure 4.2 Ivanpah Solar Electric Generating System [19]

The facility, costing \$2.2 billion was developed by Bright Source Energy and Bechtel. The largest investor in the project was NRG Energy which contributed \$300 million. Google contributed \$168 million. The United States government provided a \$1.6 billion loan guarantee and the plant is built on public land. In 2010, the project was

scaled back from its original 440 MW design to avoid disturbing the habitat of the desert tortoise.

The Ivanpah system consists of three solar thermal power plants on 4,000 acres (1,600 ha) of public land near the California–Nevada border in the Southwestern United States. Fields of heliostat mirrors focus sunlight on receivers located on centralized solar power towers. The receivers generate steam to drive specially adapted steam turbines.



Figure 4.3 Ivanpah Solar Electric Generating System [20]

For the first plant, the largest-ever fully solar-powered steam turbine generator set was ordered, with a 123 MW Siemens SST-900 single-casing reheat turbine. Siemens also supplied instrumentation and control systems. The plants use Bright Source Energy's "Luz Power Tower 550" (LPT 550) technology. Final approval for the project was granted in October 2010. The plant burns natural gas each morning to commence the operation. In 2015, the natural gas consumption had decreased to 564,814 million BTU, while the total energy output had increased to 652,300 MWh.

In August 2014, Ivanpah was awarded the "Plant of the Year" award from POWER Magazine. In February 2012, Ivanpah was awarded the CSP Project of the Year by Solar Power Generation USA.[19],[20],[114],[150],[151]

4.2.2 Solar Energy Generating Systems (SEGS)

Solar Energy Generating Systems (SEGS) in California, with the combined capacity from three separate locations at 354 megawatts (MW), is now the world's second largest solar thermal energy generating facility, after the commissioning of the even larger Ivanpah facility in 2014.

It consists of nine solar power plants in California's Mojave Desert, where isolation is among the best available in the United States. SEGS I–II (44 MW) are located at Daggett , SEGS III–VII (150 MW) are installed at Kramer Junction , and SEGS VIII–IX (160 MW) are placed at Harper Lake. NextEra Energy Resources operates and partially owns the plants located at Kramer Junction and Harper Lake. A tenth plant (SEGS X, 80 MW) had been in construction and SEGS XI and SEGS XII had been planned by Luz Industries, but the developer filed for bankruptcy in 1992, because it was unable to secure construction financing.



Figure 4.4 Solar Energy Generating Systems (SEGS) [14]

The plants have a 354 MW installed capacity. The nameplate capacity, which operating continuously, would deliver the same net power output, coming only from the solar source is around 75 MWe, representing a 21% capacity factor. In addition, the turbines can be utilized at night by burning natural gas.

NextEra claims that the solar plants power 232,500 homes (during the day, at peak power) and displace 3,800 tons of pollution per year that would have been produced if the electricity had been provided by fossil fuels, such as oil.

The facilities have a total of 936,384 mirrors and cover more than 1,600 acres. Lined up, the parabolic mirrors would extend over 229 miles (369 km). The SEGS power plants were built by Luz Industries, and commissioned between December 20, 1984 and October 1, 1990. After Luz Industries' bankruptcy in 1991 plants were sold to various investor groups as individual projects, and expansion including three more plants was halted.

The installation uses parabolic trough, solar thermal technology along with natural gas to generate electricity. About 90% of the electricity is produced by the sunlight. Natural gas is only used when the solar power is insufficient to meet the demand from Southern California Edison, the distributor of power in southern California.

The parabolic mirrors are shaped like quarter-pipes. The sun shines onto the panels made of glass, which are 94% reflective, unlike a typical mirror, which is only 70% reflective. The mirrors automatically track the sun throughout the day. The greatest source of mirror breakage is wind, with 3,000 mirrors typically replaced each year. Operators can turn the mirrors to protect them during intense wind storms. An automated washing mechanism is used to periodically clean the parabolic reflective panels.

The sunlight bounces off the mirrors and is directed to a central tube filled with synthetic oil, which heats to over 400 °C (750 °F). The reflected light focused at the central tube is 71 to 80 times more intense than the ordinary sunlight. The synthetic oil transfers its heat to water, which boils and drives the Rankine cycle steam turbine, thereby generating electricity. Synthetic oil is used to carry the heat (instead of water) to keep the pressure within manageable parameters.[14],[115],[116],[117]

4.2.3 Mojave Solar Project

The Mojave Solar Project (MSP) is a concentrated solar power (CSP) facility in the Mojave Desert in California, about 20 miles (32 km) northwest of Barstow. Surrounding the hamlet of Lockhart, Mojave Solar is adjacent to Harper Lake and the SEGS VIII–IX solar plant.

For 15 years following its construction in 1990, this was the largest commercial solar power plant in the world, generating around 160 megawatts at its peak. It is one of three separately owned sites within 40 miles of one another, that make up the nine solar fields in the Solar Electric Generating System (SEGS #1 and #2 are at Daggett, and #3 through #7 are at Kramer Junction). Harper Lake was the last of these built, and is designated as SEGS #8 and #9. It is still online, but has been surpassed by other newer facilities, including the Mojave Solar Project. MSP, with a combined nameplate capacity of 280 MW (net 250 MW), is made of two, independently-operable, solar fields.

The power plant cost an estimated \$1.6 billion in total and entered commercial operation in December 2014. The developer, Abengoa, has successfully secured a \$1.2 billion loan guarantee from the US government for the project. The plant is expected to generate 617,000 MWh of power annually, enough power for more than 88,000 households and to prevent the emission of over 430 kilotons of CO₂ a year. Pacific Gas & Electric has agreed to a 25-year power purchase agreement. The plant was commissioned on 1st December, 2014.



Figure 4.5 Mojave Solar Project (MSP) [21]

Using the desert's solar thermal energy, the facility generates steam in solar steam generators, which expands through a steam turbine generator to produce electrical power from twin, independently operable solar fields, each feeding a 125 MW power island. Generation is provided 100% from sun, no supplement from fossil-based energy sources. There is a gas-fired auxiliary boiler, for each field, only to provide equipment and heat-transfer fluid (HTF) freeze protection, when temperatures fall below 12 °C (54 °F).

The power cycle is a Rankine-with-reheat thermodynamic cycle from heat supplied via heat-transfer fluid, solar field heated up to 393 °C(740 °F). When operating, the transfer fluid enters the solar field at about 271 °C (520 °F). The steam generator steam exit temperature is about 382 °C (720 °F).

Each field utilizes 1128 solar collector arrays (SCA) sited on about 710 acres (290 ha). Each SCA, model E2 from Abengoa (derived from Luz's LS-3), is 125 m (410 ft) long and is made of 10 solar collector elements (SCE), 12 m (39 ft) long each and 5.76 m (18.9 ft) aperture. The E2 steel frame collector with monolithic glass reflector panels, yields a total aperture area of 691.2 m² (7,440 sq ft). That makes a total of 779,674 m² (8,392,340 sq ft) aperture each solar field, 1,559,347 m² (16,784,670 sq ft) total for the plant, operating about 3,024 hours per year.

Cooling is provided by wet cooling towers; water for the towers and solar collector washing, is supplied from onsite groundwater wells. Water from condensed steam exits the cooling tower pump at about 27 °C (80 °F), before cycling back to the steam generator.[21],[116],[117],[118]

4.2.4 Solana Generating Station

The Solana Generating Station is a solar power plant near Gila Bend, Arizona, about 110 km (70 miles) southwest of Phoenix, completed in 2013. When commissioned it was the largest parabolic trough plant in the world and the first U.S. solar plant with molten salt thermal energy storage. Built by the Spanish company Abengoa Solar, it has a total capacity of 280 megawatts (MW) gross, from two 140 MW gross (125 MW net) steam turbine generators, which is enough to power 70,000 homes while avoiding around 475,000 tons of CO₂ every year. Its name is the Spanish term for "sunny spot".

The plant employs a proprietary concentrating solar power (CSP) trough technology developed by Abengoa, and covers an area of 1,920 acres (780 ha). Construction was expected to create about 1,500 construction jobs with the plant employing 85 full-time workers. Solar thermal plants use substantially more water for cooling than other solar generating technologies.



Figure 4.6 Solana Generating Station [22]

One of the principal advantages of concentrated solar thermal (CST) is that thermal energy storage can be provided efficiently, so that output can be provided after the sun goes down, and output can be scheduled to meet demand requirements. The Solana Generating Station is designed to provide six hours of energy storage. This allows the plant to generate about 38 percent of its rated capacity over the course of a year.[22],[117],[118],[119],[120]

4.2.5 Genesis Solar Energy Project

The Genesis Solar Energy Project is a concentrated solar power station located in the Mojave Desert on 1,920 acres (780 ha) of Bureau of Land Management land, in eastern Riverside County, California. The Genesis Solar Energy Project is located about 40 km (25 miles) west of Blythe, in the Lower Colorado River Valley. The plant was built in the Colorado Desert along an ancient trade route that native people had traveled for thousands of years. The route traversed the Sonoran Desert and enabled trade between the Colorado River and the coast.



Figure 4.7 Genesis Solar Energy Project [39]

The solar power plant consists of two independent 125 MW net (140 MW gross) sections, using solar trough technology. This was one of three of the world's largest solar plants, that began supplying power in 2013 and 2014, located in the deserts of Riverside and San Bernardino counties. The Project power block and solar arrays occupy about 1,360 acres (550 ha) of the site. The rest are the evaporation ponds, access road, administration buildings and some fenced open area. The 1840 Solar Collector Assemblies are 1,048 m² (11,280 sq ft) each, yielding 1,928,320 m² of total solar aperture.[39],[117],[118],[121]

4.2.6 List of Solar Thermal Power Stations

Name	Capacity	Country	Type	Date
1. Ivanpah Solar Power Facility	392 MW	USA , San Benardino , California	Solar power tower	2014
2. Solar Energy Generating Systems (SEGS)	359 MW	USA , Mojave Desert , California	Parabolic through	
3. Mojave Solar Project	280 MW	USA , Barstow , California	Parabolic through	2014

4. Solana Generating Station	280 MW	USA , Gila Bend , Arizona	Parabolic through	2013
5. Genesis Solar Energy Project	250 MW	USA , Blythe , California	Parabolic through	2014
6. Solaben Solar Power Station	200 MW	Logrosan , Spain	Parabolic through	2012-2013
7. Noor I	160 MW	Morocco, Ghassate , Quarzazate Province	Parabolic through	
8. Solnova Solar Power Station	150 MW	Spain , Snlucar la Mayor	Parabolic through	2010
9. Andasol	150 MW	Spain , Guadix	Parabolic through	2008-2011
10. Extresol Solar Power Station	150 MW	Spain , Torre de Miguel Sesmero	Parabolic through	2010-2012
11. Crescent Dunes Solar Energy Project	110 MW	USA , Nye County , Nevada	Solar power tower	2015
12. Dhursar	100 MW	India , Dhursar ,Jaisalmer disstrict	Frensel reflector	2014
13 . KaXu Solar One	100 MW	South Africa ,Pofadder ,Northern Cape	Parabolic through	
14. Manchasol Power Station	100 MW	Spain , Alcazar de San Juan	Parabolic through	2011
15. Valle Solar Power Station	100 MW	Spain , San Jose del Valle	Parabolic through	2011
16. Helienergy Solar Power Station	100 MW	Spain , Ecija	Parabolic through	2011-2012
17. Aste Solar Power Station	100 MW	Spain , El Carpio	Parabolic through	2012
18. Solacor Solar Power Station	100 MW	Spain , El Carpio	Parabolic through	2012

19. Helios Solar Power Station	100 MW	Spain , Puerto Lapice	Parabolic through	2012
20. Shams Solar Power Station	100 MW	UAE , Abu Dhabi Madinat Zayed	Parabolic through	2013
21. Termosol Solar Power Station	100 MW	Spain , Navavillar de Pela	Parabolic through	2013
22. Palma del Rio I & II	100 MW	Spain , Palma del Rio	Parabolic through	2010-2011
23. Martin Next Generation Solar Energy Center	75 MW	USA , Indiantown , Florida	Parabolic through	2010
24. Nevada Solar One	64 MW	USA , Boulder City , Nevada	Parabolic through	2007
25. Guzman:	50 MW	Spain , Palma del Rio	Parabolic through	2012
26. Khi Solar One	50 MW	South Africa , Upington	Solar Power Tower	2016
27. Bokpoort	50 MW	South Africa , Groblershoop	Parabolic through	
28. Puertollano Solar Thermal Power Plant	50 MW	Spain , Puertollano , Ciudad Real	Parabolic through	2009
29. Alvarado I	50 MW	Spain , Badajoz	Parabolic through	2009
30. La Florida	50 MW	Spain , Badajoz (Alvarado)	Parabolic through	2010
31. Arenales PS	50 MW	Spain , Moron de la Frontera (Seville)	Parabolic through	2013
32. Casablanca	50 MW	Spain , Talarrubias	Parabolic through	2013
33. Majadas de Tietar	50 MW	Spain , Careres	Parabolic through	2010
34. La Dehesa	50 MW	Spain , La Garrovilla (Badajoz)	Parabolic through	2010
35. Lebrija-1	50 MW	Spain , Lebrija	Parabolic through	2011
36. Astexol 2	50 MW	Spain , Badajoz	Parabolic through	2011
37. Moron	50 MW	Spain , Moron de la Frontera	Parabolic through	2012

38. <i>La Africana</i>	50 MW	Spain , Posada	Parabolic through	2012
39. <i>Olivensa 1</i>	50 MW	Spain , Olivensa	Parabolic through	2012
40. <i>Olivensa</i>	50 MW	Spain , Orellana le Vieja	Parabolic through	2012
41. <i>Godawari Green Energy Limited</i>	50 MW	India , Naukh	Parabolic through	2013
42. <i>Enerstar Villena Power Plant</i>	50 MW	Spain , Villena	Parabolic through	2013
43. <i>Megha Solar Plant</i>	50 MW	India , Anantapur	Parabolic through	2014
44. <i>Puerto Errado</i>	31.4 MW	Spain , Murcia	Fresnel reflector	2009-2012
45. <i>Hassi R'Mel integrated solar combined cycle power station</i>	25 MW	Algeria , Hassi R'Mel	Parabolic through	2011
46. <i>Termosolar Borges</i>	22.5 MW	Spain , Borges Blanques	Parabolic through	2012
47. <i>PS20 solar power tower</i>	20 MW	Spain , Seville	Solar power tower	2009
48. <i>Karaymat Plant</i>	20 MW	Egypt , Karaymat	Parabolic through	2010
49. <i>Ain Beni Mathar Integrated Thermo Solar Combined Cycle Power</i>	20 MW	Morocco , Ain Beni Mathar	Parabolic through	2011
50. <i>Gemasolar</i>	19.9 MW	Spain , Fuentes de Andalucia (Seville)	Solar power tower	2011
51. <i>Yarz integrated Thermo Solar Combined Cycle Power Plant</i>	17 MW	: Iran , Yazd	Parabolic through	2011
52. <i>PS10 solar power tower</i>	11 MW	Spain , Seville	Solar power tower	2007
53. <i>Delingha Solar Power Plant (Supcon)</i>	10 MW	China , Delingha	Solar power tower	2013
54. <i>Greenway CSP Mersin Solar Tower Plant</i>	5 MW	Turkey , Mersin	Solar power tower	
55. <i>Kimberlina Solar Thermal Energy Plant</i>	5 MW	USA , Bakersfield , California	Fresnel reflector	

56. Sierra Sun Tower	5 MW	USA , Lancaster, California	Solar power tower	2009
57. Archimede combined cycle power plant	5 MW	Italy , Syracuse , Sicily	Parabolic through	2010
58. Thai Solar Energy (TSE) 1	5 MW	Thailand , Huai Krachao	Parabolic through	2011
59. Liddell Power Station Solar Steam Generator	9 MW	Australia , New South Wales	Fresnel reflector	
60. Acme Solar Thermal Tower	2.5 MW	India , Bikaner , Rajasthan	Solar power tower	2012
61. Keahole Solar Power	2 MW	USA , Hawaii	Parabolic through	
62. Julich Solar Tower	1.5 MW	Germany , Julich	Solar power tower	2008
63. Feranova CSP Plant	1 MW	Turkey , Aydin	Fresnel reflector	2012
64. Saguaro Solar Power Station	1 MW	USA , Red Rock , Arizona	Parabolic through	
65. Yanqing (DAHAN) Solar Power Station	1 MW	China , Yanqing	Solar power tower	2012
66. Shiraz solar power plant	0.5 MW	Iran , Shiraz	Parabolic through	
67. Augustin Fresnel Solar Power Station	0.25 MW	France , Targassonne	Fresnel reflector	2012
68. City of Medicine Hat Concentrated Solar Thermal Plant	1 MW	Canada , Medicine Hat alberta	Parabolic through	2014

Table 4.2 Solar Power Tower Stations [152],[153],[154]

4.3 Solar Power Tower Installation Under Construction

Today, many solar thermal plants are being built with solar towers in many countries of the world. Also, many projects are still under construction. So everything shows clearly that this technology will continue to be used and evolving. Here are the solar power towers that are under construction:

Name	Capacity	Country	Type
1. Noor II	200 MW	Morocco , Ghassate	Parabolic through
2. Ashalim power station 1	121 MW	Israel , Negev desert	Solar power tower
3. Cerro Dominador Solar Thermal Plant (Atacama 1)	110 MW	Chile , Maria Elena , Antofagasta	Solar power tower
4. Redstone Solar Thermal Power	100 MW	South Africa , Nothern Cape	Solar power tower
5. Xila Solar One	100 MW	South Africa , Nothern Cape	Paravolic through
6. Kathu Solar park	100 MW	South Africa , Nothern Cape	Paravolic through
7. Ilanga 1	100 MW	South Africa , Nothern Cape (Upington)	Linear Fresnel
8. El Reboso 2+3	100 MW	Spain , El Puebla den Rio (Seville)	Paravolic through
9. Diwakar	100 MW	India , Askandra	Paravolic through
10. KVK Energy Solar Project	100 MW	India , Askandra	Paravolic through
11. Noor III	100 MW	Morocco , Ghassate , Quarzazate Province	Solar power tower
12. Erdos Solar Power Plant	50 MW	China , Hanggin Banner	Paravolic through
13. CGNSEED power plant	50 MW	China , Delingha	Paravolic through
14. Jinshawan:	27.5 MW	China , China	Solar tower
15. Gujarat Solar One	25 MW	India , Kutch	Paravolic through

16. Stillwater	17 MW	USA , Nevada	Parabolic through
17. Alba Nova 1	12 MW	France , Corsica	Fresnel reflector
18. Sundt Power Plant	5 MW	USA , Arizona	Fresnel reflector
19. Airlight Energy Ait Baha Plant	3 MW	Morocco , Ait Baha	Parabolic through
20. Sundrop	1.5 MW	Australia , Port Augusta	Solar power tower
21. Tooele Army Depot	1.5 MW	USA , Tooele	Dish
22. THEMIS Solar Power Tower	1.4 MW	France , Pyrenees – Orientales	Solar power tower
23. e-Cube 1	1 MW	China , Hainan	Modular Heliostat
24. Renovalia	1 MW	Spain , Albacete	Dish

Table 4.3 Solar Power Tower Stations Under Construction[152],[153],[154]

4.4 Solar Power Tower Installation Announced

Here are the solar power towers that are announced that they will be built in the near future, as you can see this technology is increasingly being applied and future is very optimistic :

Name	Capacity	Country	Type
1. Ordos	2000 MW	China , Mongolian desert	Solar power tower
2. Sandstone Energy 10X	2000 MW	USA , Nye County , Nevada	Solar power tower
3. Solar Energy Project	1540 MW	Ain Bri Mathar , Fom Al Quad , Boujdour , Sebkhath Tah - Morocco	unknown
4. Tamarugal Solar Project	450 MW	Chile , Atacama Desert	Solar power tower
5. Likana Solar Project	390 MW	Chile , Antofagasta	Solar power tower
6. Copiapo Solar Project	260 MW	Chile , Atacama Desert	Solar power tower
7. Al – Abdaliya	280 MW	Kuwait	Parabolic through
8. Shneur Solar Power Station	120 MW	Israel , Tze'elim	Parabolic through

9. Solnova 2, 4-5	100 MW	Spain , Sevilla	Parabolic through
10. CAP SunEdison	100 MW	Chile , Atacama Desert	
11. Mashhad solar-thermal power station	72 MW	Iran , Mashhad	Parabolic through
12. Mashhad Sadde solar-thermal power station	60 MW	Israel, Mashavei Sadde , (Negev)	CSP
13. AZ 20	50 MW	Spain , Sevilla	Solar power tower
14. Archetype SW 550 solar power plant	: 30 MW	Italy , Passo Martino (CT) , Sicily	Parabolic through
15. Agua Prieta II integrated solar combined cycle power station	14 MW	Mexico , Agua Prieta (Sonora)	

Table 4.4 Solar Power Tower Stations Announced[152],[153],[154]

4.5 Solar Power Tower in Greece

By September 2013, the total installed photovoltaic capacity in Greece had reached 2,523.5 MWp from which the 987.2 MWp were installed in the period between January–September 2013 despite the unprecedented financial crisis. Greece ranks 5th worldwide with regard to per capita installed PV capacity. It is expected that PV produced energy will cover up to 7% of the country's electricity demand.

A large solar PV plant is planned for the island of Crete. Research continues into ways to make the actual solar collecting cells less expensive and more efficient. Smaller solar PV farms exist throughout the country.

Greece has potential for CSP development only in few regions. Islands of Crete and Rhodes and the south region of mainland, where the radiation levels are comparable to radiation in southern Spain, are the most attractive locations in terms of CSP development. By deploying CSP, Greece could significantly reduce its high

dependency in energy imports (roughly 70% of the energy needs are imported) and secure the energy supply, especially during the summer peak period.

In 2006, the law 3468/2006 established grants for the generation of electricity using renewable energy sources. The tariff for CSP was set at 250 €/MWh in the mainland and 270 €/MWh in the non-interconnected islands for units with an installed capacity of up to 5 MW, and for units larger than 5 MW the law established a grant of 230 €/MWh and 250 €/MWh.

Greece presented in the summer of 2010 its National Action Plan for renewable energy sources setting a target of 20% contribution of the energy produced from RES to the gross final energy consumption. In order to achieve this target the government sets specific targets for RES electricity share (40%), RES heating and cooling share (20%), and RES transport share (10%).

Although currently Greece has no CSP plant in operation or under construction, recently 2 projects, to be developed in Greece, were awarded by EU with € 86.7 M under the NER300 program. The Maximus project in the Florina region, which has been awarded with € 44.6 M, will have a total installed capacity of 75.3 MW and will consist of 25,160 parabolic dish units. On the other hand, the Minos project, awarded with € 42.1 M, will be built in the southeast of Crete with a nominal electrical capacity of 50 MW employing central tower technology.[40],[100]

Greece
<i>photovoltaic capacity (2013) : 2,523.5 MWp</i>
<i>5th position worldwide in PV installations</i>
<i>CSP development : Crete , Rhodes and south region</i>
<i>Results : reduction in energy imports , secure energy supply</i>
<i>Law 3468/2006: grants for generation of electricity using RES</i>
<i>CSP tariff : 250 €/MWh in mainland (up to 5 MW) , 230 €/MWh(larger than 5 MW) , in the non-interconnected islands 270 €/MWh(up to 5 MW) and 250 €/Mwh(larger than 5 MW) .</i>
<i>National Action Plan (2010) : 20% contribution of energy from RES to the gross final energy consumption</i>
<i>Electricity share (40%), heating and cooling share (20%), and transport share (10%).</i>

<i>Greece has no CSP plant</i>
<i>NER300 program: 2 projects awarded by EU(€ 86.7 M)</i>
<i>Maximus project (Florina, € 44.6 M, 75.3 MW capacity, 25160 parabolic dish units).</i>
<i>Minos project (Crete, € 42.1 M, 50 MW, capacity, central tower technology).</i>

Table 4.5 Summary of Renewable Energy Installations in Greece

Maximus

The Project will be a large-scale Stirling dish power plant with a total installed capacity of 75.3 MWe, located in the north west of Greece in the region of Florina. The plant consists of 25160 Stirling dish units, each of the 3 kW rated power output. The plant will be composed of 37 small power plants of modular design, built on different land plots, which will be connected to the grid via a single connection point. The Stirling dish unit consists of a cavity receiver that captures the concentrated solar irradiation from the parabolic-shaped reflector, a free-piston Stirling engine (FPSE) that converts the solar energy to electricity and a closed loop air driven cooling system. The concentrator is mounted on a structure with a two-axis tracking system to follow the sun.[111],[112],[113]

Minos

A solar thermal tower technology project in southeastern Crete, 50MWe in size, by NUR-MOH SA. The project will substantially benefit the energy independence of Crete, with technology that uses solar energy to provide guaranteed electricity at a cost competitive to fossil fuels used today. The grant amounts to € 42,041,991. The Crete Concentrated Solar Power (CSP) plant will be the first in Europe to feature Bright Source Energy's proprietary LPT 550 solar technology system and will produce electricity for approximately 13,000 homes and reduce carbon emissions by 35,000 tons annually. When completed, this will be the largest tower installation and the most technologically advanced CSP plant in Europe.

This energy system is designed to offer the industry's highest operating efficiencies and lowest capital costs. The system uses thousands of small mirrors -

called heliostats - to reflect sunlight onto a boiler atop a tower to produce high temperature steam. The steam is then piped to a conventional turbine, which generates electricity. In order to conserve water, the steam is air-cooled and piped back into the system in a closed-loop, environmentally friendly process. By using a dry-cooling technology, the plant consumes approximately 95 percent less water than competing wet-cooled solar thermal technologies.



Figure 4.8 Minos [40]

People of Crete will be provided with highly efficient, reliable and environmentally responsible power tower. This is the first CSP plant to be licensed within a portfolio of solar development activities, including large scale solar power plants in North Africa. The producer of this work is Nur Energie Ltd, an independent solar power producer in the Mediterranean region, in collaboration with Motor Oil Hellas, created Nur - MOH Heliothermal SA, in order to implement a Solar power tower installation at the site of Atherinolakkos Lassithi, Crete. Since 2008, it has focused on developing projects with CSP, PV and CPV technology in five core markets- Greece, Italy, France, Morocco and Tunisia, and has a pipeline of over 100MW of PV projects and over 2,210MW of CSP projects in development.

Motor Oil (Hellas) has been a leader in the oil and energy market in Greece for decades. Its Refinery with its ancillary plants and offsite facilities forms the largest privately held industrial complex in Greece and is considered as one of the most advanced refineries in Europe. It is active in the Greek electricity market through its

participation in the company Korinthos Power for the construction of a 437MW CCGT power plant within the refinery facilities.

Thus, Greece is evolving with the use of such systems and progressing to the next level, taking advantage of the amazing solar potential in Greece.[40],[47],[110],[111],[113],[122],[129],[142],[143]

Chapter 5

5.1 Solar Power Tower Operating Principle

The operating principle of solar power tower is based on the conversion of solar energy into many kinds before it is finally converted into electricity. Firstly solar energy is in the form of direct radiation, it is reflected by many mirror-faced surface-with an independent motion system in order to track fully and accurately the sun's trajectory. The trackers are located in a fixed position in order to reflect the direct solar radiation in the solar receiver which is located at the top of the tower. So, the receiver which includes the working medium, absorbs the reflected solar radiation from the trackers and then it becomes thermal energy, which is absorbed by a fluid. Next it is converted into mechanical energy, fluid is heated and vaporized directly or indirectly and then it performs a thermodynamic cycle. Steam from the evaporation is condensed through an air-cooled or water-cooled condenser, and saturated water is pumped to the top of the tower to complete the thermodynamic cycle and start a new one. The steam is discharged to a steam turbine and mechanical work is produced on its shaft, which is connected to a generator and there electric current is produced.

Solar power tower consists of five subsystems: Solar field, Solar receiver, Power generation system, Energy storage system and Back-up system. These technologies use ground-based field of mirrors so as to focus direct solar radiation on the receiver on the tower where it is captured and converted into heat. The solar field with the mirrors, is called heliostats, and track the sun individually in two axes. These mirrors reflect the sunlight on the central receiver where a fluid is heated up.

Current solar towers use water/steam, air or molten salt to transport the heat. The working temperatures can range from 250°C to 1000°C, temperatures of 600°C are the normal for current molten salt designs. The typical size of solar power tower plants is from 10 MW to 50 MW .

The solar field size required increases with annual electricity generation desired, which leads to a greater distance between the receiver and the outer mirrors of the solar field. This results in increasing optical losses due to atmospheric absorption,

unavoidable angular mirror deviation due to imperfections in the mirrors and slight errors in mirror tracking.

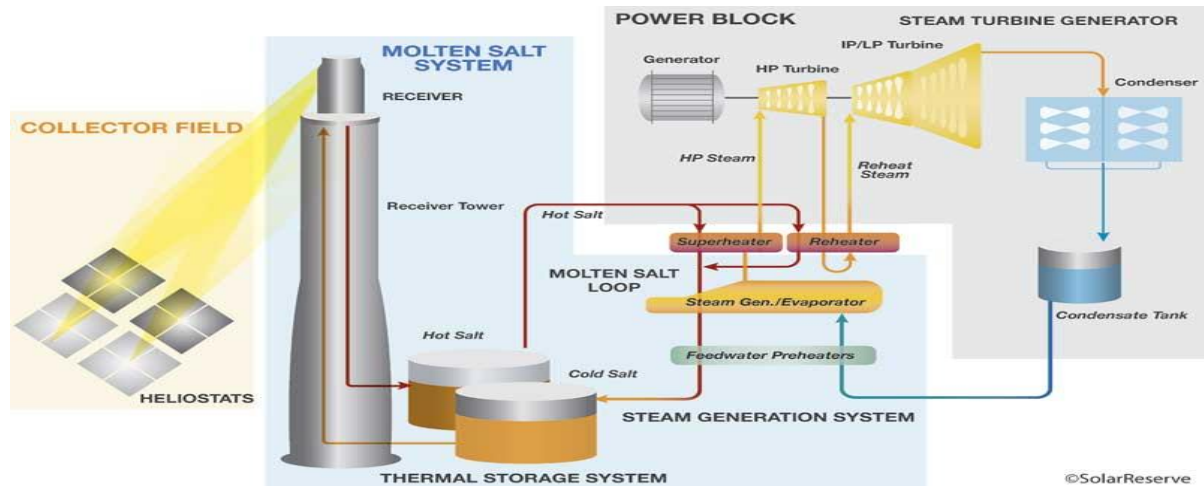


Figure 5.1 Schematic Installation of Solar Power Tower [45]

Solar towers use synthetic oils or molten salt as heat transfer fluid and as storage medium for thermal energy storage. Synthetic oils limit the operating temperature at around 390°C, resulting in limiting the efficiency of the steam cycle. Molten salt raises the potential operating temperature to between 550°C and 650°C, enough to allow higher efficiency supercritical steam cycles.

The main advantages of solar towers are:

- The higher temperature also makes the use of thermal energy storage more attractive in order to achieve schedulable power generation.
- Higher temperatures will also allow greater temperature differentials in the storage system, reducing costs or allowing greater storage for the same cost.
- The higher temperatures can potentially allow greater efficiency of the steam cycle and reduce water consumption for cooling the condenser.

The main advantage is that it can use thermal energy storage to raise capacity factors and allow a flexible generation strategy to maximize the value of the electricity generated, as well as to achieve higher efficiency levels.

Many solar power towers use energy storage systems and back-up systems conventional fuels depending on the location and the use of the facility. When solar radiation has low values for long periods either due to location or due to weather

conditions, it is necessary to use such systems for the smooth operation of the plant.[45],[71],[78],[100],[123],[124]

5.2 Solar Power Tower Subsystems

5.2.1 Solar Field

The Solar Field consists of three parts, reflective surface, support system – movement mechanism and local control system. Solar field is the place that surrounds the tower and consists of multiple mirrors with a support system. The movement of solar field is controlled by a control mechanism at the support system. The sun's motion is monitored by the heliostats so they can reflect the incident solar radiation on the receiver which is located at the top of the tower, in the best way. The central control system gives commands to the local control systems provided by the trackers depending on the demand and in general with the operation of the installation station.

The collector subsystem of a solar central receiver has as basic function the interception, redirection, and concentration of direct solar radiation. It consists of a field of tracking mirrors, called heliostats, and a tracking control system to maintain continuous focus on a receiver mounted on a tower the direct solar radiation on the receiver while energy is being collected.

When energy is not being collected, the control system must prevent the reflected energy from damaging the receiver, tower, or other structures, or creating an unsafe condition in the airspace around the plant. Because the solar field usually constitutes the largest fraction of the costs for a solar central receiver system, attention must be given to the development of low-cost designs and to estimation of mass production costs.

Two-axis tracking mirrors focus sunlight on the receiver where the working fluid absorbs the solar energy as heat. The system then converts the energy into electricity or uses it as process heat. The concentrated solar energy is absorbed by a fluid in the receiver. The absorbed thermal energy is conveyed to the base of the receiver tower where it may be used for work, such as the generation of steam for the production of electricity or the delivery of process energy.

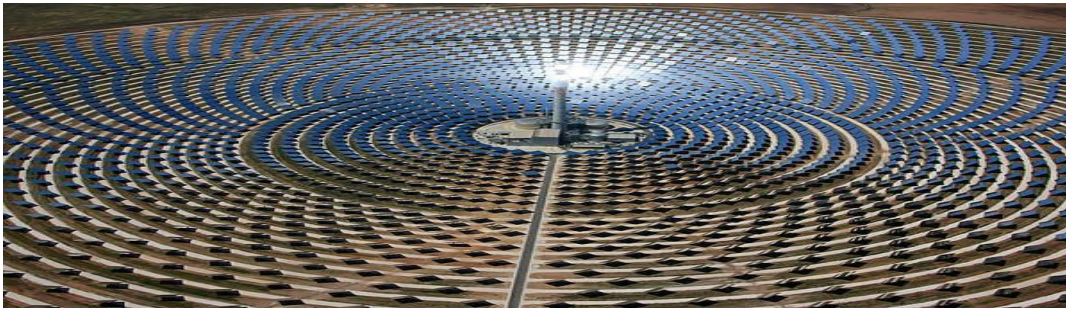


Figure 5.2 Solar Field of Solar Power Tower [46]



Figure 5.3 Heliostats [47] [48]

Tracker, with independent movement have to manage to position their reflective surface at any moment in such a way so as to achieve the best possible concentration of direct incident radiation in the central receiver at the top of the tower. The reflected beam of solar radiation has to be directed directly to the receiver, so the vector perpendicular to the surface of each transmitter must continuously bisect the angle formed by the line joining the center of the sunset with the center of the solar receiver, and the line joining the center of the sunset with the center of the sun.

The reflective surface of a typical heliostat is usually made of a steel base, an adhesive layer, a copper protective layer, a high reflectance silver coating and a thick glass layer. So far there have been built tractors in many different sizes, starting from 1 m² up to 120 m². Total reflecting surface of a large heliostat is divided into a number of

smaller surfaces to ensure a slight curvature that allows better concentration of solar radiation in the receiver. The main concern of a solar heater is high reflectivity on its surface, low relative weight and high wear resistance due to various weather phenomena.

The reflective surface has to reach the maximum reflection with the minimum weight so that the sun can move on two axes. A reflective surface technology uses large curved surfaces. Increasing the size of each tracker creates a large reflective surface while reducing the total number of heliostats required. In this way less subsystems are used and thus decreases costs. This advantage, however, is eliminated, since there are increased optical losses and therefore greater surface.



Figure 5.4 Heliostats Support System [44]

Heliostats of stretching film is a very simple technology, with much lighter construction materials. In a huge metal support ring, a stretched stainless steel sheet is placed and the front surface is coated with a high reflective material to act as a reflective surface. Vacuum conditions are created inside the membrane to give a hollow outline, and pressure can be exerted to overturn the focus. A great advantage of this technology is the very low weight compared to conventional trackers, but they are disadvantaged in strong wind conditions, since the surface of the membrane is distorted, resulting in deviations from the focal point.

A solution has already been found on this issue, since by welding a ring on the support ring, tension is induced in the membrane and the wind alterations are mitigated. Still another technology is the use of two pieces of reflective surface with a small area, resulting in good performance, very light weight and much cheaper manufacturing costs.

The characteristics of the overall collector field are defined based on cost and performance which seek to minimize the cost of annual collected energy. This includes

consideration of the receiver, tower, and piping systems in addition to the performance and cost attributes of the collector field and its related equipment.

The performance of the solar field is defined in terms of the optical efficiency, which is equal to the ratio of the net power intercepted by the receiver to the product of the direct isolation times the total mirror area. The optical efficiency includes the cosine effect, shadowing, blocking, mirror reflectivity, atmospheric transmission, and receiver spillage. The net efficiency for producing electricity includes receiver efficiency and thermalto- electric conversion efficiency.

The amount of isolation reflected by the heliostat is proportional to the amount of sunlight intercepted. The reflected power is proportional to the cosine of the angle (cosine effect) between the heliostat mirror and the incident sun rays; the ratio of the projected mirror area that is perpendicular to the sun's rays to the total area of the heliostat determines the magnitude of the cosine effect. The heliostat is oriented so that the incident sunlight is reflected on the receiver. If the sun is due south and low in the sky, as it is in the winter, then the heliostats at the north of the tower will be almost perpendicular to the sun's rays and, therefore, have almost the maximum cosine efficiency of 1.0. At the same time, heliostats at the south of the tower will have a low cosine efficiency.

Since the greatest fraction of the annual isolation occurs when the sun is in the southern sky, the annual average cosine will be greatest in the northern part of the solar field. Thus, in the northern hemisphere, solar fields are usually biased toward the north of the tower. For the same reasons, solar fields located in the southern hemisphere will be biased south of the tower. Not all the sunlight that clears the heliostats reaches the vicinity of the receiver. Some of the energy is scattered and absorbed by the atmosphere; this effect is the attenuation loss, and it will be explained below. A good visibility day will have a small percentage of energy loss per kilometer. The losses increase when water vapor or aerosol content in the atmosphere is high.

The local heliostat density at any point within the collector field is determined through a tradeoff of cost and performance parameters influencing that portion of the field. This tradeoff considers the cost of heliostats, land, and interconnecting wiring. Clearly as heliostats are packed closer together, blocking and shadowing penalties increase, but related costs for land and wiring decrease.

While both shadowing and blocking increase if the heliostats are closer together, blocking has a more pronounced effect on the layout of solar fields. As heliostats are placed at greater radial distances from the tower, the receiver appears to be closer to the horizon. Therefore, heliostats must be placed at greater radial separations to be able to see the receiver.

Heliostat control signals are first routed to local solar field controllers which in turn communicate with the heliostat controllers located at the individual heliostats. Traditionally, the control wiring network has been made up of copper wire cable which forms a serial data highway between the heliostat array controller and the field controllers and also between individual field controllers and corresponding heliostat controllers. The heliostat is the main element of the collector subsystem. The heliostat itself is the least dependent central receiver system component on overall system considerations; that is, unique heliostat designs are not required for each type of receiver heat transport fluid, receiver configuration, or end use application of thermal energy. This independence permits design emphasis to be placed on mass production as a mean of reducing the unit cost of the heliostat, recognizing that the collector system represents a major portion of the overall system cost.

There are three main types of heliostats characterized by the type of mirror module and/or structural arrangement. Glass/metal heliostats have silvered glass as the reflecting surface and a relatively stiff structure to support the mirrors and withstand wind loads. Membrane heliostats have a stressed membrane supporting a reflecting film. In a third option, the entire heliostat, either glass or membrane, may be enclosed in a pressurized bubble. Heliostats enclosed by a bubble are subjected to virtually no wind loads, and thus can have a lighter (and potentially lower cost) support structure. However, if the heliostat is enclosed in a bubble, the energy must pass through the bubble material twice, and in so doing can be absorbed and scattered by the bubble material or by dirt on the bubble material. Stressed membrane heliostats offer the potential of lower cost through reduced material cost.

The reflector or mirror module consists of a silvered glass mirror and some support structure in glass/metal heliostats or a reflective polymer-coated metal membrane in stressed membrane heliostats. Each glass/metal heliostat is made up of multiple mirror modules. Each mirror module usually has a slight concave curvature and

is also canted (aimed) with respect to the plane of the support structure to better focus the reflected sunlight on the receiver and thus improve performance.

The reflector support structure supports the array of mirror modules. Usually this structure consists of a main beam or torque tube with several cross beams. The main beam is attached to the drive system while the mirror modules are attached to the cross beams. Truss type beams are the preferred option especially for larger heliostats because their depth can be varied to provide the required stiffness, with little weight penalty. A roll-formed section, while good for small depths, has a solid web which makes deep roll-formed sections weigh more and has less stability than truss type beams.

The drive of a heliostat must have great robustness, in order to withstand the weight of the moving sections but also the strong wind loads, huge motion precision, even for very small changes in angular displacement, ability to execute very slow movements, with a reduction of 40000: 1, possibility of relatively slow reset of the heliostat [to inactive horizontal position, in case of unsuitable weather conditions, or due to need from the central solar receiver, durability in outdoor conditions, easy maintenance and small cost of construction and operation.

The motion of a tracer has to be characterized by very high accuracy so that the reflected beam beams are successfully directed to the central solar receiver. This is perceived by considering that even a small angular deviation in the movement of a tower remote from the tower may be equivalent to a deviation of many meters of the reflection of the reflected rays on the receiver. In order to carry out any movement, there is a separate local control system that collects information about the location of the sun and the meteorological data and gives the commands to the drive. The control system essentially calculates the angle at which the reflective surface must always be turned, or in the event of extreme weather conditions, instructs the positioning of the heliostats in the horizontal position.

The support system consists of two transverse steel pillars. These pillars are the two axes that allow the tracker to achieve the optimal position at any time. The vertical axis is embedded in the ground.

The movement mechanism is the system that determines the movement of each axis relative to the elevation angle and the angle of the azimuth, so that the reflective surfaces follow the Sun's position to reflect the incident solar radiation at the receiver at the top of the tower. The accuracy in the execution of any movement of the axes is

extremely important, since even a small angular deflection is able to turn the footprint of the reflected Sun rays several meters away from the focal point. Thus, the traction mechanism of the heliostat should meet certain specifications and include some specific features.

The construction of the pylons should be very robust, taking into account that the heliostats are exposed in an open field and in all weather conditions. They should be able to withstand the high loads of the winds but also their own weight and the weight of the moving parts. Also, the pylons should be rigid so they are not affected by low frequency vibrations.

The vital moves that the mechanism must make is inevitably achieved only with extremely slow motion. This becomes possible by using stepped DC motors that are capable of delivering transmission ratios up to 40000: 1. Shaft gears are commonly used for both shafts. The two gears must be proportional to the shape of the teeth and the ratio of the reduction.

Their placement must be very precise and free movement is allowed. Also, it should be ensured that the heliostat is quickly restored to an inactive horizontal position in cases of strong winds or other dangerous weather conditions, and more generally in cases where it is necessary to remove the solar receiver from the solar receiver. Its construction should be resistant to outdoor conditions, since it is exposed. Consideration should also be given to the ease of maintenance and the cost of construction and operation.

The local control system of all the field ellipses is controlled by a central control system that can be processed by a common computer. The latter provides information about the station's energy needs, the working temperature of the working medium achieved by the present focus of the reflected beams on the receiver and, more generally, is a mechanism for overall monitoring of the solar thermal station.

Each heliostat has a local control system that collects information about the location of the Sun but also meteorological data in order to give the proper command of the heliostat drive mechanism. This system is capable of calculating the angle that the heliostat should turn to reflect the solar radiation at the focal point. In case of extreme weather events, the local control system commands safety movements (e.g. horizontal position in case of strong winds). The control system is usually mounted on the mounting pylon of each tracker.

The development of local control systems is the wireless communication with the drive mechanism, but the main evolution is the autonomy. There are examples of autonomous heliostats, which operate by providing electricity from photovoltaic panels for the operation of the drive.

The local control system provided by the heliostats is controlled by the central control system. The Solar Field Control System cooperates with the Energy Production Control System, which provides information related to the station's energy needs as well as the temperature of the heat transfer fluid to the receiver. Thus, the Solar Field Control System with the elements related to the temperature and pressure of the working medium is able to alternate the focal points of each heliostat, and can alternate the heliostats during the operation of the station. With today's data, the operation of such a control system is possible through a simple computer equipped with the appropriate software.

Most central receiver system designs also include a thermal storage system which can be used to operate the plant for several hours after sunset or during cloudy weather. Depending on the heliostat design, heliostat field layout, receiver design, and receiver fluid selection, central receiver systems can be used to heat fluids from 400°C - 1000°C (750°F – 1830°F). Considerable development has focused on components designed to heat the receiver fluid to roughly 550°C - 600°C (1000°F – 1100°F), suitable for generation of steam for Rankine cycle steam turbines.

The technology of solar powered energy systems using the central receiver concept is approaching readiness for electric utility applications. Preferred locations for central receiver plants are regions with high direct normal isolation.

An important aspect of central receiver systems is the ability to store excess thermal energy efficiently. The storage of energy during daylight hours allows operation of the turbine during non-solar periods. The marginal cost of collecting and storing this energy is less than the cost of increasing turbine size to match the peak thermal output. Storage is also important for managing cloud transients during the day. Determination of the optimum storage size to fulfill the energy dispatch requirements of a particular application is a part of the central receiver design process.

The design and operation of a central receiver system is strongly influenced by the transient nature of the incident isolation. Thermal cycling of components is an important design consideration. The prediction of plant output and estimation of energy

cost are dependent on the site-specific prediction of available solar energy. Even at a given site, the reliance on short term data can be misleading and long term climatologic data is preferred.

The solar plant control system is more complex than that of conventional power plants. In addition to the turbine generator, other major subsystems such as the collector field, thermal storage, receiver, and steam generator must be controlled. This complicates control requirements during startup, shutdown, and transient (cloud) operation when the interaction of subsystems is most critical.

Four system options, distinguished by the receiver and storage fluid, are considered to be the principal options for early commercial central receiver plants. Three alternatives for receiver fluid are water/steam, molten nitrate salt, and liquid sodium. A fourth system option, in which sodium is used as the receiver working fluid and molten salt is used as the storage fluid, is referred to as a sodium/salt binary.[46],[47],[48],[71],[72],[78],[93],[100]

5.2.2 Solar Receiver

The part of the tower, and especially at the top, where solar radiation is transmitted to the working fluid, in the form of thermal energy is called central solar receiver. It is a heat exchanger and consists of many panels consisting of parallel, vertical thin tubes welded together with a common inlet and outlet head. These tubes are usually externally coated with a black dye for high absorption. The receiver subsystem intercepts and absorbs the concentrated radiant energy reflected from the collector subsystem and transfers this energy to a heat transport fluid. The heat transport fluid flows through the tubes, removing the solar energy absorbed on their outer surfaces. Thermal energy is transmitted to the heat transfer fluid so that a thermodynamic cycle can be performed.

The main parts of a central solar receiver are the absorbent surface, consisting of the piping panels, the central structure on which they are fixed, the panel interconnecting ducts, the inlet and outlet ducts of the working means and the steam tanks or steam drum, depending on the case.

The size of the solar receiver depends on the energy and is limited by the maximum flow of incoming heat flow and the leakage losses. The smaller the receiver surface, the greater the heat flow entering it. Also larger, however, are the leakage losses, from the reflected rays that fail from the surface of the receiver. The incoming heat flow is desirable to take high values as it increases the overall performance of the receiver, but it is also limited by an upper limit due to the limited strength of the receiver construction materials at very high temperatures.

Typical temperatures in which a central solar receiver operates is 300°C-1200°C, and typical values for the incoming heat flow on the absorbent surface are 200KW / m²-1200KW / m². The above values make it imperative to carefully study the materials to be used in the construction of a receiver as they are required to cope with high voltages and thermal loads during the operation of the plant. The most important features a receiver has to have is high thermal performance and high temperature resistance over a long period of time.

Depending on the construction, there are several criteria for categorizing the solar receivers. The two main categories are tubular receivers (external receivers and cavity receivers) and volumetric receivers.

Receiver design is dependent on the choice of receiver working fluid. There are three principal candidates for the receiver heat absorbing fluid for near-term, Rankine-cycle, solar power plants: water/steam, molten nitrate salts, and liquid sodium. Subsystem performance for different receiver configurations is the result of a variety of design tradeoffs among several loss mechanisms.

Two general receiver configurations occur: external and cavity. External receivers have heat absorbing surfaces that are either flat, often called a billboard, or convex toward the solar field. For a large plant, an external receiver is typically a multi panel polyhedron that approximates a cylinder, with a surround solar field.





Figure 5.5 Solar receiver[49]

The height to diameter ratio of a cylindrical receiver is generally in the range of 1:1 to 2:1. Smaller plants with external receivers typically use a north field configuration with a billboard or a partial cylinder receiver (omitting most of the south-facing panels). In a cavity receiver, the radiation reflected from the heliostats passes through an aperture into a box-like structure before impinging on the heat transfer surfaces; this box and aperture define the cavity.

A receiver may be composed of more than one cavity, each facing a different sector of the solar field. The preferred configuration is a single cavity facing a north, in the northern hemisphere, solar field. The active heat transfer surfaces within a cavity are formed from panels like those used in external receivers; however, the panel arrangement within a cavity is concave facing the heliostats.

Other internal areas of the cavity, such as the roof and floor, do not normally serve as active heat absorbing surfaces. These areas must be effectively closed and insulated to minimize heat loss and to protect structure, headers, and interconnecting piping from incident flux. Although they are not exposed to high levels of direct flux, the inactive internal areas are exposed to radiation from the hot absorber panels. The inactive surfaces are typically uncooled and can reach temperatures exceeding those of the active panels.

Radiative losses are generally larger for external receivers since the hot receiver panels are exposed and have larger view factors to the colder ambient environment. However, spillage losses are generally larger for cavity receivers because the heliostat radiation must fit through the relatively small aperture, and thermal convection losses may be larger because of the large heated surface area (active plus inactive) of the cavity. The required absorber area in a cavity receiver is larger (by roughly 25%) than that required for an external receiver with the same thermal rating, allowable peak flux

limit and flux gradient. This results from the greater difficulty in illuminating the cavity absorber area uniformly because of the cavity aperture.

The receiver mass and number of components are larger and generally more costly for a cavity than for an external receiver with a similar absorber area. Receiver piping and tank arrangements differ, depending on the receiver fluid and the flow configuration (once-through, recirculating, or multipass). Sodium and molten salt receivers have inlet and outlet surge tanks.

A water/steam receiver does not have surge tanks, but it does have a steam drum in recirculating flow configurations or a flash tank in once-through flow configurations. The inlet accumulator tank and outlet surge tank atop the tower buffer the fast-responding temperature control valves from the slower responding receiver feed pump and control valves, permitting rapid response to flux change.

During the transition from normal operation to a standby condition, these tanks may also accommodate the change in fluid and piping volumes resulting from temperature changes. If the receiver feed pumps fail, the inlet accumulator tank provides a reservoir of fluid that can be passed through the receiver for a short period, allowing time for the solar field to defocus. A compressor with storage tank maintains a constant pressure of air (for molten salt) or inert gas (for sodium) in the tank for this purpose.

The outlet surge tank is located at the highest point in the fluid-flow circuitry, providing a means for monitoring the fluid level in the receiver system to insure that the panels are filled with fluid. Fluid level is maintained by adjusting the drag valve (at the base of the tower) which controls the amount of fluid leaving the receiver. The tank also provides for flow in the event of a down blockage.

The receiver control system has two primary functions: to maintain the receiver heat transport fluid outlet conditions at set point values during normal operations, and to operate and protect the receiver during transient and emergency conditions such as start-up, shutdown, cloud passages, and equipment/component failure. Because of input power and flux distribution changes caused by diurnal and meteorological conditions, the control system must vary the receiver heat transport fluid flow rate to maintain outlet temperature and pressure at the desired set point. Sensors used in the receiver control system may include thermocouples, pressure transducers, flux transducers, flow meters, and fluid level indicators.

Pipeline (Tubular) Receiver is the most common type of solar receiver that is found in existing solar power tower installations. The thermal energy of the concentrated radiation is transferred to the transfer fluid through a metal or ceramic wall. Based on their geometrical configuration, the tubular receivers are divided into two categories, the external receivers and the cavity receivers.

The external receiver consists of cylindrical or flat tubular panels. Cylindrical panels are used in installations where the solar field is located around the tower. The panels are the absorbent surfaces consisting of thin pipes that run through the heat transfer fluid.

In the cavity receiver the reflected radiation passes through an opening into a cubic structure and impinges on the absorbent walls of the receiver. Because of its shape, the cavity receiver can only receive radiation from one orientation. Although it has been studied to have more than one aperture in order to receive radiation from more than one direction, the conclusion was that its optimal operation is with a single opening. Inside the receiver is the absorbent surface, which is a tubular panel in a concave configuration. The purpose of this receiver is to trap the energy it receives from the trackers in the cavity, and for this reason the size of the opening is of the utmost importance. The dimensions of the aperture are chosen in such a way that there is no heat loss from the cavity, but also to avoid losses from the deviation of the solar footprint in the receiver.

Comparing the two tubular receivers, it appears that the external receiver due to its direct exposure to the environment has more thermal losses, while the cavity receiver has more leakage losses because of the small size of the opening, but is much more protected than the environment and therefore has longer life.

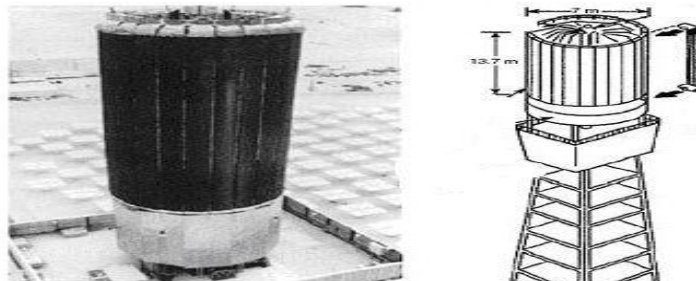


Figure 5.6 Pipeline Receiver [46]

Volumetric receivers are structures with porous characteristics and acting as heat exchangers absorb the concentrated reflected radiation through convection. Absorption takes place inside the volume and not on the surface such as the tubular receivers. The working medium, which is usually air, passes through the porous structure and is heated by sinus. It is made of thin porous materials allowing the radiation to penetrate deep into the receiver and ensure good heat transfer.

The main feature of a good receiver is the creation of the volumetric phenomenon. The side of the receiver that receives the radiation should have a lower temperature than the working medium. The volumetric receiver usually mounts exposed to the environment, however in cases where high temperature is required, it is closed by a transparent window (air outlet temperature greater than 1000 °C).

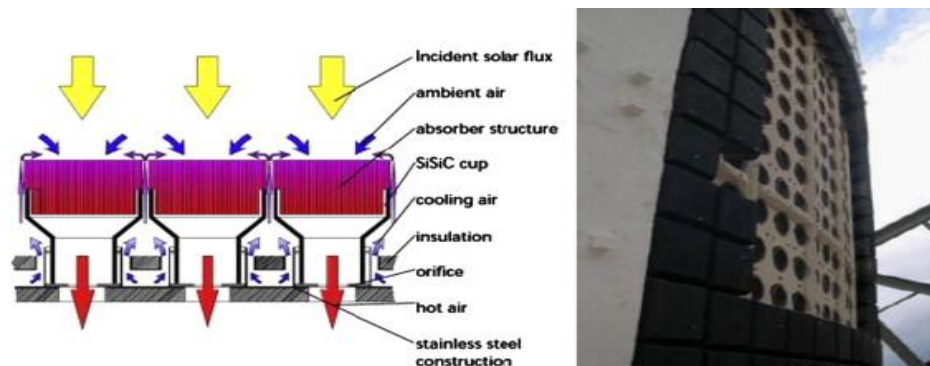


Figure 5.7 Volumetric Receiver [47]

The advantages of a volumetric receiver are the air is free and always available, there is no risk of solidification of the heat transfer fluid, very high temperatures allow the use of heat in more efficient thermodynamic cycles, the working medium does not change phase, simpler system, immediate response of the system to any changes in heat flow and it has no environmental impact.

At this stage the use of volumetric receptors is at an early stage, however the tests end up positive. They need to further improve their thermal performance and reduce radiation losses, but they need to be investigated and their resistance over time.[49],[50],[51],[71],[72],[78],[100],[103]

5.2.3 Electricity Production System

The system where the working medium runs is the Electricity Production System. There the working medium performs a thermodynamic cycle and energy is generated. Electricity Production System has steam turbines, pressure pumps, heat exchangers, condenser, degasser and electric generator (a common steam circuit). It is the same system, except that the heat supplied comes from the reflected solar radiation. One could characterize the circuits used in the power generation system as normal steam-generating circuits, with the only difference that the heat supplied by the steam generator to the fluid, in the case of solar thermal plants, is given by the concentrated solar radiation through the solar receiver. The role of the steam generator is substituted by the solar-central receiver system.

The choice of the working fluid to be used depends mainly on the operating temperature of the plant after heat absorption on the central solar receiver and on the energy storage medium if there is a storage system. The working medium, however, in turn, affects the final arrangement of them circuits that will constitute its electricity generation system installation.

Depending on the required temperature, the working medium is selected. The main heat transfer fluids and their operating temperatures are: Water - Steam (0 °C – 540 °C), Melted Salt (280 °C – 565 °C), Sodium Liquid (150 °C – 590 °C), Atmospheric Air (480 °C – 540 °C) and Compressed Air (800 °C – 1200 °C).

The electric power generating system consists of the turbine generator plant and its ancillary components. Conventional power plant equipment is suitable for central receiver plant use. Two superheated steam Rankine power conversion systems are used in the electric utility industry: reheat cycles and non-reheat cycles.

In non-reheat cycles, the steam entering the turbine expands through the turbine stages to the condenser with no intermediate energy input. In reheat cycles, the turbine steam flow is withdrawn from the turbine at an intermediate point in the expansion path and heated again to superheated conditions, after which it re-enters the turbine and undergoes further expansion.

Two types of reheating are commonly employed: direct reheat, in which expanded steam from the turbine is reheated by the same heat source which superheats the main steam and indirect reheat, in which expanded steam from the turbine is

reheated by higher temperature steam from elsewhere in the cycle (such as extraction and/or main steam).

Direct reheat allows the steam to be reheated to the same temperature as the main steam and offers the greatest thermodynamic advantage. Indirect reheat offers less thermal advantage than direct reheat but it does not require returning the steam to the steam generator.[71],[100]

5.2.3.1 Water – Steam Systems

In Water – Steam Systems, steam is produced directly at the output of the solar receiver so they are direct steam production systems. Water passes through the tubing of the receiver, so it is heated by the solar radiation and changes phase. Saturated or superheated vapor (depending on the receiver) is extinguished directly into the turbine and produces mechanical work and ultimately through the generator electricity. Then, the steaming steam passing through the condenser is again liquefied. It is then preheated before it is compressed by a pressure pump to the operating pressure of the station to climb at the top of the tower located on the solar receiver.

This technology is very mature and the most tried. Direct steam production has also the advantage that avoids the loss of the use of another heat exchanger. Water is also low cost for using it as working medium, but piping is burdened by high pressures due to the change in water phase. Also, using water-vapor is not efficient using an energy storage system due to high heat losses of water.

This system consists of a tower mounted water/steam cooled receiver heated by a field of heliostats. In this system, superheated steam from the receiver is routed directly to a steam turbine where it is used to produce electricity. High pressure steam is an uneconomical storage medium. In order to store energy in water/ steam system, the energy must be transferred to some medium with heat exchangers. One possible storage medium is oil. Transfer from steam to oil and back to steam results in energy losses.

The use of an intermediate fluid for energy storage required in a water/steam system results in efficiency losses because steam from storage is at a lower temperature and pressure than that from the receiver. This reduces the overall electrical

generating efficiency for the plant, and that requires a larger, more costly solar plant. In addition, the requirements for high fluid pressure and two phase heat transfer in the receiver directly influence receiver design, operation and control.

The major difference between water/steam and other working fluid concepts is related to the receiver, thermal storage system, and the turbine interfaces. The oil/rock thermo cline storage system used sometimes is charged by using steam from the receiver to heat a heat-transfer oil in a heat exchanger. The hot oil circulates through a tank filled with small rocks and sand, heats the rocks and sand and establishes a thermocline in the tank (25% oil and 75% rock by volume). The system is discharged by routing hot oil from the tank through a steam generator.

The maximum temperature limitation of the oil (approximately 315°C or 600°F) requires that this process is conducted at reduced steam temperature and results in the output steam being derated to 280°C (530°F), as opposed to the 510°C (950°F) steam from the receiver. This derated steam is introduced to the turbine through a special admission port in the turbine. The result of using this lower temperature derated steam is a reduction in turbine gross cycle efficiency from 34% (rated steam) to 28%.

The use of water/steam in a central receiver system together with a single pass to superheat receiver and thermocline storage has been adequately. It has successfully demonstrated the technical feasibility of this concept, the economic viability of water/steam systems does not appear to be as good as other technology options. Energy from the storage fluid is transferred to feed water and steam in the steam generator; superheated steam at design temperature and pressure is produced for use in the turbine generator. A steam generator is required in both molten salt and liquid sodium systems. For water/steam systems, steam is produced directly in the receiver, but if the water/steam system includes storage, a steam generator is required.[52],[71]

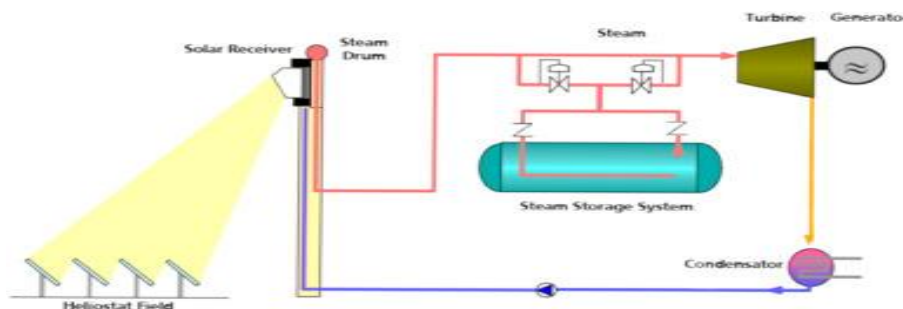


Figure 5.8 Water – Steam System [52]

5.2.3.2 Molten Salt Systems

It is an indirect steam system, so, it consists of two independent circuits, with different working means, connected to each other by a heat exchanger and produced by steam. In the first circuit, the heat transfer fluid drains the heat from the solar receiver piping and then passes through the heat exchanger, which acts as a steam generator, and from there passes the second water-vapor-flowing circuit. Thus, heat is transmitted by the hot fluid to the cold water, and superheated steam is produced. Subsequently, the steam performs the thermodynamic cycle as well as the direct production systems, and after being condensed and compressed by the pressure pump, it returns to the heat exchanger and starts a new cycle. The transfer fluid is cooled and pumped to the top of the tower to end up in the solar receiver piping and heat up again.

The advantages of using molten salts are many. It is a non-toxic material, stable, with high thermal conductivity and heat capacity and is capable of reaching high temperatures at low pressure. However, its major disadvantage is the high melting point (245 °C or 473 °F) which, in order to avoid the risk of solidification, makes it necessary to have a permanent heating system for the fluid. The use of molten salts, however, is ideal for the use of thermal energy storage technology.

Sodium liquid also has a high melting point but very high thermal conductivity. A major disadvantage, however, is the reaction of sodium water with water and air, necessarily considering safety systems.[49],[71],[72]

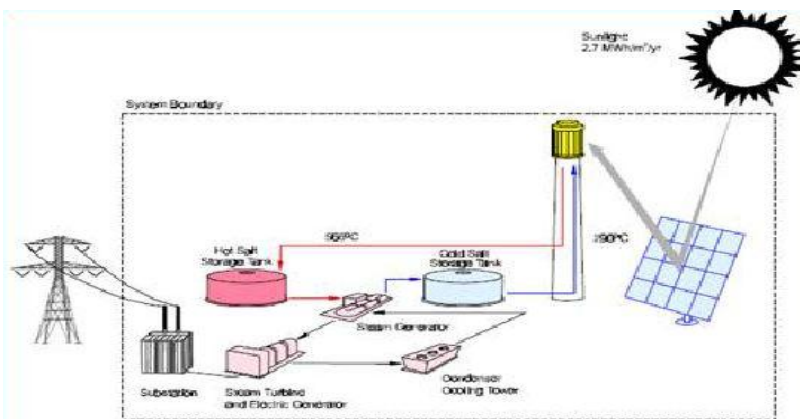


Figure 5.9 Molten Salt System [49]

5.2.3.3 Atmospheric Air Systems

Atmospheric air through a volumetric receiver is heated to temperatures of 700 °C (1292 °F) and is then used to generate steam through a heat exchanger. The advantages of using air have already been mentioned in a previous paragraph, and the conclusion that comes out is that it is a system that achieves very high temperatures but the disadvantages are the radiation losses of the receiver. However, it is possible to store energy through thermocline for a short time (3 to 6 hours). Also hybridization with additional combustion of conventional fuels improves system performance so that it is a logical choice.[71],[78]

5.2.3.4 Compressed Air Systems

In compressed air volumetric receiver systems, the air outlet temperatures from the receiver reach values above 1200 °C (2192 °F). Air is compressed at 15 bar and is driven through the receiver volume and heated. The air exiting the receiver can be used as combustion air in a gas turbine or combined cycle power plants.

For this technology, the volumetric receiver used is a window, which is made in a quartz shape to withstand the high pressures. There is the ability to connect multiple receivers in series or in parallel, essentially composing a larger scale receiver. The air exiting the receiver can be used as combustion air in a gas turbine or combined cycle power plants.

This system has a very high annual yield, above 20%, due to very high temperatures. This allows the installation of a smaller helix field and a corresponding reduction in cost. Disadvantages include the difficulty of storing energy and the construction materials required due to very high temperatures.[71],[78]

5.2.3.4.1 Tank Design

Three tank design concepts can be envisioned:

- *vertical, cylindrical hot and cold storage tanks with external insulation,*
- *vertical, cylindrical storage tanks with internal insulation for the hot tank and external insulation for the cold tank,*
- *multiple horizontal, cylindrical tanks for storing hot and cold fluid.*

Spherical tanks were considered early in some plant designs but are more expensive.

Molten salt or liquid sodium storage systems which operate at temperatures above 400°C (750°F) employ two-tank designs with separate tanks for the hot and cold fluids. The maximum fluid volume which can be contained in a tank is influenced by the storage medium temperature, tank material and tank height. The storage medium temperature and tank material determine the stresses in the tank. Tank height is limited, in part, by the allowable soil bearing strength. A heater, located in either the sump tank or storage tank, can be used to heat the storage medium during periods when the receiver is not in operation.[71]

5.2.3.4.2 Startup

The startup procedures employed when the plant is first put into operation depend primarily on the type of thermal storage medium used. For water/steam and heat transfer oils, the startup procedure consists of pumping the fluid to the solar receiver and routing the fluid directly to storage or transferring the energy by a heat exchanger to storage.

Sodium and salt are in a solid phase prior to startup. The first phase of the startup procedure involves heating the salt or sodium until approximately 20% of the total inventory is melted. This initial melting can be accomplished by either electrical resistance heating or fossil heating. In the second phase of the starting procedure, the melted medium is pumped to the solar receiver where it is heated; the hot fluid is then routed to the intermediate drainage sump tank.

The remaining bulk storage medium is gradually melted by the hot fluid. As more of the solid medium is melted, excess fluid is routed to the appropriate storage tank. This

procedure is followed until the entire inventory of the storage medium is melted. During periods of prolonged shut down of molten salt and liquid sodium systems, a system for complete temperature control is required to prevent the storage fluid from solidifying. This system may use electrical heat tracing as well as electrical immersion or fossil heating. If used correctly, this system greatly simplifies the system startup following long term shutdown.

The maintenance requirements for the thermal storage subsystem depend on the chosen storage medium. Systems using oil must be carefully maintained and monitored because oils are highly flammable. Due to thermal decomposition of oils at high temperatures, continuous make-up and blow down should be provided to maintain an acceptable fluid composition. Molten salt and liquid sodium require special attention to monitor chemical degradation, the buildup of impurities, and fluid solidification. Liquid sodium requires extra attention to prevent its oxidation and to protect equipment and personnel.[71]

5.2.4 Thermal Energy Storage System

Solar power tower systems have the ability to store excess thermal energy. Since the thermal energy accumulated in the receiver exceeds the system's operating requirements, the system stores the excess energy in order to render it back to the system in low, variable or no-sun conditions. Also, the stored thermal energy ensures the continuous operation of the plant, and avoids the many system breakdowns and system start-ups. Thus, using a storage system, the station has the ability to produce energy according to demand and stops being completely dependent on weather conditions.

Solar heating systems can optionally be used with a heat storage system. In times of high solar availability, where the thermal energy accumulated in the central receiver due to solar radiation exceeds the thermal energy that the station would need to operate under full load conditions, the storage system stores the excess heat energy, in order to give it back to the power generation system when the values of the incident direct sunlight will not be particularly high.

The storage system plays a key role in the installation of a solar power tower, as it enhances its continuous operation in low or variable sunshine conditions, or even in hours of zero irradiance. What is also important is the fact that, due to the storage system, it is avoided that the stations start abruptly and interrupt, which would be detrimental to the various components that make up the system. In a nutshell, the storage system allows changing the profile of the installed electricity from the installation in such a way that it more closely matches the current demand profile and does not depend entirely on the sunshine.

The three main types of thermal storage that have been devised to date for solar power towers are sensible heat, latent heat and thermo chemical energy. In the sensible heat storage systems, the energy is stored, in the form of thermal energy, in a storage medium which, for storage system temperatures, does not change phase. A large number of materials have been tested for this particular storage method, including oils, molten mixtures, liquid metals and solids such as stones, sand, ceramic bricks and metal spheres.

Another way of storing thermal energy is by using the latent heat emitted during the phase change of a material. Phase changes from solid to liquid occur in a relatively small range of temperatures, which must be compatible with the temperature at which the plant's storage system can operate. The two main disadvantages of latent heat storage systems are that phase change materials are expensive compared to those used to store sensible heat and that a large surface area is required to make the required heat transfer.

Thermo chemical storage is based on the storage of thermal energy released from the decomposition and re-synthesis process into reversible chemical reactions. A large number of catalytic or non-catalytic reactions have been tested in this storage method. A very positive feature of thermo chemical storage is that the components used in can be transported and stored at ambient temperatures. An obstacle, however, in the rapid development of the thermo chemical energy storage systems is the very high cost of materials, as well as the gases produced during the high temperature reactions.

Of the above types of thermal storage, the one that has been tested and more used in solar thermal installations is the storage of sensible heat. One could separate the sensible heat storage systems into direct storage systems where the working fluid in the solar receiver piping and the storage system is common and in indirect storage

systems where the working fluid is different in the two subsystems and that is why a heat exchanger is used to charge the storage system. Indirect storage systems require more heat to the receiver, hence a higher temperature, as part of it is then lost to the exchanger with the storage system.

Based on the layout of the tanks, storage systems can be divided into two categories. The first includes systems consisting of separate hot and cold tanks, while the second one is a single tank with thermoclines. The arrangement of separate hot and cold tanks usually consists of two or more tanks. The fluid in the tank has the same temperature at every point, but its amount varies during the operation of the plant due to the constant charging and discharging of the storage system. During charging, most of the fluid is directed to the hot tank, while during discharge, the working medium flows to the cold tank, giving its stored heat to the production system. During charging, the cool liquid is pumped from the bottom of the tank and heated by the solarfield (direct storage) or heat exchanger (indirect storage) and then returned to the top of the tank. During the discharge, hot liquid is pumped from the top of the tank and with the provision of thermal energy to the power generation system eventually ends up at the bottom of the tank.

The thermoclean tank is based on the thermal stratification of the storage medium, which is the result of its density variation as a function of temperature. Suitable thermoclean storage means are those that exhibit relatively low thermal conductivity and have a temperature change limit. Under plant operating conditions, the amount of fluid in the thermocouple tank remains almost constant. What is moving vertically is the layer of temperature change (thermoclean), between high and low temperature bands, charging and discharging it.

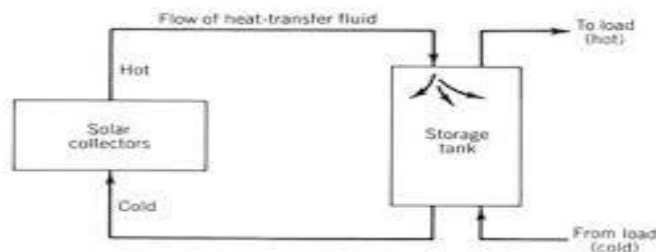


Figure 5.10 Single Tank Energy Storage System [52]

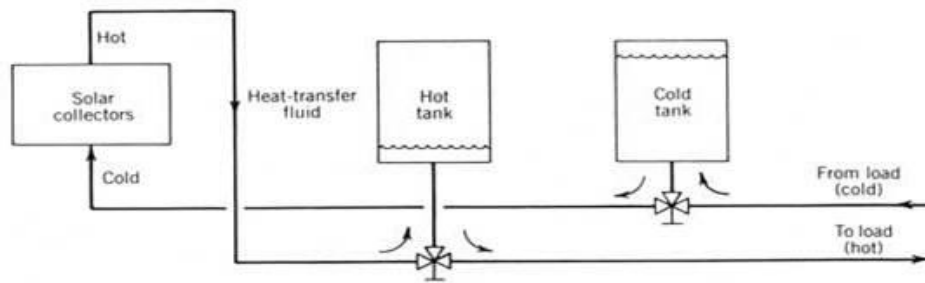


Figure 5.11 Double Tank Energy Storage System [53]

The working means used in storage systems are molten salts, sodium liquid, oils, water-vapor and various solids in cases where the solar receiver operates with air. The molten salts and the sodium liquid can be used both as a working means of transport and storage of the thermal energy of the central receiver. Storage can be done at temperatures up to 565 °C using molten salts and up to 595 °C using sodium liquid. The device used with these storage means is that of the separate cold and hot tank. The two-tank storage system with molten salts (60% sodium nitrate and 40% potassium nitrate) is the most mature and common option nowadays for solar power towers.

Heat transfer oils, such as Caloria, have higher specific heat and lower thermal conductivity than molten salts and sodium, however they can be used at relatively low temperatures up to 315 °C. This temperature limit restricts the use of oils as storage medium in installations where the central receiver uses water vapor or oil. In the case where the storage medium is the oil, the usual arrangement of the storage system consists of a thermoclean tank, although the arrangement with the two separate tanks can also be used. The high cost of oil transfer heat can be mitigated by adding stones to stockpile storage. The stones can store part of the thermal energy and replace the volume that would contain the corresponding amount of oil.

The use of water vapor as a thermal energy storage medium is also very common. The storage system arrangement includes a single reservoir in which saturated high pressure steam is stored. It is essentially a phase shift agent, as the steam condenses and evaporates again when the pressure drops during discharge. Water-steam storage systems have the advantage of being combined with a central solar water receiver that can synthesize a circuit that flows through a single fluid at each point, thus minimizing energy losses due to the absence of additional switches.

However, these storage systems are increasingly losing ground in their mineral storage systems, as they ensure the storage of heat for a short period of time. A last storage method uses air, which circulates through a large fan and transfers heat to a tank containing gravel or refractory glazing where it stores it. This avoids the use of expensive liquids, compared to cheaper solids. However, the fact that air is not the most suitable means of transporting and storing thermal energy, but also the requirement for large pipelines, compressors and fans makes this storage method less accessible.

Two tank systems use a hot and cold reservoir. During charging, the liquid is directed to the hot tank while it is directed to the cooling tank during the discharge, providing the stored energy to the power generation system.

The thermo climatic system of a tank uses a tank, and the thermal gradient separates the heat from the cold liquid. A low cost material is used to fill the tank and this acts as a storage medium, while reducing the cost of an expensive heat transfer medium. This material should be readily available, with relatively low thermal conductivity and high thermal capacity.

The thermal storage subsystem stores thermal energy captured by the receiver subsystem and delivers it to the steam generator system. Storage of thermal energy provides continuous operation of the plant during periods of variable isolation, extends plant operation into non - solar hours, avoids the potentially harmful transients arising from abrupt changes in isolation, insures power availability in emergency periods, and enables a shift of electricity generation to meet a demand profile which does not coincide with the isolation profile.

An attractive feature of thermo chemical storage is the potential for storing and transporting the constituents at ambient temperature. This aspect has generated significant interest for long term and even seasonal storage applications. Thermo chemical storage is attractive because high-grade heat could be stored at ambient temperature.

Sensible energy storage can be implemented in a central receiver plant in two ways: direct storage in which the receiver working fluid is the same as the storage media or indirect storage in which different fluids are used in the receiver and in storage. In direct storage systems, the temperature of the thermal energy delivered either from storage or from the receiver can be nearly the same. In an indirect system, an intermediate heat exchanger is used to charge storage. Temperature drops must be

provided between the receiver and storage and between storage and the load in order to transfer heat.

Therefore, the receiver must be operated at a higher temperature to charge storage than is needed to operate directly to the load; or, a lower temperature must be produced at, the load from storage than is produced directly from the receiver.[52],[53],[54],[71],[72],[78],[100]

5.2.5 Refugee Fuel Systems

The purpose of the backup combustion system is the same as the storage system, i.e. in cases of low or no sunshine, with this system being able to operate the plant. This also acts as a safety net for the station, since this does not stop the station. The difference from a thermal energy storage system is that the backup combustion system is the immediate solution for generating electricity, since it does not require charging like the system storage. Its use is optional and fossil fuel is used to heat the fluid. The devices that separate these systems are two, in series or parallel to the thermodynamic circuit.

In the most common arrangement, the backup combustion system is placed in the thermodynamic circuit parallel to the solar receiver by heating the heat transfer fluid when the temperature in the piping is low due to low solar radiation. This provision applies to direct and indirect steam generation systems. In direct steam systems, the backup burner heats the working medium intended for vaporization. In indirect steam systems, the backup burner heats the heat transfer fluid directed to the heat exchanger.

The second provision applies only to indirect steam generation systems. The backup burner is placed in the thermodynamic circuit in series with the heat exchanger. Thus, if the heat transfer fluid has a temperature that is not sufficient for steam generation through the exchanger due to low solar radiation, the backup burner heats the working medium and produces steam.

The choice of the appropriate back-up system depends on the initial design of the plant. Fuel selection depends on many parameters. When using liquid fuel (e.g. oil), storage tanks, pumping systems, etc. are required. The use of fuel gases requires piping

and compression systems, but they have less emissions of gaseous pollutants.[71],[72],[100]

5.2.6 Details of Subsystems

5.2.6.1 Master Control

The master control subsystem provides an overall command, control and data acquisition capability for a central receiver plant. This system integrates the control of the other subsystems to achieve effective single-console evaluation and control. A major part of the control system function is managing daily startup and shutdown. Since changing from one operating mode to another may involve numerous steps and considerations, the master control system may be used to automate these mode changes. Major benefits of a well-designed master control system with automation are that plant energy output is increased and reliability is improved.

The master control system is configured to control and monitor the overall plant as well as each of the major plant subsystems. Master control automatically directs heliostats to track the receiver and controls receiver flow. When desired receiver outlet conditions are achieved, the receiver fluid is directed to thermal storage. Control of the thermal storage, steam generator and turbine generator systems involves temperature, pressure and flow instrumentation to maintain and optimize energy storage and electricity generation.

When the collector field loses power, all heliostats tracking stop. If power is not restored for some time, the reflected beams will move slowly off the receiver in a direction relative to sun movement. The collector control system hardware/software design should be such that power can be restored quickly (hardware) and the field can be commanded to standby immediately after power is restored (software). The cost of these characteristics might be traded against the cost of improving the receiver design to provide some tolerance to flux levels with no fluid flow. Heliostats are built to withstand a certain wind speed. When this speed is exceeded, the heliostat should be positioned to a safe predefined orientation (high wind stow). This can be either a manual or an automatic operation.

The control system requires a number of support systems including electrical power, environmental conditioning, and fire protection. Uninterruptable power supplies (UPS) are desirable for all control electronic equipment and most other electronic equipment. The need is to provide the control system with enough power to shut the plant down safely and quickly.[71]

5.2.6.2 Water Consumption Requirements

The water consumed by a Rankine steam power conversion cycle is generally for two purposes:

- (1) evaporative removal of waste heat from the main condenser, and*
- (2) makeup of purified water to the steam cycle, to compensate for blow down leaving the steam generator.*

Of these, the evaporative removal of waste heat from the main condenser is the larger user of water. This evaporative cooling usually takes place in a wet cooling tower after the water has been heated by passage through the tubes of a surface type main condenser. Dry cooling is an alternative for plants located in regions with limited water supplies.

The amount of water consumed in the cooling tower is dependent on a number of factors, all of which can be varied during the design process to give an optimum balance between cooling efficiency, water consumption and capital costs. Significant factors include the actual atmospheric wet-bulb temperature, relative humidity when the plant is in operation, and the operating profile of the plant throughout the year. [71]

5.2.6.3 Heliostat Control

During plant operation, the heliostats require a control system to position the drive axes independently throughout the day. Two types of control systems have been considered for heliostat use: open loop and closed loop.

In an open loop system, the heliostat is programmed to point using temporal and geometric algorithms in the control computer software. In a closed loop system, a sun

sensor provides feedback to the control computer about whether the heliostat is pointing in the right direction to illuminate the receiver. Because of lower costs, an open loop system is the preferred approach. The need to control the heliostat beams accurately to insure beam safety requires an open loop control system with the same accuracy as for tracking.

Current collector subsystem control systems have three major elements: a heliostat array controller (HAC), a solar field controller (HFC) and a heliostat controller (HC). The HAC, a centrally located, oversight computer, provides information to many HFC's. Each HFC, located throughout the field, controls a group of heliostats (usually 32). The HC, located in the pedestal, controls the motors of an individual heliostat.

The control system must update the sun position and calculate new heliostat positions every few seconds since the angular relationship between the sun, the heliostat, and the receiver changes continuously as the sun moves at about 0.07 mrad/s per second.[71]

5.2.6.4 Heat Transport and Exchange Subsystem

The heat transport and exchange subsystem provides controlled fluid flow and thermal energy exchange among the solar receiver, steam generator, and thermal storage subsystems. It consists of the pumps, piping and heat exchangers which provide the physical and functional interfaces for these subsystems.

The arrangement of the heat transport and exchange subsystem is based on the heat transport medium and on the thermal storage tank configuration. The function of the heat transport and exchange subsystem can be served through combinations of three basic arrangements: common receiver and storage medium, separate receiver and storage media, and side-stream storage and heat exchange.[71]

5.2.6.5 Heat Exchangers

Heat exchangers other than the receiver and solar steam generator, are required for configurations in which the receiver and thermal storage media are different. For example, a water/steam receiver fluid will require a heat exchanger if the fluid contained in storage is oil. [71]

5.2.6.6 Insulation

Insulation is applied to all components for which heat loss or personnel safety associated with high temperature is a concern. Insulation thickness is determined by trade-offs between the added capital cost of insulation and the value of thermal energy lost over the plant life.

The insulation, typically of preformed calcium silicate, is secured to piping, valves, and other equipment. An inner layer of flexible, blanket-type insulation is occasionally applied over the heat-traced pipe and equipment. This minimizes convection losses through seams and gaps between the preformed insulation and the piping caused by the heat tracing. An exterior lagging is generally used to protect the insulation from environmental damage.[71]

5.2.6.7 Instrumentation

Typical instrumentation used in the heat transport and exchange subsystem includes flow meters, pressure gages, level sensors, thermocouples, and position indicators. This equipment is used for control and the collection of engineering data.

Pressure transducers are used for both pressure measurements and flow measurements. (Flow is determined by measuring the pressure drop across an obstruction such as a wedge or a venturi.) The pressure transducers must be isolated from the salt or sodium but at the same time must be able to sense pressure variations. This is usually accomplished with a fluid coupling through a diaphragm or bellows.[71]

5.2.6.8 Tower

The tower provides support for the solar receiver at the required height above the collector field. Tower height is primarily a function of the design point power of the plant; however, it is also influenced significantly by the receiver configuration and receiver fluid. The tower also provides support for the beam characterization system target, piping, and associated mechanical and electrical equipment. It transfers gravity loads from the tower and supported equipment to the subsurface beneath the tower foundation. It also transfers lateral wind and earthquake loads to the subsurface. The receiver is located at the top of the tower. The beam characterization system target is located on the outside of the tower just below the receiver. Electrical and control equipment for the solar receiver are located within the tower immediately beneath the receiver. Towers are constructed of steel or reinforced concrete. Principal receiver design issues and accompanying factors include: Receiver sizing (plant electrical rating, solar multiple, and required receiver thermal rating).

- *Energy collection system geometry (receiver configuration, tower height, and layout of associated collector field).*
- *Receiver heat transport fluid selection (type, inlet/outlet conditions, interface with storage and/or working fluid).*
- *Materials selection (operating temperature, mechanical properties, fabricability, sensitivity to thermal cycling, and compatibility with heat transfer media).*
- *Absorber surface design (flux limited design criteria, receiver fluid flow configuration, panel modularity).*

The overall design issues vary in importance and are interrelated when selecting and designing a receiver. Low cost is important, but it must not be obtained at the expense of high technical risk or with a design that is difficult to operate or maintain.

Receiver size is defined by its thermal rating and its active absorber area. The thermal rating needed depends on system level requirements: plant output rating (MW, for an electric plant), type of receiver fluid and storage media, nature of the electric power generating system, and solar multiple. The required receiver absorber rating for a given allowable peak flux limit, and roughly inversely related to the flux limit.

The minimum practical receiver size is largely a function of spillage considerations based on the size of the reflected heliostat beam and the size of its

target, the receiver absorber surface or cavity aperture. As heliostat size increases, the reflected beam size also increases even with focused and canted mirrors. The receiver size must also increase to keep spillage losses within reasonable values.

The minimum receiver size defined by heliostat image size is different for receiver heat transport fluids with different allowable flux levels. A fluid like sodium, for example, with a very high allowable flux level, may have very compact receiver designs, reaching the minimum receiver size based on heliostat image size at a higher thermal rating than for the lower flux fluid.[54],[71]

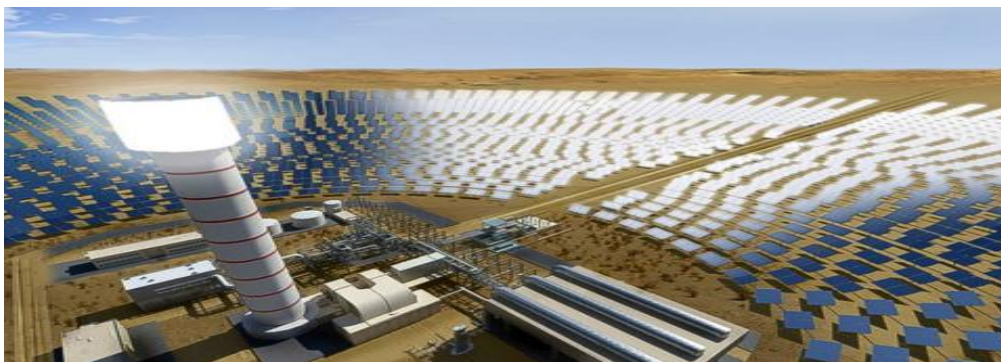


Figure 5.12 Solar Power Tower [54]

5.3 Performance and Losses

5.3.1 Evaluation

For assessing a solar energy tower, the energy losses and the performance of each subsystem is taken into account, also the percentage of incident solar energy that is converted into electricity. The main losses of a CSP are because of the solar field and the solar receiver. There are other losses from each subsystem, piping, alternators, turbines and generators.

The function of direct solar radiation ($I_{b,n}$) and the total area of the solar field (A_h) is the thermal evaluation of the CSP. The total performance of collecting energy is

$$n_{col} = \frac{Q_{useful}}{I_{b,n} n_h A_h},$$

where

Q_{useful} is the rate of thermal energy's addition in the heat transfer fluid and n_h is the number of the heliostats in the field. [72],[100]

5.3.2 Solstice Field Losses

Energy flows into our system through the solar field, but the solar field is also the main cause of losses (cosine, reflection, atmospheric attenuation, shadowing -blocking and spillage losses).

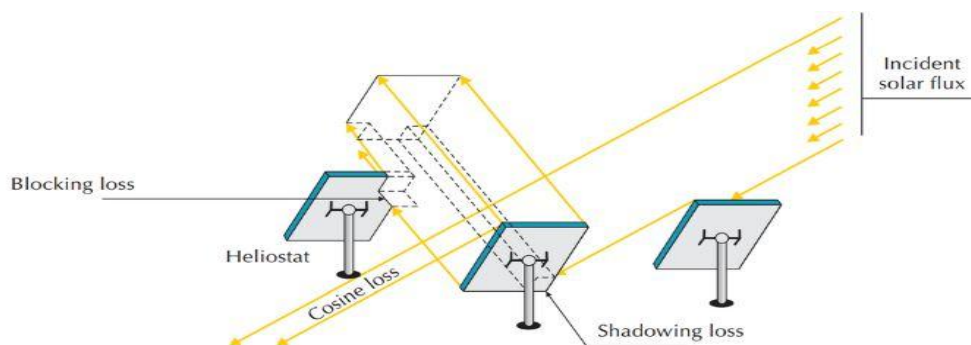


Figure 5.13 Solar Field Losses [52]

The total solar field yield is related to the product of the efficiency grades derived from the above parameters, $n_{field} = n_{cos} n_{refl} n_{att} n_{shadow} n_{blocking} n_{spil}$. It could be defined as the ratio of thermal power taken from the solar receiver to the energy caused by direct sunlight on the surface of the solar field or the ratio of the thermal power received by the solar receiver to the power incident through direct sunlight on the surface of the solar field.[71],[72],[100]

5.3.2.1 Atmospheric Attenuation

Atmospheric Attenuation losses depend on the distance between the heliostat and the tower. They are affected by the weather, and especially by humidity. Misty or humid atmosphere results in increasing these losses.

The radiation reflected by the trackers is refracted and absorbed by the atmosphere so it does not reach the solar receiver. Atmospheric permeability depends mainly on visibility and much less on the altitude of the field.

For a clear day (visibility 23km) the atmospheric permeability is

$$n_{att} = 0.99326 - 0.1046 S + 0.017S^2 - 0.002845S^3 \quad (5.1)$$

while for a misty day (visibility 5km) is

$$n_{att} = 0.98707 - 0.2748 S + 0.03394S^2 \quad (5.2)$$

where S is the distance between the heliostat and the solar receiver.[71],[72],[83],[100]

5.3.2.2 Spillage Losses

Spillage losses depend on heliostats and solar receiver, happens when the reflected rays from the heliostats do not reach the receiver due to failure, happening more often in systems with a tubular cavity receiver due to the small opening. The angle of deflection at the reflecting surface of the heliostat is responsible for these losses, it is dependent on the roughness and curvature of the surface.

The position of the heliostat is determined by the control system and is executed by the drive mechanism. It affects the deflection angles, deviation in the tracking system or in the drive mechanism, results in the wrong positioning of the heliostat surface and ultimately the diverging deflection angle resulting in spillage losses. Spillage losses increase when the solar receiver opening is small. They are reduced by using a larger opening or window operation. The bigger the opening is, the more thermal losses increase. Choosing the size of opening into a cavity receiver is a process that requires optimization.[71],[72],[74],[100]

5.3.2.3 Reflectivity Losses

Reflectivity losses depend on the efficient reflection by the heliostats of the solar radiation and are equal for all heliostats because they depend on the quality of the reflecting surface. Manufacturers have achieved reflective surfaces reflectance ratios of up to 94%. Reflection ratio is reduced as years pass.

Reflection losses also depend on the degree purity of the mirrors which depends on the location, rains, winds and ground consisting of soil. A solution to that is cleanliness of the mirrors. Reflectivity losses are equal with the product of reflection ratio and degree of purity.

The light energy from the heliostat field scattered from the receiver surface and escaping from the receiver. High absorptivity paint is used on the absorber surfaces to minimize reflective loss. Reflection loss is generally five percent or less with a freshly-painted absorber surface, but may increase during service as a result of degradation of the coating.[71],[100]

5.3.2.4 Cosine Losses

Cosine losses are the most significant losses in the solar field and depend on the position of the heliostats related to the location of the sun and the position of the solar receiver. Heliostat is positioned so that the vertical vector at its surface bisects the angle formed by the incident rays and the line between heliostat and receiver. The reflected trace of the sunset decreases in the cosine of half of that angle.

Heliostats that are placed opposite the sun have less cosine losses. The cosine performance for each heliostat is equal to the cosine of the angle of incidence θ in relation to the center of the heliostat,

$$n_{\cos} = \sqrt{\frac{\sqrt{2}}{2} [\sin \alpha \cos \lambda - \cos(\theta H - A) \cos \alpha \sin \lambda + 1]} \quad (5.3)$$

where α is the height of the Sun,

A is the azimuthal angle,

λ is the angle between the reflected radius and the vertical in the center of the sunset,

θH is the azimuthal angle of the heliostat relative to the base of the tower.

Cosine losses are also expressed by the relation

$$\cos 2\theta i = \frac{(z_0 - z_1) \sin \alpha - e \cos \alpha \sin A - n \cos \alpha \cos A}{\sqrt{[(z_0 - z_1)^2 + e^2 + n^2]}} \quad (5.4)$$

where α is sun's height,

A is the azimuthal angle, and

z , n and e are the coordinates of the tower and the heliostat. [72],[100]

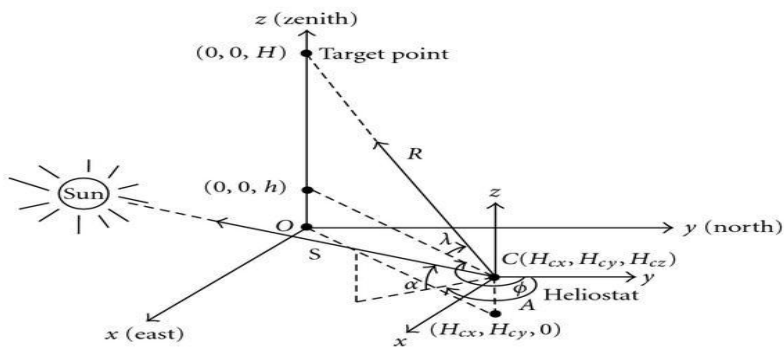


Figure 5.14 Cosine losses[55]

5.3.2.5 Shadowing and Blocking Losses

When the shadow of a heliostat covers the reflective surface of another, that is called shadowing, resulting in preventing the reflection of the incident radiation from it. When a heliostat prevents reflected radiation from a second heliostat, that is called obstruction, resulting in never reaching the solar receiver. Shadowing and Blocking Losses also include shadowing of the tower to the trackers during the hours in which the sun is behind the tower.

When the sun's height is low, the trackers are in almost vertical position, resulting in such phenomena being almost inevitably. Shadowing and obstruction losses depend on the distance of neighboring solstice, the slope of the soil, the height of the tower, the length of series of heliports, the schedule of soloists, the position of the sun and latitude. All these parameters contribute to the loss of shadowing and obstruction. The reducing these losses is an extremely complex process, as it consists of many factors that interact with each other. Minimizing these losses depends on the design of the solar field. Taking into account these parameters, the arrangement of the solar field is selected, and in this way we can control shadow and obstruction losses.[71],[72],[74],[100]

5.3.3 Solar Receiver Losses

After being reflected by the solar field the solar rays goes to the solar receiver. There is also a large percentage of its power losses installation, which we will discuss in this chapter. Losses that occur in a central solar receiver are convection, radiation, absorption and conduction losses.

The total efficiency of the solar receiver is the product of the above parameters

$$n_{receiver} = n_{conv} n_{radiation} n_{absorp} n_{conduct} \quad (5.5)$$

The efficiency of the solar receiver is also the ratio of the thermal power received by the heat transfer fluid to the receiver tubing to the total thermal power received by the outer surface of the receiver.[71],[72],[100]

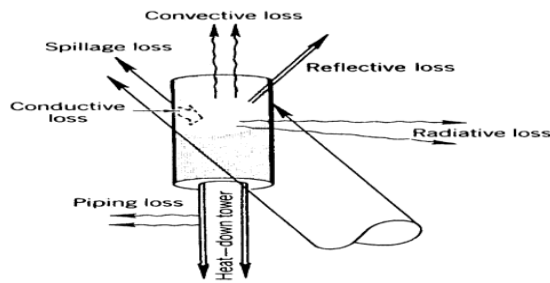


Figure 5.15 Solar Receiver Losses[55]

5.3.3.1 Absorption Losses

A percentage of the solar radiation that enters the receiver instead of being absorbed by the heat absorbing surface, it is reflected and escaped. In order to avoid this phenomenon the absorption surface of the receiver is coated with a high-absorbency black dye. The absorption losses therefore depend mainly on the receiver's surface, i.e. by the type of the coating. Over the years, aging of the dye has been observed which increases the absorption losses, so it is necessary to maintain the absorption surface of the solar receiver.

The absorption coefficient is calculated as the ratio of thermal power absorbed by the surface of the receiver to the thermal power that is incident on the surface from the solar field. Its prices absorption coefficient for a cavity receiver is at the order of 0.98.[71],[72],[100]

5.3.3.2 Convection Losses

The convection losses are the most important losses of a solar receive. Convection Losses are the thermal energy that is emitted by the colder air circulating tangentially to the surface of the receiver and result either from the air movement or the temperature difference. The magnitude of convection losses depends on the type of solar receiver, the surface area of the receiver, the tilt angle of the receiver, the temperature developed on the receiver, the temperature of the environment and the wind properties.

Convection losses in cavity receivers are increased by the size of the opening as well as the wind velocity, as also the angle of inclination of the receiver due to the greater amount of air that allows it to enter the interior of the receiver. Calculating convection losses depends on the solar receiver, the most widely used calculation method is Siebers' (1984). According to Siebers, convectional losses are

$$Q_{conv} = hA(T_w - T_a) \quad (5.6)$$

where A is the surface of the receiver,

T_w is the mean temperature of the walls of the receiver,

T_a the ambient temperature (calculated at 25 °C) and

h is the combined coefficient of free and forced convection that is calculated from

$$h = \sqrt[\alpha]{h_{fc}^\alpha + h_{nc}^\alpha} \quad (5.7)$$

where h_{fc} is the forced convection coefficient,

h_{nc} is the free-collector coefficient and

α is an empirical index analogous to the type of the solar receiver

(for a cavity receiver it is proposed $\alpha = 1$, while for an external cylindrical receiver $\alpha = 3.2$).

The free-to-air coefficient is

$$h_{nc} = 0.81(T_w - T_a)^{0.426} \quad (5.8)$$

while the forced convection coefficient is dependent on other parameters. For an external cylindrical receiver, due to the Kistler(1986), the forced convection coefficient is calculated due to the diameter (D) of the receiver. For $D \leq 4$:

$$h_{fc} = \left(\frac{1}{D}\right) [0.3 + 0.488 Re^{0.5} \left(1 + \left(\frac{Re}{282}\right)^{0.625}\right)^{0.8}] 0.04199 \quad (5.9)$$

where

$$Re = (1.751 \cdot 10^5) D \quad (5.10)$$

is the Reynolds' number.

For $4m < D < 125$, $h_{fc} = 14$ while for $D > 125m$, $h_{fc} = 33.75 D^{-0.19}$.

Kistler proposes a model of directly calculating of the losses for a solar cavity receiver, at which the convection losses are

$$Q_{conv} = Q_{forced} + Q_{nat} \quad (5.11)$$

where

$$Q_{forced} = 7,631 \frac{A}{W_{ap}^{0.2}} \quad (5.12)$$

are the forced convection losses and

$$Q_{nat} = 5,077 A_{cav} \quad (5.13)$$

are the free spill losses,

A is the area of the receiver opening,

W_{ap} is the width of the opening and

A_{cav} the area of the total surface inside the cavity. [71],[72],[78],[84],[100]

5.3.3.3 Radiation Losses

Radiation losses is the thermal energy that escapes through the emission of infrared and visible light due to the high temperatures that are developed in the solar receiver, they depend on the size of the receiver and the receiver's operating temperature.

Radiation losses are calculated from the relation

$$Q_{rad} = \sigma \varepsilon A_a (T_w^4 - T_a^4) \quad (5.14)$$

where $\sigma = 5.67 \cdot 10^{-8} \text{ W / (m}^2 \text{ K}^4)$

ε is the coefficient emission factor,

A_a is the area of the receiver opening,

T_w is the mean temperature of the receiver's walls and

T_a is the temperature of the environment.

Emission factor results from the relation

$$\varepsilon = \frac{\varepsilon_w}{\varepsilon_w + (1 - \varepsilon_w) F_r} \quad (5.15)$$

where ε_w is the emission of radiation from the walls of the receiver and

F_r is the projection coefficient, which is the ratio of the opening area of the receiver to the surface area of the receiver. [71],[84],[100]

5.3.3.4 Conduction Losses

Conduction losses is the amount of heat that escapes through the insulated surfaces and from the device that supports the receiver over the tower, depend on the insulation of all the surfaces and the contact of the receiver with the tower. Conduction losses are treated with insulation of the surfaces, minimizing the contact points between the receiver and the tower, using low thermal conductivity materials to support the receiver. Conduction losses fall below 1% if receive is designed properly, they are calculated due to the temperature difference and thermal conductivity that depends on materials and geometry.

Conduction losses result from the relation

$$Q_{\text{conduct}} = \frac{(T_{\text{rec}} - T_{\text{env}})}{R_{\text{th}}} \quad (5.16)$$

where T_{rec} is the temperature of the solar receiver,
 T_{env} is the temperature of the environment and
 R_{th} is the thermal resistance.

For one-dimensional heat loss through a single homogeneous layer of L -thickness and with thermal conductivity k , the relationship is formed

$$Q_{\text{cond}} = kA \frac{(T_{\text{rec}} - T_{\text{env}})}{L} \quad (5.17)$$

where A is the absorption surface.[71],[72],[100]

5.3.4 Other losses

Many parts of the system for their operation use electrical power that receive from the generator. The most demanding systems are those that have to heat up the fluid, when transport fluid is molten salts or nitrate, where there is a risk of solidification. Pumps of the system also consume a significant amount of energy. In power generation system we have the condensing pump and the feed pump. The required power depends on the fluid and on the required operating pressure of the system. The condenser cooling system, whether air-cooled (uses a fan) or water-cooled(uses a water pump), also needs electrical power, all these are the own consumption losses.

Piping is used so as the heat transfer fluid to take heat from the solar receiver, and then it leaks the of the power generation system. There are losses in the piping, which depend on the layout of the piping and the type of fluid, depending on the fluid, the losses vary, as also their handling. Pipe Losses may be linear along pipe lengths or point, at the points where there are valves or other accessories, possible leaks in the piping system result in thermal losses, which should be prevented by using a safety system and must be repaired immediately.[71],[92],[100]

5.3.5 Performance of a Power Generation System

After absorbing heat from the solar receiver, the transfer fluid is vaporized in the piping of the receiver or at the vaporizer via the alternator. Thermal energy that was received by the fluid during the cycle, is transformed into mechanical energy by the rotation of the turbine, that is then being converted into electricity through the generator. The ratio of the electrical power generated by the generator to the thermal power of the heat transfer fluid flowing through the solar receiver piping is the efficiency class of the power block, that shows the percentage of incoming thermal power that is eventually converted into electrical power.

Optimization of the efficiency of the power block is achieved in the design of the power generation system, it depends on the arrangement of the piping and the other components. If we know the characteristics of the fluid in the solar receiver and the turbine, i.e. the efficiency of the thermodynamic cycle it is easily calculated from the relationship

$$n_{\text{cycle}} = \frac{(m_{\text{turb}} \Delta h_{\text{turb}}) - P_{\text{pumps}}}{m_{\text{rec}} \Delta h_{\text{rec}}} = \frac{m_{\text{turb}} (h_{\text{turb},\text{in}} - h_{\text{turb},\text{out}}) - P_{\text{pumps}}}{m (h_{\text{rec},\text{out}} - h_{\text{rec},\text{in}})} \quad (5.18)$$

where m_{turb} is the steam supply to the turbine,

m_{rec} is the supply of transport fluid heat in the solar receiver,

Δh_{turb} is the enthalpy drop of steam during expansion in the turbine,

Δh_{rec} is the enthalpic increase in receiver piping and

P_{pumps} is the power consumed by the pumps in the power block.

The efficiency of the power generating system results from the product of the degrees of efficiency of the thermodynamic cycle, the storage unit and the generator,

that is $n_{\text{block}} = n_{\text{cycle}} n_{\text{gen}} n_{\text{storage}}$. (5.19)[71],[100],[125]

Chapter 6

Methodology of Designing the Solar Power Station

6.1 Design of Energy Collection System Localization - Dimension Procedure

In this chapter we will deal with the most important of the design parameters of one solar field, and we will focus on their impact on performance, these variables determine the final form of the installation. We will deal with dimensioning, with a set of criteria stemming from the current legislation, international bibliography, scientific research. The installation will be separated into two areas:

- a) the energy collection (solar field, the solar receiver, the tower and related piping) and
- b) energy recovery (steam generator, the power system, the system storage of thermal energy and conventional systems (if there are)).[71],[100]

Energy Collection system localization	Energy Collection system
Ground inclination	Solar Field
Power Block	Number of Heliostats
Design Point	Solar Field Layout
Heat and Storage Heat Transfer	Area and shape of reflective surface of Helios
Capacity Factor	Solar Multiple Ratio
Geographical Width	Solar Receiver
	Tower Height

Table 6.1 Factors that affect Energy Collection and Energy Recovery

6.1.1 Ground inclination

High-slope areas are problematic sizing areas of a CSP, due to the difficulty of accessing the road network for the construction and maintenance, and other difficulties associated with turbulence that occur more often on smooth sideways with steep slopes. The increase in the slope of the soil reduces the power output and, consequently, the energy produced. In general, for the construction of a solar field, sites with flat ground are recommended, there are cases in which one small slope of ground is inevitable and that may have an overall effect both positively and negatively in field performance, influencing the rate of its various losses.

A positive slope would considerably reduce the cosine losses as the angle of incidence of the solar rays on the surface of each heliostat would increase and the distance between heliostats and receiver would reduce, so the loss of atmospheric permeability would be reduced, in case of perimeter solar field, in the north field of the tower. A positive slope would reduce the shadow and obstruction losses, the provision would become more dense. A negative slope would have a positive effect on the cosine phenomenon in the southern part of the field, it would have a negative effect on atmospheric permeability as there will be a need for a more sparse solar field arrangement to reduce the loss of obstruction. The positive slope of the solar field in the direction of the north increases its efficiency, the negative slope throws it. For negative gradients, less than 5% of the impact on the degree of efficiency of the field is not so significant as to economically benefit the leveling of the soil.[64],[43],[100]

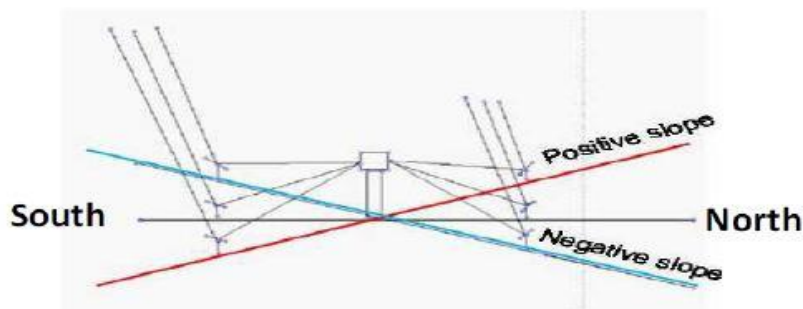


Figure 6.1 The effect of the slope of the Solar Field [43]

	NORTH part of the field				SOUTH part of the field			
	Horiz	5 %	10 %		Horiz	5 %	10 %	
Gamma cosine	0.8114	0.8073	0.8031	-	0.6750	0.6803	0.6853	+
Atmospheric effic	0.9282	0.9288	0.9294	+	0.9432	0.9426	0.9419	-
Intercept effic	0.8809	0.8841	0.8877	+	0.9369	0.9355	0.9329	-
Blocking&Shadow	0.9360	0.9423	0.9474	+	0.9455	0.9502	0.9538	+
Ann Field efficiency	58.5	58.8	59.0	+	52.3	52.8	53.3	+
Aver Power / hel (Kw)	50.0	50.3	50.4	+	44.7	45.2	45.6	+
N° heliostats	2498	2484	2464		1502	1516	1536	

Slope	-10 %	-5 %	horizontal	5 %	10 %
Ann Field eff.	56.0 %	56.6 %	57.1 %	58.1 %	58.4 %

Figure 6.2 Solar Field Efficiency Degrees vs. Ground inclination and annual Solar Field Efficiency Gradient for Ground inclination $\pm 5\%$, $\pm 10\%$ [43]

6.1.2 Power Block

The Power Block is the steam turbine - generator system. At a solar thermal station it is the same as conventional systems. Its characteristics sets the fluid requirements (pressure - inlet fluid temperature), depends on the required power and affects all other parts of the plant.[72]

6.1.3 Design Point

An important element for determining the nominal station sizes is the design point. Since sunlight differs at any time, we define a specific point in time as a design point. At the design point the station is dimensioned and the performance grades for its subsystems are calculated. Choosing the right design point is extremely important as it affects the final generation of energy over time.[71]

6.1.4 Heat and Storage Heat Transfer

Heat transfer fluid is selected due to the availability of the plant and the rated power, it affects the overall operation of the station, it depends on many factors. When water is used in systems with direct steam generation in the receiver, thermal energy storage potential is not efficient with respect to molten salts. Temperature and type of steam entering the steam turbine determines the fluid to be selected. Choice of fluid depends also on cost of the fluid, availability and thermal energy storage unit etc.[71],[72],[100]

6.1.5 Capacity Factor

The Capacity Factor is important for station dimensioning, and is calculated as the ratio of the annual energy output to the energy the unit would produce if it operated at full load per year so it depends on the design point and the station performance.

In the design and technology selection process, a range of values is initially defined as the exploitation coefficient and is determined after annual performance simulations for the optimal design of the plant. The exploitation rate is directly related to energy efficiency of the plant, but also the final annual energy production. In the design process, we can define the range of the exploitation coefficient, depending on the solar radiation. From existing studies, it has emerged that for a station without a storage system the operating rate is close to 25%, and if there is a storage system it can exceed 60%.[71],[43]

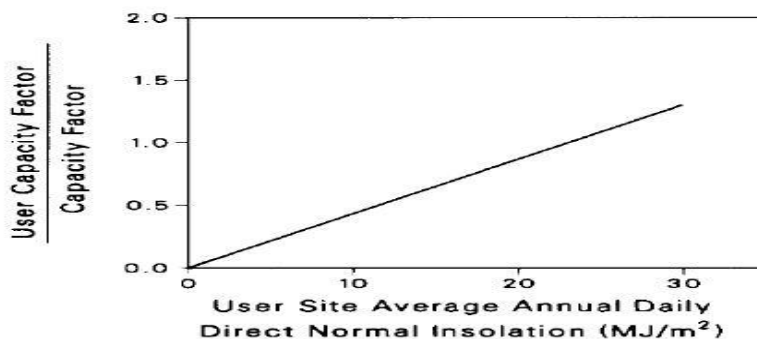


Figure 6.3 Capacity Factor- Solar Radiation [43]

6.1.6 Geographical Width

The latitude of the location indicates the maximum amount of solar energy reaching the point, so it is obvious that the location of the installation should be determined in order to know the weather conditions of the point that are affected by the altitude and the surrounding area (mountains, water and / or urban areas).

Locations that are suitable for the installation of solar thermal stations are located at latitudes from 10th to 40th and in both hemispheres. Since there are locations with similar direct solar radiation at different latitudes, we are able to look at differences in layout, tower height and receiver size-height accordingly with latitude.

The solar field in regions near the equator is smaller in extent, because the sun is constantly in a vertical position, the heliostats will be more in a horizontal position and so the height of the tower should be larger. Therefore, field performance will be bigger in smaller latitudes. This happens due to the reducing of shadowing and obstruction losses, but also due to reducing the loss of atmospheric permeability due to the low extent of the field, despite the increased cosine losses.

For a 100MWe solar power tower without storage system, 480,000 m² (4,000 solar trackers with 120 m² surface area) are reflected in the solar field for different latitudes. It is interesting to observe how the solar field evolves from circular to equatorial, to a greater extent and more northward orientation to the larger latitudes. In small latitudes, the solar field is denser due to the operation of the heliostats in a horizontal position for most of the day, while the tower should have a higher height. The area of the field at 0° latitude varies from 1.8 km², while at latitude 60° it is 3.4 km².

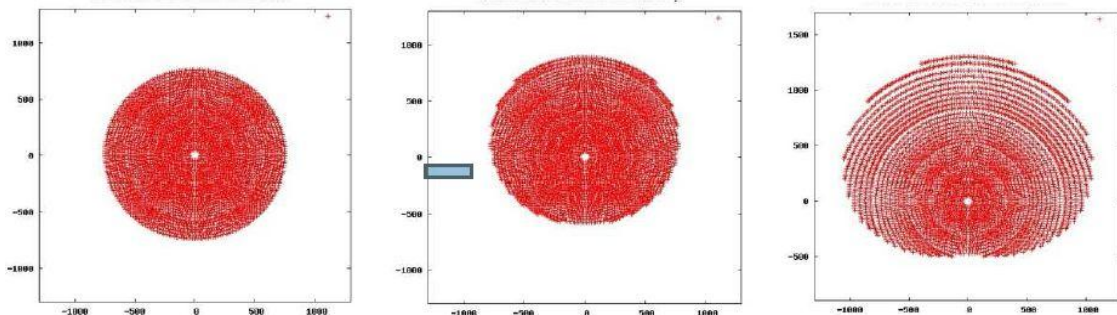


Figure 6.4 Perimeter Solar Field for Geographical Width 0°, 20°, 60° [43]

Latitude	0°	10°	20°	30°	40°	50°
Tower height	210	202	199	191	186	178
Last row north	809	871	929	987	1158	1270
Design Point Eff	67.6 %	67.2 %	66.6 %	65.3 %	64.7 %	62.4 %
Annual Field Eff	57.5 %	57.2 %	57.0 %	56.8 %	55.9 %	53.3 %

Figure 6.5 The effect of Geographic Width on the solar field [43]

We understand that appropriate Geographic Width is that of 10° -40°, the solar field near the equator is smaller and the efficiency of the field is greater in smaller Geographic Width. In small Geographic Width, the surface of the field is small, the field is denser and the tower is higher. The smaller the latitude is, the tallest the tower is, the higher design point efficiency and annual field efficiency we have.[64],[43],[127]

6.2 Design of the Energy Collection System

The plant's dimensioning is required for the optimization of the energy collection sector, the energy efficiency factors and the costs associated with the converted solar thermal energy.[71]

6.2.1 Solar Field

The design of a sun-storm field is the most difficult process that an installation faces, most losses at a solar power tower station come from the solar field, so a detailed study of all the parameters is necessary.

Many parameters are responsible for the optimal performance of a solar field and the purpose of the design is to reach the receiver the maximum possible amount of energy using the minimum possible field area, at the lowest cost. The solar field is designed and optimized due to the origin of potential losses. The degree of efficiency of the solar field is defined as the ratio of the thermal energy reaching the solar receiver to the direct solar radiation received by the trackers,

$$n_{\text{field}} = \frac{Q_{\text{inc}}}{Q_{\text{useful}}} \quad (6.1)$$

where N is the number of heliostats,

A is the surface area of the reflector surface of the heliostats,

I is the direct sunlight and

n_{avail} the availability coefficient of the solar field (usually taken as 0.99).

For a system that produces 320 MW_t with an external cylindrical receiver, the annual efficiency of the solar field ranges from 57% to 59% using sodium or molten salts as heat transfer fluid. For a corresponding cavity receiver and fluid molten salt system, the field yield was calculated at 64%. [71], [100]

6.2.1.1 Number of Heliostats

The number of solar heliostats is proportional to the power we want to be produced by the solar thermal station. The need for more heliostats may result in a reduction in the performance of the track, as the above-mentioned heliostats are placed further away from the tower and the losses are increasing.

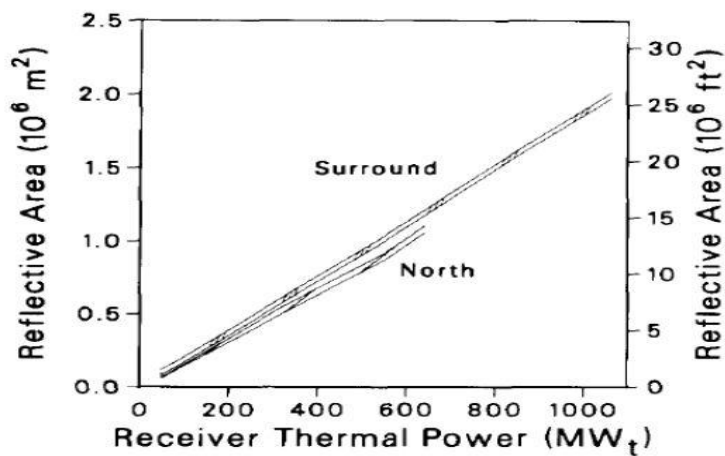


Figure 6.6 Reflective Surface Required vs Solar Thermal Required of Receiver [43]

A factor that alters the number of solar heliostats, is the choice of the solar receiver and the arrangement of the solar field. For an external receiver with a perimeter field, the heliports required are more than a cavity receiver and a northern field. In Figure 6.6, we observe the required reflective surface of the field relative to the desired thermal

energy in the receiver. Knowing the reflecting surface required, we can calculate the number of heliostats required, depending on the size of the reflector surface of the heliostat.[71],[43],[100]

6.2.1.2 Solar Field Layout

Initially we have to choose the appropriate array of the field, possible provisions are the North - South Field Layout and the Surrounding Field Layout. The choice of the device depends on the desired power and the type of solar receiver. With a cylindrical receiver, perimeter layout is selected since the receiver receives energy around it. With a cavity receiver, the opening is on one side, the North or South layout is selected. If we want to increase the power, more heliostats have to be used, resulting in a greater distance from the tower. Due to atmospheric permeability, the losses would increase so that it would not be advantageous to add heliostats. Stations with higher power, the arrangement of the field of elusive is perimeter.

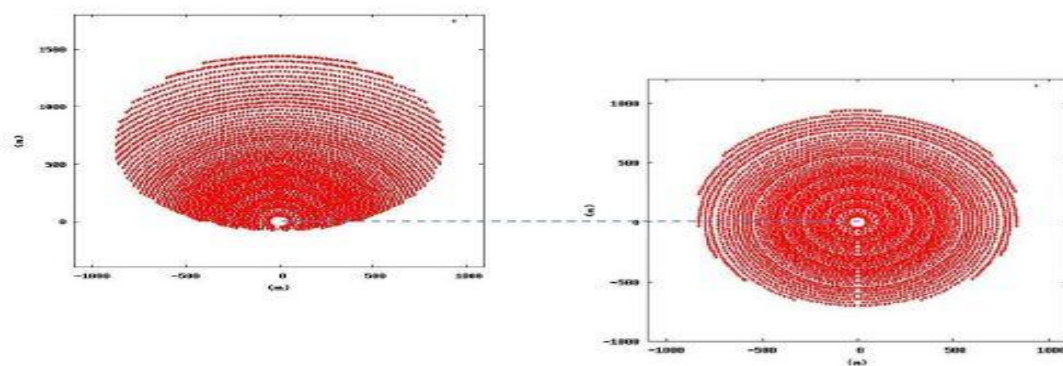


Figure 6.7 Northern vs Perimeter Solar Fields for Power Plant 90 MWe[43]

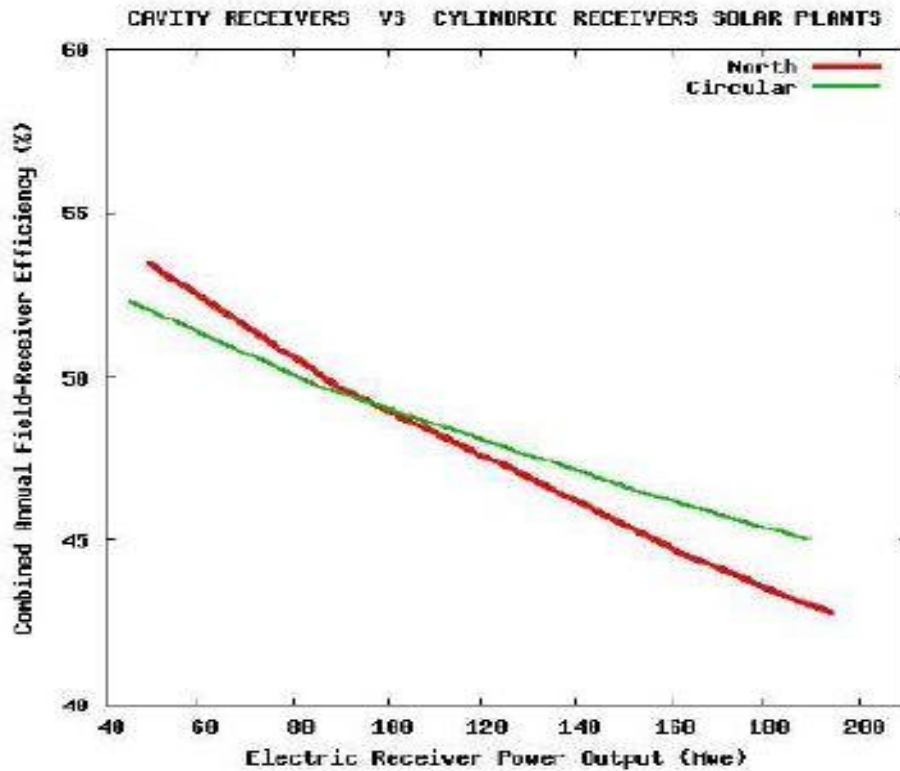


Figure 6.8 Combined performance Degree of Solar field - Receiver, for Northern and Perimeter Solar field vs. Power [43]

To minimize the loss of shadows between the heliostats, the trackers should not be placed too close together so the footprint of each tracker will be able to reach the solar receiver. By increasing this distance, we increase the cost due to the need for a larger area of the solar field. For North or South towers, there are two predominant motifs for the trackers, the Cornfield type, in which the trackers are placed in straight lines and at a uniform rectangular distance and the Staggered Field, where the trackers are aligned radially along the concentric circles centered on the tower, so no sunbird is placed behind or in front of another tracker.

The radial staggered device is the most efficient for a given extent, most tower solar thermal stations are designed like this, as the required field size and consequently atmospheric permeability losses are minimized. The northern array layout requires more heliostats at a distance from the tower in relation to the perimeter; this is negative for the cavity receivers, since as the size increases, the shadowing, obstruction and atmospheric permeability increases, while fewer cosine losses occur. In installations with

high power it is preferable to select the circumferential arrangement with a cylindrical receiver, while for stations with lower power the northern cavity receiver arrangement is preferable. The dividing point between north and perimeter field is about 90 MWe without a storage system (Figure 6.8). The combined efficiency of a solar field-receiver for a 50 MWe power station without a storage system would be 3% higher with a northern cavity arrangement and receiver. For a power station of 150 MWe without a storage system the efficiency would be 4% higher with perimeter layout and cylindrical receiver. For stations with the possibility of storage of thermal energy for 6 hours, the separation point would be at 50 MWe.[43],[64],[71],[72],[100]

6.2.1.3 Area and shape of reflective surface of Heliostats

It is widely perceived that the use of larger surfaces per heliostat reduces the cost of the installation. Reducing the number of trackers, the cost of the control and movement systems of each tracker is reduced, as also the operating and maintenance costs. Heliostats are built with a reflective surface of more than 100m².

Comparing two solar fields consisting of 10m² and 200m² surface heliostats, the size of the reflector surface of the heliostat has no effect on the annual performance. The criterion of selecting a small or large surface area of a tracer remains the cost per m². Assessing costs, soil preparation, electronic systems and communication systems, as well as estimated operating and maintenance costs, play an important role. Studies show that the largest reflecting surfaces of a heliostat are cost-effective, but the size of the heliostat has a significant impact on the size of the receiver. Sliders with a lower reflective surface require a relatively smaller receiver and this is a positive effect for cost and thermal loss. From the first solar thermal stations, the shape of the solar heaters is almost square, and the width to height ratio plays an important role in field performance.

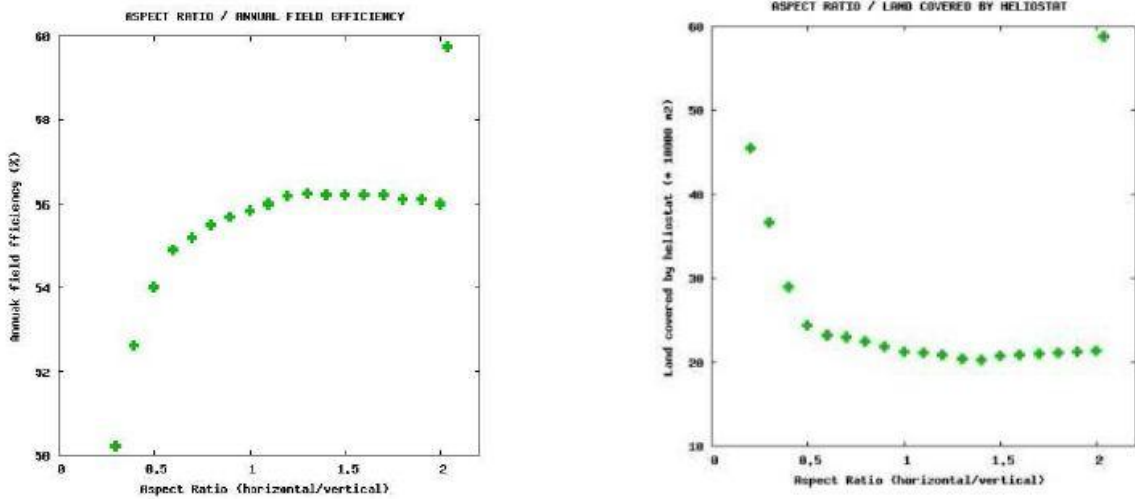


Figure 6.9 Solar Field Performance and Required Area to Width-Height ratio [43]

By increasing the height of the heliostat in relation to the width (Figure 6.9), the annual field yield is reduced due to the increase in shading and obstruction losses, while the required area of the field is increased. By increasing the width of the helix with respect to height, the degree of efficiency is minimally increased, but the area of the field decreases. The optimal shape of a helix could be a width ratio - 1.2, which would help to increase the annual field yield rate by 1% compared to a square-shaped helix.[43],[64],[73],[100]

6.2.1.4 Solar Field

An important factor for installing CSP is the proper placement of the trackers. The points to be placed arise after studies and depend on many parameters. This complicated process is designed to transfer the maximum possible solar radiation to the receiver with the least possible loss.

We have to select the arrangement of the field and according to the required power of the station and location, and after simulations, a northern or circumferential arrangement is selected. Then, the solar field pattern is selected. After research on the correct determination of the coordinates of the solar trackers in the field, codes have

been developed for the automatic calculation and optimization of the solar field. Optimized radial scaling devices were developed at the University of Houston (Lipps & Vant-Hull, 1978), resulting in a means of determining the spatial positioning and density of an early field helix. The radial distance between the ΔR solar trackers and the azimuthal distance ΔA was defined by Dellin (DELSOL 2, 1981) and is reported by Knightler (DELSOL 3, 1986) for highly reflective ($> 90\%$) helixes in large fields. So it is true that the radial distance should be

$$\Delta R = (1.4424 \cot \theta_L - 1.0935 + 3.0684 \theta_L - 1.125 \theta_L^2) \quad (6.2)$$

and

$$\Delta A = WM \left(1.7491 + 0.6396 \theta_L + \frac{0.2873}{\theta_L - 0.04902} \right) (m) \quad (6.3)$$

where WM the width of the heliport.

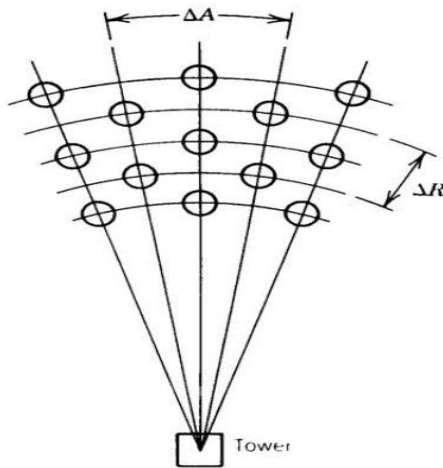


Figure 6.10 Radial Staggered Layout [43]

The angle formed between the ground and the line joining the center of the sunset with the solar receiver is the angle of altitude of the receiver, θ_L , and is denoted by the relation

$$\theta_L = \tan^{-1} \frac{TH}{R} (\text{deg}) \quad (6.4)$$

where TH is the height of the tower and
 R is the distance of the heliport from the base of the tower.

The azimuthal angle θ_L between two successive heliostats located at the same radial distance is defined as

$$\theta_A = \frac{\Delta A}{R} \quad (6.5)$$

The area around the tower is divided into concentric zones during spatialization of the solar field, where radial and azimuthal distance is used to determine the mean or center pattern for each zone. The density of the heliostats of each band is defined by the relation

$$\rho_F = \frac{2DM \cdot DMHM}{\Delta R \Delta A} \quad (6.6)$$

where DM is the ratio of the reflecting surface to the total surface of the heliostat.

There is the possibility, if large bands are selected, the azimuth distance ΔA cannot be maintained. Heliostats that are close to the inner ring of each zone are more likely to experience mechanical interference or unacceptable loss of shading and blocking. The demarcation of the solar field is determined by the height of the tower and the type of solar receiver. The radial distance of the first and last series of transmitters as defined by the DELSOL code is successively

$$R_{min} = 0.8 TH \quad (6.7)$$

and

$$R_{max} = 7.15 TH \quad (6.8)$$

The maximum azimuthal distance for systems north of the tower is calculated geometrically according to the solar receiver, i.e. the shape of the receiver opening, the angle of inclination and the angle of reception. So after separating the solar field into zones and knowing the density of each belt in the trackers, we are able to find the coordinates of each tracker in the field, knowing the azimuthal angle for successive radial heliostats, we can find the coordinates of all the heliostats in the same radius.

The first belt hunter on the y axis will have a abscissa equal to 0 and ordinarily equal to the smallest possible distance from the base of the tower in accordance with the belt constraints or boundaries. The next tracer in the first quadrant will have a ordinate defined by the relation

$$y = R \cos\left(\frac{\Delta A}{R}\right) \quad (6.9)$$

while the abscissa will be

$$x = R \sin\left(\frac{\Delta A}{R}\right) \quad (6.10)$$

where R is the distance from the base of the tower. The second runner in the series will have an ordered

$$y = R \cos\left(2 \frac{\Delta A}{R}\right) \quad (6.11)$$

and a cut

$$x = R \sin\left(2 \frac{\Delta A}{R}\right) \quad (6.12)$$

and so on. The abscissae in the second quadrant are the same as the first with a changed sign. For the third and fourth quadrants, the coordinates are the same as those located above the x-axis with opposite signs. Knowing where a series of soloists is placed, the variables change according to the distance of each row from the base of the tower R for the next rows. The calculation of the distance R is calculated differently for the even rows than for the single rows. The third row is calculated as the sum of the distance of the first row and the radial distance ΔR .

The distance of the second row can be calculated, knowing the distance of the third row, using relation

$$R_2 = R_1 + \frac{R_3 - R_1}{2} \quad (6.13)$$

This calculation is different for the even rows, as the y-axis is not mounted on the y-axis. In the first quadrant the first soloist will have an ordered

$$y = R \cos\left(0.5 \frac{\Delta A}{R}\right) \quad (6.14)$$

and a cut-off

$$x = R \sin\left(0.5 \frac{\Delta A}{R}\right) \quad (6.15)$$

The other one will have an ordered

$$y = R \cos\left[(0.5 + 1) \frac{\Delta A}{R}\right] \quad (6.16)$$

and a cut-off

$$x = R \sin\left[(0.5 + 1) \frac{\Delta A}{R}\right] \quad (6.17)$$

and so on. In the remaining quadrants it is true that it was mentioned above for the first series of Heliostats. We see that the azimuthal distance ΔA is increased enough to allow other trackers to be placed between as we continue the process, it is necessary when this distance exceeds at least twice the required space of each tracker. In this case, we re-calculate the coordinates of the series, reducing the azimuthal angle θ_A by $\frac{1}{2}$. [43],[71],[72],[74],[79],[80],[82],[83],[84],[100]

6.2.1.5 Optimization Codes

Due to complexity of spatialisation of the solar field, errors are likely to be made. This process is very time-consuming, and as a solution codes have been developed, calculating and positioning the field tracers in the solar field. They minimize losses and costs, to be able to spatially position and optimize the field of sunshine. The RCELL code (Houston University) simulates field operation, places the heliostats in space, calculates the heat flow for each or all of the field (TieSOL application). The DELSOL 3 code (Kistler, 1986) is the most widespread. Firstly basic parameters must be inserted (height of the tower and the geometry of the solar receiver), and this code divide the field into zones and give us the density of heliostats in each zone, but also specific coordinates DELSOL 3 produces heat flow maps for the receiver and can calculate their system performance degrees in all areas of the installation.

More recent codes are HFLD code by Chinese Academy of Sciences, optimizing the field of sunshine and HFLCAL, which is the evolution of the first code developed by

MIRVAL, and now belongs to the German Aerospace Center (DLR).[71],[74],[80],[81],[100]

6.2.2 Solar Multiple Ratio

Solar multiple ratio is determined at the design point, defining the energy collection and is defined as the ratio of thermal energy in the solar receiver to the input of thermal energy to the turbine. Over-dimensional ratio is greater than 1, since excess heat can be stored. Although it is linked with the rate of exploitation, it is important to understand their differences. The over-dimensioning ratio is a design and sizing variable, while the exploitation coefficient is a parameter of energy efficiency.

While the over-dimensional ratio is constant, the operating factor can be reduced by a number of factors (e.g. weather). The range of the over-dimensional ratio depends on the thermal energy required by the system. Its price should be increased to cover the need for excess energy, as there is a thermal energy storage system. By increasing the ratio of over-dimensioning, a larger field surface area is required, resulting in increased cost. A 100 MWe system with solar multiple ratio of 1.5 can store thermal energy for about 3 hours and requires an area of 2.6 km², while a system with a ratio of 2.1 can store thermal energy for about 9 hours.[43],[71],[100]

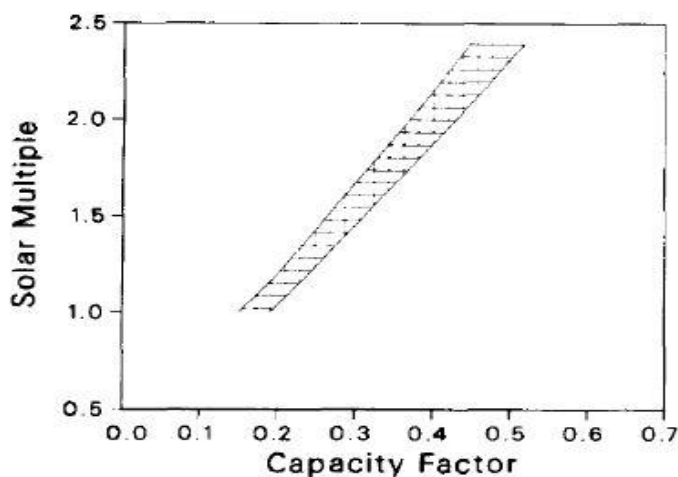


Figure 6.11 Solar multiple to Capacity factor[43]

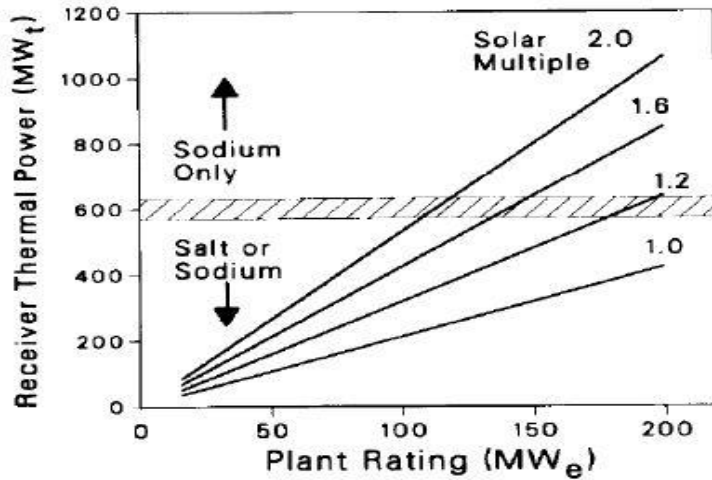


Figure 6.12 Thermal Power of the Solar Receiver with respect to Power and Ratio of Over-Diffusion of the System [43]

6.2.3 Solar Receiver

Solar receiver sets the boundaries of the solar field and determines the layout, depended on the thermal capacity of the heat transfer fluid. Tower is also constructed to handle its weight, depending on the receiver. Cylindrical receivers are selected for the perimeter of the tower, while for devices north of the tower, reflected radiation is focused on one side, the cavity receiver is selected for its low heat losses.

When cavity receiver, the geometric limits of the solar field are set by the area of the aperture and the angle of inclination. Larger open area means a larger solar field, resulting in increased losses (atmospheric permeability and thermal losses of the receiver). The change in receiver slope changes the demarcation of the solar field, resulting in a possible reduction in field performance. The efficiency of the solar receiver is defined as the ratio of the thermal energy received by the transfer fluid in the piping to the thermal energy received by the receiver from the solar field,

$$n_{\text{receiver}} = \frac{Q_{\text{net}}}{Q_{\text{inc}}} \quad (6.18)$$

The thermal energy that fluid receives is $Q_{net} = m \Delta h$,
 where m is the flow rate of the transfer fluid to the receiver piping and
 Δh is the difference in enthalpy $h_{outrec} - h_{inrec}$.

The thermal energy received by the receiver from the field of the heliostat can be defined as $Q_{inc} = N A_{heliostat} I n_{field} n_{avail}$ (6.19),

where N number of heliostats,

$A_{heliostat}$ the area of reflector surface of the heliostat,

I direct sunlight,

n_{field} the degree of efficiency of the solar field and

n_{avail} the availability coefficient of the solar field (usually obtained by 0.99).

For defining the dimensions of the solar receiver, basic factor is the active or radiant absorption surface. For given design and thermal constraints, such as the thermal flow limit, the absorption surface is proportional to the maximum thermal power of the receiver. Shape of the receiver depends on the size, and is characterized by the height - width of the opening of the cavity receiver or by the height - diameter ratio of the outer cylindrical receiver. The width of the opening width for the cavity receiver ranges from 0.7 for small receivers to slightly above 1 for large receivers. Height-to-diameter ratio for external cylindrical receivers ranges from 1 to 2 for very large systems.

The selection of the solar receiver type depends on the heat transfer fluid and on the technology of the production power system. The receiver's typical sizes is affected by thermal energy absorbing surface, as for specific design modes and defined heat flow limits, the absorption surface depends on the maximum thermal energy required. A limit of thermal energy flow should be set, so as to dimension the receiver.

The heat flux in the solar receiver requires the crash and stress tests of the receiver piping in a particular thermal or hydraulic design. The heat flow is dependent on the heat transfer fluid and the piping construction materials. The heat that the solar receiver receives from the solar field must be distributed evenly. Detailed analysis is required to determine the proper targeting of the radiation from the transmitters to the receiver (footprint) so that the heat levels on the receiver surface are properly distributed by minimizing leakage losses.

When tunnel footprints are defined in the receiver, the sliders with the smallest shadow and obstruction losses are selected for targeting at a point other than the center of the solar receiver to distribute the heat flux across the receiver surface. Since it is not possible to obtain an appropriate heat flow in the receiver, the process is repeated by increasing the size of the receiver to reduce the losses. The limit of the thermal flow is based on the working fluid and the materials made by the piping of the receiver.

In the outer cylindrical receivers, due to the better optical performance of the heliostats located north of the tower, the maximum heat flow is located on the northern surface of the receiver. Based on this pattern of heat flow on the surface of the receiver, the local flow of the heat transfer fluid can be examined as well as the maximum temperature in the piping of the receiver.[72],[79],[100]

6.2.4 Tower height

Tower provides support for the solar receiver at the appropriate height, but also support for piping and all relevant electromechanical equipment, it transports the gravity loads of the tower and the equipment, and the loads of winds and earthquakes at levels below its foundations. The design determines the height and is significantly influenced by the properties of the receiver but also from the heat transfer fluid. The appropriate height of a tower depends on parameters, like cost and performance of other subsystems, on solar field, the arrangement of which is determined by the height of the tower.

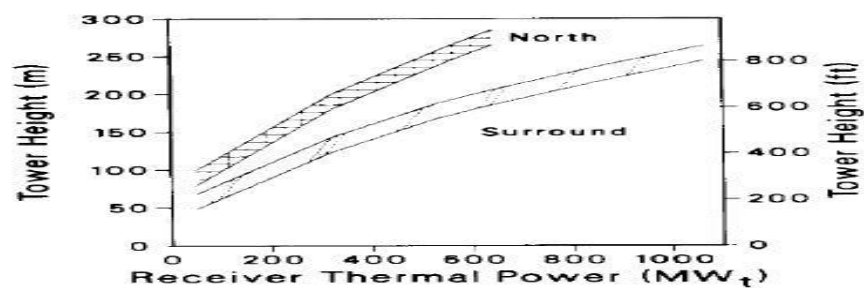


Figure 6.13 Height of Tower vs Thermal Energy of Solar Receiver for Northern and Perimeter Solar Field [43]

Cost can limit the height of the tower. Factors that affect the construction of the tower are the loads of the winds, the weight, the seismic activity and the heat transfer fluid used. There are two way of construction, a concrete and a steel frame (mesh).When concrete, the chimney construction techniques are followed. When steel frame, the technique followed is the same as the construction of an oil drilling tower.

Steel construction is cheaper at tower heights of less than 120m and the construction with concrete is cheaper at higher heights. A solar field north of the cavity receiver tower requires a taller tower than a tower around the tower and a cylindrical receiver. The height of the tower affects the cosine, field obstruction and shadow losses. Higher tower height reduces these losses but increases the cost. A taller tower provides a denser layout of the field, increasing the height of the tower, increases atmospheric permeability losses due to the greater distance the reflected rays have to travel.[43],[71],[72],[100],[127]

6.3 Use of Energy - Design of Thermal Energy Storage System Size

Optimization of the energy sector leads to production of thermal energy at the lowest cost. The dimensioning of energy utilization parameters is an assessment of the use of energy rather than detailed optimization. The size of the storage system is related to energy requirements throughout the station and with the energy collection sector. The basic factors affecting the size of the storage system are :

- a) Turbine performance
- b) Thermodynamic efficiency of the cycle
- c) Operating factor and
- d) Mode of operation of the plan.

Left in Figure 6.14, we see the operating hours of the storage system to the maximum energy efficiency of the turbine as a function of the capacity factor. The hours displayed in the graph result from the minimum stored energy requirement associated with purely stored thermal energy. This quantity is determined by the difference between

the energy in the collection section and the energy required to supply the turbine. Right on Figure 6.14, we see the storage capacity for different turbine sizes as a function of the capacity factor. Thermal energy storage tanks do not differ from large oil reservoirs and their dimensions have a height-diameter ratio of less than 1. The fluid transport systems consist of pumps for fluid circulation. [43],[71],[100]

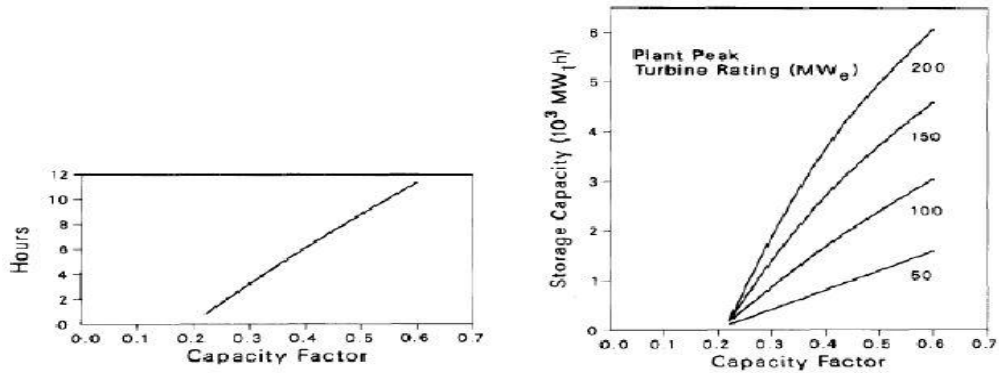


Figure 6.14 Energy Storage System Size vs Capacity factor [43]

6.4 Annual Electricity Production Assessment

Annual energy production calculation depends on weather conditions and station mode, so it is difficult to accurately estimate using simplified design rules. Computational models for the energy flow in a station are used, using real meteorological data and realistic estimates for the supply of subsystems.

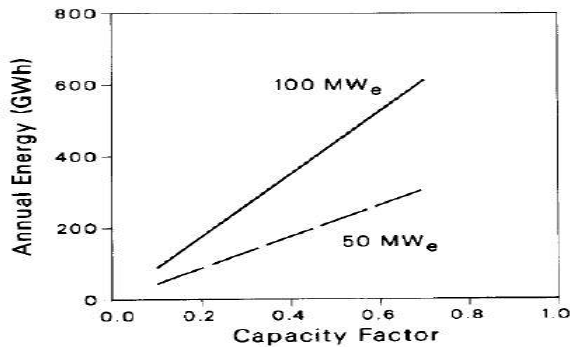


Figure 6.15 Annual Produced Energy vs Capacity factor [43]

Studies show that based on the relationship between the operating factor and the over-estimation factor, we can calculate the annual energy output of the system. The operating factor is defined as the ratio of the average annual energy produced by the system to the energy generated annually at the design point, knowing the operating factor we can find the annual energy output, or

$$\text{operating factor} = \frac{\text{average energy produced annually}}{\text{energy generated at the optimal design point annually}} .$$

[71],[43],[127]

6.5 Energy Cost

Energy cost is weighted cost, derived from the ratio of the plant's annual cost to annual energy production. Sum of the costs of each station sector, capital cost, which includes all the costs incurred before the operation of the station is firstly calculated, necessary for the calculation of the weighted energy cost. This include direct and indirect costs, unexpected costs and the cost of starting the plant. It is estimated that indirect costs, unexpected costs and start-up costs amount to 20% - 35% of direct costs. Cost of the energy collection, solar receiver, tower, transmission cost, energy storage system, power conversion system and plant operating systems are calculated for the calculation of the total cost of capital. Operating and maintenance costs are also important, including labor costs and materials for the operation and maintenance of the plant, replacement of storage facilities and overheads incurred during its operation.[71],[127]

6.6 Energy Balance Sheet

6.6.1 Solar Energy

Based on energy balance of the solar power tower station, we can see all the energy conversions, from the solar radiation received by the receiver, the conversion to thermal energy in the solar receiver and finally the electricity generated by the generator.

Years of measurement must pass to find the available solar energy of the area of the installation. Using the meteorological data of the area, we find the direct solar radiation (I). The amount of this radiation reflected by the heliostats at the central receiver, is defined by the relation

$$Q_{\text{useful}} = N_h A_h I n_{\text{avail}} \quad (6.20) ,$$

where N_h the number of heliostats,

A_h the area of the reflective surface of each heliostat and

n_{avail} the availability factor of the solar field (usually taken equal to 0.99).

Thermal energy reaching the receiver is calculated by

$$Q_{\text{inc}} = n_{\text{field}} Q_{\text{useful}} \quad (6.21) ,$$

where n_{field} is the degree of efficiency of the solar field. The efficiency of the solar field is equal to the sum of the coefficients of any possible loss, so

$$n_{\text{field}} = n_{\text{cos}} n_{\text{refl}} n_{\text{att}} n_{\text{shadow}} n_{\text{blocking}} n_{\text{spill}} \quad (6.22)[72],[100]$$

6.6.2 Thermal Energy

Thermal energy reaches the solar receiver and is transferred to the heat transfer fluid. There are losses during transport determining the efficiency of the receiver absorption behavior

$$n_{\text{receiver}} = n_{\text{conv}} n_{\text{radiation}} n_{\text{absorp}} n_{\text{conduct}} \quad (6.23)$$

The efficiency of the solar receiver is defined as the ratio of the thermal energy that the fluid receives in the pipeline of the receiver to the thermal energy that reaches the solar receiver from the solar field[72]

$$n_{\text{receiver}} = \frac{Q_{\text{net}}}{Q_{\text{inc}}} \quad (6.24)$$

6.6.3 Production of Electricity

Thermal energy of the fluid through the power block is converted into electrical energy. The efficiency of the power block is calculated by examining losses resulting from the output of the fluid from the solar receiver to the conversion of the thermal to electrical energy at the generator terminals, is defined as

$$n_{\text{block}} = \frac{P_{\text{el.gross}}}{Q_{\text{net}}} \quad (6.25)$$

In the fluid path from the solar receiver to the steam turbine, there are piping and heat exchangers losses. The degree of performance of the power block is calculated if the degree of efficiency of the thermodynamic cycle is given. The degree of efficiency of the thermodynamic cycle can be calculated from the relationship

$$n_{\text{cycle}} = \frac{(m_{\text{turb}} * \Delta h_{\text{turb}}) - P_{\text{pumps}}}{m_{\text{rec}} * \Delta h_{\text{rec}}} = \frac{m_{\text{turb}} * (h_{\text{turb, in}} - h_{\text{turb, out}}) - P_{\text{pumps}}}{m_{\text{rec}} * (h_{\text{rec, out}} - h_{\text{rec, in}})} \quad (6.26)$$

where m_{turb} is the flow of steam in the turbine,
 m_{rec} is the supply of the heat transfer fluid to the solar receiver,
 Δh_{turb} is the enthalpy drop of the steam at the turbine expansion,
 Δh_{rec} is the enthalpic increase in the receiver piping and
 P_{pumps} is the power consumed by the pumps in the power block.

The efficiency of the power generation system results from the sum of the efficiency grades of the thermodynamic cycle and the generator, so

$$n_{\text{block}} = n_{\text{cycle}} n_{\text{gen}} \quad (6.27).$$

When there is energy storage system, the degree of storage performance is included in the performance block strength.[71],[78],[100]

6.6.4 Gross to Net Conversion

There are losses when the electricity generated by the generator ends up in the network. These losses include self-consumption losses, the power supply of the

substations of the plant that require electricity to operate. The degree of efficiency of transferring electricity from the generator to the grid is

$$n_{el} = \frac{P_{el,net}}{P_{el,gross}} \quad (6.28).[72]$$

6.6.5 Reflecting Surface Calculation - Energy Balance

Now it is time to find the relation, defines the final electrical energy entering the grid in relation to the solar radiation of the area planned for the station, and calculate the required field of solstice. Given the required electricity production,

$$P_{el,net} = P_{el,gross} n_{el} \quad (6.29) ,$$

where the energy generated by the generator is

$$P_{el,gross} = n_{block} Q_{net} \quad (6.30)$$

so(7.29) becomes

$$P_{el,net} = n_{el} n_{block} Q_{net} \quad (6.31).$$

Thermal energy of the transfer fluid at the output of the solar receiver is

$$Q_{net} = n_{receiver} Q_{inc} \quad (6.32),$$

and (7.31) becomes

$$P_{el,net} = n_{el} n_{block} n_{receiver} Q_{inc} \quad (6.33),$$

where energy reaching the solar receiver from the solar field is

$$Q_{inc} = n_{field} Q_{useful} \quad (6.34)$$

and(6.33) becomes

$$P_{el,net} = n_{el} n_{block} n_{receiver} n_{field} Q_{useful} \quad (6.35).$$

Solar energy reflected by the solar trackers is

$$Q_{useful} = N_h A_h I n_{avail} \quad (6.36),$$

where $N_h A_h$ is the total reflective surface of the solar field A_{refl} . Relation (6.35) becomes

$$P_{el,net} = n_{el} n_{block} n_{receiver} n_{field} n_{avail} A_{refl} I \quad (6.37).$$

The efficiency of the plant is equal to the ratio of the electricity produced to the reflected solar radiation by the heliostats ,

$$n_{plant} = \frac{P_{el,net}}{Q_{useful}} = \frac{P_{el,net}}{n_{avail} A_{refl} I} \quad (6.38),$$

and because of

$$P_{el,net} = n_{el} n_{block} n_{receiver} n_{field} n_{avail} A_{refl} I \quad (6.37)$$

it is

$$n_{plant} = n_{el} n_{block} n_{receiver} n_{field} \quad (6.39).$$

We will take data from PS10 station, located near Seville, Spain and is the world's first solar power tower trading station in operation since 2007. The plant's power is 11MW and generates electricity of 23.4 GWh per year. The average annual direct sunlight in the area is 2012 kWh / m² and its solar field consists of 624 heliostats with a reflective surface area of 120m² each.

From all these relationships we now calculate the required solar field having as data the direct solar radiation at the design point and the required electricity production. Our design point is the 21st June between 12:00 and 13:00, where direct sunlight is

$$I_{dp} = 861 \text{ Wh/m}^2 \quad (6.40)$$

and electricity generation should be $P_{el,net} = 11 \text{ MWh}$. From the relation

$$P_{el,net} = n_{el} n_{block} n_{receiver} n_{field} n_{avail} A_{refl} I \quad (6.37)$$

total reflective surface of the solar field is found. The performance grades of the different system segments are empirically obtained, since we are unable to know any real size of the system but we can make the calculations with actual performance grades. For the calculation of the efficiency of the solar field, cosine coefficient is $n_{cos} = 0.859$, atmospheric transmittance is $n_{atm} = 0.954$, shadow coefficient and inhibitory factor are $n_{shadow} n_{blocking} = 0.9255$ and reflectivity coefficient $n_{refl} = 0.88$. So the average annual efficiency of the solar field is

$$n_{field} = n_{cos} n_{att} n_{shadow} n_{blocking} n_{refl} = 0.859 \cdot 0.954 \cdot 0.9255 \cdot 0.88 = 0.6674 \quad (6.41).$$

The efficiency of the solar receiver is $n_{receiver} = 0.92$ and the efficiency of the power block and the net efficiency of the net electricity is

$$n_{block} n_{el} = 0.307 \quad (6.42).$$

The relation $P_{el,net} = n_{el} n_{block} n_{receiver} n_{field} n_{avail} A_{refl} I$ (6.37) becomes

$$A_{refl} = \frac{P_{el,net}}{(n_{el} n_{block} n_{receiver} n_{field} n_{avail}) A_{refl} I} \quad (6.43)$$

and from all above

$$A_{refl} = \frac{11 \cdot 10^6}{0.307 \cdot 0.92 \cdot 0.6674 \cdot 0.99 \cdot 861 \frac{Wh}{m^2}} = 68,460.8 m^2 \quad (6.44)$$

The magnitude of the solar trackers $A_h = 120 m^2$, the number of the heliostats will be $N_h = \frac{A_{refl}}{A_h} = \frac{68460.8}{120} m^2/m^2 = 571$ (6.45).

The deviation of the theoretical calculation from the actual result results from the degree of yield of the solar field, which changes during the year. We know the true magnitude of the solar field, we can find the station's annual efficiency. The total reflective surface of the solar field will be

$$A_{refl} = N_h A_h = 624 \cdot 120 m^2 = 74,880 m^2 \quad (6.46)$$

and the field availability is $n_{avail} = 0.99$, so the total annual reflected solar energy will be $Q_{useful} = A_{refl} I n_{avail} = 74880 m^2 \cdot 2012 kWh / m^2 \cdot 0.99 = 149.15 GWh$ (6.47).

Due to the relation (7.38) the efficiency of the installation is,

$$n_{plant} = \frac{P_{el,net}}{Q_{useful}} = \frac{23.4 GWh}{149.15 GWh} = 0.157 \quad (6.48).$$

This was calculated according to the actual annual energy output. [71],[72],[75],[76],[77],[100],[127]

6.7 Theoretical approach

6.7.1 Theoretical Modeling

Thermal energy required by the solar receiver is necessary to determine the required surface of the solar field (Q_{inc}). For that reason, we need to get approximate performance grades for the rest of the system. R.A.E's assessment guide provides us indicative grades of performance for the modeling of such stations.

To make an initial estimate of the annual electricity produced, we should calculate the station's operating hours at its nominal load. For the operation of the plant, according to the R.A.E., no solar radiation below the threshold set at $200W/m^2$ is taken into account. Meteorological data calculated the hours when the sunshine exceeds the threshold and the result is that it exceeds 3,500 hours per year. Taking into account storage and backup system, its operating hours can reach 10-12 hours a day.

A realistic estimate of annual electricity generation according to the operating hours and nominal power of the plant is about $P_{el,net} = 200,000MWh_e$. The operating time of the storage unit and the backup system will not be taken into account when there is no sunshine for calculating correctly the input energy required in the system and determine the solar field.

For the hours of partial sunshine, the storage unit's supportive function is taken into account, as it was stored during the system receiving excess energy from the Sun. So we will calculate the energy sizes for 8 hours per day operation at full load. The annual operating hours are $h_{annual} = 8 \times 365 = 2,920$ hour and net energy production is $P_{el,net} = h_{annual} P_{nameplate} = 2,920 \text{ hours } 52 \text{ MW} = 151,840 \text{ MWh}$.

The net electricity transfer factor in the network is $n_{el} = n_{parasitics} n_{start} n_{el,avail}$, where $n_{parasitics}$ is the self-consumption losses coefficient ($n_{parasitics} = 0.884$ due to R.A.E.), n_{start} is the degree of start-up efficiency ($n_{start} = 0.983$ due to R.A.E.) and $n_{el,avail}$ is the availability to the network ($n_{el,avail} = 0.94$ due to R.A.E), so the net energy transfer rate to the network due to R.A.E will be $n_{el} = n_{parasitics} n_{start} n_{el,avail} = 0.884 \cdot 0.983 \cdot 0.94 = 0.816$.

The efficiency class of the power block is $n_{block} = n_{cycle} n_{gen} n_{storage}$, where n_{cycle} is the degree of performance of the cycle for reheating cycle ($n_{cycle} = 0.375$ due to R.A.E.), n_{gen} is the efficiency of the generator calculated empirically from existing systems ($n_{gen} = 0.95$ due to R.A.E.), and $n_{storage}$ is the degree of energy storage performance ($n_{storage} = 0.993$ due to R.A.E.). So n_{block} due to R.A.E will be $n_{block} = n_{cycle} n_{gen} n_{storage} = 0.375 \times 0.95 \times 0.993 = 0.354$.

The efficiency of the solar receiver, (due to R.A.E) is $n_{receiver} = 0.783$. The efficiency of the solar field is $n_{field} = 0.56$ (due to R.A.E). Thermal energy needed by the solar receiver from the solar field is $Q_{inc} = \frac{Q_{net}}{n_{receiver}}$, where $Q_{net} = \frac{P_{el,gross}}{n_{block}}$ is the thermal energy at the output of the solar receiver and $P_{el,gross} = \frac{P_{el,net}}{n_{el}} = \frac{151840 \text{ MWh}}{0.816} = 186.08 \text{ GWh}_e$, where $P_{el,net}$ is net electricity attributable to the grid. So $Q_{net} = \frac{P_{el,gross}}{n_{block}} = \frac{186.08 \text{ GWh}_e}{0.354} = 525.64 \text{ GWh}_{th}$ and finally $Q_{inc} = \frac{Q_{net}}{n_{receiver}} = \frac{525.64 \text{ GWh}_{th}}{0.783} = 671.32 \text{ GWh}_{th}$.

The reflected solar radiation required by the system is $Q_{useful} = \frac{Q_{inc}}{n_{field}} = \frac{671.32 \text{ GWh}_{th}}{0.56} = 1,198.8 \text{ GWh}$. The required total reflection surface of the field is $Q_{useful} = A_{field} I n_{avail}$. The direct annual solar radiation is $I = 2,100 \text{ kWh/m}^2$ and the availability coefficient of the heliostats structure field is $n_{avail} = 0.99$. The total required reflective surface of the solar field is $A_{field} = \frac{Q_{useful}}{I n_{avail}} = \frac{1198.8 \text{ GWh}}{\frac{2100 \text{ kWh}}{\text{m}^2} \times 0.99} = 576,623.4 \text{ m}^2$. The dimensions of each heliostat is $A_h = 14.625 \text{ m}^2$, so the total number of heliostats needed to cover the area is theoretically $N_h = \frac{A_{field}}{A_h} = \frac{576623.4 \text{ m}^2}{14.625 \text{ m}^2} = 39,428$ heliostats.

These performance grades are theoretical and differ from the actual ones, so the results that are based on them are the theoretical aspect of the design, and are useful only to know the range of sizes. [72],[76],[90]

Radiation threshold 200 W/m^2	$P_{el,net} = 200,000 \text{ MWh}_e$	$h_{annual} = 8 \times 365 = 2,920 \text{ h}$
$P_{el,net} = h_{annual} P_{nameplace} = 2920 \text{ h} \times 52 \text{ MW} = 151,840 \text{ MWh}$	$n_{el} = n_{parasitics} n_{start} n_{el,avail} = 0.816$	$n_{parasitics} = 0.884$ due to R.A.E.

$n_{start} = 0.983$ due to R.A.E.	$n_{el,avail} = 0.94$ due to R.A.E.	$n_{block} = n_{cycle} n_{gen} n_{storage} = 0.354$
$n_{cycle} = 0.375$ due to R.A.E.	$n_{gen} = 0.95$ due to R.A.E.	$n_{storage} = 0.993$ due to R.A.E.
$n_{receiver} = 0.783$ due to R.A.E.	$n_{field} = 0.56$ due to R.A.E.	$Q_{inc} = \frac{Q_{net}}{n_{receiver}} = 671.32$ GWh _{th}
$Q_{net} = \frac{P_{el,gross}}{n_{block}} = 525.64$ GWh _{th}	$P_{el,gross} = \frac{P_{el,net}}{n_{el}} = 186.08$ GWh _e	$Q_{useful} = \frac{Q_{inc}}{n_{field}} = 1,198.8$ GWh
$Q_{useful} = A_{field} I n_{avail}$	$I = 2,100$ kWh / m ²	$n_{avail} = 0.99$
$A_{field} = \frac{Q_{useful}}{I n_{avail}} = 576,623.4$ m ²	$A_h = 14.625$ m ²	$N_h = \frac{A_{field}}{A_h} = 39,428$

Table 6.2 Summary of Theoretical Modeling

6.7.2 Theoretical Optimization

The capacity factor is the ratio of the annual electricity generated to the annual electricity that would be produced if the plant was continuously operating at the design point. The annual energy production is $P_{el,net} = 200,000$ MWh and the annual electricity at the design point is $P_{el,dp,annual} = 52\text{MW} \cdot 8760\text{h} = 455,520$ MWh. So, the operating rate will be $C_f = (P_{el,net}) / (P_{el,dp,annual}) = 200,000\text{MWh}_e / (455,520 \text{ MWh}) = 0.439 = 43.9\%$.

Knowing the exploitation coefficient, we can define the solar multiple. The solar multiple varies between 1.9 and 2.3, and if we want for the station to function more efficiently, the solar energy received by the solar receiver should be nearly twice as high as the thermal energy entering the turbine. These data enable us to redefine the magnitude of the solar field, revising the system's performance levels in order to have a more realistic picture of station sizes. New performance grades will come from existing facilities or studies.

The degree of solar field performance for devices around the tower may in some cases reach 75%, but this is judged by the location and pattern chosen for the installation. In our case, the degree of yield of the solar field will be $n_{field} = 0.68$, a feasible and realistic value.

The efficiency of the solar receiver is mainly determined by its construction, and for its external cylindrical receiver its values are close to 90%. Taking the degree of efficiency of existing CSP, the degree of efficiency will be $n_{\text{receiver}} = 0.88$ which is achievable.

The thermodynamic cycle of Rankine with re-heating would be preferable to be used, as the degree of its performance exceeds in some cases 42%. Including storage system losses and generator performance in the power block performance class, it is possible to approximate the yield to $n_{\text{block}} = 0.4$.

The efficiency of clean electricity transmission in most existing installations is 92%. The efficiency of clean electricity transmission in our installation will be lower as it has high self-consumption, there is an energy storage system and hence a higher power requirement for the plant to operate. The efficiency of transmission of clean electricity will be defined to a logical size of $n_{\text{el}} = 0.87$.

The degrees of efficiency and the ratio of over-dimensioning is now known, so we can re-calculate the required field of solstice. The overdimension ratio is equal to $SM = \frac{Q_{\text{inc}}}{Q_{\text{turb}}} = \frac{Q_{\text{inc}}}{Q_{\text{netnstorage}}} = 1.9$ up to 2.3. We will take the average price of overdimension ratio so $SM = 2.1$. According to that new data $SM = 2.1$, $Q_{\text{inc}} = 310.653$, $Q_{\text{useful}} = 456.8426$, $A_{\text{field}} = 562067.2585$ and $N_h = 38432$.-----

Gross electricity at the design point is $P_{\text{el,gross}} = \frac{P_{\text{el,net}}}{n_{\text{el}}} = \frac{52\text{MWh}}{0.87} = 59.77\text{MWh}$ and the thermal energy at solar receiver output is $Q_{\text{net}} = \frac{P_{\text{el,gross}}}{n_{\text{block}}} = \frac{59.77\text{MWh}}{0.4} = 149.43\text{MWh}_{\text{th}}$. The thermal energy storage coefficient is $n_{\text{storage}} = 0.99$. The thermal energy entering the turbine is $Q_{\text{turb}} = Q_{\text{net}} n_{\text{storage}} = 149.43\text{MWh} \cdot 0.99 = 147.93\text{MWh}_{\text{th}}$.

These results are not exactly real, as each tracker contributes differently to the system. The effect of each tracker depends on its position, heliostats that are located far from the tower will have greater losses of atmospheric permeability, as the heliostats that are located south of the tower will have greater cosine losses. The final number of heliostats will arise after modeling and optimization of the solar field.[71],[92],[93],[94]

$P_{\text{el,net}} = 200,000\text{ MWh}$	$P_{\text{el,dp,annual}} = 455,520\text{ MWh}$	$C_f = \frac{P_{\text{el,net}}}{P_{\text{el,dp,annual}}} = 43.9\%$
--	--	--

$n_{field} = 0.68$	$n_{receiver} = 0.88$	$n_{block} = 0.4$
$n_{el} = 0.87$	$SM = 2.1$ (average)	$Q_{inc} = 310.653$
$Q_{useful} = 456.8426$	$A_{field} = 562067.2585$	$N_h = 38432$
$SM = \frac{Q_{inc}}{Q_{turb}} = \frac{Q_{inc}}{Q_{net} n_{storage}} = 1.9 = 2.3$	$P_{el,gross} = \frac{P_{el,net}}{n_{el}} = 59.77 MWh_e$	$Q_{net} = \frac{P_{el,gross}}{n_{block}} = 149.43 MWh_{th}$
$n_{storage} = 0.99$	$Q_{turb} = Q_{net} n_{storage} = 147.93 MWh_{th}$	

Table 6.3 Summary of Theoretical optimization

6.7.3 Theoretical Installation at The Design Point

We will take as design point 21st June (summer solstice). Design point is the time period we choose to dimension the installation. The weather during this time period is the best and direct solar radiation as derived from meteorological data in the installation site at the design point is $I_{dp} = 821 Wh/m^2$.

For calculating the magnitude of the solar field at the design point, we need the performance grades of R.A.E.'s rating. Due to the rated power of the plant $P_{net} = 52MW$, the power output for one hour of operation is $P_{el,net} = 52MWh_e$. The net electricity transmission factor for the design point is equal to the self-consumption coefficient, as there are no starts or restarts and the availability factor is equal to $n_{el\ avail} = 1$.

The generator generates electricity equal to $P_{el,gross} = \frac{P_{el,net}}{n_{el}} = \frac{52MWh_e}{0.884} = 58.82MWh_e$. The thermal energy at the receiver output is $Q_{net} = \frac{P_{el,gross}}{n_{block}} = \frac{58.82MWh_e}{0.354} = 166.16 MWh_{th}$. The receiver receives thermal energy from the field of solstice equal to $Q_{inc} = \frac{Q_{net}}{n_{receiver}} = \frac{166.16 MWh_{th}}{0.783} = 212.22 MWh_{th}$. The required reflected solar radiation from the solar field is $Q_{useful} = \frac{Q_{inc}}{n_{field}} = \frac{212.22 MWh_{th}}{0.56} = 378.96 MWh_{th}$. The total reflecting surface area will be $A_{field} = \frac{Q_{useful}}{I_{dp} n_{avail}} = \frac{378.96 MWh_{th}}{821 Wh\ ms. \times 0.99} =$

466,251m². So the number of soldiers finally required will be $N_h = \frac{A_{field}}{A_h} = \frac{466251 \text{ m}^2}{14625 \text{ m}^2} = 31,880$.

It can be noticed that the number of heliostats we found here is significantly smaller than the actual one. This happens due to the fact that we did not take into account neither the thermal energy storage system nor the over-dimensional ratio.[76]

Latitude 35.012 °	Longitude 26.134 °	$I = 2100 \text{ kWh} / \text{m}^2$
$A_h = (2 \times 3.25 \text{ m}) \times 2.25 \text{ m} = 6.5 \text{ m} \times 2.25 \text{ m} = 14.625 \text{ m}^2$	$I_{dp} = 821 \text{ Wh} / \text{m}^s$	$P_{net} = 52 \text{ MW}$
$P_{el,net} = 52 \text{ MWhe}$	$n_{el\text{ avail}} = 1$	$P_{el,gross} = \frac{P_{el,net}}{n_{el}} = \frac{52 \text{ MWhe}}{0.884} = 58.82 \text{ MWhe}$
$Q_{net} = \frac{P_{el,gross}}{n_{block}} = \frac{58.82 \text{ MWhe}}{0.354} = 166.16 \text{ MWh}_{th}$	$Q_{inc} = \frac{Q_{net}}{n_{receiver}} = \frac{166.16 \text{ MWh}_{th}}{0.783} = 212.22 \text{ MWh}_{th}$	$Q_{useful} = \frac{Q_{inc}}{n_{field}} = \frac{212.22 \text{ MWh}_{th}}{0.56} = 378.96 \text{ MWh}_{th}$
$A_{field} = \frac{Q_{useful}}{I_{dp} * n_{avail}} = \frac{378.96 \text{ MWh}_{th}}{821 \text{ Wh m.s.} \times 0.99} = 466,251 \text{ m}^2$	$N_h = \frac{A_{field}}{A_h} = \frac{466251 \text{ m}^2}{14625 \text{ m}^2} = 31,880$	

Table 6.4 Summary of Theoretical Installation at The Design Point

6.8 Software for Solar Power Tower Modeling

At the initial stage of this work, I had to search in order to find the right free software, that would be the best for the simulation of the solar tower. During that investigation, for the most suitable software, a lot of software were found that could meet the needs of this thesis, but I came to the SAM (System Advisor Model), for reasons that will be explained below. Initially I will make a presentation of all the software that were found and then a presentation of the SAM. The inquiry found the following software available. Here is a small presentation for each, showing their characteristics and capabilities.[108]

1.TRNSYS: *an extremely versatile graphics software, that is used for the simulation of the transient behavior of systems. This software deals with evaluating the performance of thermal and electrical energy systems, but it has also the ability to configure and other systems such as traffic flow, or biological processes. TRNSYS consists of two parts, the core that reads and processes the input file, specifies thermophysical properties, determines the convergence and other variables, performs linear regressions, and inserts external data files. The second part of TRNSYS is a library comprising about 150 models such as pumps in multi-zone buildings, wind, weather data processors and basic HVAC equipment at the cutting edge emerging technologies. The models are constructed in such a way that the users can modify existing components or write their own, expanding the capabilities of the software. After 35 years of commercial availability, TRNSYS is still a flexible, component-based software package that houses the ever-changing needs of both researchers and practitioners in energy simulation community.* [23]

2.SolarPILOT: *The optimizer produces and characterizes the power tower systems. The software was developed by the National Renewable Energy Laboratory (NREL). SolarPILOT comprises a graphical user interface (GUI) and an application program (API), through which external programs can access the functionality. This software enables the creation tracker considering local solar and atmospheric conditions, the geometry of the receiver, the height of the tower, factors of market pricing etc. It can determine the position of the heliostat associated with applications such as Google Earth. SolarPILOT models a wide variety of solar configurations and systems with multiple trackers or different geometries, considering the time and the position of the sun. It even optimizes solar provisions in order to minimize the total expected cost of energy and calculates the cost of installation. This software implements methods so as to reduce the overall computational burden and it produces accurate results.* [24] [25]

3.RETScreen: *Clean Energy Management Software system for feasibility analysis of energy efficiency projects, renewable energy and cogeneration of energy, as well as the analysis of the current energy efficiency. RETScreen Expert is an advanced privileged software version, and it is available for free. The RETScreen empowers professionals*

and decision makers to quickly identify, assess and optimize the technical and economic viability of potential clean energy projects. This decision software platform also allows easy measurement and verification of actual performance of facilities, but also it helps finding additional savings and energy production opportunities.[29],[109]

4.HOMER Legacy: a computer model that simplifies the task of evaluating the design options for both off-grid and grid power systems for remote, stand-alone and distributed generation (DG) applications. Optimization and sensitivity analysis Homer algorithms allow the user to evaluate the economic and technical feasibility of a large number of technological options and to account for the uncertainty of technology cost, availability of energy resources, and other variables. HOMER Legacy is the original version of HOMER software that was created at the National Renewable Energy Laboratory (NREL). This software was for free. From April 14, 2015, the HOMER is available only for academics and students working in teaching and research, or energy projects, organizations working in the energy sector non-profit. [26]

5.Skelion: this software enables the design of solar - thermal or solar - photovoltaic installations starting from a 3D model. There is the possibility of housing design or installation of power plants with a few clicks using SketchUp and Google Earth, you thus reducing the time of the simulation. With Skelion software the users import photovoltaic and other thermal components in a surface and Skelion has the ability to place solar panels very quickly and it quickly makes the studies on renewable solar energy sources. In addition Skelion allows the user to place 3D solar installation models, to use the PV module database that is available or to add new valuation model from each user and to be connected to Google Earth in order to determine the position. [27]

6.EasySolar App -EasySolar Web Platform: The EasySolar App is the first application for designing solar or photovoltaic systems which expands EasySolar Web Platform, that is a photovoltaic software which has much more possibilities for design drawings, project management and creation of financial analysis. There is the possibility to the user to create PV Design (image, Google Maps, sketch) and to create financial analysis and sales management. [28]

7.Hybrid2: *The software package Hybrid2 is a tool which examines the performance and economic analysis in a wide variety of hybrid power systems. This program is no longer supported. The Hybrid2 software uses time series data loads, wind speed, solar radiation, temperature and power system that are designed or selected by the user to predict the performance of the hybrid power system. The changes in wind speed and the load at each time step are taken into account. The model is based on the time series but uses statistical methods to represent each time step variations in the wind and the load.* [30]

8.Viessman ESOP: *the online tool is used only for collectors and Viessman systems which have the potential to make solar calculations and simulation of solar thermal systems. It gives the user results in solar efficiency, solar fractions, efficiency and intensity.* [31]

9.Kalkener: *the online Kalkener solar simulation software allows the calculation of solar thermal water heating systems: the size of its main components, according to the monthly, weekly and daily water consumption. It also allows the solar site survey, shading, orientation and inclination of solar panels, the optimum position for those on sloping roofs, it calculates the annual output of solar energy (taking in account losses) and its main profitability indicators, (IRR and NPV). The goal of this software is to calculate accurately, fast and in a cheap way all the necessary data in order to make the right decision about whether is good or not to invest in this type of facilities.*[32]

10.CEC-Fchart: *is a user-friendly program designed to calculate the solar fraction for solar water heating systems in California. This online tool calculates solar heat water for a system and it is designed for the calculation of the thermal solar water heating for solar systems. The solar fraction generated is based on compliance with the standards of the 2013 Title 24 Building Energy Efficiency and should not be used for any other purpose.*[65]

11.FreeGreenius: is the free version of Greenius software which has been developed at the Solar Research Institute of the German Aerospace Center (DLR) several years ago. It is made to measure quickly and simply the performance of solar power (CSP) systems and other renewable energy sources and is based on an hourly simulation of system performance. The initial focus was on the production of electricity from renewable sources by focusing on concentrating solar power generated by parabolic trough plants. The Greenius software continuously expands e.g. for simulating solar towers, production of solar heat and solar cooling. It offers fast technical calculations, financial calculations and user interfaces for handling parameters and analyzing the results. Weather maps and performance data that were created with other software tools can be easily integrated into this software. In the past, the available public version was limited in modeling capabilities and only users who have purchased the full version had access to all options. There were many requests from users, but due to limited resources, users could not use it. Plus there is a full version of Greenius for all free. [33]

12.Combisun: this tool makes estimations of combisystems. Combisun can calculate and simulate the performance of many different combisystem, under different climates and different loads.[34]

Combisystem: A solar combisystem provides both solar heating and cooling, but also hot water from a common set of solar thermal collectors, that are usually accompanied by an auxiliary non-solar heat source.[66]

13.OVENTROP: is an easy to use tool, which calculates and simulates solar thermal systems with solar collectors. The user after modeling gets results about Solar Efficiency, Solar fraction, the efficiency etc. OVENTROP is a global database on climate. [35]

14.SOLO - TECSOL: a free online software to calculate the solar output of hot water systems. This software calculates the energy output depending on the location, the water needs, the nature and volume of the water tank, the collector region and the slope. SOLO - TECSOL is a global database on climate.[67]

15.ScanTheSun: program that calculates the direction and solar radiation of a solar collector considering trees, buildings or other shading sources that maybe are around it. ScanTheSun allows the calculation of solar energy reaching the collector, it can find the energy loss due to the shadow of objects in the area, it can design thermal collectors and it can even calculates the hours of hot water or production of electricity during the day – it prepares a complex documentation of the solar radiation and the solar plant efficiency.[68]

16.Energy2D: Energy2D is an interactive modeling simulation program for the three modes of heat transfer, treatment, convection and radiation, as well as their connection with the dynamics of particles. This program allows the user to design "computer experiments" to test a scientific hypothesis or solve an engineering problem without resorting to complex mathematics. In addition to heat transfer, it can also include other types of energy and transformations (e.g. phase changes and chemical reactions), and it supports multiple types of fluids (e.g. air and water), it provides an interface with sensor for creating a mixed reality applications. The goal of Energy2D is to create a flexible system through virtual experiments and the ability to create complex simulations of physical phenomena. [36]

17.SAM (System Advisor Model): is a free tool available from the National Renewable Energy Laboratory (NREL). SAM is designed to facilitate decision making for people engaged in the renewable energy sector. This tool includes high performance models for the following technologies[38]: Photovoltaic, Battery Storage Model for photovoltaic systems, Parabolic trough concentrating solar power, Power tower concentrating solar power (salt and steam), Linear Fresnel concentrating solar power, Dish-Stirling concentrating solar power, Conventional Thermal Energy, Solar water heating for residential or commercial buildings, Wind power (large and small), Geothermal energy and geothermal cogeneration and Electricity from biomass. [38]

6.9 Software Used in the Present Thesis

To draw safer conclusions it was necessary to model and optimize the solar tower using software. The software that will eventually be used in our case for modeling is the SAM (System Advisor Model), which models and optimizes energy installations for almost all aggregated solar technologies and therefore the solar tower in our case.

Greece generally is ideal due to its solar potential for installing such a system, according to the requirements of a solar thermal station in direct sunlight and because of the form of the soil, so has attracted in the recent years interest for investment in the energy industry from many countries worldwide.

Sam includes information for only a system in Greece, and enable us to analyze it, so in this thesis we will use the given data, to analyze a solar tower system, making our work more connected to reality, using real data, making our work more reliable, so from now on all the information used will be about that system whose characteristics can be found in SAM , and its location is at 37.9° latitude and 23.73° longitude.

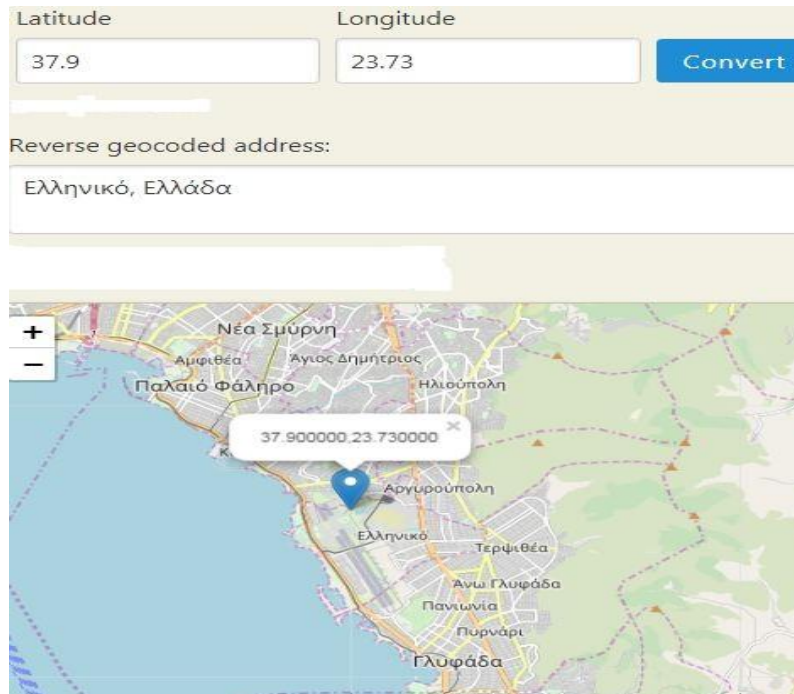


Figure 6.16 The exact location of the designed system(latitude 37.9° and longitude 23.73°)

The weather-meteorological data and the direct sunlight of the area that the system is designed to be installed are collected by the program and are available for the users to study them. The ideal days in one year for the operation of a solar thermal station exceed 160 and the maximum output power of the plant will be 52MWe(estimated net output at design (nameplate)). Annual meteorological data from previous years helped to find the real annual direct solar radiation of the area, whose location is at 37.9 ° latitude and 23.73 ° longitude, so due to global maps and meteorological data, annual direct solar radiation of that area is $I = 2,100 \text{ kWh} / \text{m}^2$. [56]

The company that will install the system is Brightsource company, the solar thermal station will consist of a cylindrical Brightsource receiver and a Brightsource solar field around the receiver. Each tracker consists of two mirror-width mirror mirrors 3.25 2.25 m. The reflective area of each tracker is $A_h = (2 \cdot 3.25 \text{ m}) \cdot 2.25 \text{ m} = 14.625 \text{ m}^2$, as you can also see in SAM that number is used as data(single heliostat area).

When opening and starting SAM as it will be analyzed below, we select the type of system we want to model, in our case CSP, and SAM gives us a Schematic Representation of the Solar Power Tower, as you can see in Figure 6.17. The system includes a thermal energy storage system that consists of two salt tanks. These tanks make the plant operate at its rated load for 5 hours(full load hours of storage).

The heat transfer fluid (HTF type) used in our case is molten salts, and especially Hitec Solar Salt, consisting of 60% sodium nitrate (NaNO_3) and 40% potassium nitrate (KNO_3),as you can see in SAM, with melting point at 238 °C, and maximum operating temperature is 593 °C.

In the two-tank thermal energy storage system, the liquid in the cold tank at 290°C is pumped to the top of the tower and is heated to 565°C through the solar receiver piping and enters the hot tank. From the hot tank, it is pumped and divided into two circuits. The first circuit is introduced through a super heater into the heat exchanger (steam generator) where the water vaporizes, then enters the pre-heater and finally ends up in the cold tank. The second circuit enters the re - heater and ends at the first circuit before the steam generator. Finally, the cold fluid ends up in the cold tank to start the process again.

If steam pressure and temperature are increased, the efficiency of a Rankine thermodynamic cycle will be increased too. The properties of the inlet vapor are selected according to the turbine and the desired thermodynamic cycle. The water is pumped at

ambient temperature (19°C) (ambient temperature at design) and through the pre-heater passes through the steam generator where it vaporizes. It then enters the super heater and superheated steam flows at a temperature of 565°C (HTF hot temperature) and a pressure of 100 bar (boiler operating pressure). Superheated steam enters the high pressure turbine and then into the re - heater before it reaches the low pressure turbine. Subsequently, saturated water flows out of the low pressure turbine at a temperature of 35°C which ends at the air-cooled condenser where it exits at ambient temperature before the cycle begins again. [71],[76],[86],[87],[88],[89],[90]

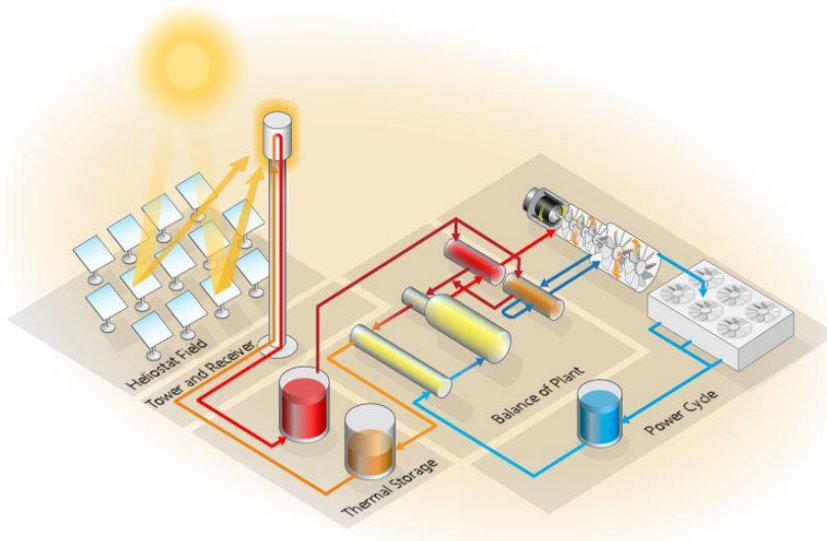


Figure 6.17 Schematic Representation of a Solar Power Tower Using Molten Salts

Chapter 7

7.1 The Proposed Modeling in SAM

This section includes the modeling and the optimization of the solar power tower using software, so that we can make safer conclusions about the features of the system. Our software System Advisor Model (SAM) is available from the National Renewable Energy Laboratory (NREL) and it models and optimizes energy facilities for virtually all "sun" technologies. More specifically, version SAM 2016.3.14 was used in this work because of the compatibility with the computer we used.

Modeling of a solar power tower system includes the optimization of the solar field using DELSOL3 code. That code needs to know the required thermal energy on the surface of the receiver and some other basic properties of the solar field, the tower height and the dimensions of the solar receiver for optimization and after optimization, as a result, we receive the number of solar heliostats, the total reflecting surface of the field that our system will have, the exact dimensions of the solar receiver and other important results for the CSP.

After inserting the values of potential losses and the financial data, the simulation of our system is performed. The simulation function of SAM uses TRNSYS16, a software that simulates and models constantly changing systems. TRNSYS models our system according to the parameters and meteorological data we have set and simulates the operation of the station. SAM gives as a result the basic results associated with the installation of the simulation of the station, and extracts multiple results and charts, except from the results associated with the installation and operation of the station, it performs a detailed techno-economic (LC-cycle) analysis for the system.[38]

7.1.1 Starting the Program

First the basic frames of SAM are presented, where we inserted the prices of the variables in order to continue with the simulation of the CSP system.

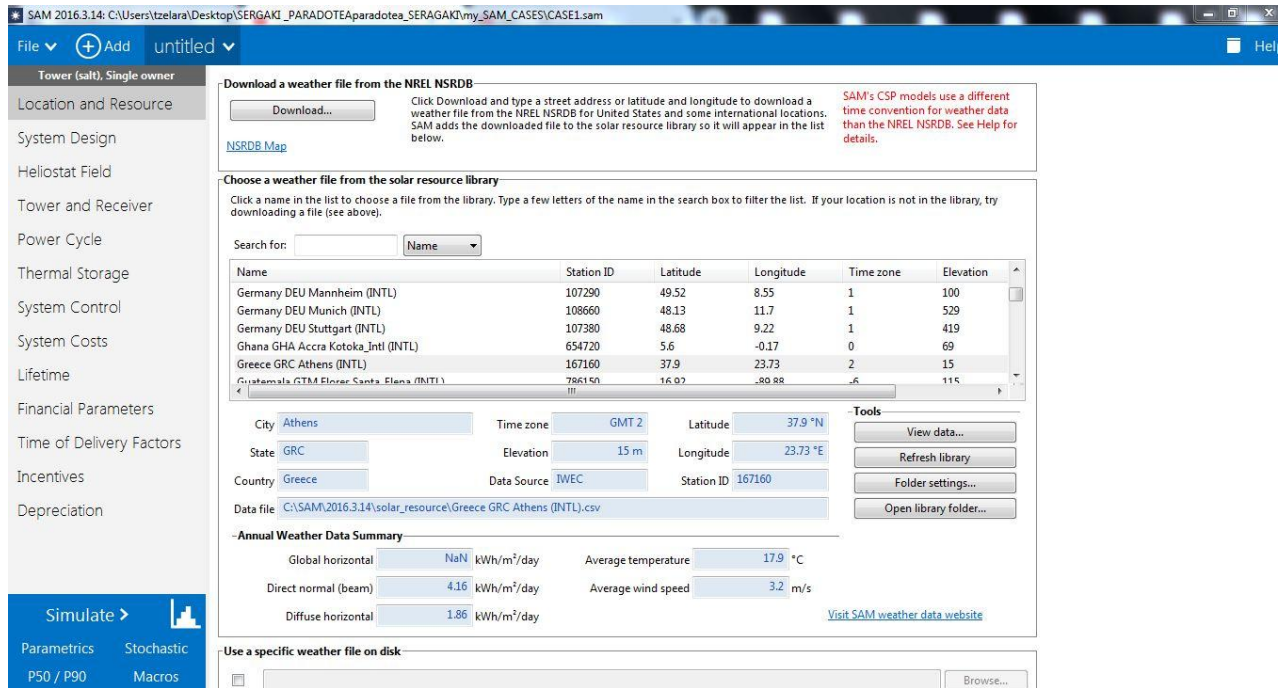


Figure 7.1 Location and Resource Frame in SAM

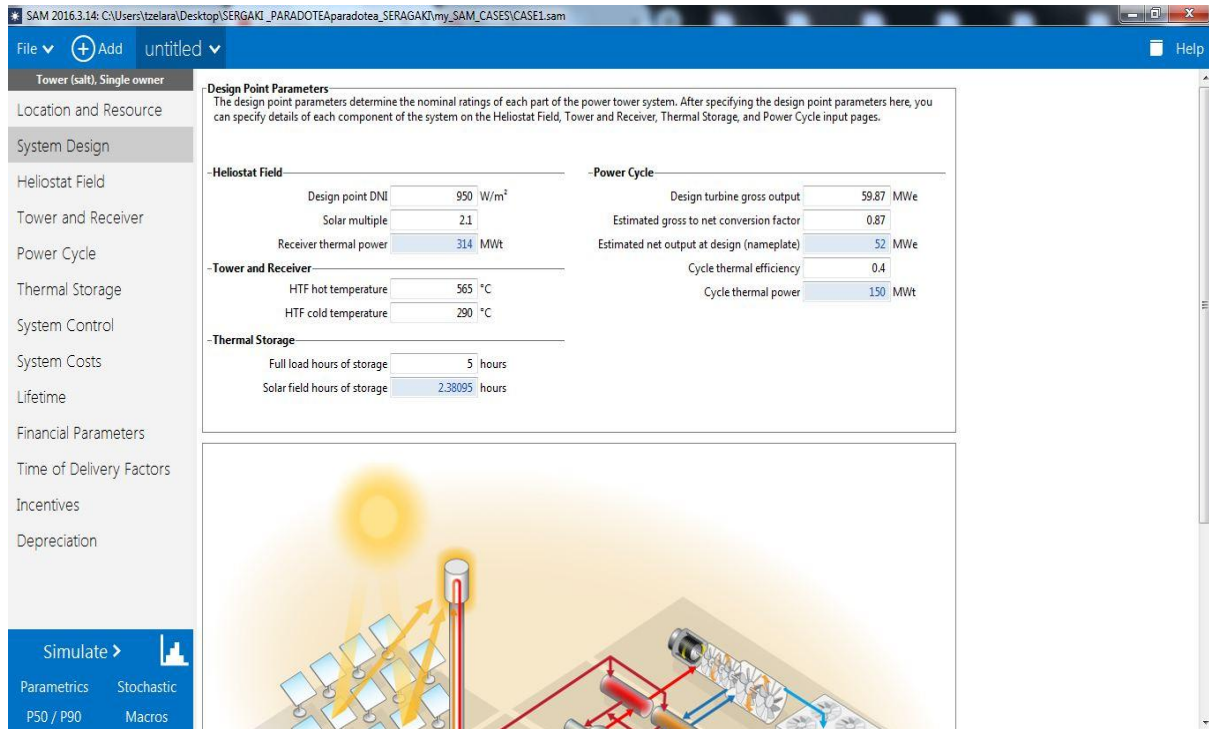


Figure 7.2 System Design Frame in SAM

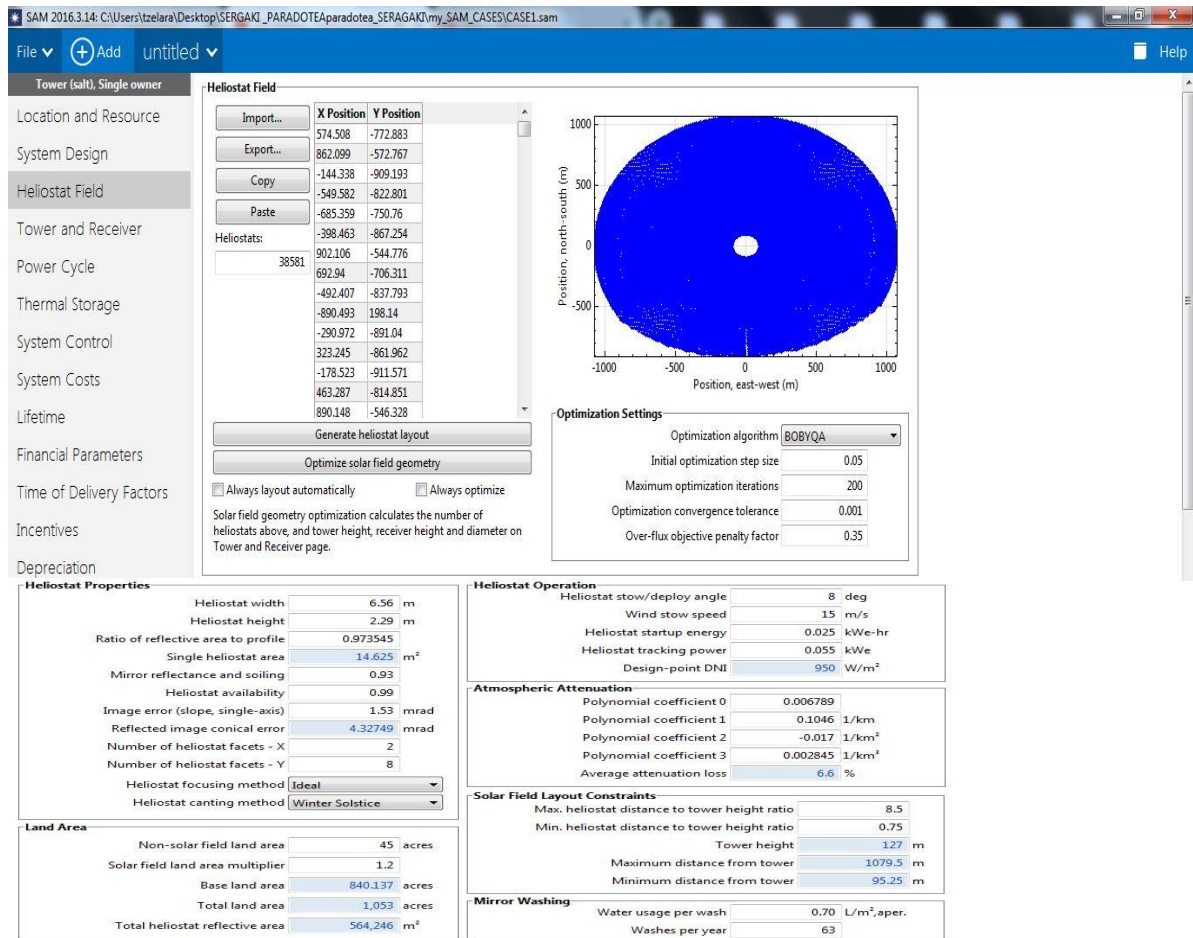


Figure 7.3 Heliostat Field Frame in SAM

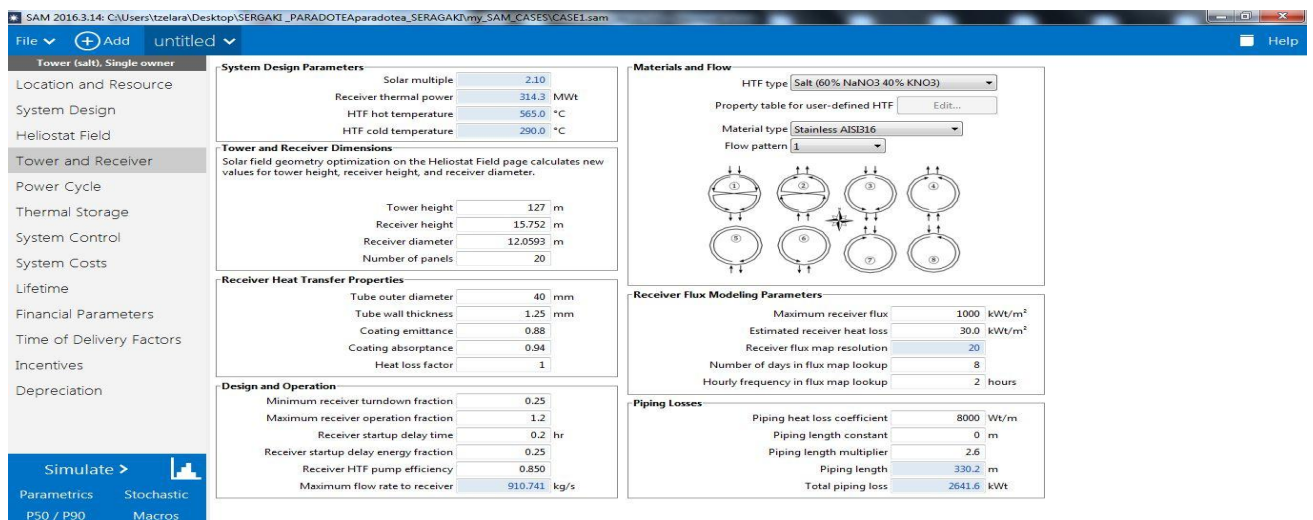


Figure 7.4 Tower and Receiver Field Frame in SAM

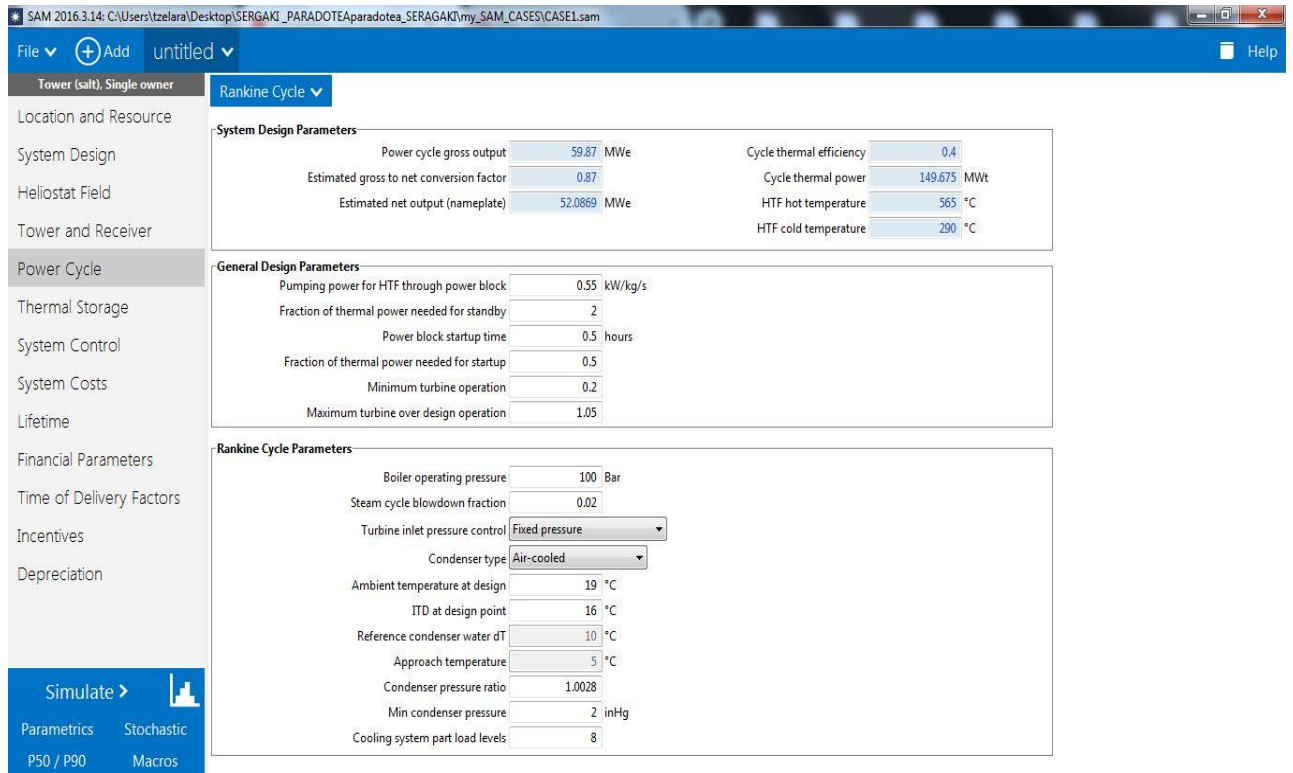


Figure 7.5 Power Cycle Frame in SAM

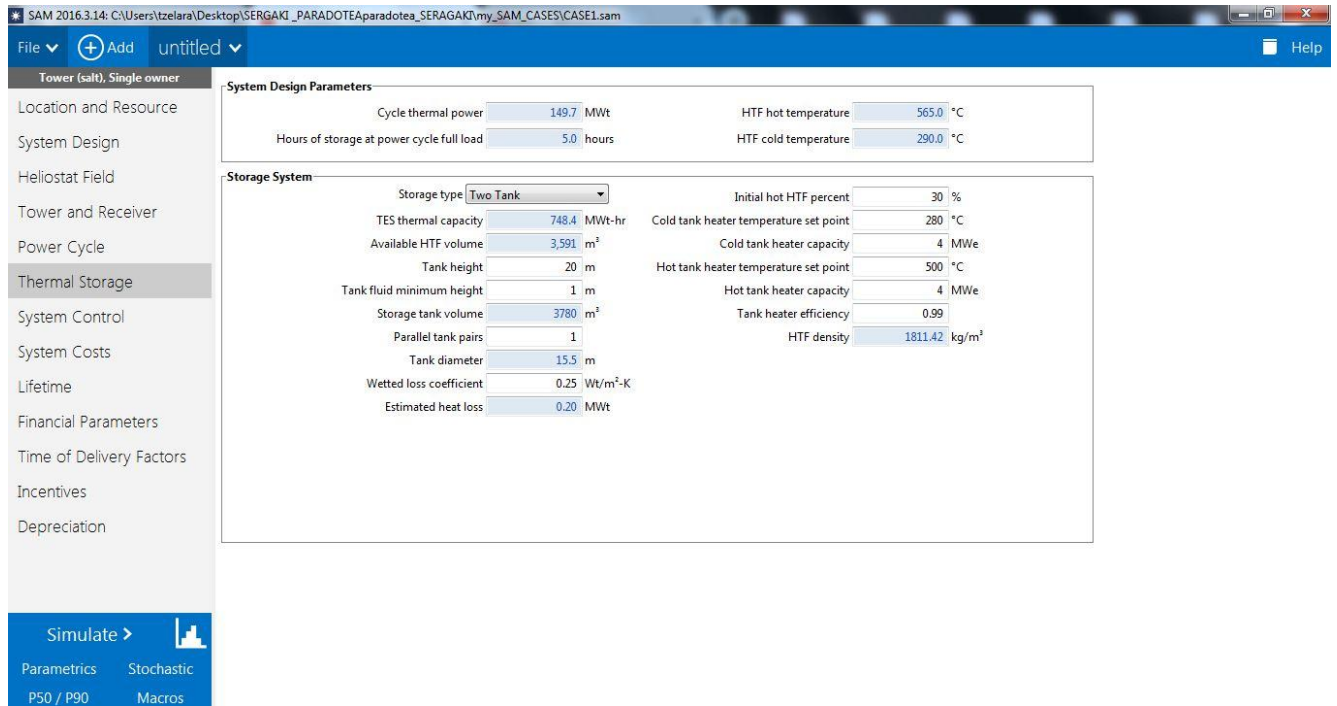


Figure 7.6 Thermal Storage Field Frame in SAM

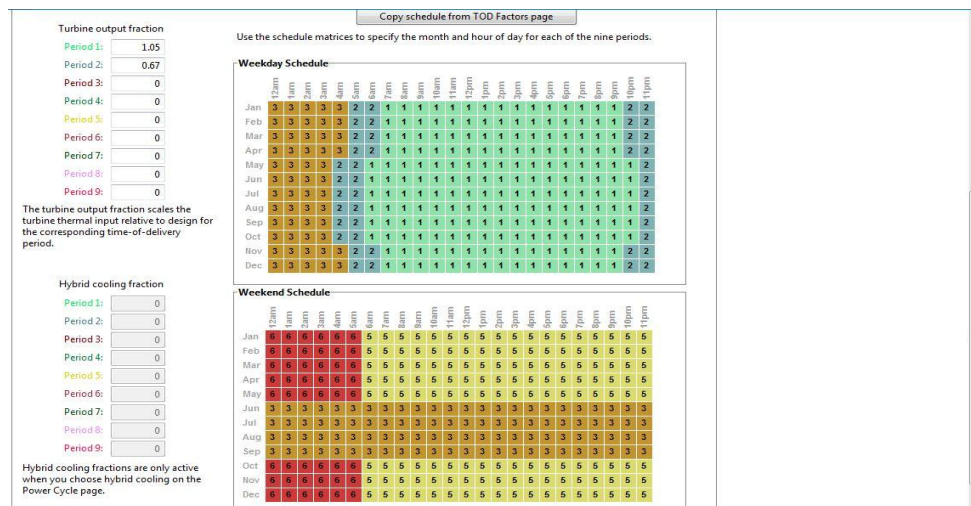
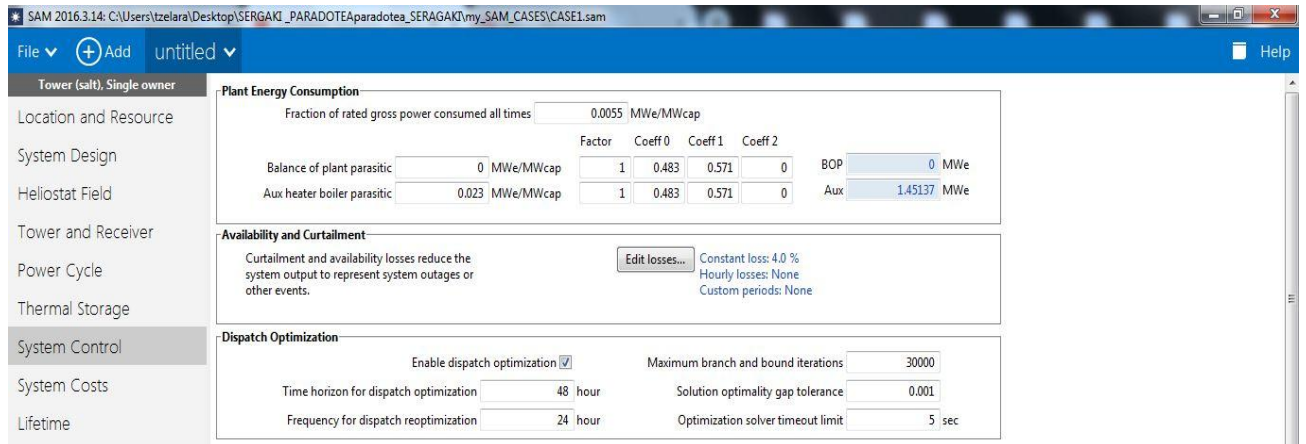


Figure 7.7 System Control Frame in SAM

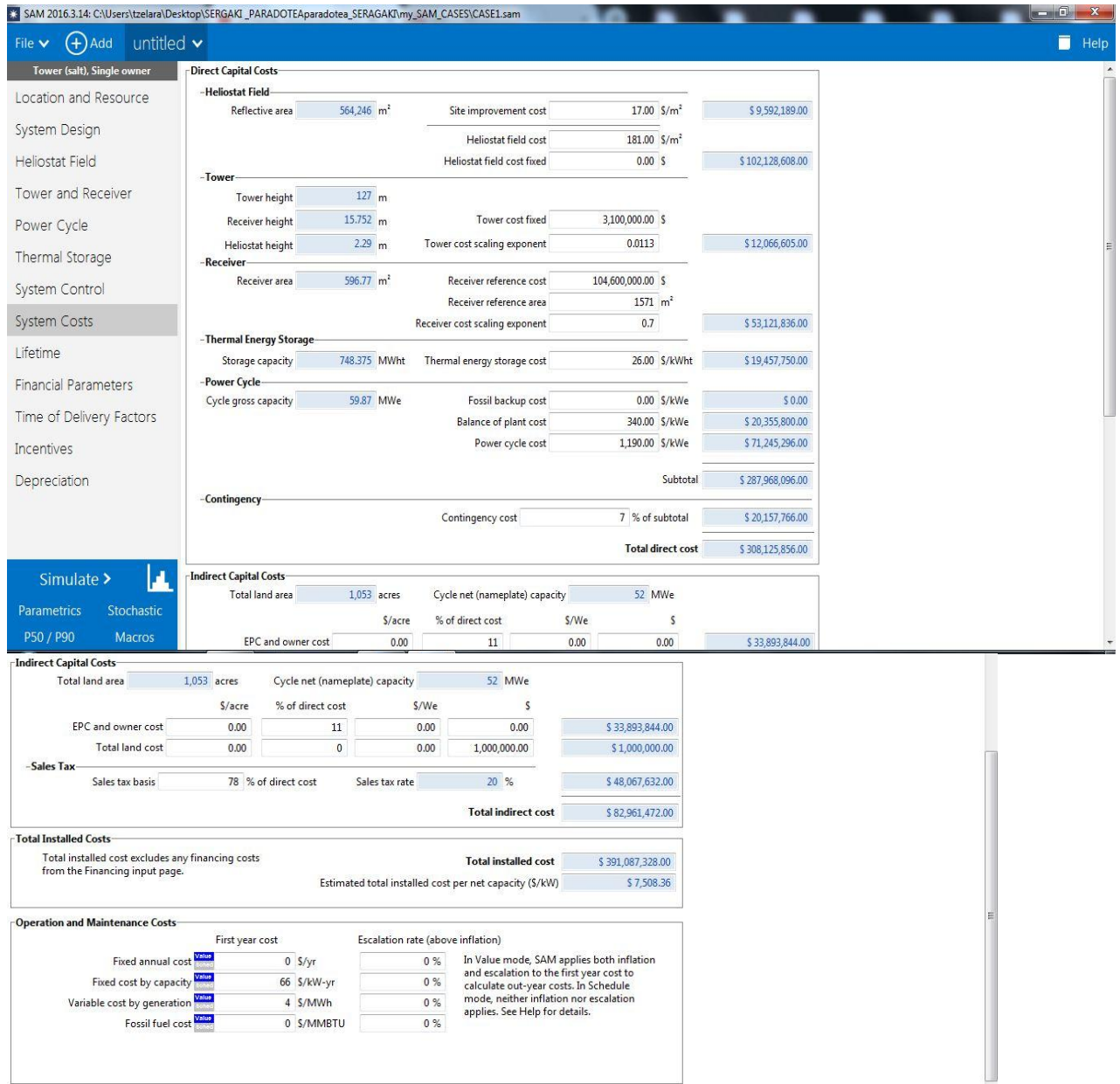


Figure 7.8 System Costs Field Frame in SAM

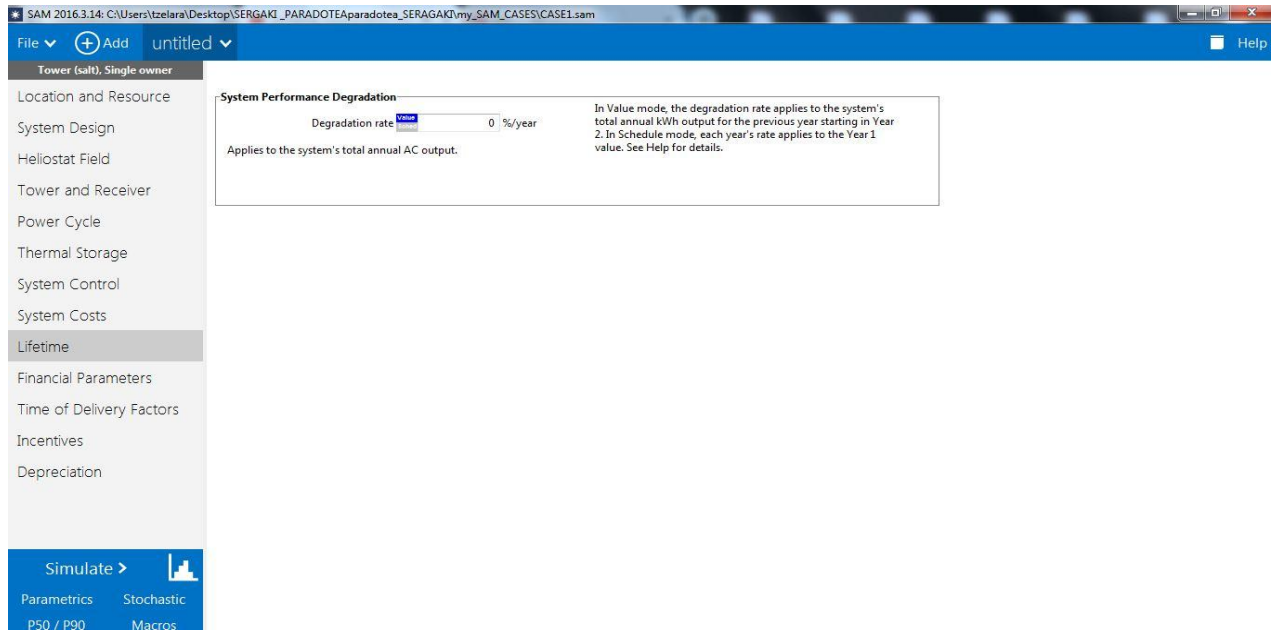


Figure 7.9 Lifetime Frame in SAM

SAM 2016.3.14: C:\Users\tzelara\Desktop\SERGAKI_PARADOTE\paradotea_SERGAKI\my_SAM_CASES\CASE1.sam

File Add untyped Help

Tower (salt), Single owner

Location and Resource
System Design
Heliostat Field
Tower and Receiver
Power Cycle
Thermal Storage
System Control
System Costs
Lifetime
Financial Parameters
Time of Delivery Factors
Incentives
Depreciation

Solution Mode

Specify IRR target IRR target 11 % IRR target year 20
 Specify PPA price PPA price 0.13 \$/kWh

Escalation Rate

PPA price escalation 1 %/year
 Inflation does not apply to the PPA price.

Analysis Parameters

Analysis period 25 years Inflation rate 2 %/year
 Real discount rate 8.2 %/year
 Nominal discount rate 10.36 %/year

Tax and Insurance Rates

Federal income tax rate 0 %/year
 State income tax rate 3 %/year
 Sales tax 20 % of total direct cost
 Insurance rate (annual) 1 % of installed cost

Property Tax

Assessed percentage 100 % of installed cost
 Assessed value \$ 391,087,328.00
 Annual decline 0 %/year
 Property tax rate 2 %/year

Salvage Value

Net salvage value 0 % of installed cost End of analysis period value \$ 0

Project Term Debt

Project Term Debt

Debt percent 75 % of total cap. cost
 DSCR 0

Tenor 10 years
 Annual interest rate 5 %
 Debt closing costs 450,000.00 \$
 Up-front fee 2.75 % of total debt

Choose "Debt percent" to size the debt manually as a percentage of total installed cost. Choose "DSCR" to size the debt based on cash available for debt service. See Help for details.

For a project with no debt, set the either the debt percent or the DSCR to zero.

Be sure to verify that all debt-related costs are appropriate for your analysis: Debt closing costs, up-front fee, and debt service reserve account. Note that debt interest payments are tax deductible, so a project with more debt may have higher net after-tax annual cash flows than a project with less debt.

You are modeling a project with no debt, but the debt closing costs are not zero. To be sure that all debt-related costs are zero, set the debt closing costs to zero.

Cost of Acquiring Financing

Cost of Acquiring Financing

Financing cost 580,000,000.00 \$

SAM includes the financing cost (and the working capital reserve) in the project's financing cost, which is part of the project's total equity capital reported in the project cash flow. See Help for details.

Construction Financing

Construction Period Debt

Specify the terms of up to five optional short-term construction loans. SAM calculates the total financing cost and adds it to the project's investment cost. The sum of percentages in the Percent of Installed Costs column must equal 100%.

Construction loans	Percent of installed costs	Up-front fee (% of principal)	Months prior to operation	Annual interest rate (%)	Principal (\$)	Interest (\$)	Total construction financing cost (\$)
Loan 1	100	1	24	4	391,087,328.00	15,643,493.00	19,554,366.00
Loan 2	0	0	0	0	0.00	0.00	0.00
Loan 3	0	0	0	0	0.00	0.00	0.00
Loan 4	0	0	0	0	0.00	0.00	0.00
Loan 5	0	0	0	0	0.00	0.00	0.00
Totals:	100				391,087,328.00	15,643,493.00	19,554,366.00

Reserve Accounts

Reserve Accounts

Interest on reserves 1.75 %/year
 Working capital reserve 6 months of operating costs
 Debt service reserve account 6 months of principal and interest (P&I) payments

Interest on Reserves applies to all reserve accounts, including debt, working capital, and replacement reserves.

Major Equipment Replacement Reserve Accounts

	Replacement cost (\$/W)	Year 1 dollars (\$)	Replacement frequency (years)	Depreciation treatment (applies to all major equipment expenditures)
Replacement Reserve 1	0	0.00	12	Federal 5-yr MACRS
Replacement Reserve 2	0	0.00	15	State 5-yr MACRS
Replacement Reserve 3	0	0.00	3	

Figure 7.10 Financial Parameters Frame in SAM

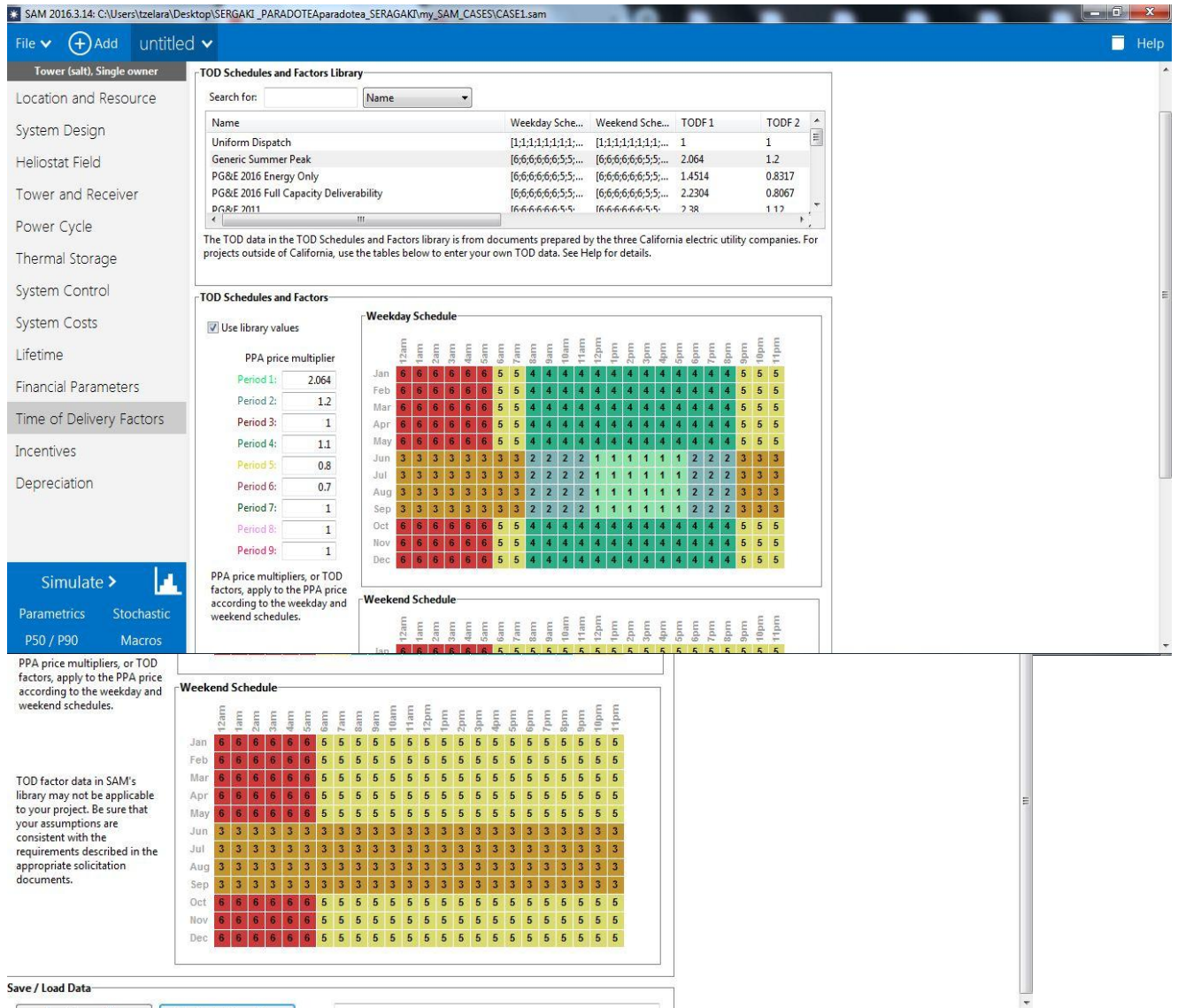


Figure 7.11 Time of Delivery Factors Frame in SAM

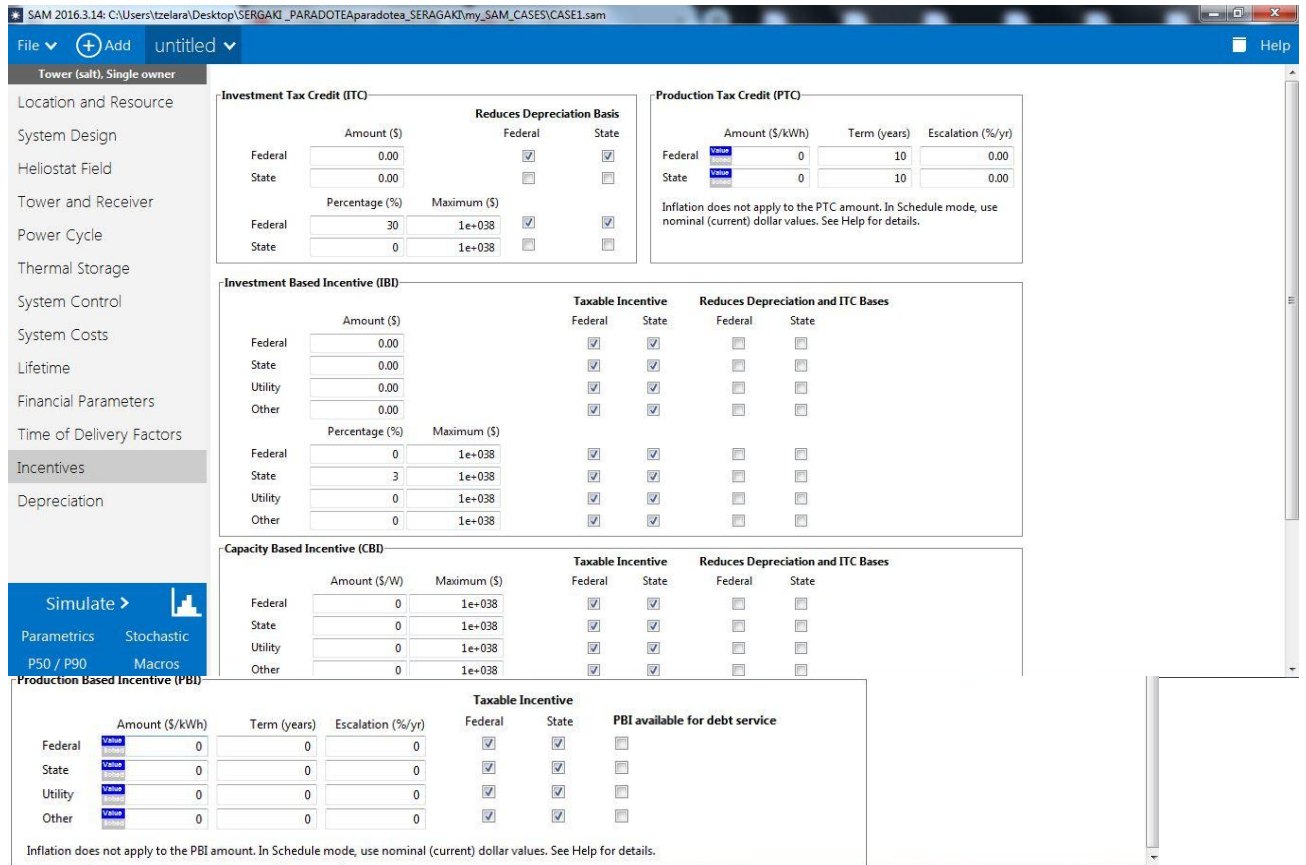


Figure 7.12 Incentives Frame in SAM

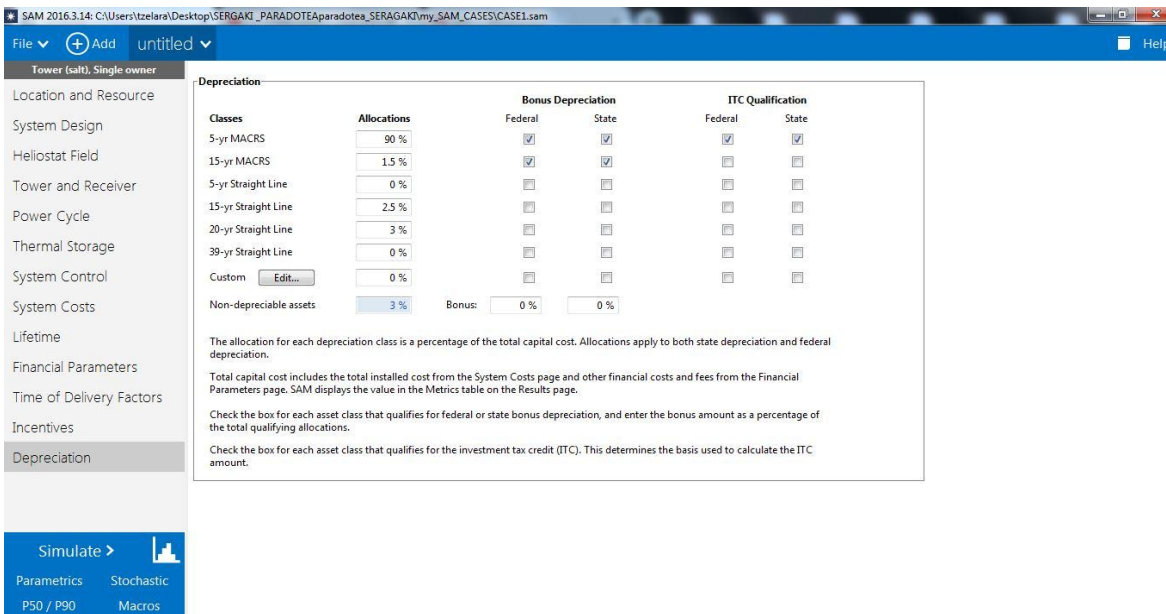


Figure 7.13 Depreciation Frame in SAM

Starting with SAM we create a new file, and choose the type of installation to be simulated. All our available technologies are listed on our menu, Concentrating Solar power Molten Salt is chosen, and after that the program offers additional options for techno-economic analysis (Figure 7.14).

The first option for techno-economic analysis is for installations by private electricity generators, and more production cases follow (with more options). Our interest obviously concerns private producers with a PPA, so we chose the first available option. In this economic model, an internal rate of return (IRR) is calculated if we know the agreed sale price or alternatively the ideal selling price is calculated for a certain internal rate of return.

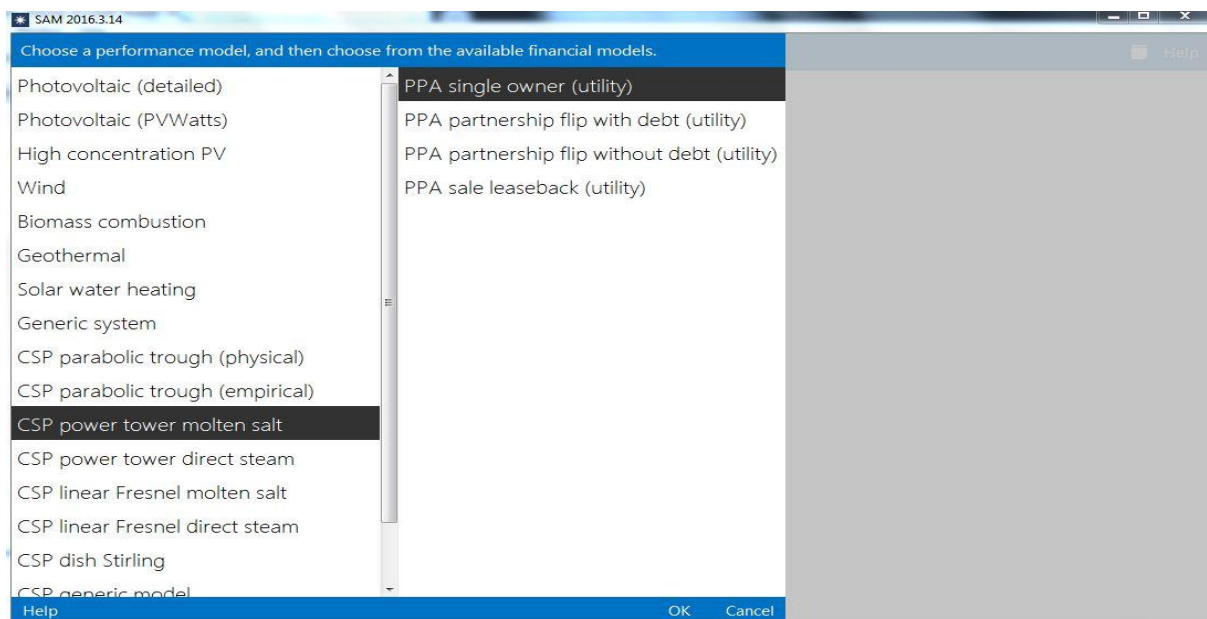


Figure 7.14 System choices and economic models - Start Menu of SAM

7.1.2 Data Used in the Proposed Modeling in SAM

In this software, as we have already said, there is only one choice related to CSP in Greece, so we chose to model and optimize that only solar power tower available in SAM located in our country with 37.9 ° latitude and 23.73 ° longitude, and its features appear on the screen (Figure 7.16).

By selecting the power tower located in our country, we see the area's information, latitude and longitude, altitude and time zone. At the bottom of the screen are the annual meteorological data, such as annual solar radiation, average annual temperature and average annual wind speed. Once we have defined the area of the plant, we can now set the station's nominal values.

By selecting the power cycle (Power Cycle of the window design system), we define the estimated net electricity transfer coefficient of $n_{el} = 0.87$ (estimated gross to net conversion factor), and after the nominal power we want is $P_{el,net} = 52 \text{ MWe}$ (estimated power output at design given), we calculate the gross turbine power equal $P_{el,gros} = \frac{P_{el,net}}{n_{el}} = \frac{52 \text{ MWe}}{0.87} = 59.78 \text{ MWe}$ (Figure 7.15).

Power Cycle		
Design turbine gross output	59.87	MWe
Estimated gross to net conversion factor	0.87	
Estimated net output at design (nameplate)	52	MWe
Cycle thermal efficiency	0.4	
Cycle thermal power	150	MWt

Figure 7.15 Properties of a solar thermal station in SAM

Next step is the properties of the power block, defining the power block yield strength of 0.4 (Cycle Thermal Efficiency) and the required cycle thermal power at the turbine is equal to 149.45MWth, which is calculated by the software according to the estimated net energy transfer rate in the grid. The inlet and outlet temperature of the fluid follows (565 °C - 290 °C), the operating pressure at 100 bar and the steam cycle blow down fraction at 0.02(Figure 7.17 and 7.19).

The station control values follow, setting the hot tank heater temperature at 500°C, the fraction of thermal power needed for standby at 2, the minimum turbine operation at 0.2, the start time of the power block to 30 minutes (0.5 hours) and the thermal energy required to start should be at 50%. The minimum rate of operation of the turbine will be 0.2 while the maximum operating torque of the turbine will be 1.05(Figure 7.18).

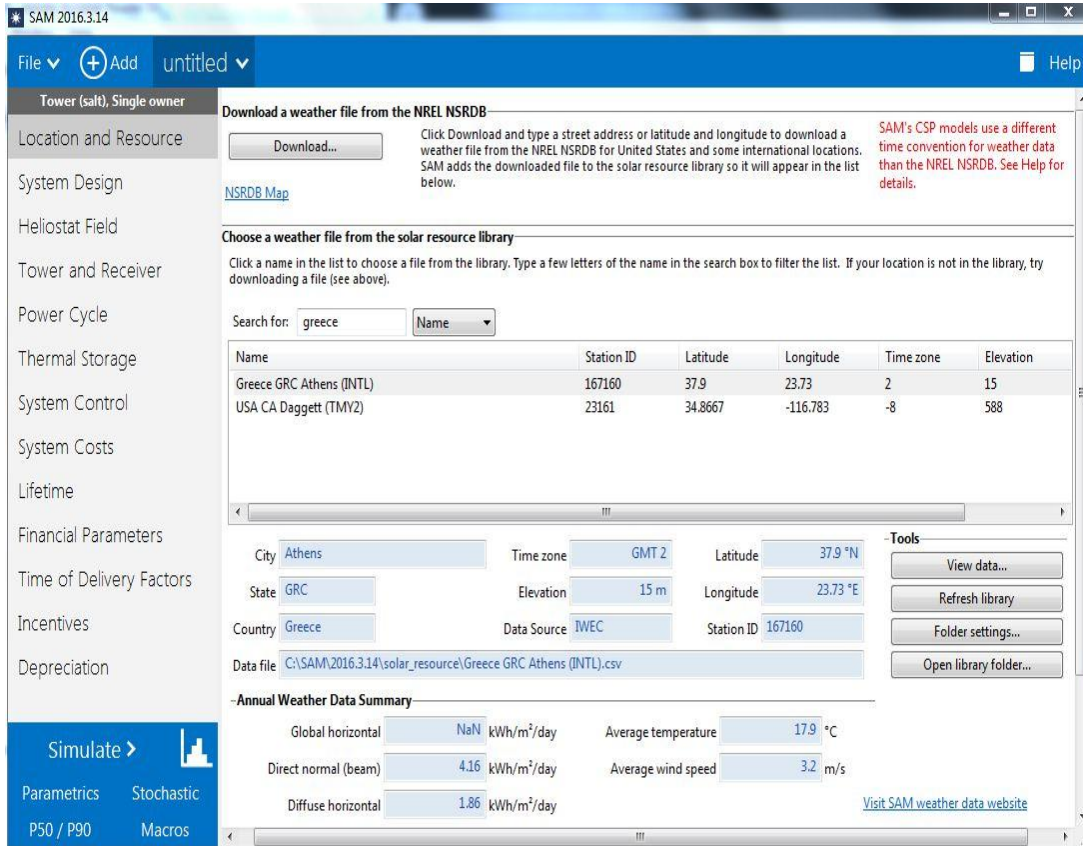


Figure 7.16 Location options of CSP in SAM

System Design Parameters			
Power cycle gross output	<input type="text" value="59.87"/> MWe	Cycle thermal efficiency	<input type="text" value="0.4"/>
Estimated gross to net conversion factor	<input type="text" value="0.87"/>	Cycle thermal power	<input type="text" value="149.675"/> MWt
Estimated net output (nameplate)	<input type="text" value="52.0869"/> MWe	HTF hot temperature	<input type="text" value="565"/> °C
		HTF cold temperature	<input type="text" value="290"/> °C

Figure 7.17 Design of the Power Block in SAM

General Design Parameters	
Pumping power for HTF through power block	0.55 kW/kg/s
Fraction of thermal power needed for standby	2
Power block startup time	0.5 hours
Fraction of thermal power needed for startup	0.5
Minimum turbine operation	0.2
Maximum turbine over design operation	1.05

Figure 7.18 Control of the Solar Thermal Station in SAM

Next step is the introduction of cooling system properties, the options given to us for the condenser are evaporative, air-cooled or hybrid. We choose to install an air-cooled condenser to restrict water use. We set the ambient temperature = 19 °C, the original temperature difference of the atmospheric air from the steam exiting the turbine to the design point = 10 °C, the pressure drop across the condenser = 1.0028, which is used by SAM to calculate the energy required to maintain airflow. Then we set the minimum condenser pressure = 2 inHg to protect the system. The heat rejection function is set according to the time points of the operation that we want to discharge. Thus, the system will know the time points that will reject heat in cases where the station is not operating at full load. The input pressure on the turbine is selected to be fixed(Fixed Pressure)(Figure 7.19).

Rankine Cycle Parameters	
Boiler operating pressure	100 Bar
Steam cycle blowdown fraction	0.02
Turbine inlet pressure control	Fixed pressure
Condenser type	Air-cooled
Ambient temperature at design	19 °C
ITD at design point	16 °C
Reference condenser water dT	10 °C
Approach temperature	5 °C
Condenser pressure ratio	1.0028
Min condenser pressure	2 inHg
Cooling system part load levels	8

Figure 7.19 Condenser properties in SAM

Now we will look at the Tower and the Solar Receiver, where we set an external cylindrical solar receiver, with heat transfer fluid salts: 60% NaNO₃ and 40% KNO₃. The material used to make the piping in most solar receivers is a stainless steel alloy (Stainless AISI316). For fluid flow pattern among the 8 choices that are given, we select the first one (1), as it is ideal for the particular installation (Figure 7.20).

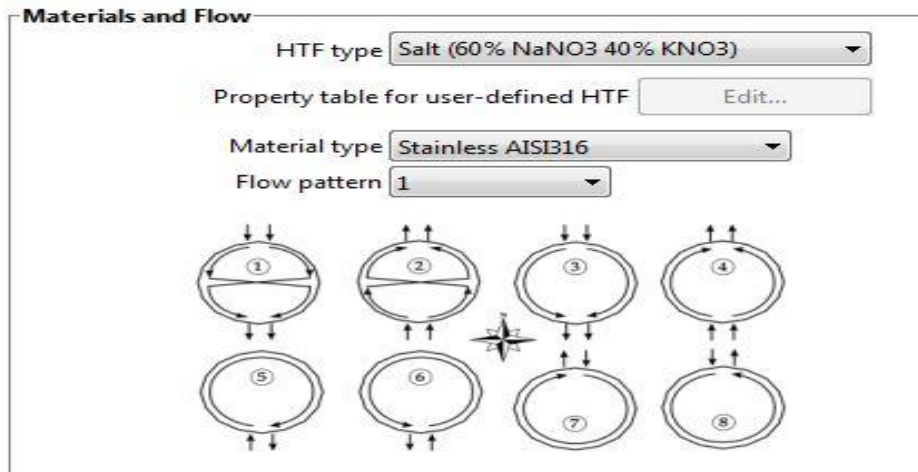


Figure 7.20 Selection of Liquid Heat Transfer, Piping Construction Material and Flow Pattern in SAM

The operating parameters of the solar receiver will be defined, starting from setting the minimum and maximum heat flux rates in the receiver according to flow at the design point. The minimum flow rate will be 0.25 and maximum 1.2. We have already entered the data required for the cycle to work, SAM knows the thermal energy required to receive the solar receiver from the solar field, which is calculated according to the ratio of the over-dimensioning, so the required thermal energy in the solar receiver will be $Q_{inc} = \frac{Q_{net}}{SM} = \frac{149.675}{2.1} MW_{th} = 314.3 MW_{th}$. The ideal solar multiple ratio for this installation will be $SM = 2.1$. The parameters of starting the solar receiver will be now defined, during the simulation, the receiver starts its operation when during the previous time the sunlight is not enough for the receiver to function and the next hour is sufficient. SAM calculates the thermal start energy as a percentage of the thermal energy that will occur at the start time. Thus, we define the time required to start the receiver at 0.2 hours (12 minutes) and the amount of energy required to start at 0.25 (Figure 7.21 and Figure 7.22).

-Design and Operation		
Minimum receiver turndown fraction	0.25	
Maximum receiver operation fraction	1.2	
Receiver startup delay time	0.2	hr
Receiver startup delay energy fraction	0.25	
Receiver HTF pump efficiency	0.850	
Maximum flow rate to receiver	910.741	kg/s

Figure 7.21 Operating Parameters of the Solar Receiver in SAM

System Design Parameters		
Solar multiple	2.10	
Receiver thermal power	314.3	MWt
HTF hot temperature	565.0	°C
HTF cold temperature	290.0	°C

Figure 7.22 Operating Parameters of the Solar Receiver in SAM

In the thermodynamic characteristics of the solar receiver, we set the diameter of the pipelines penetrating the receiver = 40mm and the wall thickness = 1.25mm. The absorption coefficient of the coating of the receiver tubing is usually between 0.91-0.95. A feasible value of this factor is 0.94. We set the heat loss factor if after the simulation there are deviations from the expected values. Then, we introduce the transmittance coefficient of the solar receiver coating equal to 0.88. SAM uses this factor as a black body constant for all wavelengths. (Figure 7.23).

The above data contributes to the optimization of the solar field. The dimensions of the solar receiver are also calculated afterwards optimization using the DELSOL code, which we will see below.

Receiver Heat Transfer Properties		
Tube outer diameter	40	mm
Tube wall thickness	1.25	mm
Coating emittance	0.88	
Coating absorptance	0.94	
Heat loss factor	1	

Figure 7.23 Thermodynamic Characteristics of the Solar Receiver in SAM

The process of modeling the solar field is an extremely complex process. SAM wants to know the properties of the heliostats, the efficiency grades that depend on the construction of the heliostats and the terrain of the field, the boundary of the field and the required thermal energy of the solar receiver. These data of the heliostats depends on

the construction, here will be used BrightSource heliostats, which means 6.50m 2.25m so their reflective area is 14.625m².

The ratio of the total surface of the transmitter to the reflecting surface must be defined. The real total surface area of each heliostat is 15m², but due to the mirror brackets, the actual dimensions are 6.56m 2.29m. SAM has calculated the reflecting surface of each heliostat is default 0.973545. After that the coefficient of reflectivity and purity is defined, where for our heliostats the factor reflectivity is 0.95 and the purity factor is 0.98, so the total mirror reflectance soiling is 0.95 0.98 = 0.93.

The availability factor is equal to 0.99 and the optical error, which is the reflection of each reflector of the ideal reflector so as to determine the heat flux formation in the solar receiver. This value is true for every single heliostat regardless of its position in the field and its distance from the tower. Visual error includes errors of all parameters such as sun detection error, motion system errors, mirror ripple, alignment errors, atmospheric refraction, and tower oscillations. This value is equal to 0.00153rad = 1.53 mrad. The sunset threshold where the solar field will operate is set at 8 deg, and the maximum wind speed limit, where the solar field will stop is equal to 15 m/s(Figure 7.24 and Figure 7.25).

Heliostat Properties		
Heliostat width	6.56	m
Heliostat height	2.29	m
Ratio of reflective area to profile	0.973545	
Single heliostat area	14.625	m ²
Mirror reflectance and soiling	0.93	
Heliostat availability	0.99	
Image error (slope, single-axis)	1.53	mrad
Reflected image conical error	4.32749	mrad
Number of heliostat facets - X	2	
Number of heliostat facets - Y	8	
Heliostat focusing method	Flat	
Heliostat canting method	Winter Solstice	

Figure 7.24 Heliostats properties in SAM

Heliostat Operation		
Heliostat stow/deploy angle	8	deg
Wind stow speed	15	m/s
Heliostat startup energy	0.025	kWe-hr
Heliostat tracking power	0.055	kWe
Design-point DNI	950	W/m ²

Figure 7.25 Heliostats properties in SAM

7.1.3 Optimization Procedure of Solar Power Tower in SAM

It is time for the optimization, since all the characteristics of the heliostats are determined. We first generate the solar field and then we run the code - optimize solar field geometry, and we take the result.

In Figure 7.26 the density of the solar field is presented. We observe that we have a uniform density of heliostats around the tower. The variable prices used for that optimization are the optimized one that are given by laws, scientific experiments and other official investigation. The code optimizes the solar field and the solar receiver for 128.17 m tower height. The height of the solar receiver will be 15.7455 m and the diameter of the solar receiver will be 12.0708 m. The diameter of the receiver is equal to the distance from the center of the receiver to the middle of a receiver panel. The total number of the heliostats at the solar field is 38,570. The 'previous values' are the non-optimized one. (Figure 7.27)

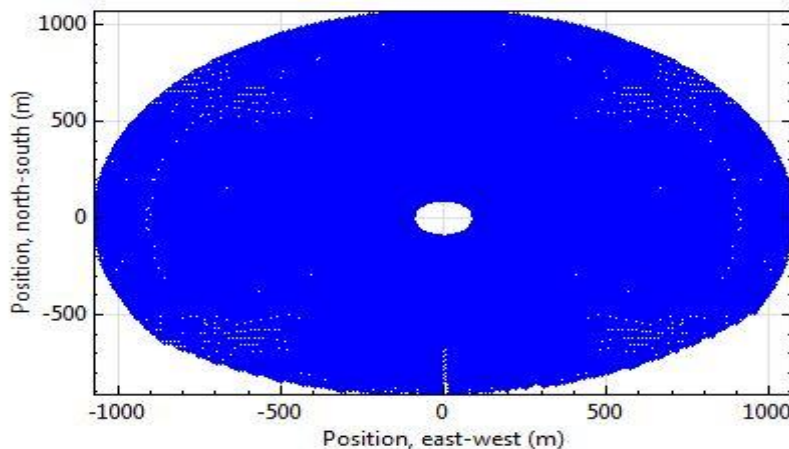


Figure 7.26 Layout of Solar Field in SAM

Item	Units	Update Value	Previous
Receiver height	m	15.7455	15.752
Receiver diameter	m	12.0708	12.0593
Tower height	m	128.17	127
Heliostat count		38570	38735

Figure 7.27 Optimization Results in SAM

7.1.4 Optimization Procedure of the Storage system of Solar Power Tower in SAM

This result is automatically entered into the SAM frame for the features of the solar receiver (Figure 7.28). We define the number of panels that make up the solar receiver. This number should be a multiple of 2 if we have chosen for the flow of the heat transfer fluid pattern passing through the receiver here have been defined 20 panels from the program.

Tower and Receiver Dimensions	
Solar field geometry optimization on the Heliostat Field page calculates new values for tower height, receiver height, and receiver diameter.	
Tower height	128.17 m
Receiver height	15.7455 m
Receiver diameter	12.0708 m
Number of panels	20

Figure 7.28 Features of the Solar Receiver in SAM

SAM has calculated the total reflective surface, optimizing the solar field, these limits were found according to the height of the tower resulting from the optimization. The tower has a height of 128.17m, due to the distance factors, the shortest field distance from the base of the tower is 95.25m and the largest is 1079.5m. DELSOL code, due to these limits, computes the total reflective surface and after introducing the dimensions of the heliostats, the number of the heliostats also is found. The total reflective surface is 564,217 m² and consists of 38,570 heliostats.

SAM calculates the total area of the facility. We calculate the extent required for parts of the system outside the solar field. A typical price for this area is 45 acres (non-solar field land area). The total area of the solar field is expressed using a multiplier indicating the extra surface occupying the field relative to the total reflecting surface. The standard value of the multiplier is 1.2 (solar field land area multiplier). Finally, SAM calculates the total area of the plant to calculate the cost of land. The total area of the solar field equals the product of the surface area of the bands forming the field and the multiplier of the extra surface. From the sum of this area and the surface outside the solar field, the total area of the plant, which will be about 841.245 acres (base land area) is derived (Figure 7.29).

Land Area	
Non-solar field land area	45 acres
Solar field land area multiplier	1.2
Base land area	841,245 acres
Total land area	1,054 acres
Total heliostat reflective area	564,217 m ²

Figure 7.29 Station Data in SAM

In the calculation of the amount of water required by the station for its operation, the amount of washing water of the heliostats is included. According to typical values, we define the amount of water we need for each wash as 0.7 L/m^2 and we define the frequency at 63 washes per year (Figure 7.30).

Mirror Washing	
Water usage per wash	0.70 L/m ² ,aper.
Washes per year	63

Figure 7.30 Water required by the station in SAM

For the storage system, the amount of time we require the system to run at full load(Full Load Hours of TES) must be defined and they are equal to 5. The storage system between a two-tank system must be selected and our choice is the ideal Two Tank Storage Type. From the installation authorization it is known that the station will be able to operate for 5 hours at full load using a two-tank storage system. SAM calculates the total stored salt volume at $3,780 \text{ m}^3$ (Storage Tank Volume). We require two tanks, SAM also finds the diameter of each tank and it is equal to 15.5 m, and the height of the tanks is determined 20m and the minimum storage limit at 1m(Tank Fluid Minimum Height).The maximum stored salt volume to use is $3,591 \text{ m}^3$ (available HTF volume).Wetted loss coefficient in the tank has been estimated as $0.25 \text{ Wt/ m}^2\text{- K}$. Heat and cold heat transfer fluid temperatures for starting the simulation are defined as in the cycle properties, HTC hot temperature is equal to 565°C and HTC cold temperature is equal to 290°C . The percentage of the heat transfer fluid originally in the hot tank (Initial Hot HTC Percent) is set at 30%.

We have to set the minimum safety limit of the temperature of the two tanks, if this limit is not observed during operation, there is a risk of solidification of the fluid, so the backup PC should be activated to heat the fluid up to the acceptable limits. The limit for the cold tank is 280 °C (Cold Tank Heater Temperature Set Point) and for the hot tank at 500 °C (Hot Tank Heater Temperature Set Point), while the power of the electric power will be 4MWe (Cold and Hot Heater Capacity) with an efficiency rating of 0.99 (Tank Heater Efficiency)(Figure 7.31).

System Design Parameters	
Cycle thermal power	149.7 MWt
Hours of storage at power cycle full load	5.0 hours
HTF hot temperature	565.0 °C
HTF cold temperature	290.0 °C

Storage System	
Storage type	Two Tank
TES thermal capacity	748.4 MWt-hr
Available HTF volume	3,591 m ³
Tank height	20 m
Tank fluid minimum height	1 m
Storage tank volume	3780 m ³
Parallel tank pairs	1
Tank diameter	15.5 m
Wetted loss coefficient	0.25 Wt/m ² -K
Estimated heat loss	0.20 MWt
Initial hot HTF percent	30 %
Cold tank heater temperature set point	280 °C
Cold tank heater capacity	4 MWe
Hot tank heater temperature set point	500 °C
Hot tank heater capacity	4 MWe
Tank heater efficiency	0.99
HTF density	1811.42 kg/m ³

Figure 7.31 Properties of Thermal Energy Storage System in SAM

Now we can define how the stored thermal energy penetrates the system. SAM calculates an amount of stored thermal energy sufficient to operate the plant, and sets the penetration limit. We can separate the year into periods, so for each of these periods the system operates differently. For our station, we would like to operate at full load during the day, where there is the greatest demand, for the whole year.

We define the 1st period for full load operation, in the 2nd period it will operate with the stored thermal energy but without the backup boiler to reduce the fuel cost. During the 2nd period the station practically works to start the system in the morning hours and

partially cover the demand in the evening. In the 3rd period it will not work at all (Figure 7.32).

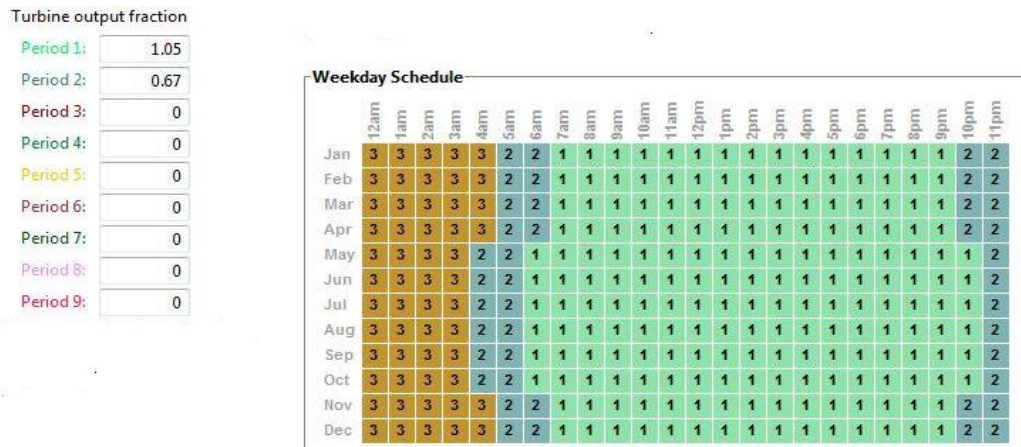


Figure 7.32 Hourly Schedule of Operation of the Station during the Year in SAM

The way the storage system works, varies depending on the conditions prevailing in the system. For periods of time there is sunshine that overlaps production, the system stores thermal energy. In case the storage unit reaches the maximum limit, some heliostats should exit the system (defocus) to reduce the thermal energy that the solar receiver receives. In case the sunshine is not enough for production, the system controls the levels of stored energy and works partly from the solar field and partly from the storage system. Simulation checks at the beginning of each hour the levels of stored thermal energy and decides whether to operate the system or not. In the case there is not enough sunshine to operate the station at full load, SAM checks whether the stored energy is enough for the power system to operate. In case of no sunshine, SAM checks if the stored thermal energy levels are above the penetration limit and acts accordingly.

We define a coefficient indicating the thermal energy that will have to penetrate the system from the storage unit relative to the thermal energy required by the turbine. This factor should be equal to or greater than 1 to cover potential losses of thermal energy penetration in the system. For the second period, we will define the penetration of stored thermal energy as in the first period, but to partially meet the demands of the turbine. Thus, we will define the penetration to 2/3 of the nominal load without infiltration of the conventional boiler. In 3rd period and for all the next periods, we do not allow the

penetration of the stored thermal energy, nor the penetration of the backup boiler, since the system should not operate in this period so it is equal to 0.

Self-consumption losses are separated by SAM into two types, total losses and hourly losses. Total self-consumption losses are used to calculate the actual net electricity transmission coefficient in the simulation on the grid, and therefore the required thermal energy is calculated on the turbine. We import the electric power that the heliostats need at the start of field operation, which will be 0.025kWh for each heliostat. During the operation of the system, each tracer requires 0.055kWh of electrical power for the sun's motion detection. Then we introduce the electromechanical efficiency of the heat transfer fluid pump, which will be 0.85.

We have to set a coefficient corresponding to other self-consumption losses, expressed as a ratio of electric power to thermal power, and it is 0.0055 MWh/MWh (Fraction of rated gross power consumed all times) (Figure 7.33). The pipe length is calculated due to the height of the tower. In SAM we set a multiplier that corresponds to the height of the tower, this multiplier should be greater than 2, as pipes go up and down the tower. The value of that multiplier is equal to 2.6, and the total length of pipelines is calculated 330.2 m. Thermal pipeline losses have been thoroughly researched by previous plants, and have been achieved low values of 8000 W_{th}/m (Piping Heat Loss Coefficient).

We set coefficients or performance grades for the system (Balance Of Plant Parasitic), but also for the conventional boiler (Aux Heater, Boiler Parasitic). SAM calculates the electricity required for the boiler operation. We empirically set the factor of 0.023 MWh/MWh_{cap} (Aux heater boiler parasitic), where MWh_{cap} is the rated power of the station. Two other empirical coefficients for the boiler efficiency have been set (Coeff0 and Coeff1), and the electricity required by the boiler will be calculated and the result is 1.45137 MWh (Aux). All these are shown in Figure 7.33, Figure 7.34, Figure 7.35 and Figure 7.36.

Plant Energy Consumption

Fraction of rated gross power consumed all times MWe/MWcap

	Factor	Coeff 0	Coeff 1	Coeff 2		
Balance of plant parasitic	<input type="text" value="0"/>	<input type="text" value="0.483"/>	<input type="text" value="0.571"/>	<input type="text" value="0"/>	BOP	<input type="text" value="0"/> MWe
Aux heater boiler parasitic	<input type="text" value="0.023"/>	<input type="text" value="0.483"/>	<input type="text" value="0.571"/>	<input type="text" value="0"/>	Aux	<input type="text" value="1.45137"/> MWe

Figure 7.33 Own consumption in SAM

Piping Losses

Piping heat loss coefficient	<input type="text" value="8000"/>	Wt/m
Piping length constant	<input type="text" value="0"/>	m
Piping length multiplier	<input type="text" value="2.6"/>	
Piping length	<input type="text" value="330.2"/>	m
Total piping loss	<input type="text" value="2641.6"/>	kWt

Figure 7.34 Piping Losses in SAM

Heliostat Operation

Heliostat stow/deploy angle	<input type="text" value="8"/>	deg
Wind stow speed	<input type="text" value="15"/>	m/s
Heliostat startup energy	<input type="text" value="0.025"/>	kWe-hr
Heliostat tracking power	<input type="text" value="0.055"/>	kWe
Design-point DNI	<input type="text" value="950"/>	W/m ²

Figure 7.35 Heliostat Operation Parameters

Design and Operation

Minimum receiver turndown fraction	<input type="text" value="0.25"/>	
Maximum receiver operation fraction	<input type="text" value="1.2"/>	
Receiver startup delay time	<input type="text" value="0.2"/>	hr
Receiver startup delay energy fraction	<input type="text" value="0.25"/>	
Receiver HTF pump efficiency	<input type="text" value="0.850"/>	
Maximum flow rate to receiver	<input type="text" value="910.741"/>	kg/s

Figure 7.36 Design and Operation Parameters in SAM

7.1.5 Financial -Cost analysis Procedure in SAM

SAM divides costs into three categories:

- a) The direct capital cost for equipment purchase and labor cost of installation,*
- b) The indirect capital cost for licensing, planning and land costs and*
- c) The labor costs of operation and maintenance, equipment costs and various costs for the operation of the station.*

SAM must also know the costs associated with financing the installation, such as construction loan costs, borrowing costs of an installation, taxation and insurance and cost of use. SAM must know user's cost data for all the parts of the system and calculates NPV (net present value) and internal IRR (internal rate of return). The prices that will be used here, are based on many years of studies so as to reduce costs. In particular, we will get prices from the latest study in 2013 by Turchi and Heath on the economic model of solar power tower using molten salts.[69],[70]

In the direct capital cost field, we set the specific costs for all the parts of the system. The first price concerns the cost of improving the site, our location includes low vegetation, so this cost is equal to 17 \$/m². The special cost of the solar field includes the cost of manufacturing all parts of the heliostat, the wiring, the mechanical parts, the labor costs and the equipment. This cost is equal to 181\$/m².

The specific costs for the other parts and the specific cost of the power block are set. Other costs include the cost of building, the cost of installing equipment associated with electricity production and the cost of control systems. All costs include labor costs and equipment costs. Due to recent study, the specific costs of the other parts is 340 \$/MWe (Balance of the Plant Cost), and the power block cost will be 1,190 \$/MW (Power Cycle Cost). The conventional boiler cost is included in the other costs. The energy storage system cost is equal to 26 \$/kWh_{th} (Thermal Energy Storage Cost).

For calculating the direct capital cost of the tower, a scale indicator is used ($T_{sc} = 0.0113$) (tower cost scaling exponent) that defines the non-linear relation between the tower's cost and its height. A tower reference cost is equal to $FTC = 3,100,000$ \$ (tower

cost fixed). The final price for tower construction is derived from the relation $TTC=FTCe^{THTT^{sc}}$, where THT is the height of the tower. SAM calculates the tower construction cost and it is equal to $TTC = 12,062,426\$$.

For the cost of the solar receiver we set the reference cost of the receiver equal to $RRC = 104,600,000\$$ (receiver reference cost) and the reference area of the receiver equal to $RRA = 1571m^2$ (receiver reference cost). The scale factor of the solar receiver determines the non-linear relation between the receiver's cost and its surface area, it is equal to $R_{sc} = 0.7$ (Receiver cost scaling exponent). The final cost of the solar receiver is calculated from the relation $TRC= RRC\left(\frac{2\pi \times Rh \times Rr}{RRA}\right)^{R_{sc}}$,

where $R_h = 15.8133m$ is the receiver height and $R_r = 12.6525/2 = 6.32625 m$ is the radius of the receiver.

The solar collector's surface area is $564.276 m$, and the total cost of the solar receiver is $TRC = 55,087,516\$(Figure 7.37)$.

Direct Capital Costs			
-Heliostat Field-			
Reflective area	564,276 m ²	Site improvement cost	17.00 \$/m ² \$ 9,592,687.00
		Heliostat field cost	181.00 \$/m ²
		Heliostat field cost fixed	0.00 \$ \$ 102,133,896.00
-Tower-			
Tower height	127 m	Tower cost fixed	3,100,000.00 \$
Receiver height	15.8133 m	Tower cost scaling exponent	0.0113 \$ 12,062,426.00
Heliostat height	2.29 m		
-Receiver-			
Receiver area	628.564 m ²	Receiver reference cost	104,600,000.00 \$
		Receiver reference area	1571 m ²
		Receiver cost scaling exponent	0.7 \$ 55,087,516.00
-Thermal Energy Storage-			
Storage capacity	748.375 MWht	Thermal energy storage cost	26.00 \$/kWht \$ 19,457,750.00
-Power Cycle-			
Cycle gross capacity	59.87 MWe	Fossil backup cost	0.00 \$/kWe \$ 0.00
		Balance of plant cost	340.00 \$/kWe \$ 20,355,800.00
		Power cycle cost	1,190.00 \$/kWe \$ 71,245,296.00
		Subtotal	\$ 289,935,392.00
-Contingency-			
		Contingency cost	7 % of subtotal \$ 20,295,476.00
		Total direct cost	\$ 310,230,848.00

Figure 7.37 Direct Capital Cost in SAM

Summing up all the capital costs mentioned above, the final capital cost is DC=289,935,372\$ (total direct cost - contingency cost 7% of subtotal). However, we set a 7% unexpected cost (Contingency Cost), including the improvements that may occur in all of the above areas of the plant. Summing up this percentage to the final cost also results in total direct costs capital equal to TDC = 310,230,848 \$(total direct cost) (Figure 7.37).

The indirect capital cost is the cost that is not calculated in the cost analysis of specific system segments. For calculating it correctly, the program should know the total area of the station and the rated power. The first indirect cost that is calculated is the cost of design - procurement - construction (Engineer - Procure - Construct or EPC). This includes the costs of licensing, usage rights, advisory services, legal supplies, geotechnical and environmental studies, interconnection, spare parts, and the cost of the design process borne by the plant owner. EPC costs is calculated by SAM by three methods, depending on the size of the station, depending on the rated power or percentage of the direct cost of capital. According to the latest cost study for solar thermal systems, the EPC costs represent 11% of the direct cost of capital, in the present case it will be EPC = \$ 34,125,396 (Figure 7.38).

Indirect Capital Costs					
Total land area	1,061	acres	Cycle net (nameplate) capacity	52	MWe
		\$/acre	% of direct cost	\$/We	\$
EPC and owner cost	0.00		11	0.00	0.00
					\$ 34,125,396.00
Total land cost	0.00		0	0.00	1,000,000.00
					\$ 1,000,000.00
- Sales Tax					
Sales tax basis	78	% of direct cost	Sales tax rate	20	%
					\$ 48,396,012.00
Total indirect cost					\$ 83,521,408.00

Figure 7.38 Indirect Capital Costs in SAM

Land costs are also included in indirect capital cost. In our case, it is estimated that the cost of renting land in the area is \$1,000,000. The same cost includes the taxation for the purchase of equipment, which is calculated by SAM with the definition of the tax rate and the rate of taxation.

Since the capital cost includes equipment and labor costs, the taxable amount will correspond to the proportion of capital destined for the purchase of equipment. In Greece, the average tax on purchasing equipment is estimated at 20%. According to the bibliography, the percentage of this tax will be 78%, and finally the tax cost is \$48,396,012. Therefore, the total indirect cost of the CSP is \$83,521,408 (Figure 7.38).

The total installation cost of the system is estimated at \$ 393,752,256 (total direct cost + total indirect cost). This cost does not include the cost of borrowing, which will be calculated later. Operating and maintenance costs reflect the annual costs of equipment and services incurred after construction of the system. SAM gets data input to calculate cost in three ways, total fixed cost per year, fixed cost in relation to rated power and variable costs in relation to electricity generation. The variable cost is set in relation to the electricity production, which is equal to 4 \$/MWh. This cost includes the costs of materials used by the system for production, such as heat transfer fluid, and water and power supplies consumed for production. The above prices do not remain constant over time, but they are rising. Thus, we will set a percentage increase in prices, 1% per year, which will be calculated by SAM in addition to inflation.

<input type="radio"/> Debt percent	<input type="checkbox"/>	75 % of total cap. cost
<input checked="" type="radio"/> DSCR	<input type="checkbox"/>	0
Tenor		10 years
Annual interest rate		5 %
Debt closing costs		450,000.00 \$
Up-front fee		2.75 % of total debt

Figure 7.39 Loan Parameters in SAM

SAM calculates the cash flow and returns us as a result of the IRR if we know the PPA Price. For Greece, according to the legislation of the RES. (L.3851 / 2010), the selling price for a thermal power station with a thermal energy storage system that ensures at least 2 hours of operation at nominal load, is set at PPA = 284.85 €/MWh = 0.28485 €/kWh = 0.394 \$/kWh. We also have the ability to set a yearly increase rate selling price to partially cover inflation (since no calculated by SAM for the sale price). We will set the annual an increase of 1% and we will choose the IRR solution.

On the loan parameters, we determine the percentage of the capital that we will borrow for the construction of the station. The RAE restricts funding. The Debt Service Coverage Ratio or DSCR should exceed the value of 1.2. After many trials for smoother cash flow and taking into account the limit imposed by RAE, we have borrowed 75% of the total cost of capital, \$ 295,314,192. Today's lending rates for this amount for a long time range between 4% and 6%, so we will set a 5% borrowing rate and payback time at 10 years. Equity accounts for 25% of the cost of capital, \$ 98,438,064. SAM, having calculated the cost of each source of funding, also calculates the weighted average cost of capital, which reflects the cost of raising capital. The weighted average cost of capital is given by the program for reference purposes of 6.23%, but it is not taken into account.

We define the analysis period, 25 years, the Inflation Rate (IR) equal to 2% per year, due to the most recent Euro stat data. We set the real discount rate (d_{real}) equal to 8.2% per year. The Nominal Discount Rate ($d_{nominal}$) is calculated using $d_{nominal} = (1 + d_{real}) \times (1 + IR) - 1$ and it is 10.36% per year (Figure 7.40).

Analysis Parameters	
Analysis period	25 years
Inflation rate	2 %/year
Real discount rate	8.2 %/year
Nominal discount rate	10.36 %/year

Figure 7.40 Economic Analysis Parameters in SAM

Tax and Insurance Rates	
Federal income tax rate	0 %/year
State income tax rate	3 %/year
Sales tax	20 % of total direct cost
Insurance rate (annual)	1 % of installed cost
-Property Tax-	
Assessed percentage	100 % of installed cost
Assessed value	\$ 393,752,256.00
Annual decline	0 %/year
Property tax rate	2 %/year

Figure 7.41 Tax and Insurance Contributors in SAM

According to the existing legislation, the tax rate for companies that are active in the production of electricity through RES is equal to 3% per year (state income tax rate). For the calculation of capital cost, the tax rate for the purchase of equipment is 20% of total direct cost. The Annual insurance rate (annual insurance costs) is 1% of installed

cost. For calculating the real estate tax, we should know the objective value of the facilities which is 100% of the capital cost required for the installation (assessed percentage 100% of installed cost). The objective value of the area will not change for the next years. The property tax is 2% per year (Figure 7.41).

At the end of the 25-year operation of the solar thermal station, the equipment that can be re-used, through a sale to third parties (sales tax) is utilized. We define this value as a percentage of the capital cost, which is typically calculated at 20%. SAM adds the amount that will result from this process to the yearly operating income of the last year of operation of the plant. Finally, with SAM gives us the possibility of defining subsidies, tax reliefs and tax exemptions. A corresponding project in Greece has received a grant from the NER300 program of the European Commission of € 42 million (\$ 58,000,000). Also, there is possibility to set specific depreciation or repayment methods. After the introduction of the financial data has been completed, the simulation of the operation of the station and the economic analysis follows.

7.2 Scenarios Simulation and Results in SAM

In the first scenario (scenario 1.1) we used the parameters presented in the previous paragraph. In this thesis we will examine the behavior of the Solar Power Tower in cases where we change the tower height, the solar multiple and the Design Point DNI and we will see how these parameters affect the system. In this scenario, scenario 1.1, these variables have these prices:

1. Tower Height = 127 m
2. Solar Multiple = 2.1
3. Design Point DNI = 950 W/m²

Simulation of the operation of the station is carried out for scenario 1.1. While the model of the installation is generated, simulation of the function of the station for 25 years and the LC-cycle analysis is carried out for this whole duration. After the simulation, the SAM informs us about the performance of the system for scenario 1.1 through a table (Figure 7.42)

Annual electricity production (year 1) was calculated to be equal to $P_{el,net}=121,964,560$ kWh, the capacity factor (year 1) is equal to 26.7% and the annual water use is equal to $35,385$ m³. Regarding the financial data, SAM informs us of the sales price (PPA price (year 1) = 66.12\$/kWh) and also of the increase in the sales price (PPA Escalation = 1% / year). We can see the nominal Levelized PPA price which is equal to 90.89\$/kWh, the real Levelized price which is equal to 76.46\$/kWh and the Levelized Cost of Energy (LCOE), which reflects the cost of installation and operation in relation to the generation of electricity throughout its operation. Nominal LCOE is derived without taking inflation into account, while Real COE calculates the value of the currency in line with inflation so in our case Levelized COE (nominal) is equal to 83.69\$/kWh. The Net Present Value (NPV) is \$89,357,592 and the IRR (internal rate of return) of the investment is 11%, we can see that year IRR is achieved (20) and IRR at the end of the project is equal to 11.84%. The net capital cost is equal to \$987,397,504, the equity is also equal to \$987,397,504 and finally the size of debt is equal to \$0.

Metric	Value
Annual energy (year 1)	121,964,560 kWh
Capacity factor (year 1)	26.7%
Annual Water Usage	35,385 m ³
PPA price (year 1)	66.12 ¢/kWh
PPA price escalation	1.00 %/year
Levelized PPA price (nominal)	90.89 ¢/kWh
Levelized PPA price (real)	76.46 ¢/kWh
Levelized COE (nominal)	83.69 ¢/kWh
Net present value	\$89,357,592
Internal rate of return (IRR)	11.00 %
Year IRR is achieved	20
IRR at end of project	11.84 %
Net capital cost	\$987,397,504
Equity	\$987,397,504
Size of debt	\$0

Figure 7.42 CSP 's Performance results as simulated in SAM (scenario 1.1)

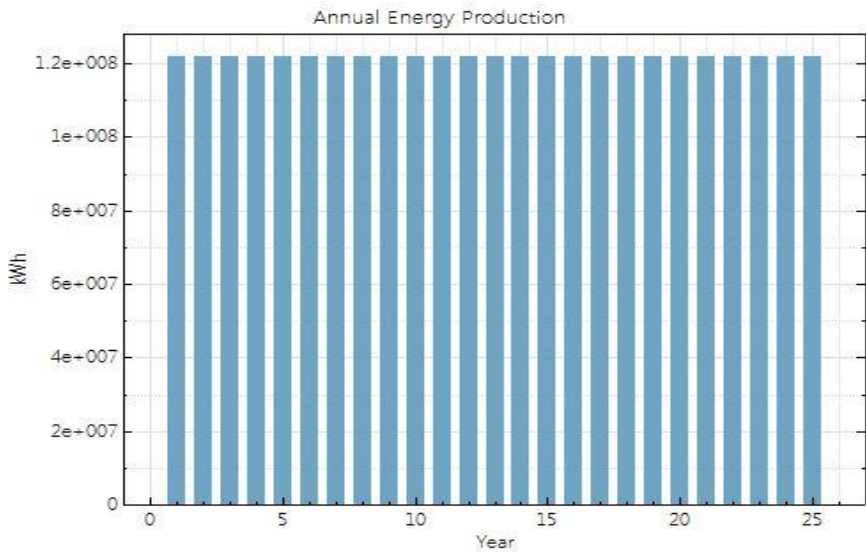


Figure 7.43 CSP 's Annual Electricity Production as simulated in SAM (scenario 1.1)

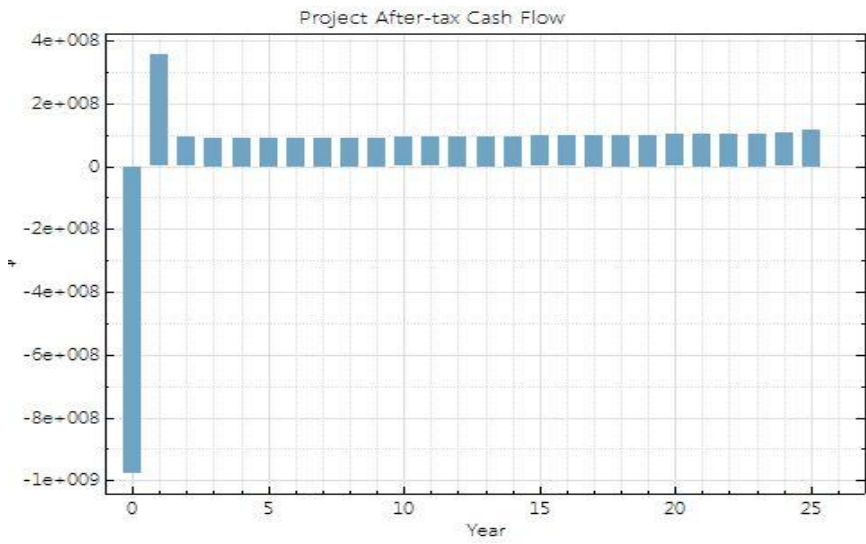


Figure 7.44 CSP 's Cash Flow as simulated in SAM (scenario1.1)

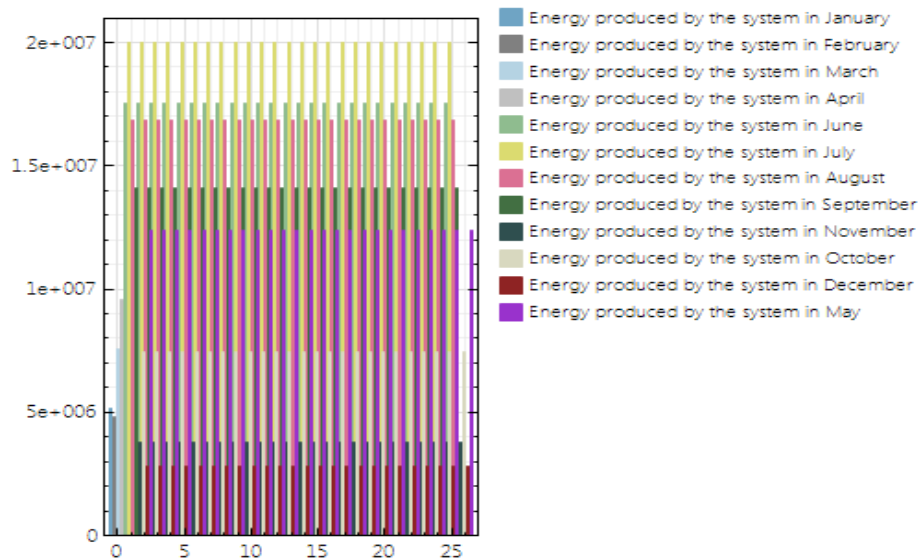


Figure 7.45 CSP 's Energy Production as simulated in SAM (scenario1.1)

For the operation of the system during the year, we will see the monthly electricity output (Figure 7.45). The most productive month of operation of the plant is July with a production of more than 2,00E+12 kWh, and this is ideal due to the higher demand during summer.

Now we have finished our first scenario, we have taken the results and we are going to change some variables in order to see the changes we will have in our results.

7.2.1 Tower Height Scenarios

In the scenarios that follow we will change the price of tower height to get our results. We will examine the system starting from low tower height ending up with a high tower height, taking the results and understanding the behavior of the system due to that change.

Scenario 1.2: Tower Height = 63.5 m

In this scenario we changed the tower height of the system, especially here tower height is the half of that at scenario 1.1, so now tower height is $127 \text{ m} / 2 = 63.5 \text{ m}$ and the results are shown in Figure 7.46.

Metric	Value
Annual energy (year 1)	23,678,514 kWh
Capacity factor (year 1)	5.2%
Annual Water Usage	12,370 m ³
PPA price (year 1)	217.77 €/kWh
PPA price escalation	1.00 %/year
Levelized PPA price (nominal)	397.38 €/kWh
Levelized PPA price (real)	334.30 €/kWh
Levelized COE (nominal)	364.10 €/kWh
Net present value	\$77,494,144
Internal rate of return (IRR)	11.00 %
Year IRR is achieved	20
IRR at end of project	11.83 %
Net capital cost	\$855,297,856
Equity	\$855,297,856
Size of debt	\$0

Figure 7.46 CSP 's Performance results as simulated in SAM (scenario1.2)

Annual electricity production (year 1) was now calculated to be equal to $P_{el,net}=23,678,514\text{kWh}$, we can see that it has decreased, the capacity factor (year 1) has decreased and it is now equal to 5.2% and the annual water use is now equal to $12,370\text{ m}^3$. Regarding the financial data, about the sales price (PPA price (year 1) = 217.77\$/kWh) and the increase in the sales price (PPA Escalation = 1% / year), same as scenario 1.1. The nominal Levelized PPA price has increased and it is now equal to 397.38\$/kWh, the real Levelized price has increased and it is now equal to 334.30 \$/kWh and the Levelized Cost of Energy (LCOE) has increased and it is now equal to 364.10\$/kWh. The Net Present Value (NPV) has decreased and it is now \$ 77,494,144 and the IRR (internal rate of return) of the investment is again equal to 11%, we can see that year IRR is again achieved (20) and IRR at the end of the project is equal to 11.83% (11.84% in scenario 1.1). The net capital cost has decreased and it is now equal to \$855,297,856, the equity is also equal to \$855,297,856 and the size of debt is again equal to \$0.

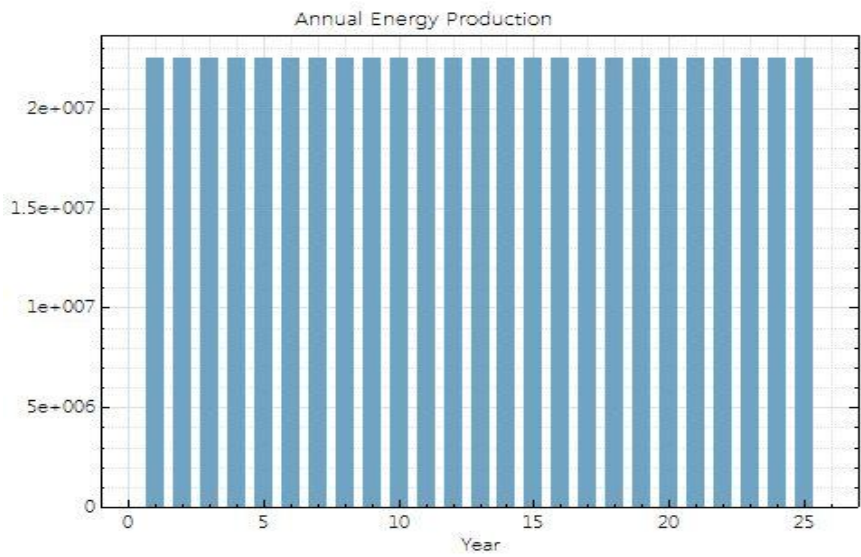


Figure 7.47 CSP 's Annual Electricity Production as simulated in SAM (scenario1.2)

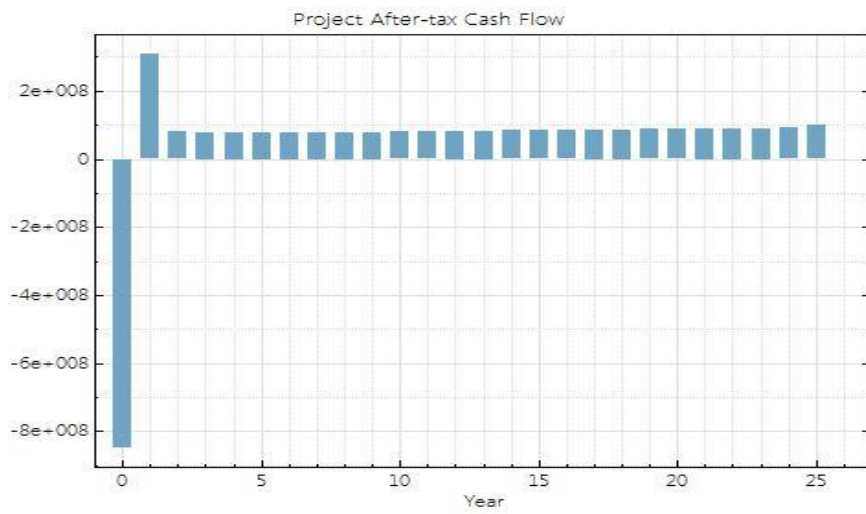


Figure 7.48 CSP 's Cash Flow as simulated in SAM (scenario1.2)

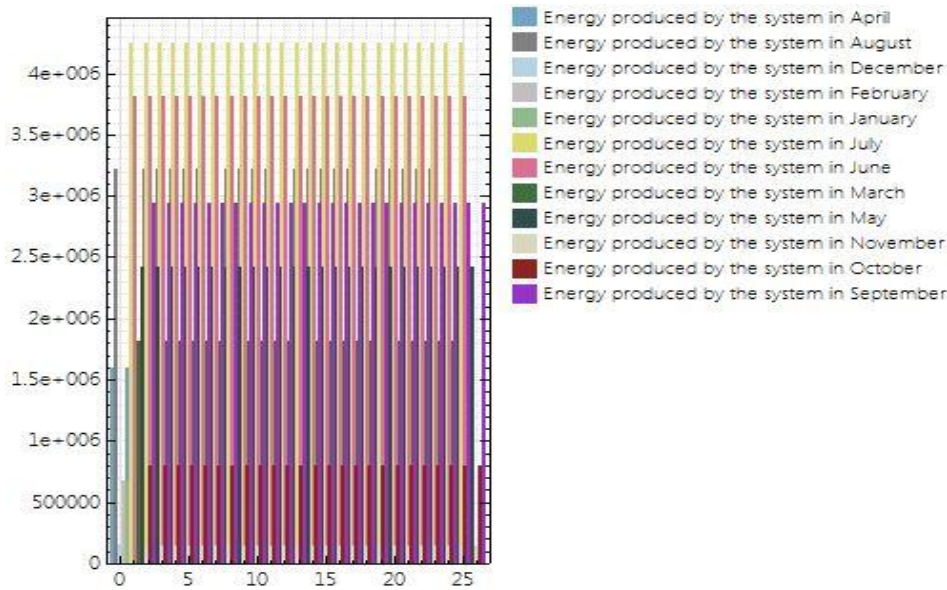


Figure 7.49 CSP 's Energy Production as simulated in SAM (scenario1.2)

Scenario 1.3: Tower Height = 190.5 m

In this scenario we changed the tower height of the system, especially here tower height is +1/2 of that at scenario1.1, so now tower height is 127 m + 63.5= 190.5 m and the results are shown in Figure 7.50.

Metric	Value
Annual energy (year 1)	118,598,840 kWh
Capacity factor (year 1)	26.0%
Annual Water Usage	33,799 m ³
PPA price (year 1)	69.40 ¢/kWh
PPA price escalation	1.00 %/year
Levelized PPA price (nominal)	95.76 ¢/kWh
Levelized PPA price (real)	80.56 ¢/kWh
Levelized COE (nominal)	88.22 ¢/kWh
Net present value	\$91,348,424
Internal rate of return (IRR)	11.00 %
Year IRR is achieved	20
IRR at end of project	11.84 %
Net capital cost	\$1,009,518,528
Equity	\$1,009,518,528
Size of debt	\$0

Figure 7.50 CSP 's Performance results as simulated in SAM (scenario1.3)

Annual electricity production (year 1) was now calculated to be equal to $P_{el,net}=118,598,840$ kWh, we can see that it has decreased, the capacity factor (year 1) has is now equal to 26 % and the annual water use has decreased and it is now equal to $33,799$ m³. Regarding the financial data, about the sales price (PPA price (year 1) = 69.40\$/kWh) and the increase in the sales price (PPA Escalation = 1% / year), same as scenario 1.1. The nominal Levelized PPA price has increased and it is now equal to 95.76\$/kWh, the real Levelized price has increased and it is now equal to 80.56 \$/kWh and the Levelized Cost of Energy (LCOE) has increased and it is now equal to 88.22 \$/kWh. The Net Present Value (NPV) has decreased and it is now \$ 91,348,424 and the IRR (internal rate of return) of the investment is again equal to 11%, we can see that year IRR is again achieved (20) and IRR at the end of the project is equal to 11.84% (same as scenario 1.1). The net capital cost has increased and it is now equal to \$1,009,518,528, the equity is also equal to \$1,009,518,528 and the size of debt is again equal to \$0.

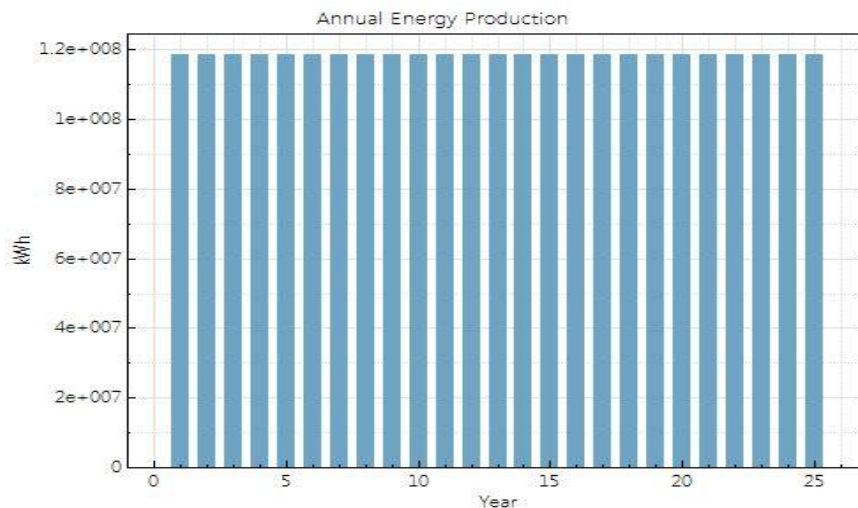


Figure 7.51 CSP 's Annual Electricity Production as simulated in SAM (scenario1.3)

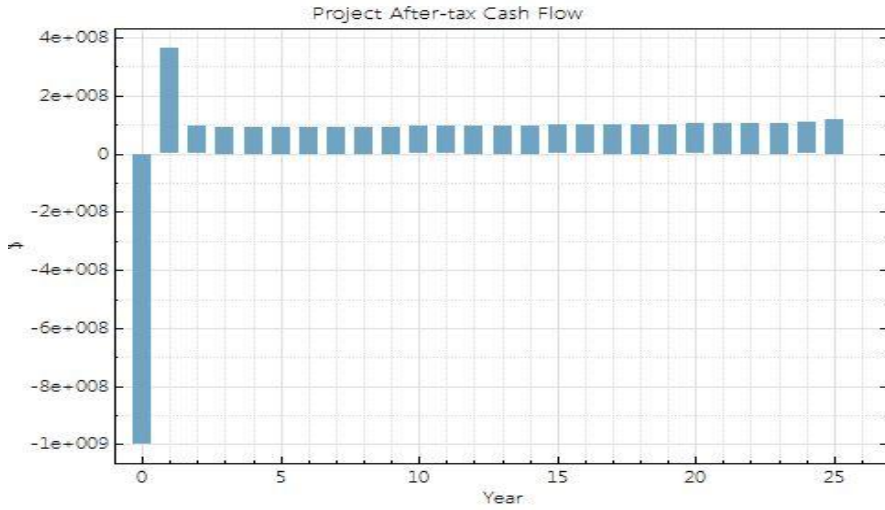


Figure 7.52 CSP 's Cash Flow as simulated in SAM (scenario1.3)

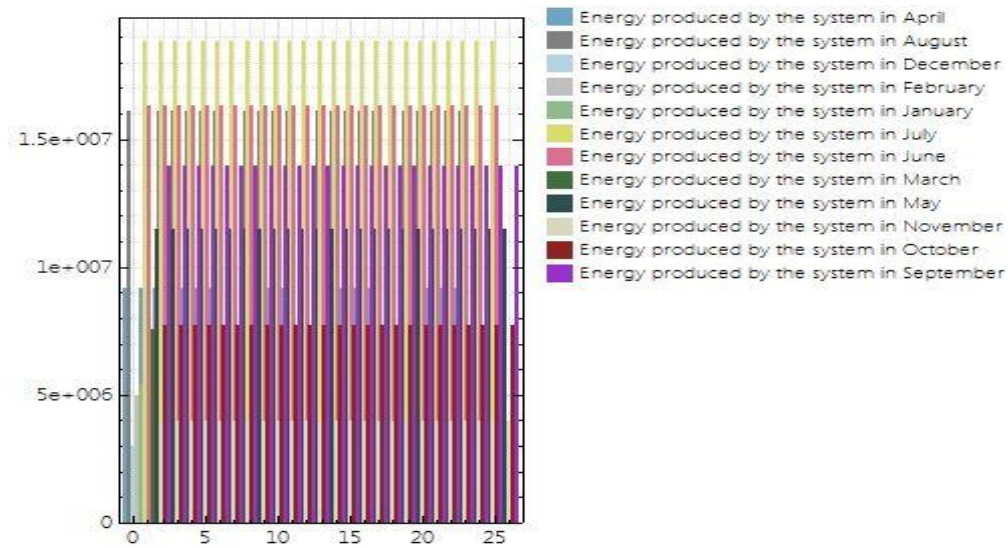


Figure 7.53 CSP 's Energy Production as simulated in SAM (scenario1.3)

Scenario 1.4: Tower Height = 254 m

In this scenario we changed again the tower height of the system, especially here tower height is twice of that at scenario 1.1, so now tower height is equal to $127\text{ m} \times 2 = 254\text{ m}$ and the results are shown in Figure 7.54.

Metric	Value
Annual energy (year 1)	114,133,232 kWh
Capacity factor (year 1)	25.0%
Annual Water Usage	33,652 m ³
PPA price (year 1)	73.62 ¢/kWh
PPA price escalation	1.00 %/year
Levelized PPA price (nominal)	102.20 ¢/kWh
Levelized PPA price (real)	85.97 ¢/kWh
Levelized COE (nominal)	94.21 ¢/kWh
Net present value	\$93,598,376
Internal rate of return (IRR)	11.00 %
Year IRR is achieved	20
IRR at end of project	11.84 %
Net capital cost	\$1,034,517,184
Equity	\$1,034,517,184
Size of debt	\$0

Figure 7.54 CSP 's Performance results as simulated in SAM (scenario1.4)

Annual electricity production (year 1) was now calculated to be equal to $P_{el,net}=114,133,232\text{kWh}$, we can see that it has decreased a little, the capacity factor (year 1) is now equal to 25% and the annual water use has decreased and it is now equal to $33,652\text{ m}^3$. Regarding the financial data, about the sales price (PPA price (year 1) = $73.62\$/\text{kWh}$) and the increase in the sales price (PPA Escalation = 1% / year), same as scenario 1.1. The nominal Levelized PPA price is now equal to $102.2\ \$/\text{kWh}$, it has increased, the real Levelized price is now equal to $85.97\ \$/\text{kWh}$ and the Levelized Cost of Energy (LCOE) is now equal to $94.21\ \$/\text{kWh}$, it has increased. The Net Present Value (NPV) is now $\$93,598,376$ and the IRR (internal rate of return) of the investment is again equal to 11%, we can see that year IRR is again achieved (20) and IRR at the end of the project is again equal to 11.84%. The net capital cost has increased and it is now equal to $\$1,034,517,184$, the equity is also equal to $\$1,034,517,184$ and the size of debt is again equal to $\$0$.

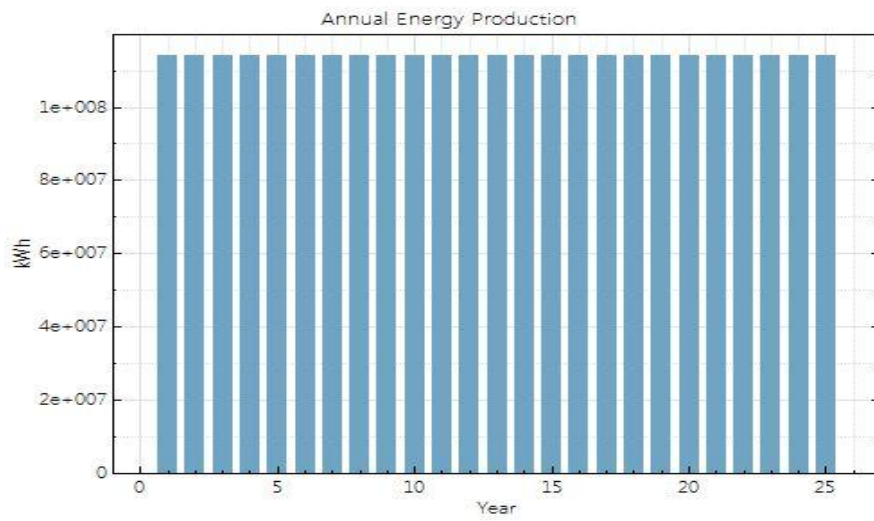


Figure 7.55 CSP 's Annual Electricity Production as simulated in SAM (scenario 1.4)

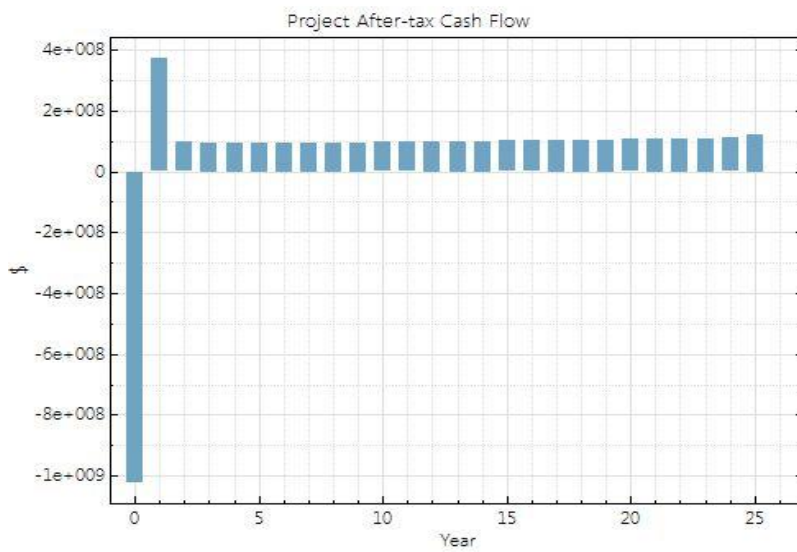


Figure 7.56 CSP 's Cash Flow as simulated in SAM (scenario 1.4)

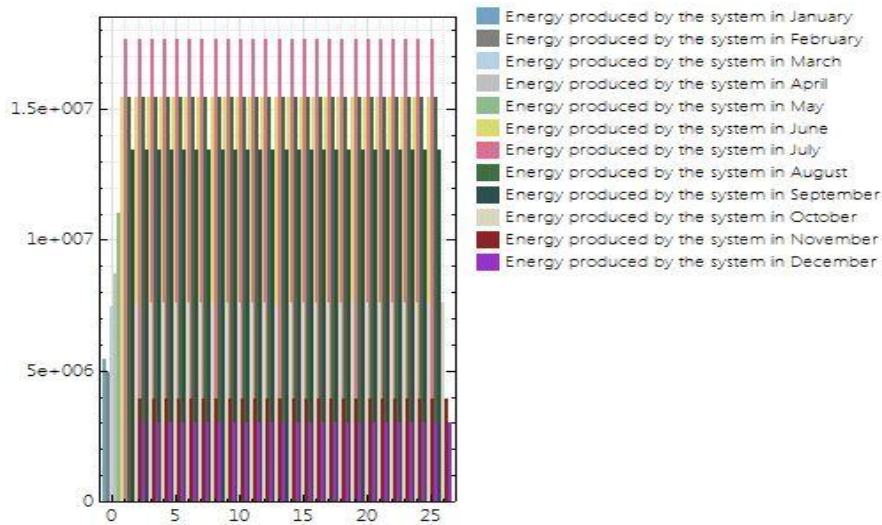


Figure 7.57 CSP 's Energy Production as simulated in SAM (scenario1.4)

Scenario 1.5: Tower Height = 317.5 m

In this scenario we changed again the tower height of the system, especially here tower height is equal to 317.5 m and the results are shown in Figure 7.58.

Metric	Value
Annual energy (year 1)	112,432,120 kWh
Capacity factor (year 1)	24.6%
Annual Water Usage	33,683 m ³
PPA price (year 1)	75.42 €/kWh
PPA price escalation	1.00 %/year
Levelized PPA price (nominal)	104.89 €/kWh
Levelized PPA price (real)	88.24 €/kWh
Levelized COE (nominal)	96.72 €/kWh
Net present value	\$94,545,176
Internal rate of return (IRR)	11.00 %
Year IRR is achieved	20
IRR at end of project	11.84 %
Net capital cost	\$1,045,037,248
Equity	\$1,045,037,248
Size of debt	\$0

Figure 7.58 CSP 's Performance results as simulated in SAM (scenario1.5)

Annual electricity production (year 1) was now calculated to be equal to $P_{el,net}=112,432,120$ kWh, we can see that it has decreased a little, the capacity factor (year 1) is now equal to 24.6% and the annual water use has decreased and it is now

equal to $33,683 \text{ m}^3$. Regarding the financial data, about the sales price (PPA price (year 1) = 75.42 \$/kWh) and the increase in the sales price (PPA Escalation = 1% / year), same as scenario 1.1. The nominal Levelized PPA price is now equal to 104.89 \$/kWh, it has increased, the real Levelized price is now equal to 88.24\$/kWh and the Levelized Cost of Energy (LCOE) is now equal to 96.72 \$/kWh, it has increased. The Net Present Value (NPV) is now \$ 94,545,176 and the IRR (internal rate of return) of the investment is again equal to 11%, we can see that year IRR is again achieved (20) and IRR at the end of the project is again equal to 11.84%. The net capital cost has increased and it is now equal to \$1,045,037,248, the equity is also equal to \$1,045,037,248 and the size of debt is again equal to \$0.

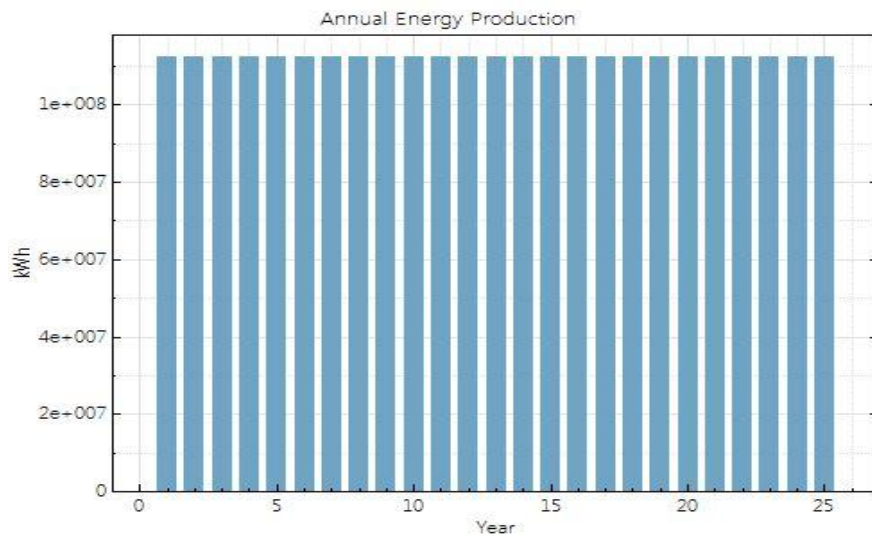


Figure7.59 CSP 's Annual Electricity Production as simulated in SAM (scenario1.5)

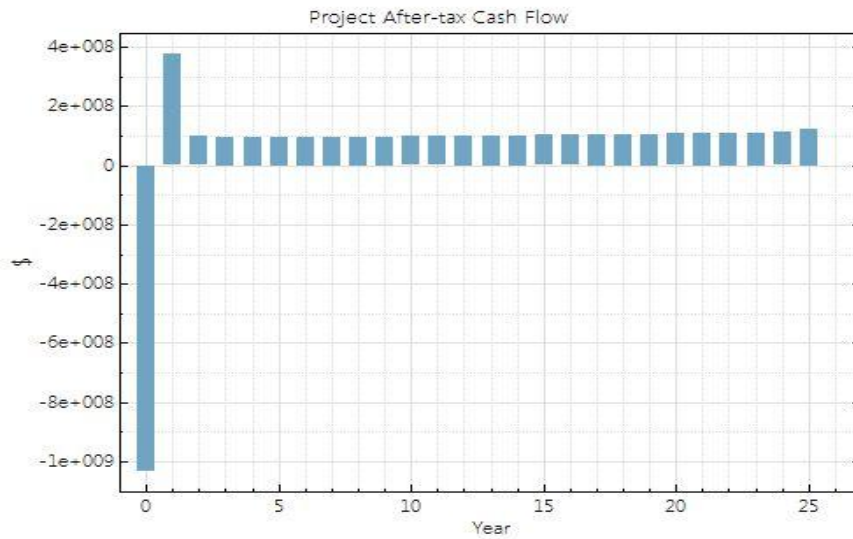


Figure 7.60 CSP 's Cash Flow as simulated in SAM (scenario1.5)

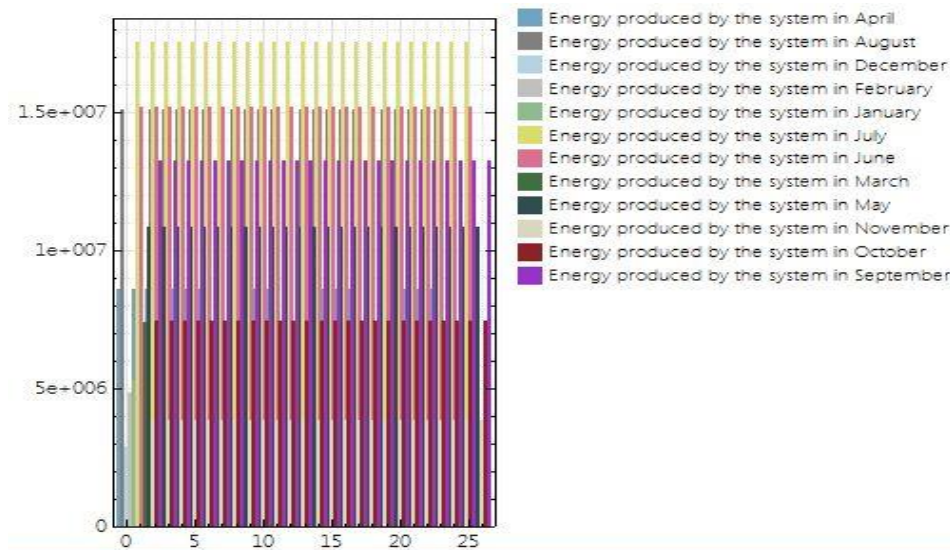


Figure 7.61 CSP 's Energy Production as simulated in SAM (scenario1.5)

Scenario 1.6: Tower height = 400 m

In this scenario we changed again the tower height of the system, especially here tower height is three times of that at scenario1.1, so now tower height is equal to $127\text{ m} \times 3 = 381\text{ m} \approx 400\text{ m}$ and the results are shown in Figure 7.62.

Metric	Value
Annual energy (year 1)	120,853,616 kWh
Capacity factor (year 1)	26.5%
Annual Water Usage	34,838 m ³
PPA price (year 1)	67.81 ¢/kWh
PPA price escalation	1.00 %/year
Levelized PPA price (nominal)	93.33 ¢/kWh
Levelized PPA price (real)	78.51 ¢/kWh
Levelized COE (nominal)	85.97 ¢/kWh
Net present value	\$90,770,976
Internal rate of return (IRR)	11.00 %
Year IRR is achieved	20
IRR at end of project	11.84 %
Net capital cost	\$1,003,105,280
Equity	\$1,003,105,280
Size of debt	\$0

Figure 7.62 CSP 's Performance results as simulated in SAM (scenario1.6)

Annual electricity production (year 1) was now calculated to be equal to $P_{el,net}=120,853,616$ kWh, we can see that it has decreased, the capacity factor (year 1) is now equal to 26.5% and the annual water use has decreased and it is now equal to 34,838 m³. Regarding the financial data, about the sales price (PPA price (year 1) = 67.81\$/kWh) and the increase in the sales price (PPA Escalation= 1% / year), same as scenario 1.1. The nominal Levelized PPA price is now equal to 93.33 \$/kWh, it has increased, the real Levelized price is now equal to 78.51 \$/kWh and the Levelized Cost of Energy (LCOE) is now equal to 85.97\$/kWh, it has increased. The Net Present Value (NPV) is now \$ 90,770,976 and the IRR (internal rate of return) of the investment is again equal to 11%, we can see that year IRR is again achieved (20) and IRR at the end of the project is again equal to 11.84%. The net capital cost has increased and it is now equal to \$1,003,105,280, the equity is also equal to \$1,003,105,280 and the size of debt is again equal to \$0.

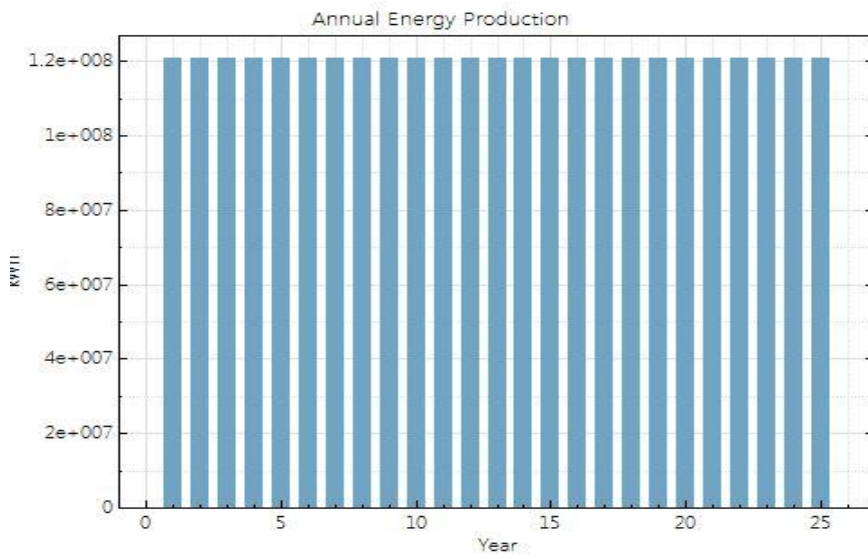


Figure 7.63 CSP 's Annual Electricity Production as simulated in SAM (scenario 1.6)

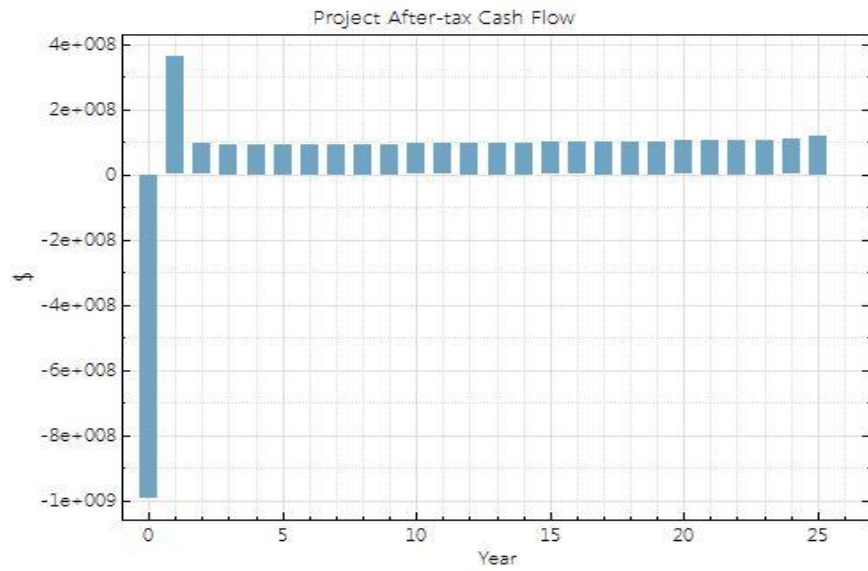


Figure 7.64 CSP 's Cash Flow as simulated in SAM (scenario 1.6)

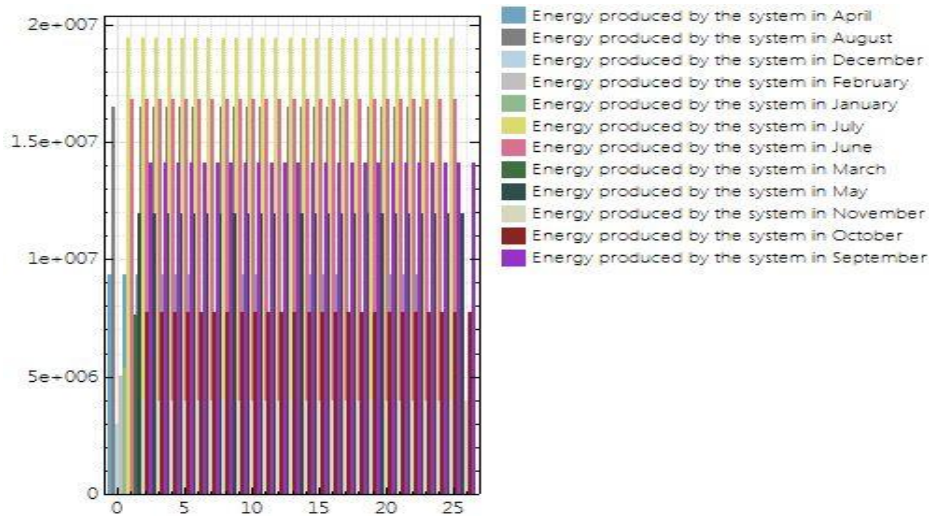


Figure 7.65 CSP 's Energy Production as simulated in SAM (scenario 1.6)

Scenario 1.7: Tower height = 450 m

In this scenario we changed again the tower height of the system, especially here tower height 450 m and the results are shown in Figure 7.66.

Metric	Value
Annual energy (year 1)	121,755,232 kWh
Capacity factor (year 1)	26.7%
Annual Water Usage	35,103 m ³
PPA price (year 1)	66.64 ¢/kWh
PPA price escalation	1.00 %/year
Levelized PPA price (nominal)	91.67 ¢/kWh
Levelized PPA price (real)	77.12 ¢/kWh
Levelized COE (nominal)	84.41 ¢/kWh
Net present value	\$89,907,760
Internal rate of return (IRR)	11.00 %
Year IRR is achieved	20
IRR at end of project	11.84 %
Net capital cost	\$993,512,384
Equity	\$993,512,384
Size of debt	\$0

Figure 7.66 CSP 's Performance results as simulated in SAM (scenario 1.7)

Annual electricity production (year 1) was now calculated to be equal to $P_{el,net}=121,755,232$ kWh, we can see that it has decreased, the capacity factor (year 1)

is now equal to 26.7% and the annual water use is now equal to 35,103 m³. Regarding the financial data, about the sales price (PPA price (year 1) = 66.64\$/kWh) and the increase in the sales price (PPA Escalation = 1% / year), same as scenario 1.1. The nominal Levelized PPA price is now equal to 91.67 \$/kWh, it has increased, the real Levelized price is now equal to 77.12 \$/kWh and the Levelized Cost of Energy (LCOE) is now equal to 84.41 \$/kWh, it has increased. The Net Present Value (NPV) is now \$ 89,907,760 and the IRR (internal rate of return) of the investment is again equal to 11%, we can see that year IRR is again achieved (20) and IRR at the end of the project is again equal to 11.84%. The net capital cost has increased and it is now equal to \$993,512,384, the equity is also equal to \$993,512,384 and the size of debt is again equal to \$0.

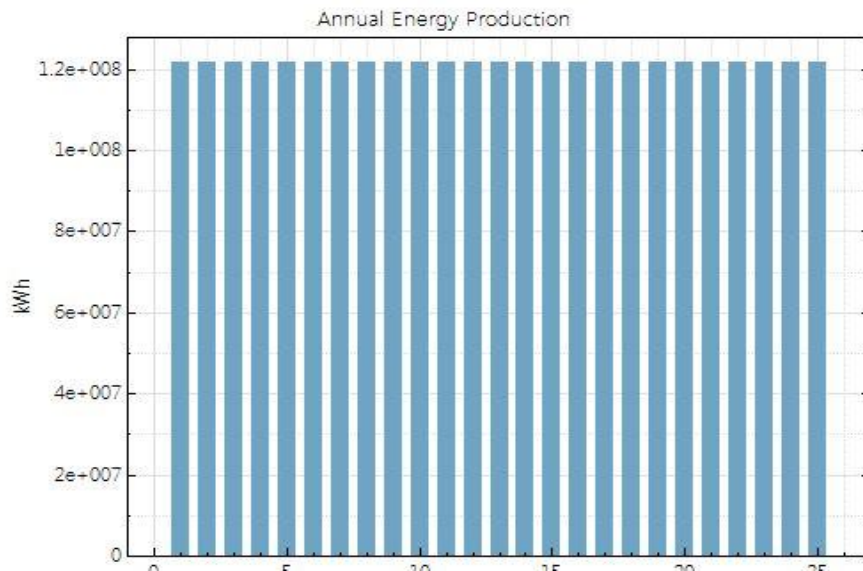


Figure7.67 CSP 's Annual Electricity Production as simulated in SAM (scenario1.7)

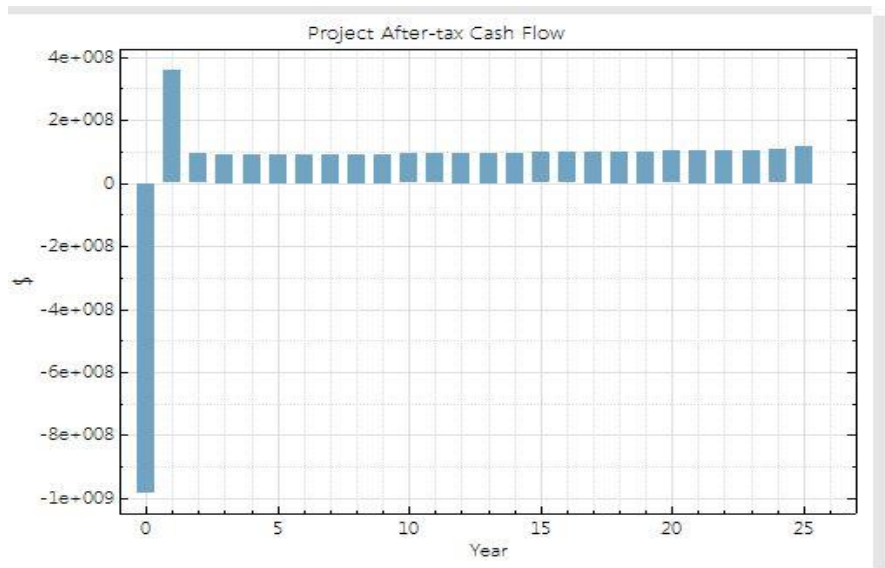


Figure 7.68 CSP 's Cash Flow as simulated in SAM (scenario1.7)

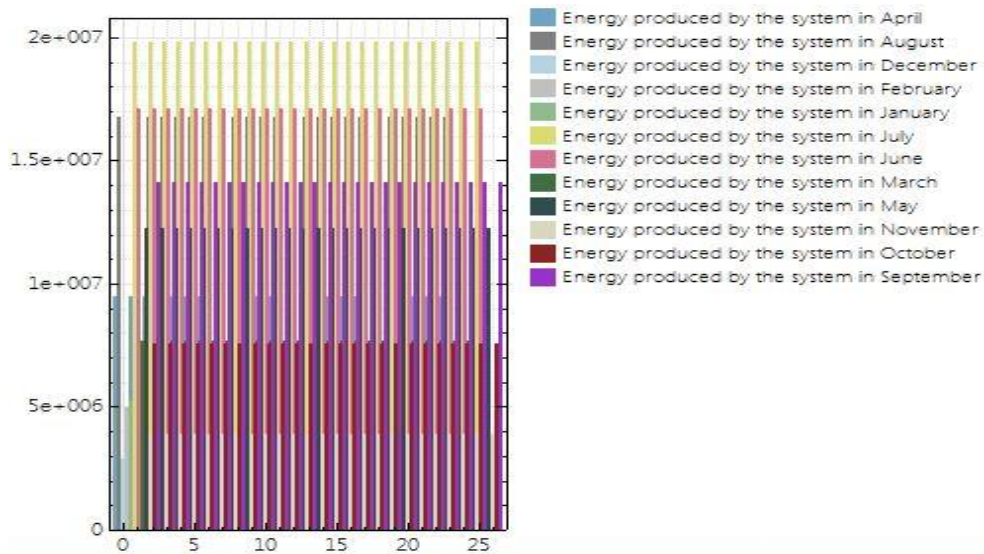


Figure 7.69 CSP 's Energy Production as simulated in SAM (scenario1.7)

Scenario 1.8: Tower Height = 480 m

In this scenario we changed again the tower height of the system, especially here tower height is four times of that at scenario 1.1, (this price is the biggest we could achieve as if bigger price is put the program crashed) so now tower height is equal to $127\text{ m} \cdot 4 = 508\text{ m} \approx 480\text{ m}$ and the results are shown in Figure 7.70.

Metric	Value
Annual energy (year 1)	89,403,344 kWh
Capacity factor (year 1)	19.6%
Annual Water Usage	35,021 m ³
PPA price (year 1)	101.80 ¢/kWh
PPA price escalation	1.00 %/year
Levelized PPA price (nominal)	146.04 ¢/kWh
Levelized PPA price (real)	122.85 ¢/kWh
Levelized COE (nominal)	134.96 ¢/kWh
Net present value	\$103,825,816
Internal rate of return (IRR)	11.00 %
Year IRR is achieved	20
IRR at end of project	11.84 %
Net capital cost	\$1,148,141,184
Equity	\$1,148,141,184
Size of debt	\$0

Figure 7.70 CSP 's Performance results as simulated in SAM (scenario 1.8)

Annual electricity production (year 1) was now calculated to be equal to $P_{el,net} = 89,403,344\text{ kWh}$, we can see that it has decreased, the capacity factor (year 1) is now equal to 19.6 % and the annual water use has decreased and it is now equal to $35,021\text{ m}^3$. Regarding the financial data, about the sales price (PPA price (year 1) = 101.80\$/kWh) and the increase in the sales price (PPA Escalation = 1% / year), same as scenario 1.1. The nominal Levelized PPA price is now equal to 146.04 \$/kWh, it has increased, the real Levelized price is now equal to 122.85 \$/kWh and the Levelized Cost of Energy (LCOE) is now equal to 134.96\$/kWh, it has increased. The Net Present Value (NPV) is now \$ 103,825,8216 and the IRR (internal rate of return) of the investment is again equal to 11%, we can see that year IRR is again achieved (20) and IRR at the end of the project is again equal to 11.84%. The net capital cost has increased and it is now equal to \$1,148,141,184, the equity is also equal to \$1,148,141,184 and the size of debt is again equal to \$0.

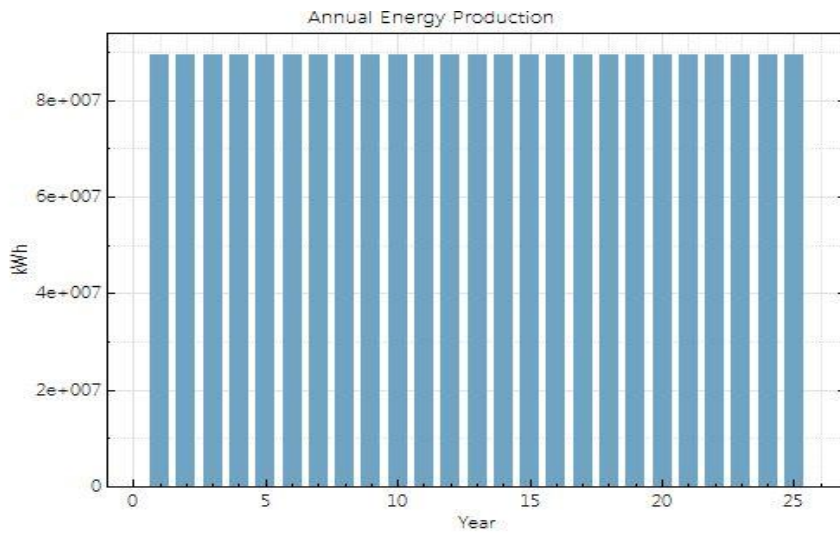


Figure 7.71 CSP 's Annual Electricity Production as simulated in SAM (scenario 1.8)

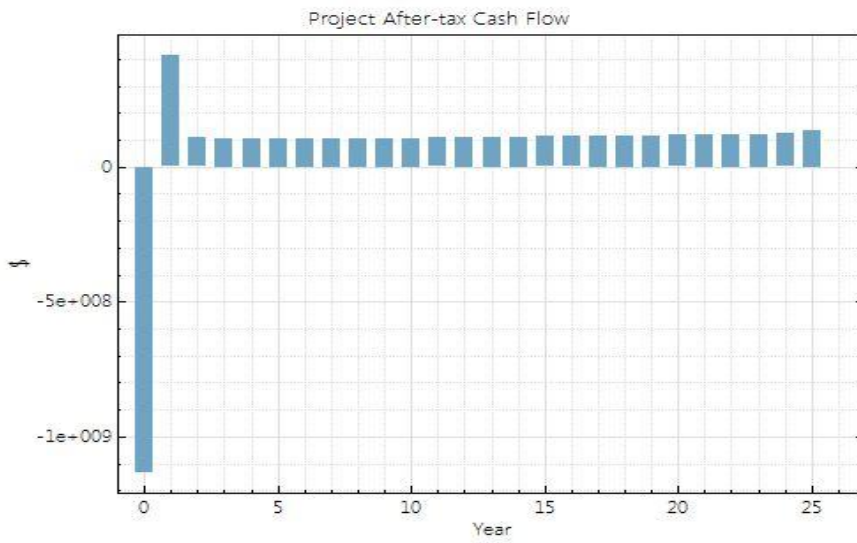


Figure 7.72 CSP 's Cash Flow as simulated in SAM (scenario 1.8)

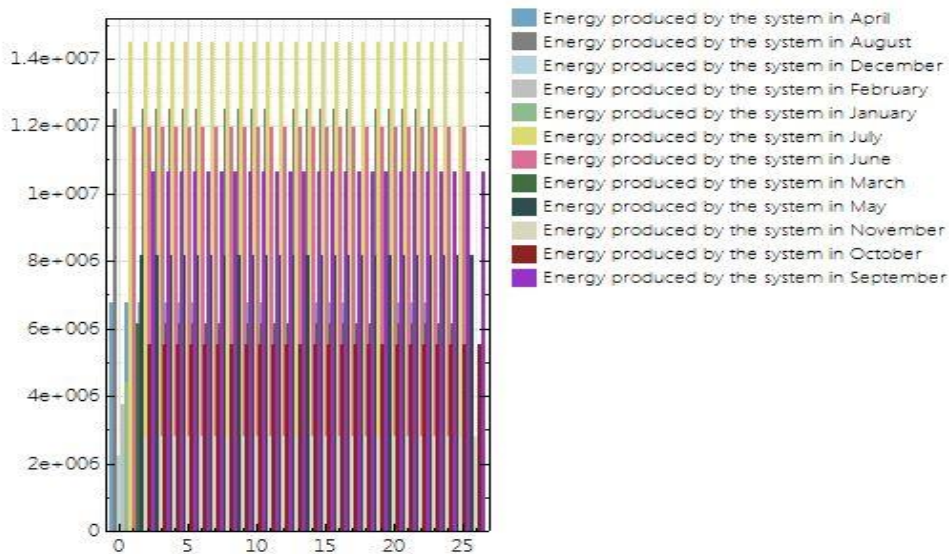


Figure 7.73 CSP 's Energy Production as simulated in SAM (scenario 1.8)

7.2.2 Solar Multiple Scenarios

In the scenarios that follow we will change the price of solar multiple to get our results. We will examine the system starting from low solar multiple ending up with a high solar multiple, taking the results and understanding the behavior of the system due to that change.

Solar multiple is a measure of the solar field aperture area as a function of the power block's nameplate capacity. $\text{Solar Multiple} = \text{Aperture Reflective Area} / \text{Exact Aperture Reflective Area}$. The solar multiple is a way to express the solar field aperture area as a function of the power cycle capacity. A solar multiple of 1 is the aperture area required to deliver sufficient thermal energy to the power cycle to drive it at its nameplate capacity under design conditions. The solar multiple is useful for optimizing the solar field size for a given power cycle capacity and location.

Solar multiple ratio is determined at the design point, defining the energy collection and is defined as the ratio of thermal energy in the solar receiver to the input of thermal energy to the turbine. Over-dimensional ratio is greater than 1, since excess

heat can be stored. Although it is linked with the rate of exploitation, it is important to understand their differences. The over-dimensioning ratio is a design and sizing variable, while the exploitation coefficient is a parameter of energy efficiency.

While the over-dimensional ratio is constant, the operating factor can be reduced by a number of factors (e.g. weather). The range of the over-dimensional ratio depends on the thermal energy required by the system. Its price should be increased to cover the need for excess energy, as there is a thermal energy storage system. By increasing the ratio of over-dimensioning, a larger field surface area is required, resulting in increased cost. A 100 MWe system with solar multiple ratio of 1.5 can store thermal energy for about 3 hours and requires an area of 2.6 km², while a system with a ratio of 2.1 can store thermal energy for about 9 hours.[58],[59],[63]

Scenario 2.1: Solar multiple = 1.05

In this scenario we changed the solar multiple of the system, especially here solar multiple is the half of that at scenario 1, so now it is $2.1/2 = 1.05$ and the results are shown in Figure 7.74.

Metric	Value
Annual energy (year 1)	52,386,520 kWh
Capacity factor (year 1)	11.5%
Annual Water Usage	16,623 m ³
PPA price (year 1)	117.66 ¢/kWh
PPA price escalation	1.00 %/year
Levelized PPA price (nominal)	190.24 ¢/kWh
Levelized PPA price (real)	160.04 ¢/kWh
Levelized COE (nominal)	174.62 ¢/kWh
Net present value	\$81,446,136
Internal rate of return (IRR)	11.00 %
Year IRR is achieved	20
IRR at end of project	11.83 %
Net capital cost	\$899,293,760
Equity	\$899,293,760
Size of debt	\$0

Figure 7.74 CSP 's Performance results as simulated in SAM (scenario2.1)

Annual electricity production (year 1) was now calculated to be equal to $P_{el,net}=52,386,520$ kWh, we can see that it has decreased, the capacity factor (year 1)

has decreased and it is now equal to 11.5% and the annual water use) has decreased and it is now equal to 16,623 m³. Regarding the financial data, about the sales price (PPA price (year 1) = 117.66\$/kWh) and the increase in the sales price (PPA Escalation= 1% / year), same as scenario 1.1. The nominal Levelized PPA price has increased and it is now equal to 190.24 \$/kWh, the real Levelized price has increased and it is now equal to 160.04 \$/kWh and the Levelized Cost of Energy (LCOE) has increased and it is now equal to 174.62 \$/kWh. The Net Present Value (NPV) has decreased and it is now \$ 81,446,136 and the IRR (internal rate of return) of the investment is again equal to 11%, we can see that year IRR is again achieved (20) and IRR at the end of the project is equal to 11.84% (same as scenario 1.1). The net capital cost has decreased and it is now equal to \$899,293,760, the equity is also equal to \$ 899,293,760 and the size of debt is again equal to \$0.

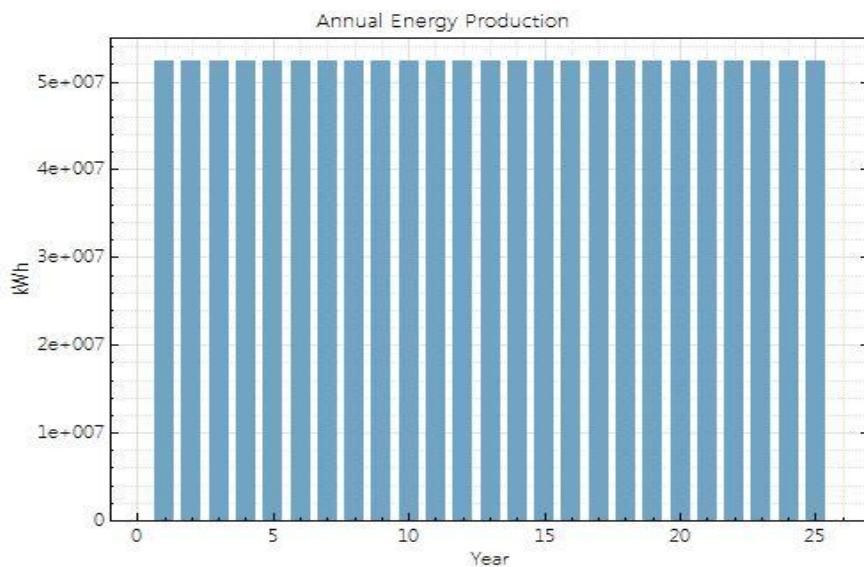


Figure 7.75 CSP 's Annual Electricity Production as simulated in SAM (scenario2.1)

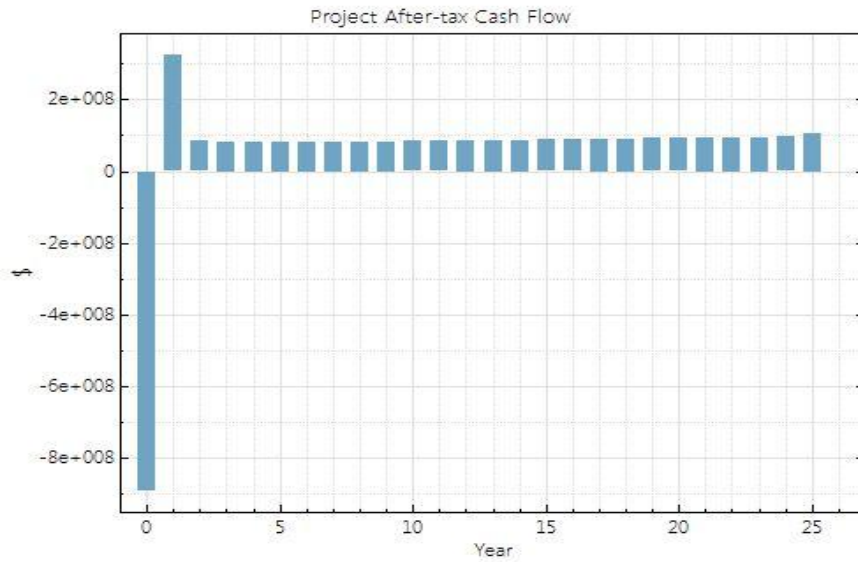


Figure 7.76 CSP 's Cash Flow as simulated in SAM (scenario2.1)

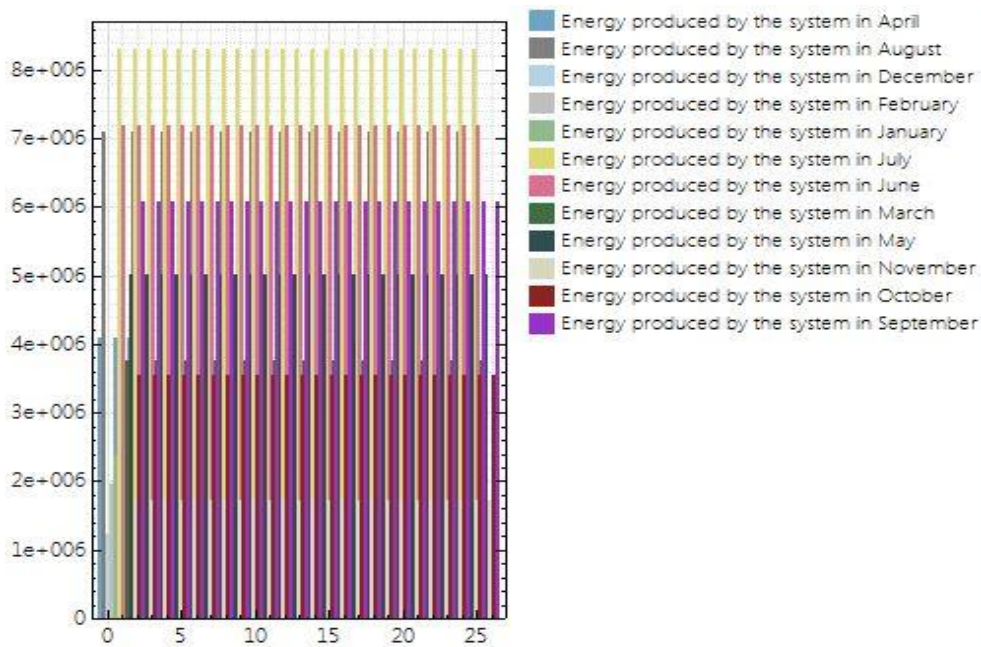


Figure 7.77 CSP 's Energy Production as simulated in SAM (scenario2.1)

Scenario 2.2: Solar multiple = 1.6

In this scenario we changed the solar multiple of the system, especially here we set the solar multiple equal to 1.6 and the results are shown in Figure 7.78.

Metric	Value
Annual energy (year 1)	90,592,800 kWh
Capacity factor (year 1)	19.9%
Annual Water Usage	26,397 m ³
PPA price (year 1)	79.78 ¢/kWh
PPA price escalation	1.00 %/year
Levelized PPA price (nominal)	115.99 ¢/kWh
Levelized PPA price (real)	97.58 ¢/kWh
Levelized COE (nominal)	106.64 ¢/kWh
Net present value	\$85,260,832
Internal rate of return (IRR)	11.00 %
Year IRR is achieved	20
IRR at end of project	11.84 %
Net capital cost	\$941,786,112
Equity	\$941,786,112
Size of debt	\$0

Figure 7.78 CSP 's Performance results as simulated in SAM (scenario 2.2)

Annual electricity production (year 1) was now calculated to be equal to $P_{el,net}=90,592,800$ kWh, we can see that it has decreased, the capacity factor (year 1) has decreased and it is now equal to 19.9% and the annual water use) has decreased and it is now equal to 26,397 m³. Regarding the financial data, about the sales price (PPA price (year 1) = 79.78\$/kWh) and the increase in the sales price (PPA Escalation = 1% / year), same as scenario 1.1. The nominal Levelized PPA price has increased and it is now equal to 115.99 \$/kWh, the real Levelized price has increased and it is now equal to 97.58\$/kWh and the Levelized Cost of Energy (LCOE) has increased and it is now equal to 106.64 \$/kWh. The Net Present Value (NPV) has decreased and it is now \$85,260,832 and the IRR (internal rate of return) of the investment is again equal to 11%, we can see that year IRR is again achieved (20) and IRR at the end of the project is equal to 11.84% (same as case 1). The net capital cost has decreased and it is now equal to \$947,786,112, the equity is also equal to \$947,786,112 and the size of debt is again equal to \$0.

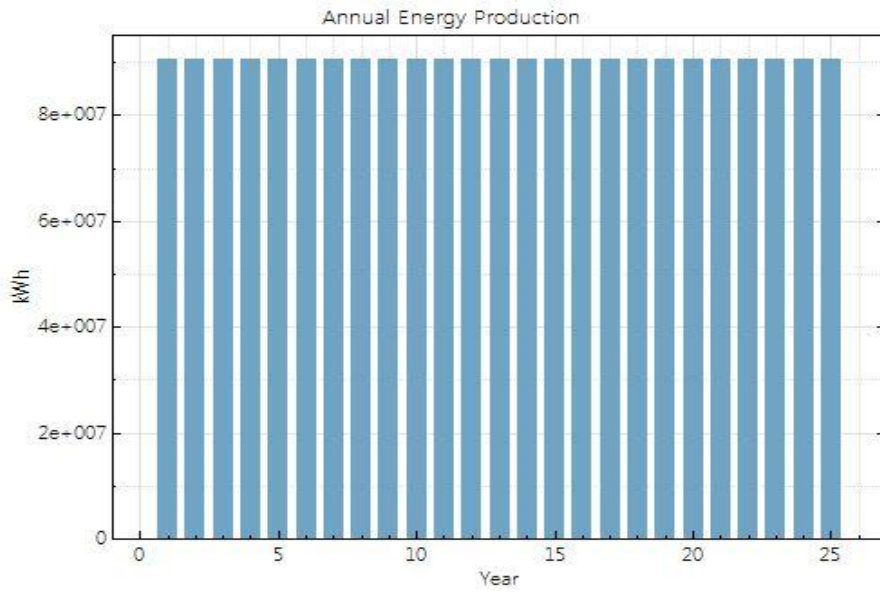


Figure 7.79 CSP 's Annual Electricity Production as simulated in SAM (scenario 2.2)

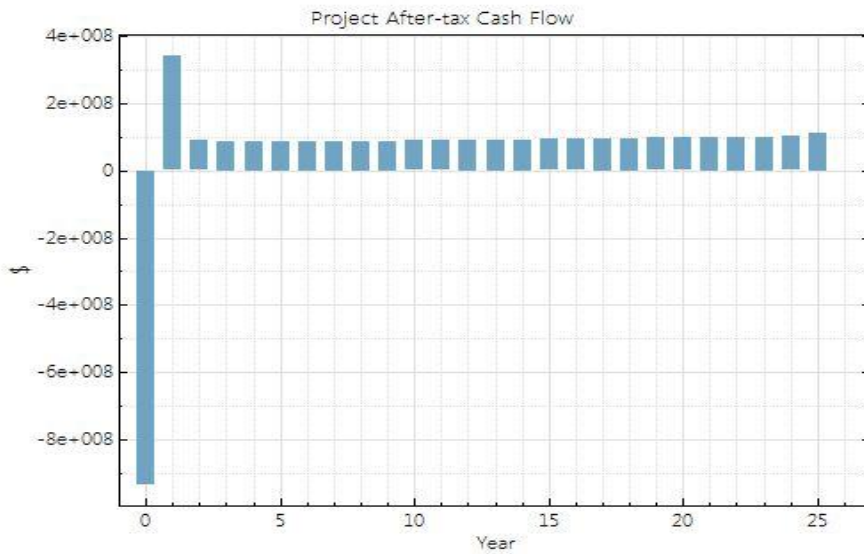


Figure 7.80 CSP 's Cash Flow as simulated in SAM (scenario 2.2)

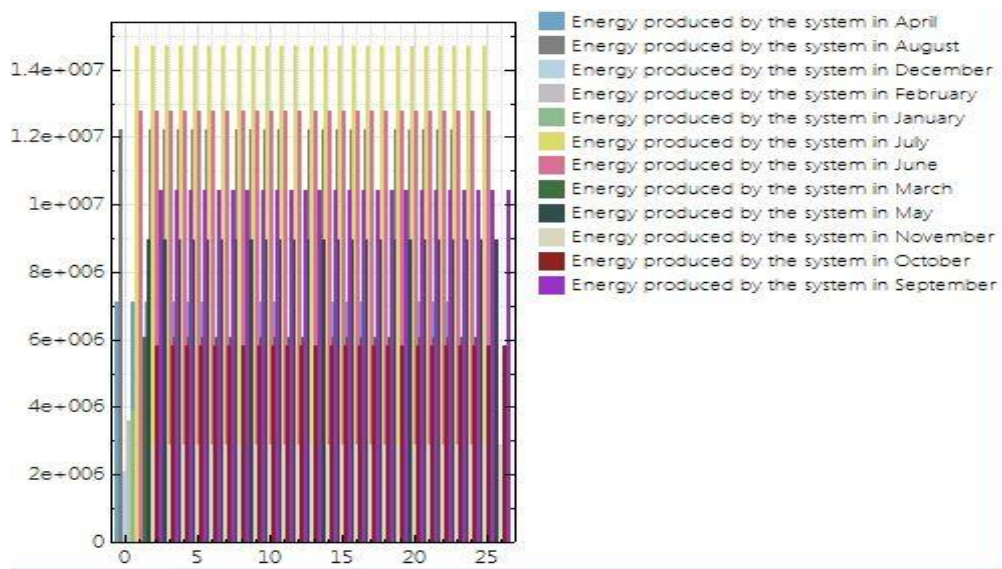


Figure 7.81 CSP 's Energy Production as simulated in SAM (scenario 2.2)

Scenario 2.3: Solar multiple = 2.6

In this scenario we changed the solar multiple of the system, especially here we set the solar multiple equal to 2.6 a little higher than that of the scenario 1.1, and the results are shown in Figure 7.82.

Metric	Value
Annual energy (year 1)	139,210,688 kWh
Capacity factor (year 1)	30.5%
Annual Water Usage	42,823 m ³
PPA price (year 1)	62.46 ¢/kWh
PPA price escalation	1.00 %/year
Levelized PPA price (nominal)	83.91 ¢/kWh
Levelized PPA price (real)	70.59 ¢/kWh
Levelized COE (nominal)	77.36 ¢/kWh
Net present value	\$93,633,368
Internal rate of return (IRR)	11.00 %
Year IRR is achieved	20
IRR at end of project	11.84 %
Net capital cost	\$1,034,965,440
Equity	\$1,034,965,440
Size of debt	\$0

Figure 7.82 CSP 's Performance results as simulated in SAM (scenario 2.3)

Annual electricity production (year 1) was now calculated to be equal to $P_{el,net}=139,210,688$ kWh, we can see that it has increased, the capacity factor (year 1) has increased and it is now equal to 30.5% and the annual water use) has increased and it is now equal to $42,823$ m³. Regarding the financial data, about the sales price (PPA price (year 1) = 62.46\$/kWh) and the increase in the sales price (PPA Escalation = 1% / year), same as scenario 1.1. The nominal Levelized PPA price has decreased and it is now equal to 83.91\$/kWh, the real Levelized price has decreased and it is now equal to 70.59\$/kWh and the Levelized Cost of Energy (LCOE) has decreased and it is now equal to 77.36 \$/kWh. The Net Present Value (NPV) has increased and it is now \$ 93,633,368 and the IRR (internal rate of return) of the investment is again equal to 11%, we can see that year IRR is again achieved (20) and IRR at the end of the project is equal to 11.84% (same as scenario 1.1). The net capital cost has increased and it is now equal to \$1,034,965,440, the equity is also equal to \$1,034,965,440 and the size of debt is again equal to \$0.

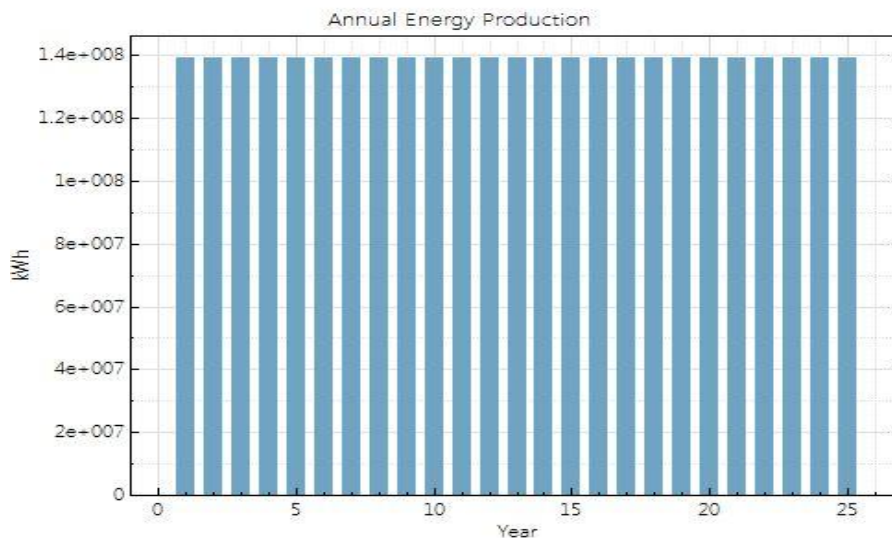


Figure 7.83 CSP 's Annual Electricity Production as simulated in SAM (scenario2.3)

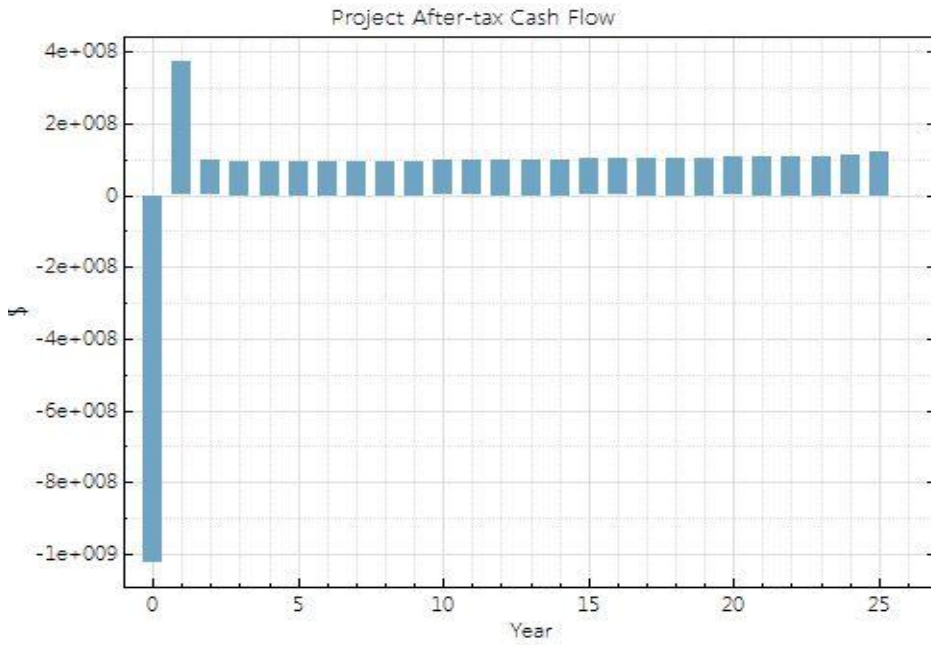


Figure 7.84 CSP 's Cash Flow as simulated in SAM (scenario2.3)

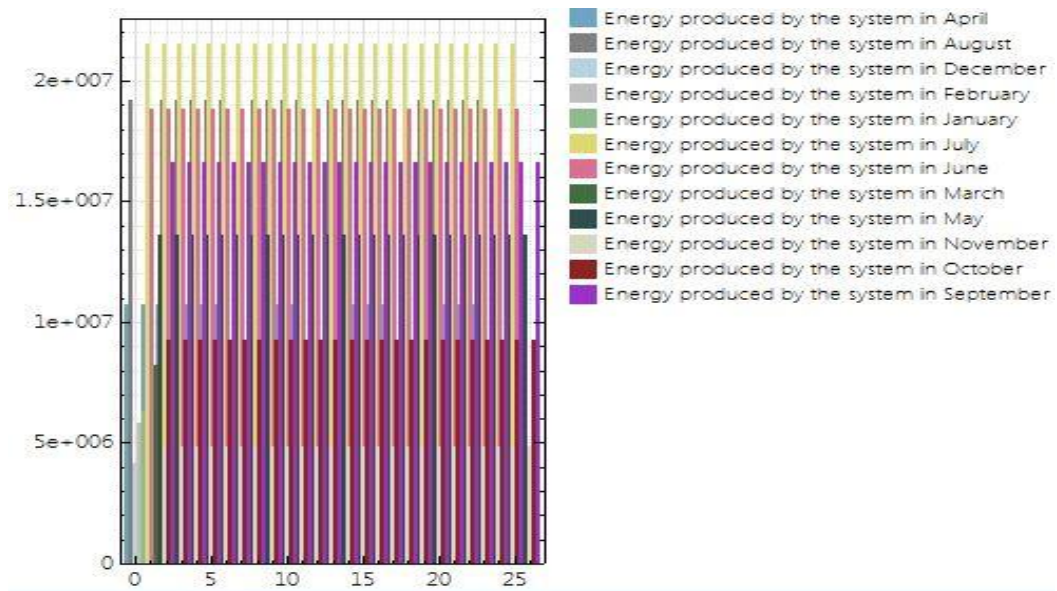


Figure 7.85 CSP 's Energy Production as simulated in SAM (scenario2.3)

Scenario 2.4: Solar multiple = 4.2

In this scenario we changed again the solar multiple of the system, especially here solar multiple is twice of that at scenario 1.1, so now it is equal to $2.1 \times 2 = 4.2$ and the results are shown in Figure 7.86.

Metric	Value
Annual energy (year 1)	74,956,984 kWh
Capacity factor (year 1)	16.4%
Annual Water Usage	57,414 m ³
PPA price (year 1)	153.37 ¢/kWh
PPA price escalation	1.00 %/year
Levelized PPA price (nominal)	183.10 ¢/kWh
Levelized PPA price (real)	154.03 ¢/kWh
Levelized COE (nominal)	169.38 ¢/kWh
Net present value	\$108,745,392
Internal rate of return (IRR)	11.00 %
Year IRR is achieved	20
IRR at end of project	11.84 %
Net capital cost	\$1,202,790,144
Equity	\$1,202,790,144
Size of debt	\$0

Figure 7.86 CSP 's Performance results as simulated in SAM (scenario 2.4)

Annual electricity production (year 1) was now calculated to be equal to $P_{el,net}=74,956,984$ kWh, we can see that it has decreased, the capacity factor (year 1) is now equal to 16.4% and the annual water use has increased and it is now equal to 57,414 m³. Regarding the financial data, about the sales price (PPA price (year 1) = 153.37\$/kWh) and the increase in the sales price (PPA Escalation = 1% / year), same as scenario 1.1. The nominal Levelized PPA price is now equal to 183.10 \$/kWh, it has increased, the real Levelized price is now equal to 154.03 \$/kWh and the Levelized Cost of Energy (LCOE) is now equal to 169.38 \$/kWh, it has increased. The Net Present Value (NPV) is now \$ 108,745,392 and the IRR (internal rate of return) of the investment is again equal to 11%, we can see that year IRR is again achieved (20) and IRR at the end of the project is again equal to 11.84%. The net capital cost has increased and it is now equal to \$1,202,790,144, the equity is also equal to \$1,202,790,144 and the size of debt is again equal to \$0.

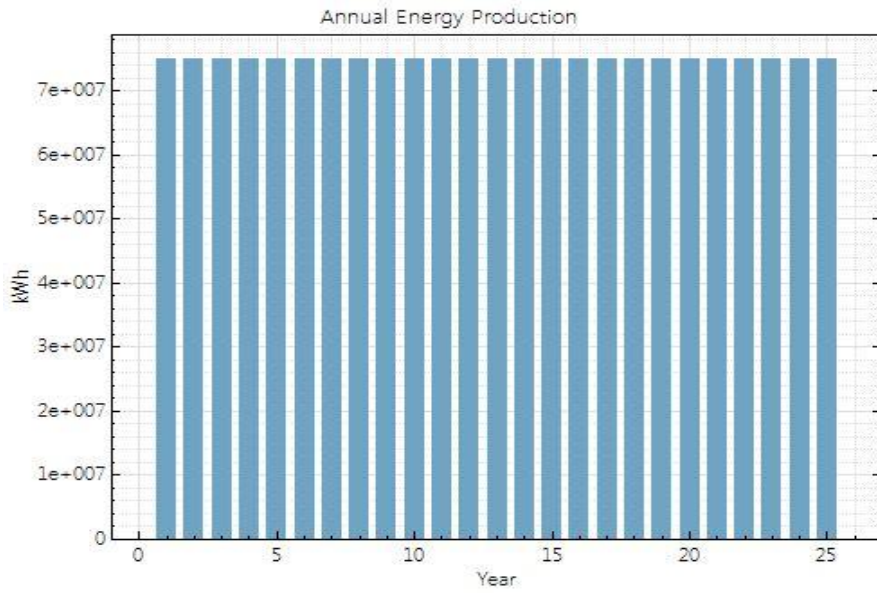


Figure 7.87 CSP 's Annual Electricity Production as simulated in SAM (scenario 2.4)

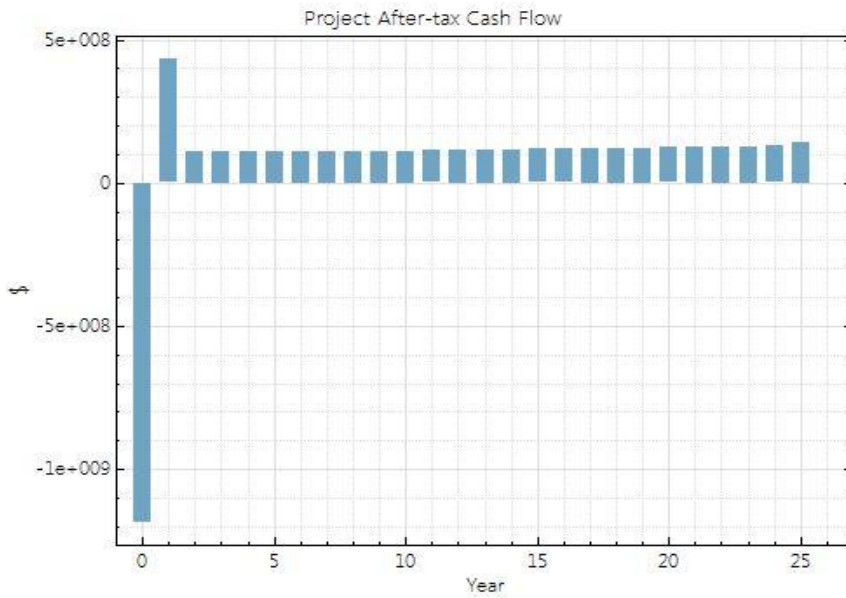


Figure 7.88 CSP 's Cash Flow as simulated in SAM (scenario 2.4)

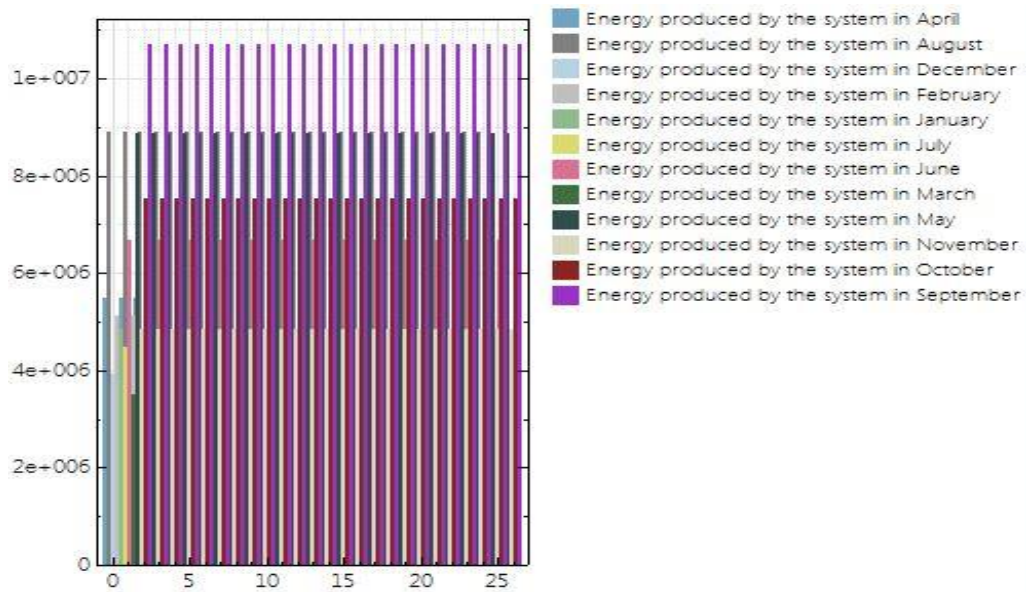


Figure 7.89 CSP 's Energy Production as simulated in SAM (scenario 2.4)

Scenario 2.5: Solar multiple = 8.4

In this case we changed again the solar multiple of the system, especially here solar multiple is four times of that at scenario 1.1, so now it is equal to $2.1 \times 4 = 8.4$ and the results are shown in Figure 7.90.

Metric	Value
Annual energy (year 1)	28,285,772 kWh
Capacity factor (year 1)	6.2%
Annual Water Usage	108,188 m ³
PPA price (year 1)	612.80 €/kWh
PPA price escalation	1.00 %/year
Levelized PPA price (nominal)	707.10 €/kWh
Levelized PPA price (real)	594.84 €/kWh
Levelized COE (nominal)	658.30 €/kWh
Net present value	\$154,627,168
Internal rate of return (IRR)	11.00 %
Year IRR is achieved	20
IRR at end of project	11.84 %
Net capital cost	\$1,712,675,584
Equity	\$1,712,675,584
Size of debt	\$0

Figure 7.90 CSP 's Performance results as simulated in SAM (scenario 2.5)

Annual electricity production (year 1) was now calculated to be equal to $P_{el,net}=28,285,772$ kWh, we can see that it has decreased, the capacity factor (year 1) is now equal to 6.2% and the annual water use has increased and it is now equal to $108,188$ m³. Regarding the financial data, about the sales price (PPA price (year 1) = 612.80\$ / kWh) and the increase in the sales price (PPA Escalation = 1% / year), same as scenario 1.1. The nominal Levelized PPA price is now equal to 707.10 \$/kWh, it has increased, the real Levelized price is now equal to 594.84 \$/kWh and the Levelized Cost of Energy (LCOE) is now equal to 658.30 \$/kW, it has increased. The Net Present Value (NPV) is now \$ 154,627,168 and the IRR (internal rate of return) of the investment is again equal to 11%, we can see that year IRR is again achieved (20) and IRR at the end of the project is again equal to 11.84%. The net capital cost has increased and it is now equal to \$1,712,675,584, the equity is also equal to \$1,712,675,584 and the size of debt is again equal to \$0.

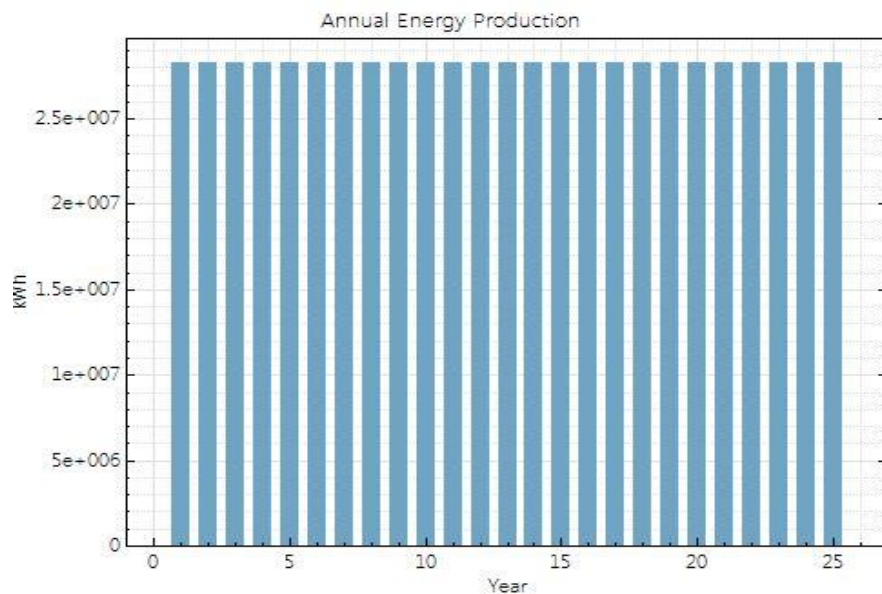


Figure7.91 CSP 's Annual Electricity Production as simulated in SAM (scenario 2.5)

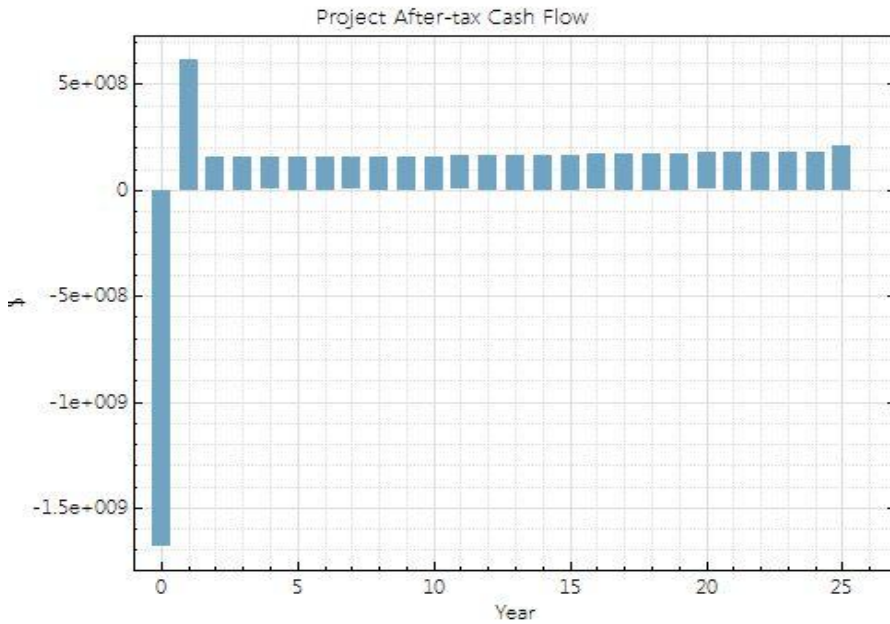


Figure 7.92 CSP 's Cash Flow as simulated in SAM (scenario 2.5)

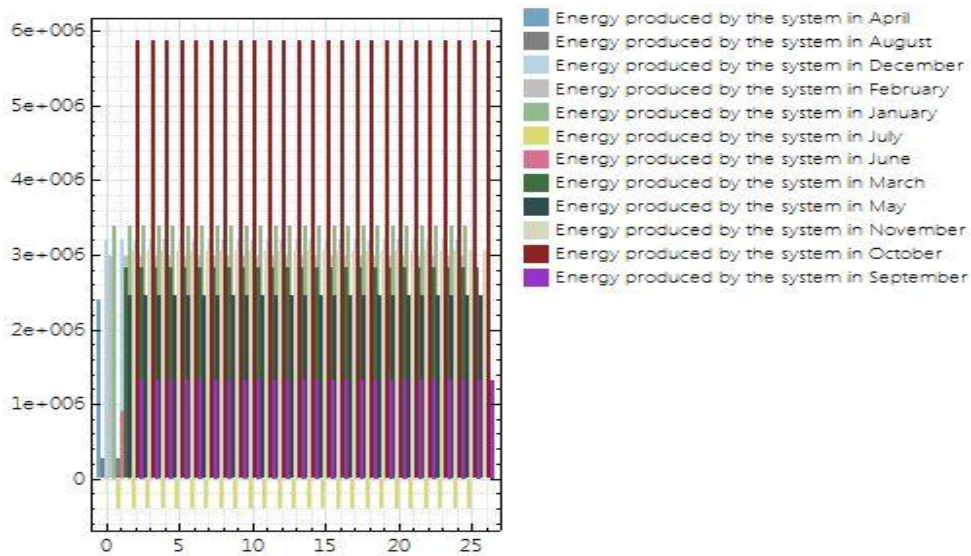


Figure 7.93 CSP 's Energy Production as simulated in SAM (scenario 2.5)

Scenario 2.6: Solar multiple = 16.8

In this scenario we changed again the solar multiple of the system, especially here solar multiple is eight times of that at scenario 1.1, so now it is equal to $2.1 \times 8 = 16.8$ and the results are shown in Figure 7.94.

Metric	Value
Annual energy (year 1)	-23,933,500 kWh
Capacity factor (year 1)	-5.2%
Annual Water Usage	220,739 m ³
PPA price (year 1)	1000.00 €/kWh
PPA price escalation	1.00 %/year
Levelized PPA price (nominal)	1604.91 €/kWh
Levelized PPA price (real)	1350.13 €/kWh
Levelized COE (nominal)	-1150.24 €/kWh
Net present value	\$-5,761,561,600
Internal rate of return (IRR)	NaN
Year IRR is achieved	NaN
IRR at end of project	NaN
Net capital cost	\$2,659,069,440
Equity	\$2,659,069,440
Size of debt	\$0

Figure 7.94 CSP 's Performance results as simulated in SAM (scenario 2.6)

Annual electricity production (year 1) was now calculated to be negative for first time and equal to $P_{el,net} = -23,933,500$ kWh, that means that there is not energy production from the system, the capacity factor (year 1) is also negative and it is equal to -5.2% and the annual water use has increased and it is now equal to 220,739 m³. Regarding the financial data, about the sales price (PPA price (year 1) = 1000 \$/kWh) and the increase in the sales price (PPA Escalation = 1% / year), same as scenario 1.1. The nominal Levelized PPA price is now equal to 1604.91 \$/kWh, it has increased a lot, the real Levelized price is now equal to 1350.13 \$/kWh and the Levelized Cost of Energy (LCOE) is now negative and it is equal to -1150.24 \$/kWh. The Net Present Value (NPV) is also negative \$ -5,761,561,600 and the IRR (internal rate of return) of the investment is NaN, we can see that year IRR is also NaN and IRR at the end of the project is again NaN. The net capital cost has increased and it is now equal to \$2,659,069,440, it has increased, the equity is also equal to \$2,659,069,440 and the size of debt is again equal to \$0. The negative and NaN prices to our variables means that combination of very large solar field relative to the power cycle capacity and no storage does not seem like a realistic design. I suspect that the system is forced to dump large

quantities of energy, causing the LCOE to be negative. Also, with the longer header piping runs, I expect the thermal losses are high.

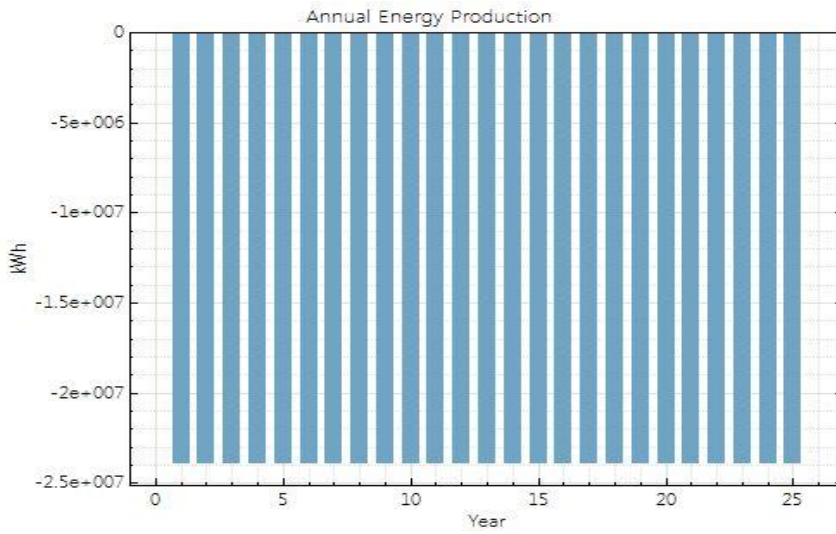


Figure 7.95 CSP 's Annual Electricity Production as simulated in SAM (scenario 2.6)

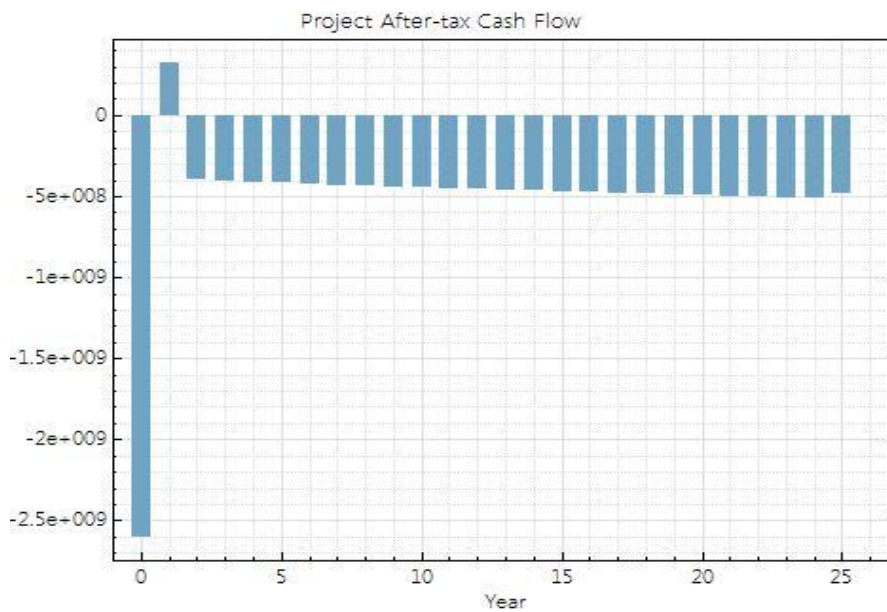


Figure 7.96 CSP 's Cash Flow as simulated in SAM (scenario 2.6)

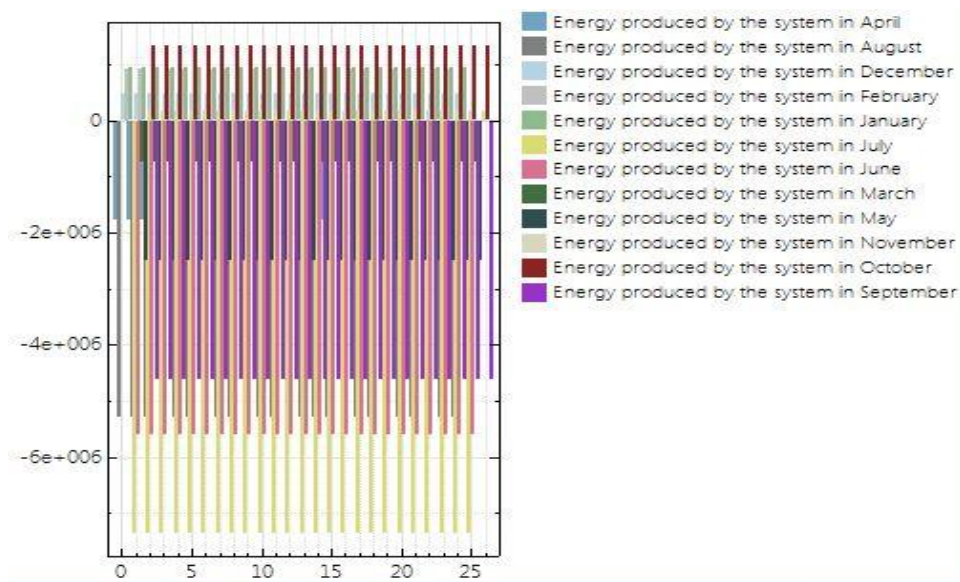


Figure 7.97 CSP 's Energy Production as simulated in SAM (scenario 2.6)

Scenario 2.7: Solar multiple = 21

In this scenario we changed again the solar multiple of the system, especially here solar multiple is ten times of that at scenario 1.1, so now it is equal to $2.1 \times 10 = 21$ and the results are shown in Figure 7.98.

Metric	Value
Annual energy (year 1)	1,776,612 kWh
Capacity factor (year 1)	0.4%
Annual Water Usage	90,320 m ³
PPA price (year 1)	1000.00 €/kWh
PPA price escalation	1.00 %/year
Levelized PPA price (nominal)	2175.09 €/kWh
Levelized PPA price (real)	1829.79 €/kWh
Levelized COE (nominal)	10737.77 €/kWh
Net present value	\$-1,307,879,680
Internal rate of return (IRR)	NaN
Year IRR is achieved	NaN
IRR at end of project	NaN
Net capital cost	\$1,797,018,496
Equity	\$1,797,018,496
Size of debt	\$0

Figure 7.98 CSP 's Performance results as simulated in SAM (scenario 2.7)

Annual electricity production (year 1) was now calculated to be equal to $P_{el,net}=1,776,612$ kWh, we can see that it has decreased, the capacity factor (year 1) is now equal to 0.4% and the annual water use has increased and it is now equal to 90,320 m^3 . Regarding the financial data, about the sales price (PPA price (year 1) = 1000\$/kWh) and the increase in the sales price (PPA Escalation = 1% / year), same as scenario 1.1. The nominal Levelized PPA price is now equal to 2175.09\$/kWh, it has increased a lot, the real Levelized price is now equal to 1829.79\$/kWh and the Levelized Cost of Energy (LCOE) is now equal to 10737.77 \$/kWh, it has increased a lot. The Net Present Value (NPV) is now negative\$ -1,307,879,680 and the IRR (internal rate of return) of the investment is NaN, we can see that year IRR is also NaN and IRR at the end of the project is again NaN. The net capital cost has increased and it is now equal to \$1,797,018,496, it has increased, the equity is also equal to \$1,797,018,496 and the size of debt is again equal to \$0. The negative and NaN prices to our variables means that combination of very large solar field relative to the power cycle capacity and no storage does not seem like a realistic design. I suspect that the system is forced to dump large quantities of energy, causing the LCOE to be negative. Also, with the longer header piping runs, I expect the thermal losses are high.

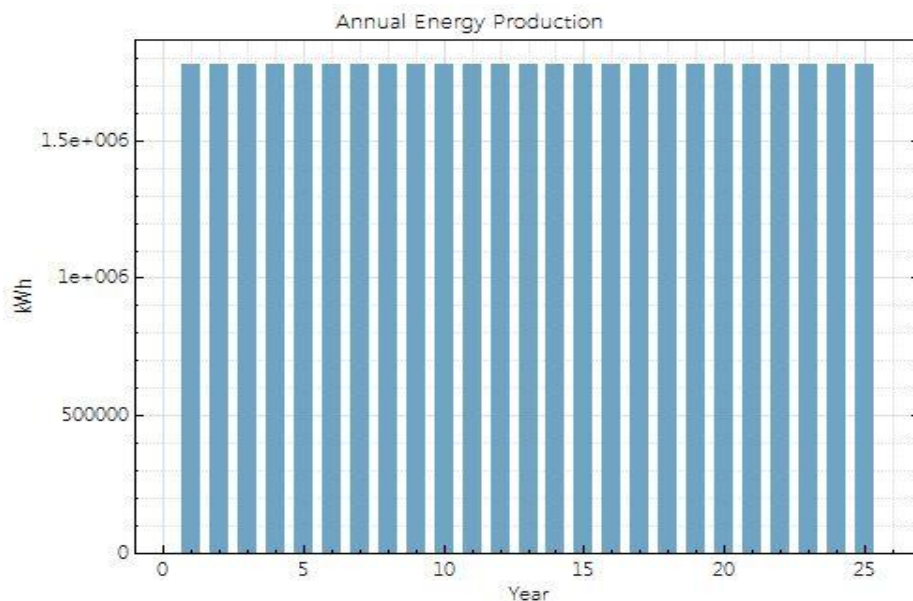


Figure 7.99 CSP 's Annual Electricity Production as simulated in SAM (scenario 2.7)

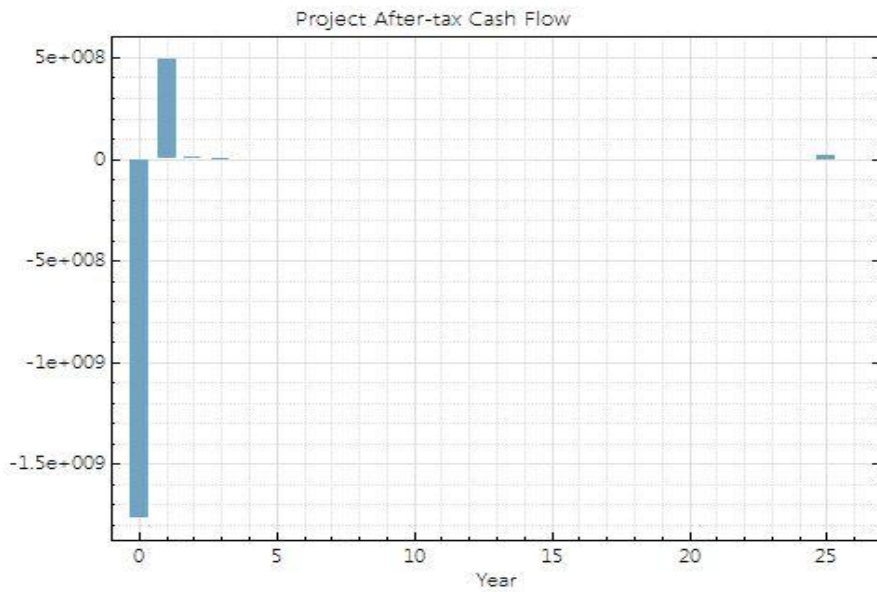


Figure 7.100 CSP 's Cash Flow as simulated in SAM (scenario2.7)

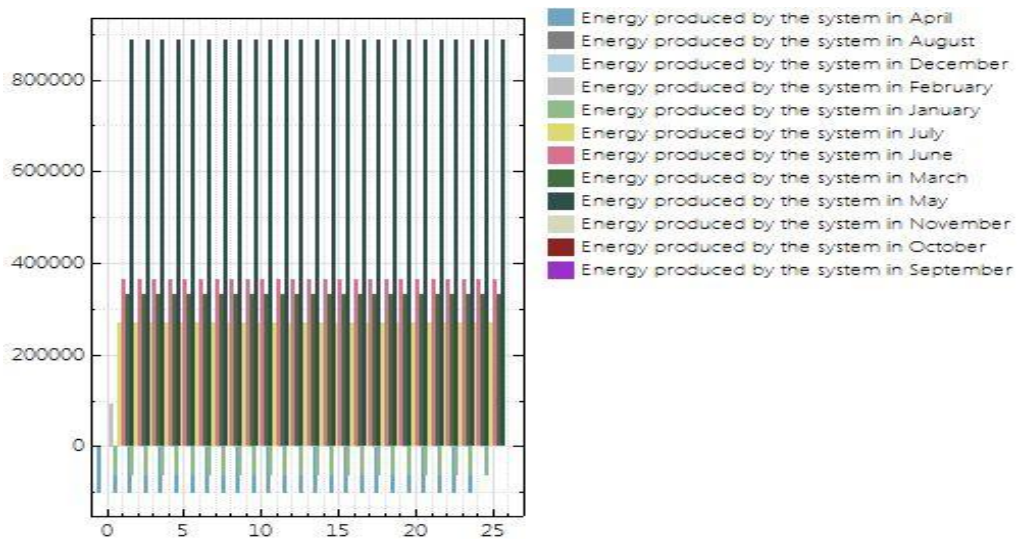


Figure 7.101 CSP 's Energy Production as simulated in SAM (scenario2.7)

7.2.3 Design Point DNI Scenarios

In the Scenarios that follow we will change the price of Design Point DNI to get our results. We will examine the system starting from low Design Point DNI ending up with a high Design Point DNI price, taking the results and understanding the behavior of the system due to that change.

DNI is the direct normal irradiance, the irradiation at design value is the reference DNI, or the DNI at which the system operates at its design point, the irradiation at design value, at which the system operates at its design point. For example, a 100 MW system with a value of 950 W/m^2 for irradiation at design would produce 100 MW of electricity when the actual DNI is 950 W/m^2 (and the other reference parameters are met, including ambient temperature etc.) Solar irradiance is the power per unit area received from the Sun in the form of electromagnetic radiation in the wavelength range of the measuring instrument. Irradiance may be measured in space or at the Earth's surface after atmospheric absorption and scattering. It is measured perpendicular to the incoming sunlight. Total solar irradiance, is a measure of the solar power over all wavelengths per unit area incident on the Earth's upper atmosphere. Irradiance is a function of distance from the Sun, the solar cycle, and cross-cycle changes. The SI unit of irradiance is watt per square meter (W/m^2).[60]

Scenario 3.1: Design Point DNI = 475 W/m^2

In this scenario we changed the Design Point DNI of the system, especially here Design Point DNI is the half of that at scenario1,1, so now it is $950\text{W/m}^2 / 2 = 475 \text{ W/m}^2$ and the results are shown in Figure 7.102.

Metric	Value
Annual energy (year 1)	164,662,480 kWh
Capacity factor (year 1)	36.1%
Annual Water Usage	66,985 m ³
PPA price (year 1)	63.73 €/kWh
PPA price escalation	1.00 %/year
Levelized PPA price (nominal)	83.20 €/kWh
Levelized PPA price (real)	69.99 €/kWh
Levelized COE (nominal)	76.98 €/kWh
Net present value	\$108,246,400
Internal rate of return (IRR)	11.00 %
Year IRR is achieved	20
IRR at end of project	11.84 %
Net capital cost	\$1,197,455,744
Equity	\$1,197,455,744
Size of debt	\$0

Figure 7.102 CSP 's Performance results as simulated in SAM (scenario 3.1)

Annual electricity production (year 1) was now calculated to be equal to $P_{el,net}=164,662,480$ kWh, we can see that it has increased, the capacity factor (year 1) has increased and it is now equal to 36.1% and the annual water use) has increased and it is now equal to 66,985 m³. Regarding the financial data, about the sales price (PPA price (year 1) = 63.73\$/kWh) and the increase in the sales price (PPA Escalation = 1% / year), same as scenario 1.1. The nominal Levelized PPA price has decreased and it is now equal to 83.20\$/kWh, the real Levelized price has decreased and it is now equal to 69.99\$/kWh and the Levelized Cost of Energy (LCOE) has decreased and it is now equal to 76.98 \$/kWh. The Net Present Value (NPV) has increased and it is now \$108,246,400 and the IRR (internal rate of return) of the investment is again equal to 11%, we can see that year IRR is again achieved (20) and IRR at the end of the project is equal to 11.84% (same as scenario 1.1). The net capital cost has increased and it is now equal to \$1,197,455,744, the equity is also equal to \$1,197,455,744 and the size of debt is again equal to \$0.

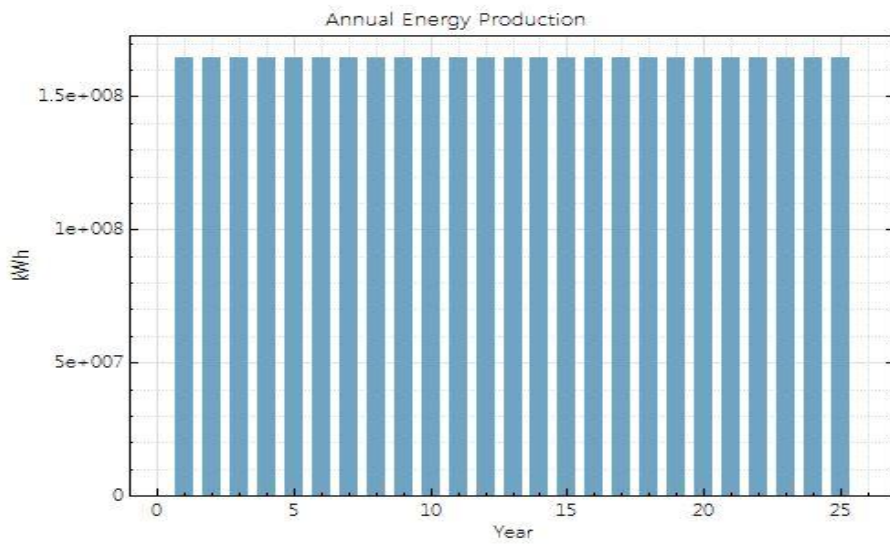


Figure 7.103 CSP 's Annual Electricity Production as simulated in SAM (scenario3.1)

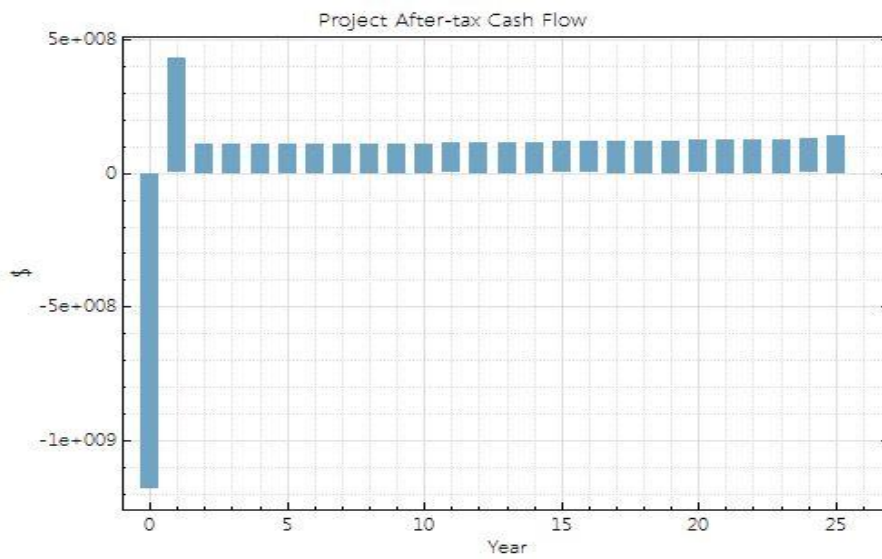


Figure 7.104 CSP 's Cash Flow as simulated in SAM (scenario3.1)

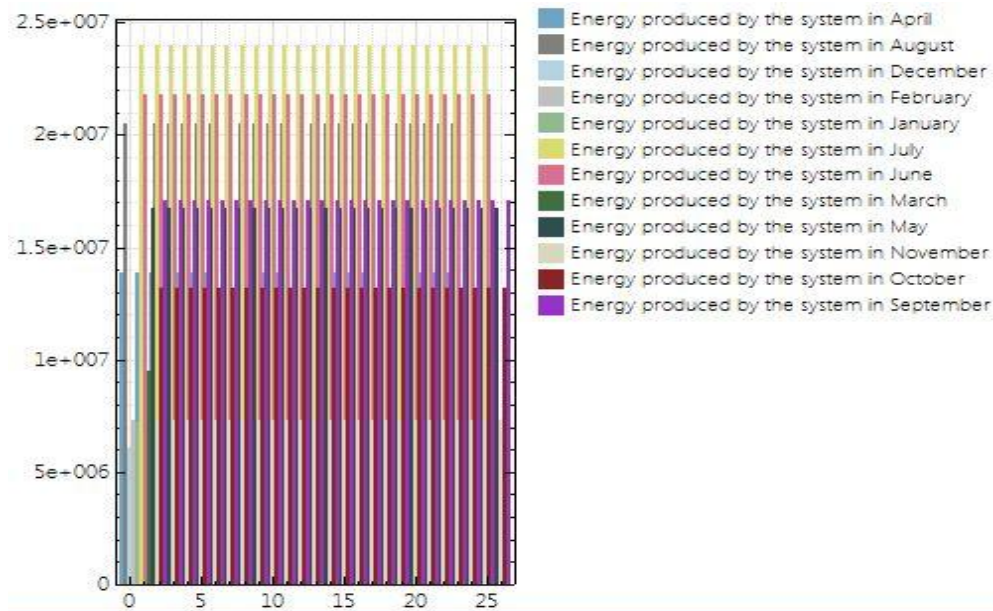


Figure 7.105 CSP 's Energy Production as simulated in SAM (scenario 3.1)

Scenario 3.2: Design Point DNI = 700 W/m²

In this scenario we changed the Design Point DNI of the system, especially here Design Point DNI is equal to 700W / m² and the results are shown in Figure 7.106.

Metric	Value
Annual energy (year 1)	152,287,760 kWh
Capacity factor (year 1)	33.4%
Annual Water Usage	47,391 m ³
PPA price (year 1)	59.56 ¢/kWh
PPA price escalation	1.00 %/year
Levelized PPA price (nominal)	78.84 ¢/kWh
Levelized PPA price (real)	66.33 ¢/kWh
Levelized COE (nominal)	72.74 ¢/kWh
Net present value	\$95,960,120
Internal rate of return (IRR)	11.00 %
Year IRR is achieved	20
IRR at end of project	11.84 %
Net capital cost	\$1,060,859,200
Equity	\$1,060,859,200
Size of debt	\$0

Figure 7.106 CSP 's Performance results as simulated in SAM (scenario 3.2)

Annual electricity production (year 1) was now calculated to be equal to $P_{el,net}=152,287,760$ kWh, we can see that it has increased, the capacity factor (year 1) has increased and it is now equal to 33.4% and the annual water use is now equal to $47,391 \text{ m}^3$. Regarding the financial data, about the sales price (PPA price (year 1) = $59.56\$/\text{kWh}$) and the increase in the sales price (PPA Escalation = 1% / year), same as scenario 1.1. The nominal Levelized PPA price has decreased and it is now equal to $78.84\$/\text{kWh}$, the real Levelized price has decreased and it is now equal to $66.33\$/\text{kWh}$ and the Levelized Cost of Energy (LCOE) has decreased and it is now equal to $72.74 \text{ \$/kWh}$. The Net Present Value (NPV) has increased and it is now $\$95,960,120$ and the IRR (internal rate of return) of the investment is again equal to 11%, we can see that year IRR is again achieved (20) and IRR at the end of the project is equal to 11.84% (same as scenario 1.1). The net capital cost has increased and it is now equal to $\$1,060,859,200$, the equity is also equal to $\$1,060,859,200$ and the size of debt is again equal to $\$0$.

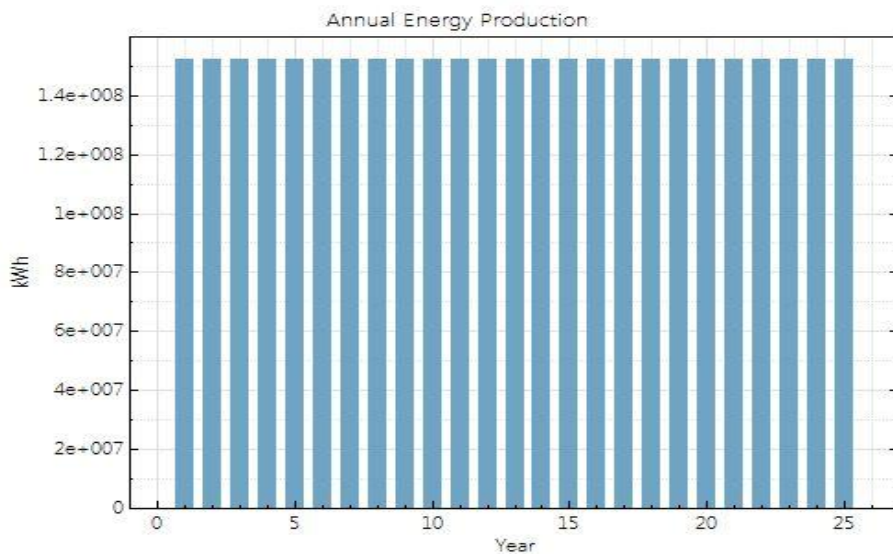


Figure 7.107 CSP 's Annual Electricity Production as simulated in SAM (scenario 3.2)

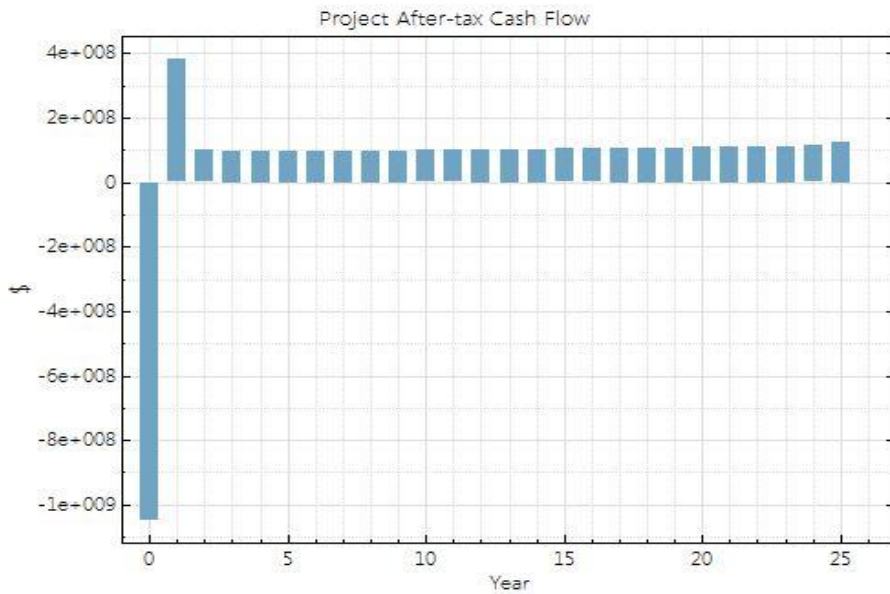


Figure 7.108 CSP 's Cash Flow as simulated in SAM (scenario 3.2)

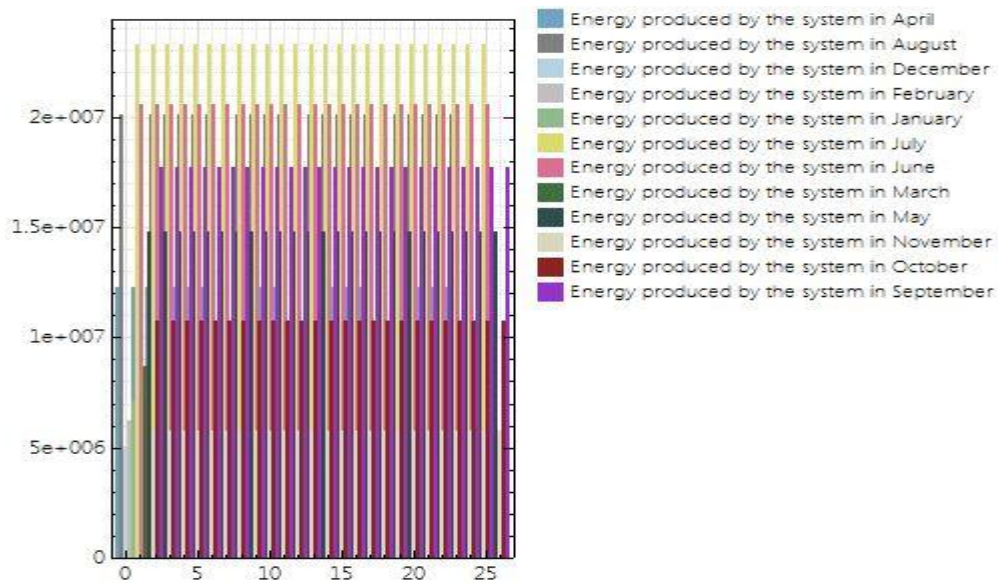


Figure 7.109 CSP 's Energy Production as simulated in SAM (scenario 3.2)

Scenario 3.3: Design Point DNI = 800 W/m²

In this scenario we changed the Design Point DNI of the system, especially here Design Point DNI is equal to 800 W/m² and the results are shown in Figure 7.110.

Metric	Value
Annual energy (year 1)	141,965,136 kWh
Capacity factor (year 1)	31.1%
Annual Water Usage	42,190 m ³
PPA price (year 1)	60.81 ¢/kWh
PPA price escalation	1.00 %/year
Levelized PPA price (nominal)	81.41 ¢/kWh
Levelized PPA price (real)	68.48 ¢/kWh
Levelized COE (nominal)	75.03 ¢/kWh
Net present value	\$92,719,448
Internal rate of return (IRR)	11.00 %
Year IRR is achieved	20
IRR at end of project	11.84 %
Net capital cost	\$1,024,813,312
Equity	\$1,024,813,312
Size of debt	\$0

Figure 7.110 CSP 's Performance results as simulated in SAM (scenario3.3)

Annual electricity production (year 1) was now calculated to be equal to $P_{el,net}=141,965,136$ kWh, we can see that it has increased, the capacity factor (year 1) has increased and it is now equal to 31.1% and the annual water use is now equal to 42,190 m³. Regarding the financial data, about the sales price (PPA price (year 1) = 60.81\$ / kWh) and the increase in the sales price (PPA Escalation = 1% / year), same as scenario 1.1. The nominal Levelized PPA price has decreased and it is now equal to 81.41\$/kWh, the real Levelized price has decreased and it is now equal to 68.48 \$/kWh and the Levelized Cost of Energy (LCOE) has decreased and it is now equal to 75.03\$/kWh. The Net Present Value (NPV) has increased and it is now \$92,719,448 and the IRR (internal rate of return) of the investment is again equal to 11%, we can see that year IRR is again achieved (20) and IRR at the end of the project is equal to 11.84% (same as scenario 1.1). The net capital cost has increased and it is now equal to \$1,024,813,312, the equity is also equal to \$1,024,813,312 and the size of debt is again equal to \$0.

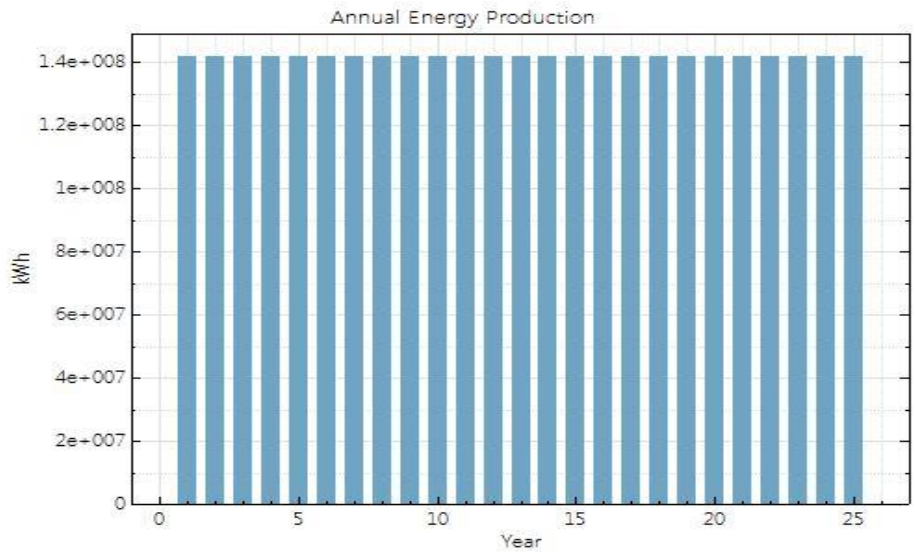


Figure 7.111 CSP 's Annual Electricity Production as simulated in SAM (scenario3.3)

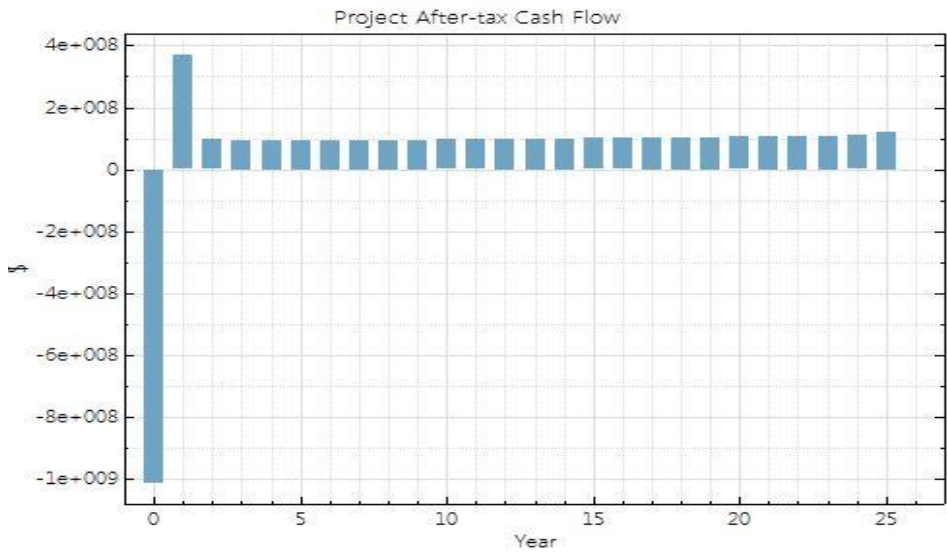


Figure 7.112 CSP 's Cash Flow as simulated in SAM (scenario 3.3)

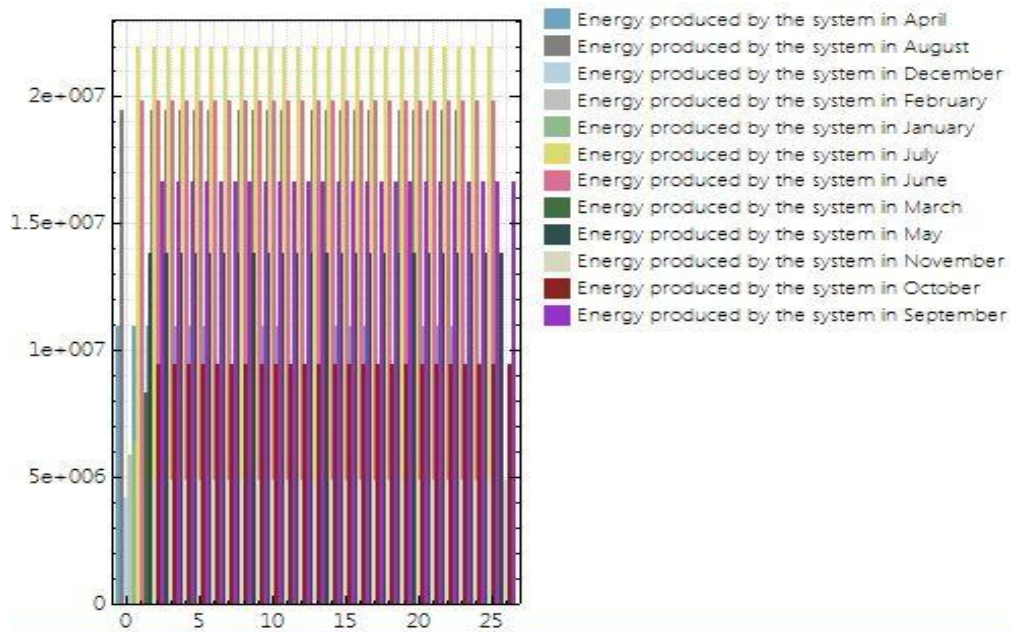


Figure 7.113 CSP 's Energy Production as simulated in SAM (scenario 3.3)

Scenario 3.4: Design Point DNI = 1000 W/m²

In this scenario we changed the Design Point DNI of the system, especially here Design Point DNI is equal to 1000 W/m² and the results are shown in Figure 7.114.

Metric	Value
Annual energy (year 1)	114,111,152 kWh
Capacity factor (year 1)	25.0%
Annual Water Usage	33,251 m ³
PPA price (year 1)	69.26 ¢/kWh
PPA price escalation	1.00 %/year
Levelized PPA price (nominal)	96.33 ¢/kWh
Levelized PPA price (real)	81.03 ¢/kWh
Levelized COE (nominal)	88.66 ¢/kWh
Net present value	\$88,700,696
Internal rate of return (IRR)	11.00 %
Year IRR is achieved	20
IRR at end of project	11.84 %
Net capital cost	\$980,077,312
Equity	\$980,077,312
Size of debt	\$0

Figure 7.114 CSP 's Performance results as simulated in SAM (scenario 3.4)

Annual electricity production (year 1) was now calculated to be equal to $P_{el,net}=114,111,152$ kWh, we can see that it has decreased, the capacity factor (year 1) has decreased and it is now equal to 25% and the annual water use is now equal to $33,251$ m³. Regarding the financial data, about the sales price (PPA price (year 1) = 69.26\$/kWh) and the increase in the sales price (PPA Escalation = 1% / year), same as scenario 1.1. The nominal Levelized PPA price has increased and it is now equal to 96.33 \$/kWh, the real Levelized price has increased and it is now equal to 81.03 \$/kWh and the Levelized Cost of Energy (LCOE) has increased and it is now equal to 88.66 \$/kWh. The Net Present Value (NPV) has decreased and it is now \$88,700,696 and the IRR (internal rate of return) of the investment is again equal to 11%, we can see that year IRR is again achieved (20) and IRR at the end of the project is equal to 11.84% (same as scenario 1.1). The net capital cost has decreased and it is now equal to \$980,077,312, the equity is also equal to \$980,077,312 and the size of debt is again equal to \$0.

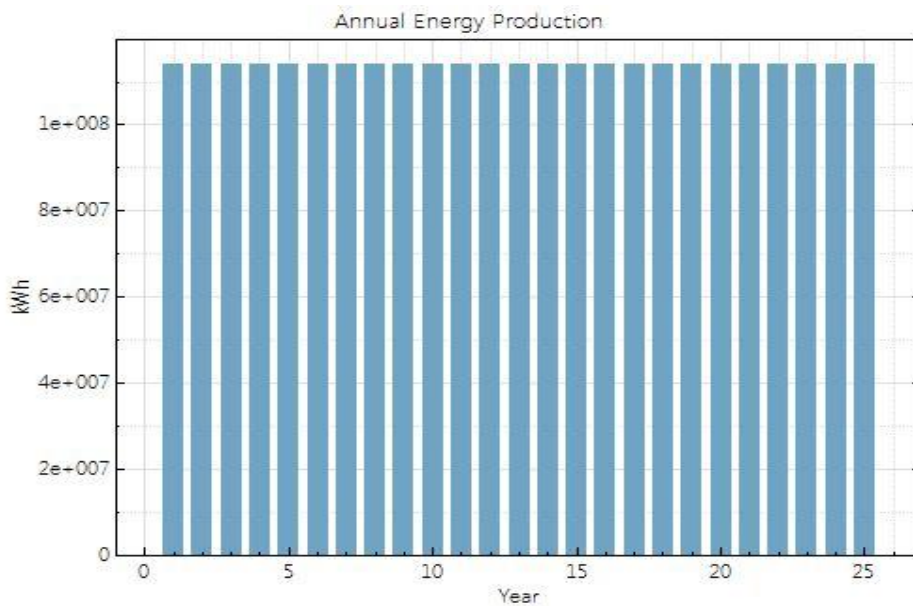


Figure 7.115 CSP 's Annual Electricity Production as simulated in SAM (scenario 3.4)

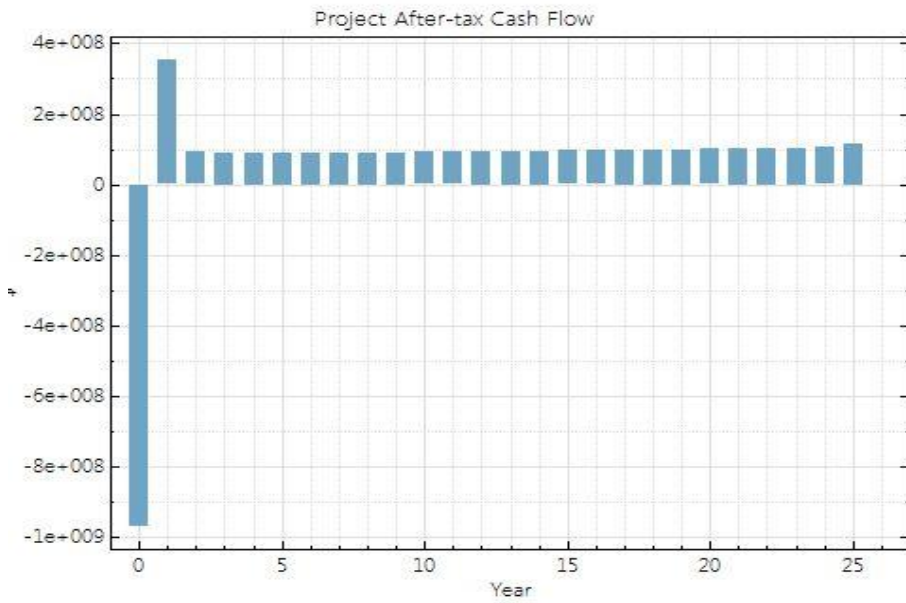


Figure 7.116 CSP 's Cash Flow as simulated in SAM (scenario3.4)

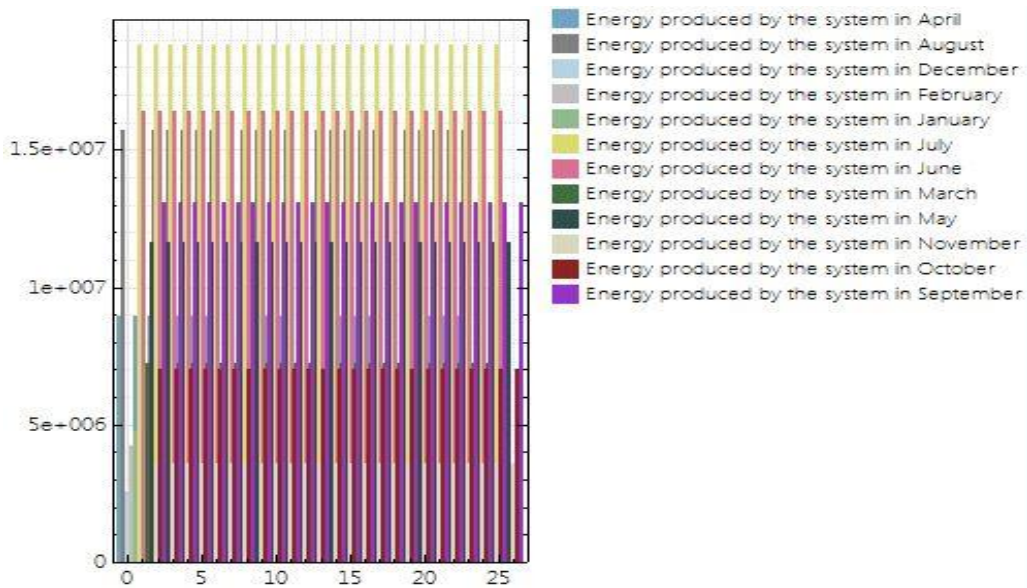


Figure 7.117 CSP 's Energy Production as simulated in SAM (scenario 3.4)

Scenario 3.5: Design Point DNI = 1100 W/m²

In this scenario we changed again the Design Point DNI of the system, especially here Design Point DNI is +250 W/m² of that at scenario1.1, so now it is equal to 950 W/m² + 250W/m²= 1100W/m² and the results are shown in Figure 7.118.

Metric	Value
Annual energy (year 1)	99,450,616 kWh
Capacity factor (year 1)	21.8%
Annual Water Usage	29,720 m ³
PPA price (year 1)	75.70 €/kWh
PPA price escalation	1.00 %/year
Levelized PPA price (nominal)	108.22 €/kWh
Levelized PPA price (real)	91.04 €/kWh
Levelized COE (nominal)	99.55 €/kWh
Net present value	\$87,080,840
Internal rate of return (IRR)	11.00 %
Year IRR is achieved	20
IRR at end of project	11.84 %
Net capital cost	\$962,037,248
Equity	\$962,037,248
Size of debt	\$0

Figure 7.118 CSP 's Performance results as simulated in SAM (scenario3.5)

Annual electricity production (year 1) was now calculated to be equal to $P_{el,net}=99,450,616$ kWh, we can see that it has decreased, the capacity factor (year 1) is now equal to 21.8% and the annual water use has decreased and it is now equal to 29,720 m³. Regarding the financial data, about the sales price (PPA price (year 1) = 75.70 \$/kWh) and the increase in the sales price (PPA Escalation = 1% / year), same as scenario 1.1. The nominal Levelized PPA price is now equal to 108.22 \$/kWh, it has increased, the real Levelized price is now equal to 91.04 \$/kWh and the Levelized Cost of Energy (LCOE) is now equal to 99.55 \$/kWh, it has increased. The Net Present Value (NPV) is now \$87,080,840 and the IRR (internal rate of return) of the investment is again equal to 11%, we can see that year IRR is again achieved (20) and IRR at the end of the project is again equal to 11.84%. The net capital cost has decreased and it is now equal to \$962,037,248, the equity is also equal to \$962,037,248 and the size of debt is again equal to \$0.

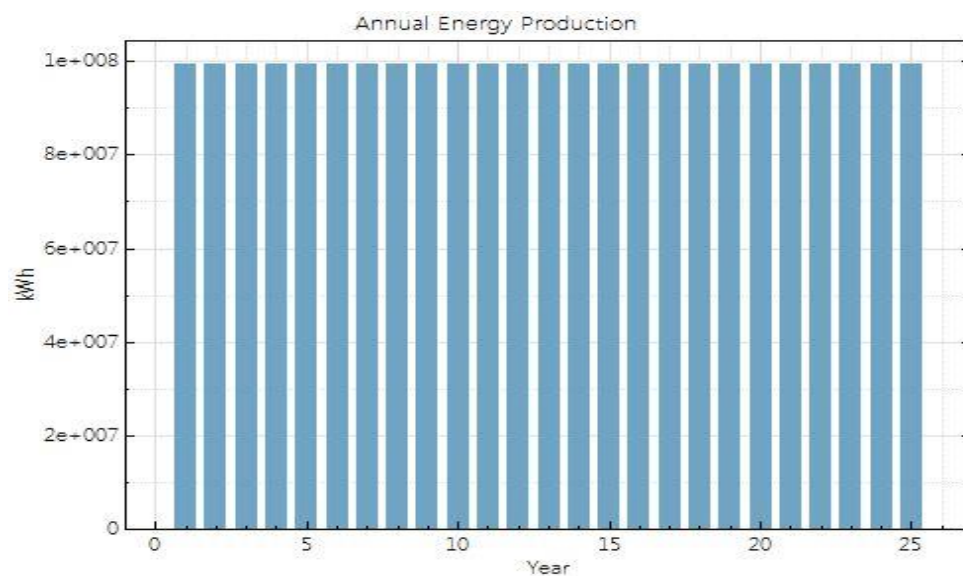


Figure 7.119 CSP 's Annual Electricity Production as simulated in SAM (scenario3.5)

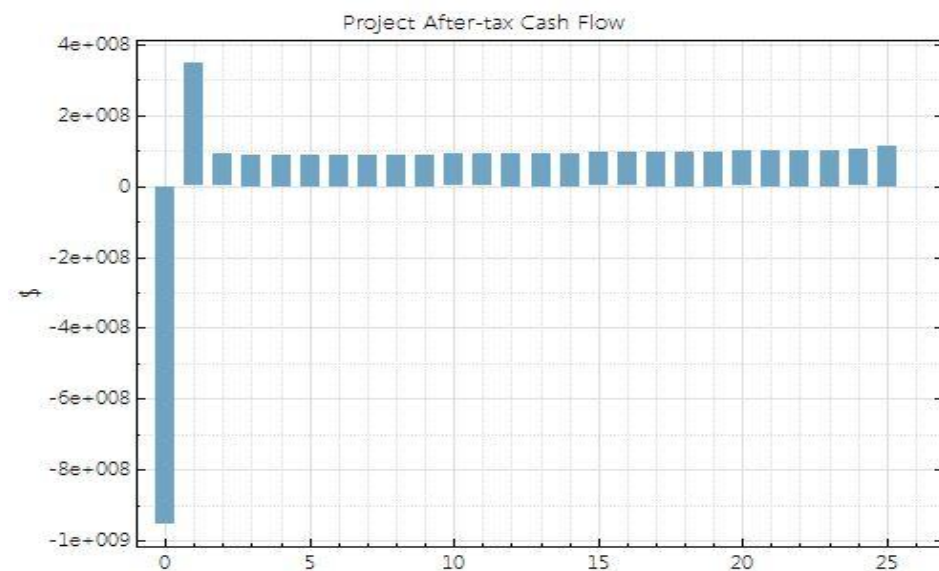


Figure 7.120 CSP 's Cash Flow as simulated in SAM (scenario3.5)

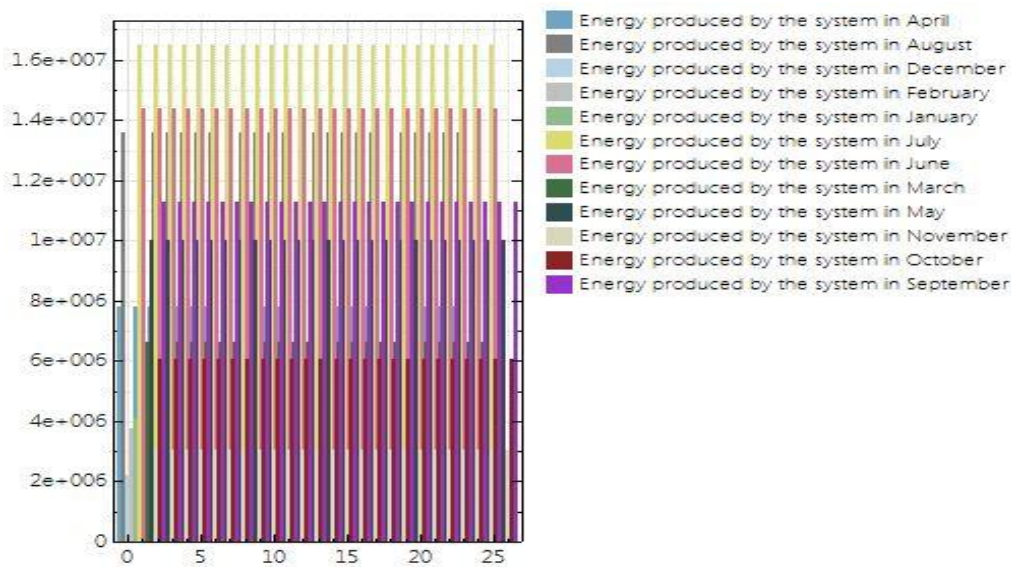


Figure 7.121 CSP 's Energy Production as simulated in SAM (scenario3.5)

Scenario 3.6: Design Point DNI = 1475 W/m²

In this scenario we changed again the Design Point DNI of the system, especially here Design Point DNI is +1/2 of that at scenario1,1, so now it is equal to 950W/m² + 475 W/m²= 1475W/m², (this increase of Design Point DNI is chosen as we wanted to show a high price but SAM crashed so there was not many choices) and the results are shown in Figure 7.122.

Metric	Value
Annual energy (year 1)	63,103,792 kWh
Capacity factor (year 1)	13.8%
Annual Water Usage	21,359 m ³
PPA price (year 1)	106.23 €/kWh
PPA price escalation	1.00 %/year
Levelized PPA price (nominal)	166.06 €/kWh
Levelized PPA price (real)	139.70 €/kWh
Levelized COE (nominal)	152.64 €/kWh
Net present value	\$85,147,600
Internal rate of return (IRR)	11.00 %
Year IRR is achieved	20
IRR at end of project	11.84 %
Net capital cost	\$940,462,528
Equity	\$940,462,528
Size of debt	\$0

Figure 7.122 CSP 's Performance results as simulated in SAM (scenario3.6)

Annual electricity production (year 1) was now calculated to be equal to $P_{el,net}=63,103,792$ kWh, we can see that it has decreased, the capacity factor (year 1) is now equal to 13.8% and the annual water use has decreased and it is now equal to $21,359$ m³. Regarding the financial data, about the sales price (PPA price (year 1) = 106.23\$/kWh) and the increase in the sales price (PPA Escalation = 1% / year), same as scenario 1.1. The nominal Levelized PPA price is now equal to 166.06 \$/kWh, it has increased, the real Levelized price is now equal to 139.70 \$/kWh and the Levelized Cost of Energy (LCOE) is now equal to 152.64 \$/kWh, it has increased. The Net Present Value (NPV) is now \$ 85,147,600 and the IRR (internal rate of return) of the investment is again equal to 11%, we can see that year IRR is again achieved (20) and IRR at the end of the project is again equal to 11.84%. The net capital cost has decreased and it is now equal to \$940,462,528, it has increased, the equity is also equal to \$940,462,528 and the size of debt is again equal to \$0.

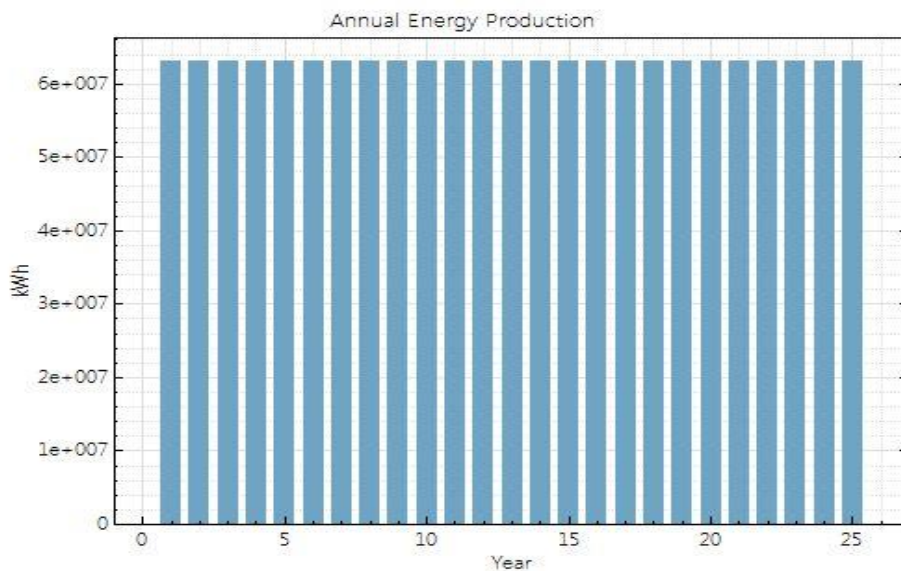


Figure 7.123 CSP 's Annual Electricity Production as simulated in SAM (scenario 3.6)

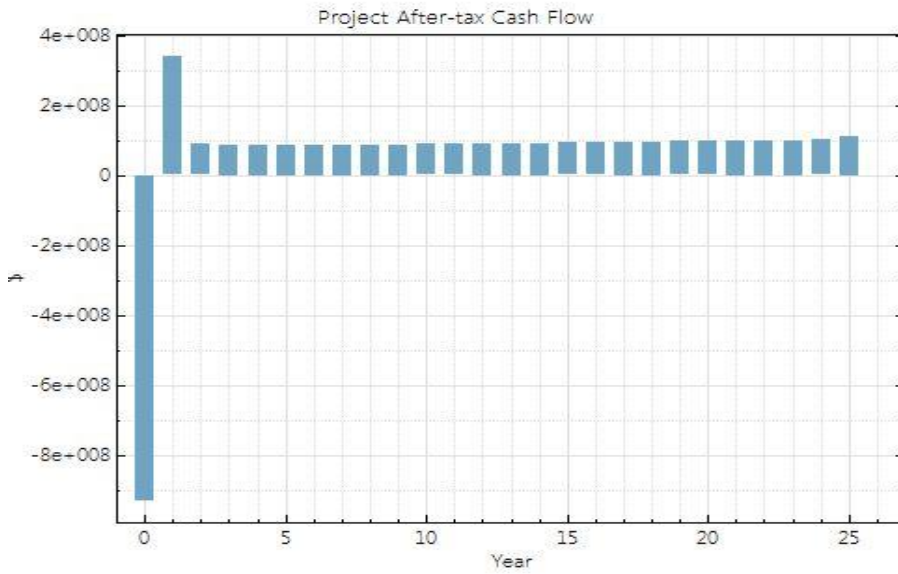


Figure 7.124 CSP 's Cash Flow as simulated in SAM (scenario3.6)

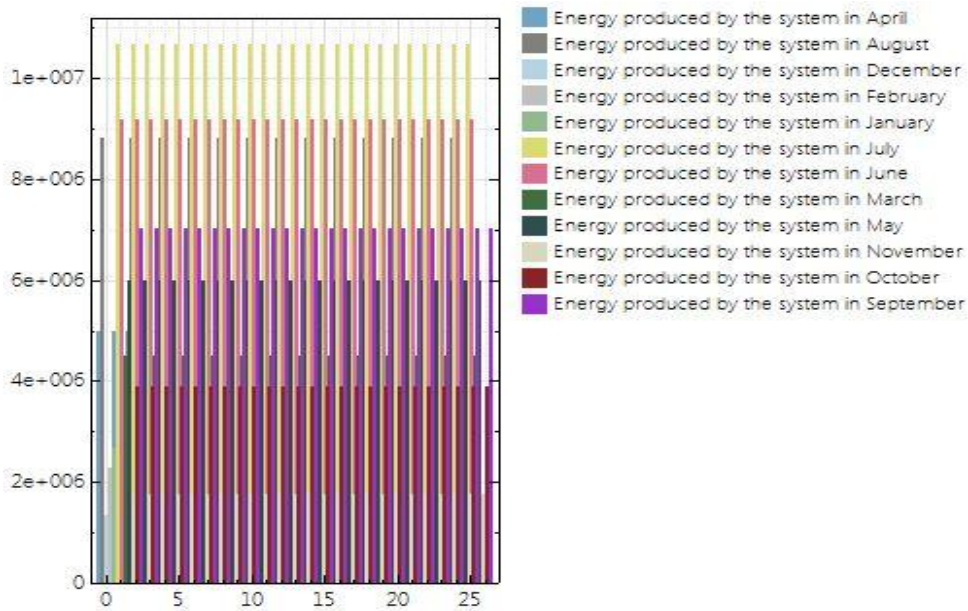


Figure 7.125 CSP 's Energy Production as simulated in SAM (scenario3.6)

7.3 Scenarios Results

7.3.1 Tower Height Scenarios: Much effort is spent to improve individual components and subsystems. For a given thermal power requirement, there is no such thing as an optimum tower height. SAM model defines tower height as the distance from the heliostat hinge point to the center of the receiver. Heliostats are often characterized and even compared using the main parameter cost per square meter'. This was correct if the heliostats to be compared were otherwise identical. Unfortunately, this is never the case in reality. Therefore this approach is not satisfactory. In practice, apart from cost per square meter, more factors like optical and tracking accuracy, shape, structural deformation under operation loads and maybe even power consumption have to be factored in to allow for a meaningful comparison.

For the overall layout process of heliostat field, tower and receiver the complete system is modeled using System Advisor Model (SAM) to determine investment cost, annual electricity generation and resulting levelized electricity costs. By doing so, different tower heights be directly compared using LCoE as a reasonable figure of merit. The overall target is to minimize Levelized Costs of Electricity (LCoE). Here a more recent curve is used from an investigation, where we can see that the higher the tower is, the bigger the LCOE cost are (Figure 7.126).[61],[62]

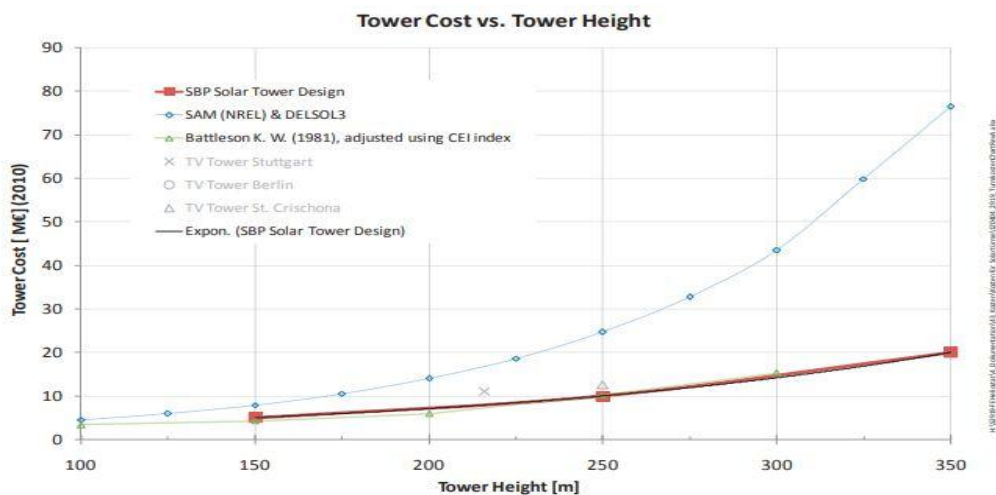


Figure 7.126 Tower cost vs Tower height [61]

Our results for the tower cases we set are below:

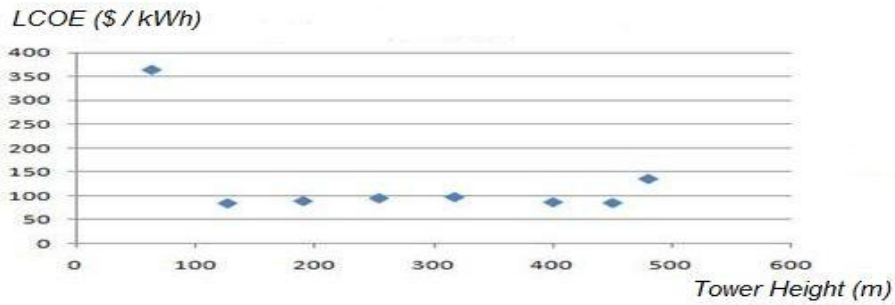


Figure 7.127 Summary Diagram of Tower height vs Tower cost in our Scenarios

A lower LCOE suggests a more profitable project. This implies lower cost, with more energy production. We can see that between our different tower height scenarios the lowest tower height gives a big LCOE price. The next scenarios follow the paper's line (the higher the tower is, the bigger the LCOE costs are). The aim is to minimize Levelised Costs of Electricity (LCoE). Here the lowest LCOE prices as you can see are for the scenario 1.1 (tower height = 127 m) and then scenario 1.6, where tower height = 400 m follows with a higher LCOE price than scenario 1.1, but it is very close. In order to get safer conclusions we can see what annual energy is produced in this two scenarios to get a more reliable conclusion. As you can see in Figure 7.128 the scenario 1.1 (tower height = 127 m) gives higher annual Energy than that of scenario 1.6 (tower height = 400 m) with a good LCOE price, so we conclude that the best case for tower height is that of 127 m, scenario 1.1, where we have the lowest LCOE price as asked, combined with the produced annual energy. In Table 7.1, there is a summary presentation of Tower Height scenarios, the produced Energy and the LCOE price in every case.

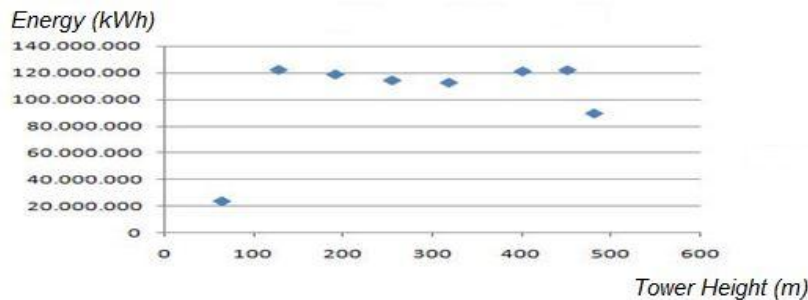


Figure 7.128 Summary Diagram of Tower height vs Energy in our Scenarios

Scenarios	Height	Energy	Lcoe
-----------	--------	--------	------

Scenario 1.2	63.5 m	23,678,514 kWh	364.10 \$/kWh
Scenario 1.1	127 m	121,964,560 kWh	83.69 \$/kWh
Scenario 1.3	190.5 m	118,598,840 kWh	88.22 \$/kWh
Scenario 1.4	254 m	114,133,232 kWh	94.21 \$/kWh
Scenario 1.5	317.5 m	112,432,120 kWh	96.72 \$/kWh
Scenario 1.6	400 m	120,853,616 kWh	85.97 \$/kWh
Scenario 1.7	450 m	121,755,232 kWh	84.41 \$/kWh
Scenario 1.8	480 m	89,403,314 kWh	134.96 \$/kWh

Table 7.1 Summary of Tower Height Scenarios Results

7.3.2 Solar Multiple Scenarios: *Solar multiple represents one of the most important parameters which has a significant effect on the Levelized Cost of Energy (LCOE) of the electricity produced by the CSP system. Solar multiple can be defined as the ratio of the actual solar field size to the minimum size required to run the power block at full capacity under normal irradiation conditions. The increase in the solar multiple, combined with thermal energy storage, can increase the utilization of the power block which reduce the LCOE of the whole plant. However, increasing the solar multiple also increases the capital cost of the system. This contradiction effect of this parameter need to be optimized to determine the solar multiple which give the minimum LCOE at the design condition of the proposed power plant.*

Due to papers simulations of the performance of the proposed plant under range of solar multiple has been conducted. The other design parameters of the plant are kept constant. The simulation results of the paper's optimization process is shown in Figure 7.129. This leads to the conclusion that solar multiple must provide the minimum LCOE of the electricity produced at this design parameters of the plant.[58],[59],[63]

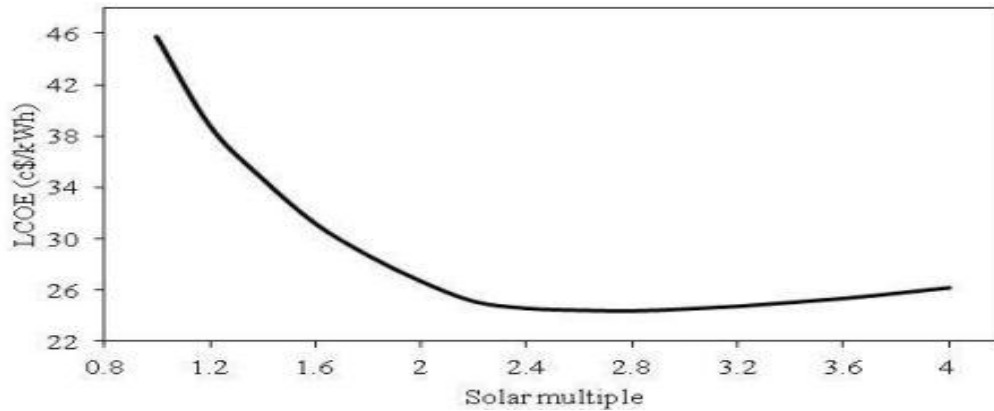


Figure 7.129 Solar multiple vs Tower cost [63]

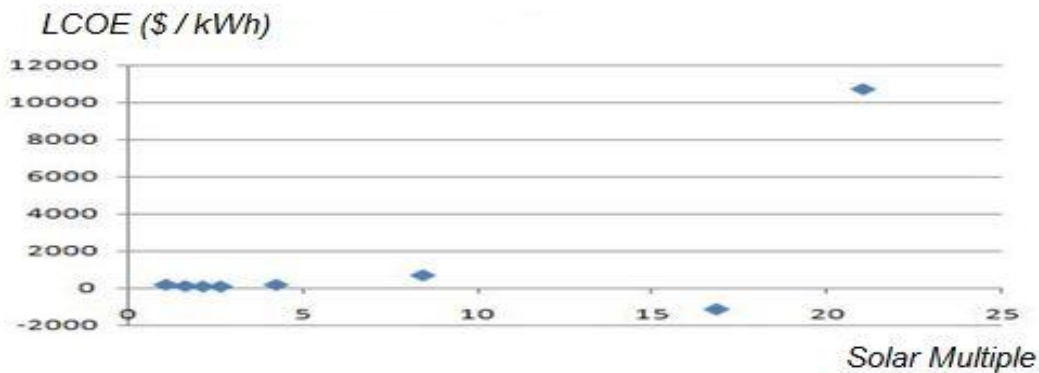


Figure 7.130 Summary Diagram of Solar multiple vs Tower cost in our Scenarios

A lower LCOE suggests a more profitable project. This implies lower cost, with more energy production. We can see that between our solar multiple scenarios the highest solar multiple gives a high LCOE price. The other scenarios follow the paper's line (the higher solar multiple is, the higher the LCOE cost are with an negative LCOE here in case of solar multiple is 16.8, which means that it is not a realistic design as we have explained). The aim is to minimize Levelized Costs of Electricity (LCoE).

Here the lowest LCOE prices as you can see are for the scenario 1.1 (solar multiple=2.1) and then case for scenario 2.3, solar multiple=2.6 follows with the lowest LCOE price. In order to get safer conclusions we can see what annual energy is produced in this two scenarios to get a more reliable conclusion. As you can see in Figure 7.131 scenario 1.1 gives lower annual Energy than that of scenario 2.3, solar multiple=2.6 with a good LCOE price, so we conclude that the best case for solar multiple is not that of scenario 1.1 but the best choice is that of scenario 2.3, solar

multiple=2.6, where we have the lowest LCOE price as asked, combined with the produced annual energy. In Table 7.2, there is a summary presentation of Solar multiple scenarios, the produced Energy and the LCOE price in every case.

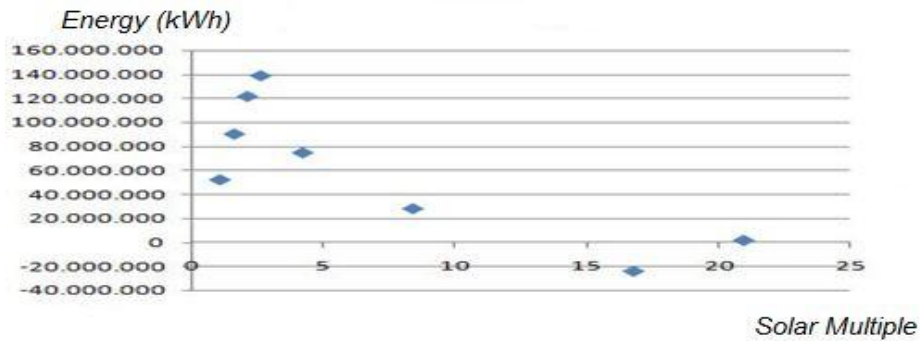


Figure 7.131 Summary Diagram of Solar multiple vs Energy in our Scenarios

Scenarios	Solar Multiple	Energy (kWh)	LCOE (\$/kWh)
Scenario 2.1	1.05	52,386,520	174.62
Scenario 2.2	1.6	90,592,800	106.64
Scenario 1.1	2.1	121,964,560	83.69
Scenario 2.3	2.6	139,210,688	77.36
Scenario 2.4	4.2	74,956,984	169.38
Scenario 2.5	8.4	28,285,772	658.30
Scenario 2.6	16.8	23,933,500	1150.24
Scenario 2.7	21	1,776,612	10737.77

Table 7.2 Summary of Solar Multiple Scenarios Results

7.3.3 Design Point DNI Scenarios: CSP systems must cope with unpredictable operating conditions and they are designed to accommodate their locations' geographical and meteorological properties. The design point generally consists of a set of the operating conditions and the resulting output. For the collector field of a CSP, DNI is the most relevant operating condition, as it determines the amount of solar power

incident on the CSP. Studies on the design, analysis and optimization of CSP systems have shown that no clear consensus exists on the choice of its design point. The majority of the studies use the conditions at the equinox (usually March 21) or the summer solstice (June 21 in the northern hemisphere), less commonly, the conditions at the winter solstice are used.

With suitable DNI values, the performance of the system can be assessed at the design point and over the entire year. In studies about the design point significant differences are found in the modeled behavior, in which they focus on maximizing the system's efficiency. The choice of operating conditions, the design point used as an input to the model has an influence on the result of the optimization process and it has a crucial effect on predictions of a system's nominal efficiency. Our analysis is repeated at the first chosen location in Greece changing in every case the design point DNI in order to see the behavior of our system if the that meteorological condition change.[60]

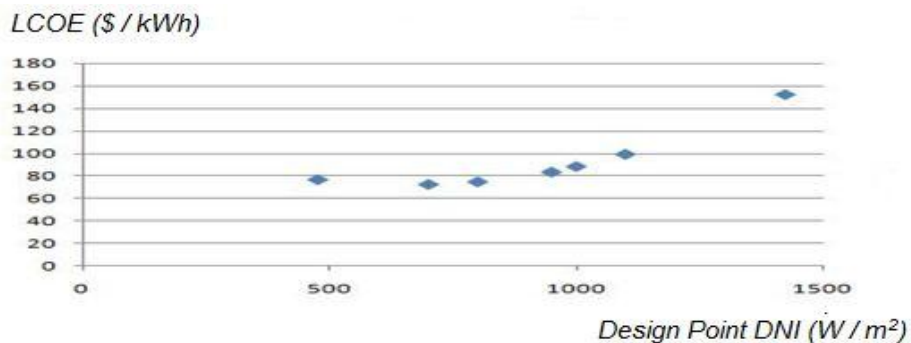


Figure 7.132 Summary Diagram of Design point DNI vs Tower cost in our Scenarios

A lower LCOE suggests a more profitable project. This implies lower cost, with more energy production. We can see that between our Design Point DNI scenarios the highest DNI gives a high LCOE price. The higher Design Point DNI is, the higher the LCOE cost are. The aim in the other examined cases was to minimize Levelized Costs of Electricity (LCoE). So if we continue keeping that criterion, it can be seen that in the DNI scenarios, the lowest LCOE prices is for scenario 3.2, Design Point DNI = 700 W / m². In order to get safer conclusions we can see what annual energy is produced to get a more reliable conclusion. As you can see in Figure 7.133 cases that gives the lowest

LCOE are for scenario 3.2, Design Point DNI = 700 W / m² and for scenario 3.3 , Design Point DNI = 800W/m².

Scenario 3.2, Design Point DNI = 700 W/m² scenario gives higher annual Energy than that of scenario 3.3, Design Point DNI = 800 W/m² with a higher Annual energy production price, so we conclude that the best scenario for Design Point DNI is not that of scenario 3.3, but the best choice is that of scenario 3.2, Design Point DNI = 700 W/m², where we have the lowest LCOE price, combined with the produced annual energy. In Table 7.3, there is a summary presentation of Design Point DNI scenarios, the produced Energy and the LCOE price in every case.

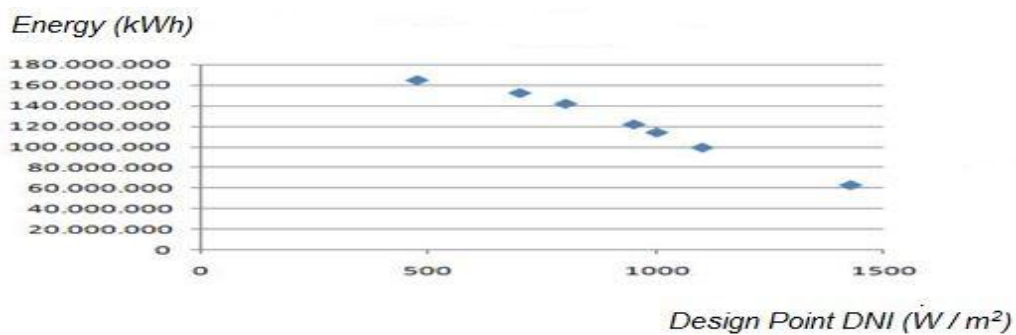


Figure 7.133 Summary Diagram of Design point DNI vs Energy in our Scenarios

Scenarios	Design Point DNI (W/m²)	Energy (kWh)	LCOE (\$/kWh)
Scenario 3.1	475	164,662,480	76.98
Scenario 3.2	700	152,287,760	72.74
Scenario 3.3	800	141,965,136	75.03
Scenario 1.1	950	121,964,560	83.69
Scenario 3.4	1000	114,111,152	88.66
Scenario 3.5	1100	99,450,616	99.55
Scenario 3.6	1475	63,103,792	152.64

Table 7.3 Summary of Design Point DNI Scenarios Results

7.4 Solar Field Geometry

7.4.1 Tower height

Scenario 1.1: Tower Height = 127 m

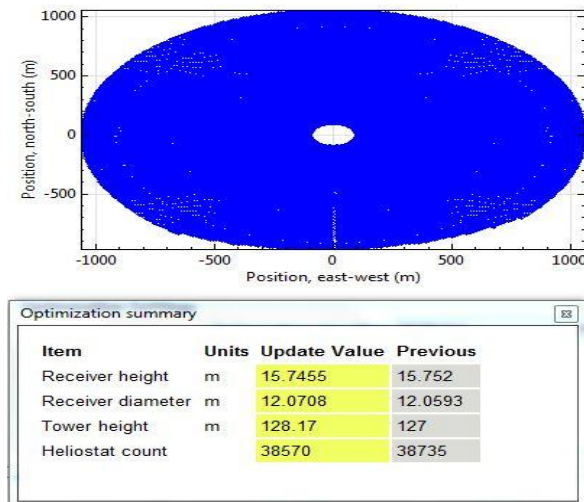


Figure 7.134 Solar Field Geometry and Characteristics of Scenario 1.1

Scenario 1.2: Tower Height = 63.5 m

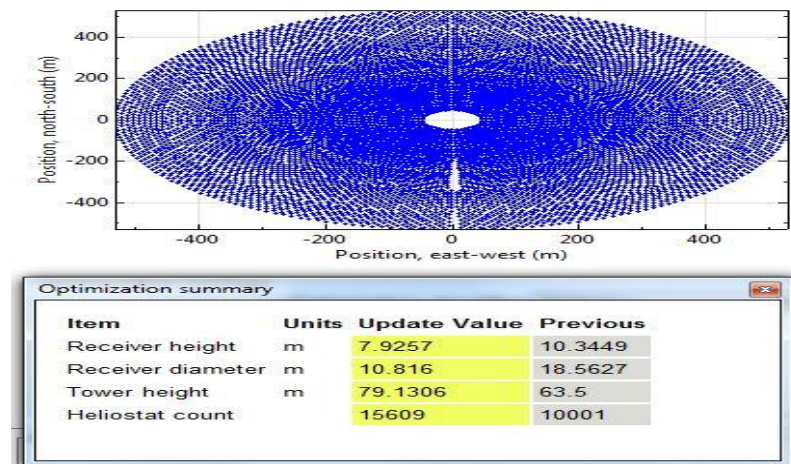


Figure 7.135 Solar Field Geometry and Characteristics of Scenario 1.2

Scenario 1.3: Tower Height = 190.5 m

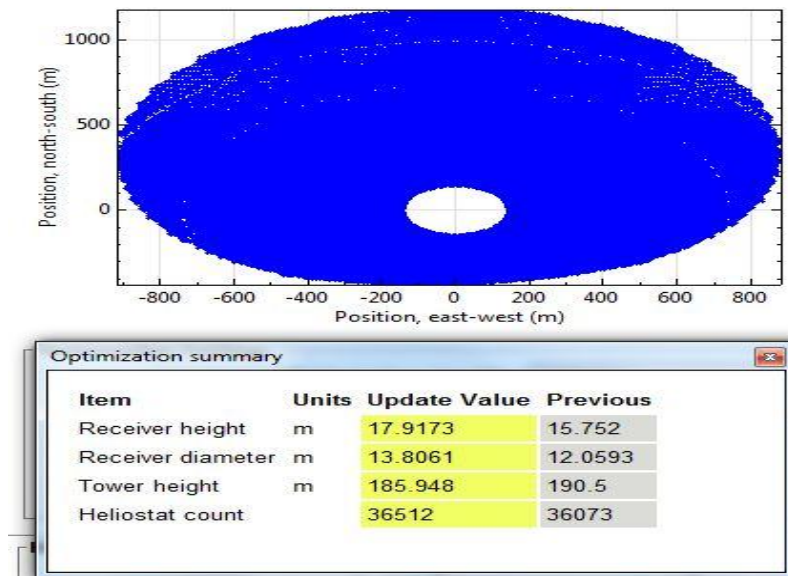


Figure 7.136 Solar Field Geometry and Characteristics of Scenario 1.3

Scenario 1.4: Tower Height = 254 m

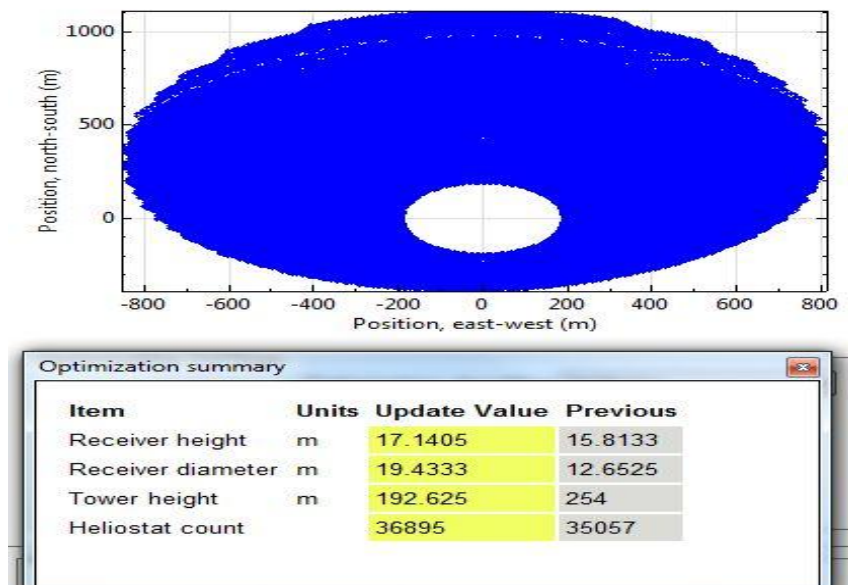


Figure 7.137 Solar Field Geometry and Characteristics of Scenario 1.4

Scenario 1.5: Tower Height = 317.5 m

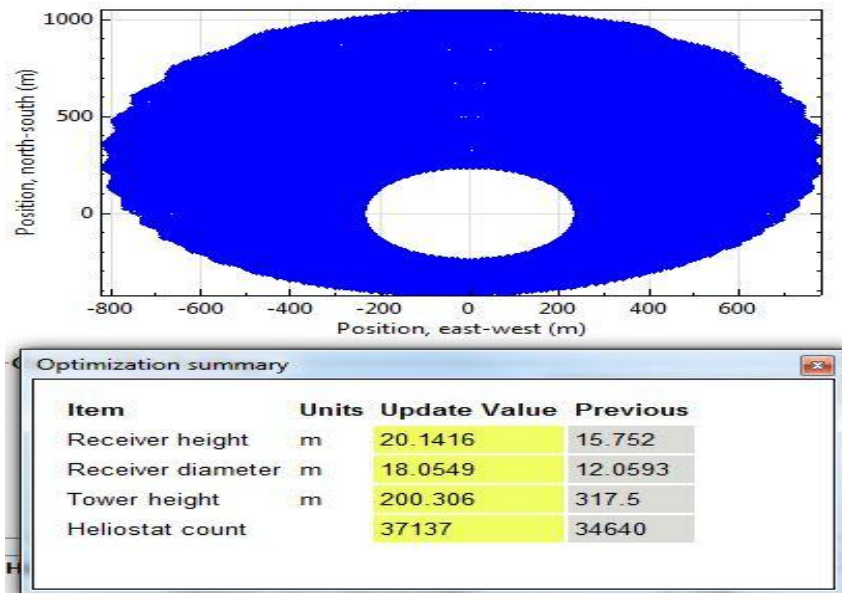


Figure 7.138 Solar Field Geometry and Characteristics of Scenario 1.5

Scenario 1.6: Tower Height = 400 m

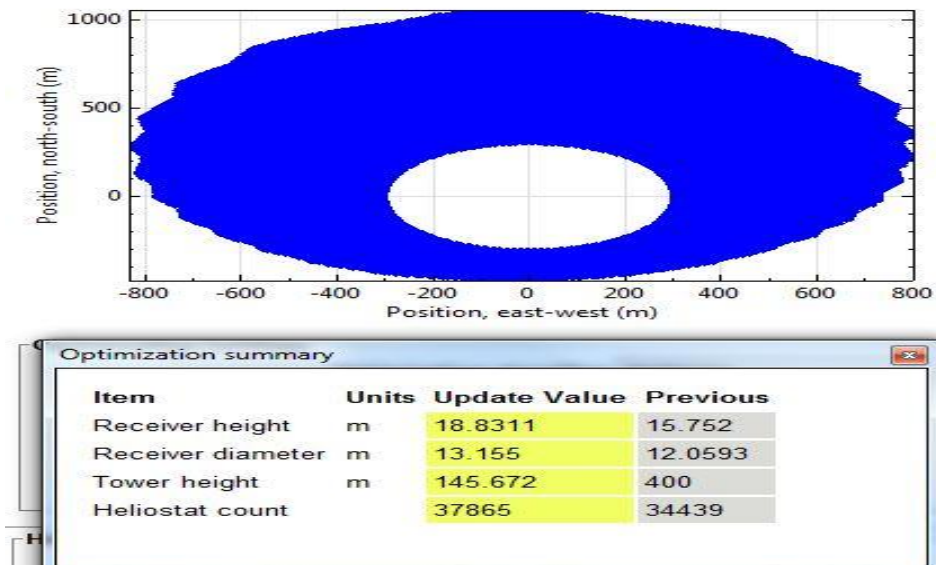


Figure 7.139 Solar Field Geometry and Characteristics of Scenario 1.6

Scenario 1.7: Tower Height = 450 m

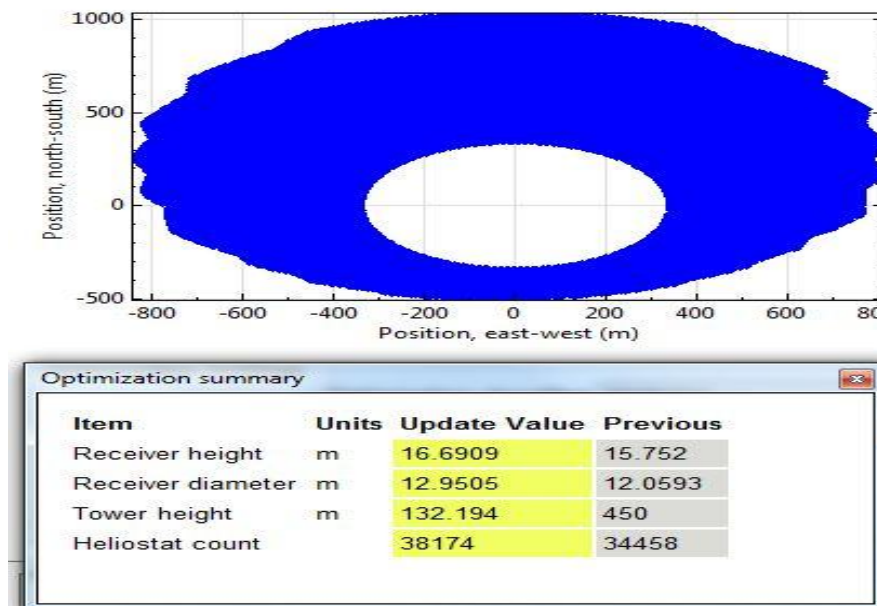


Figure 7.140 Solar Field Geometry and Characteristics of Scenario 1.7

Scenario 1.8: Tower Height = 480 m

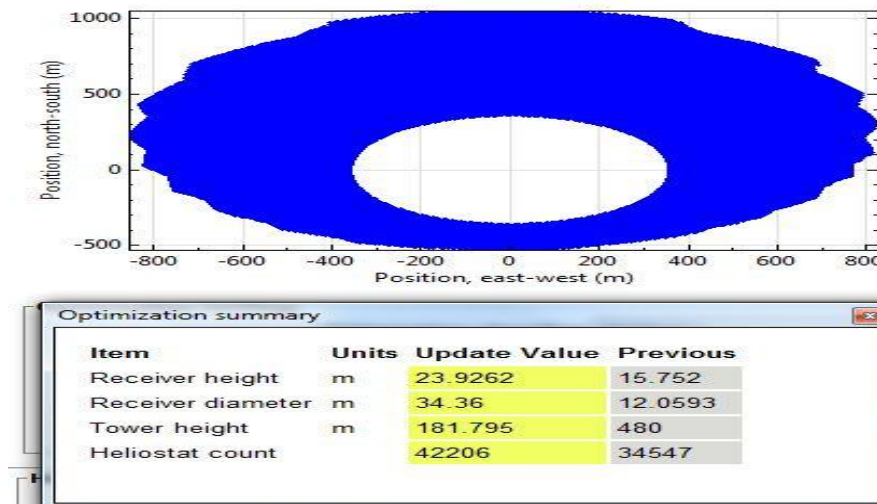


Figure 7.141 Solar Field Geometry and Characteristics of Scenario 1.8

In the case of the lowest height, the solar field is relatively light at first, the lightest of all tower cases, and the tower is placed at the center of the area, with the heliostats around it in a light field as we said. In the optimal case the tower is also at the center but the heliostats are placed with more density around the tower, and in cases that follow we have density but the geometry changes in a way that the tower is gradually moved southwards in the area, and as the height gets bigger, less heliostats are placed near the tower, so as you can see it seems like a hole around the tower and as we increase the height this hole gets bigger. The surface of the solar field begins from 800m x 800 m, it increases and then it is 2,000 m x 2,000 m and at the final scenario it is 1,500 m x 1,600 m.

The previous values in the tables are the non-optimized values and we would expect to be higher than the optimized values (yellow) but in many cases the optimized values are greater. In case of tower height it is obvious that there is a limit to the height as we insert heights near to 400 m, 450 m, 480 m (non optimized values), but it was optimized at the scale up to 200m and no higher. Another observation of this solar field geometry is that the receiver height does not get over 24 m, it increases as the tower height increases but not analogical, it has its ups and downs, as well as the same happens to the receiver diameter. The number of the heliostats is analogical to the tower height, so the higher the tower is the more heliostats we have in the solar field, and as we said they go southwards, making a hole around the tower, so they have more density as they are more in the number in a smaller area as they removed from the tower.

7.4.2 Solar Multiple

Scenario 2.1: Solar multiple = 1.05

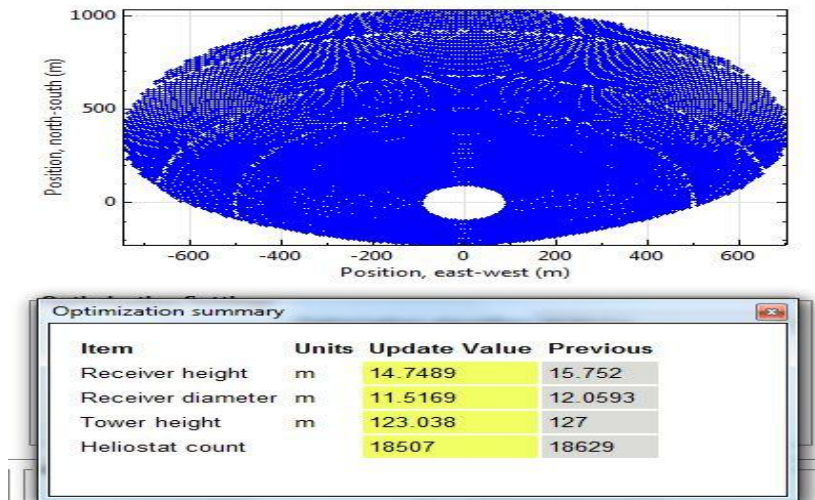


Figure 7.142 Solar Field Geometry and Characteristics of Scenario 2.1

Scenario 2.2: Solar multiple = 1.6

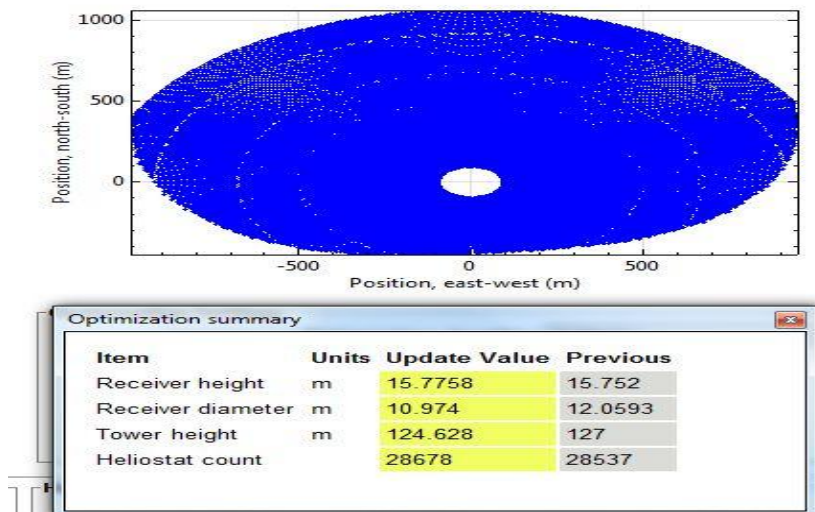


Figure 7.143 Solar Field Geometry and Characteristics of Scenario 2.2

Scenario 2.3: Solar multiple = 2.6

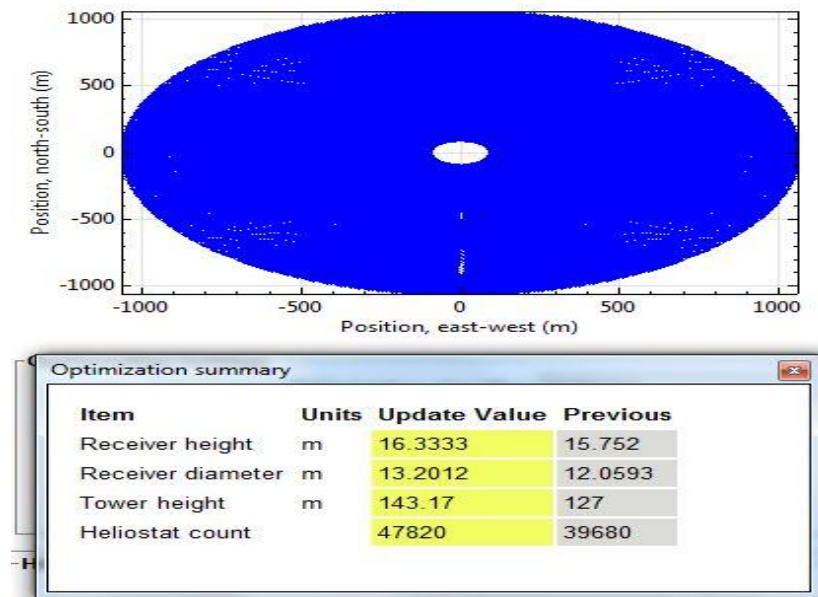


Figure 7.144 Solar Field Geometry and Characteristics of Scenario 2.3

Scenario 2.4: Solar multiple = 4.2

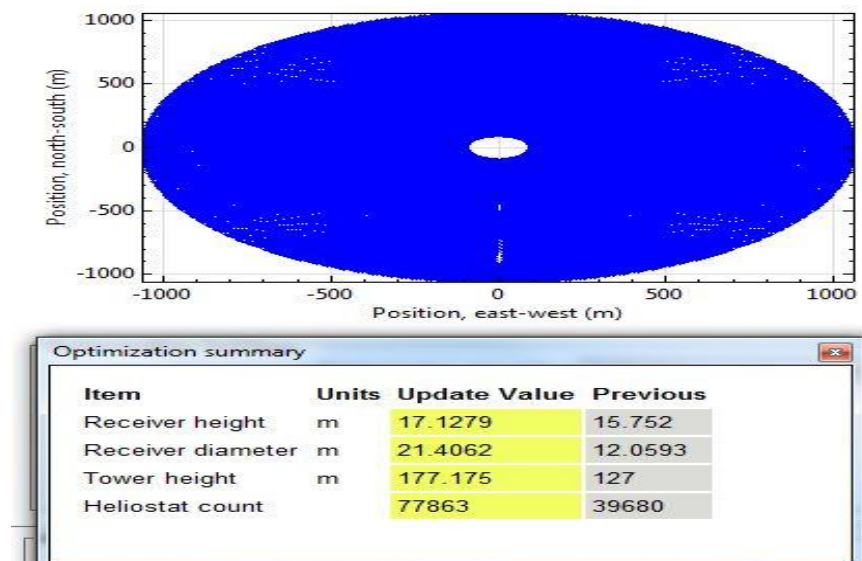


Figure 7.145 Solar Field Geometry and Characteristics of Scenario 2.4

Scenario 2.5: Solar multiple = 8.4

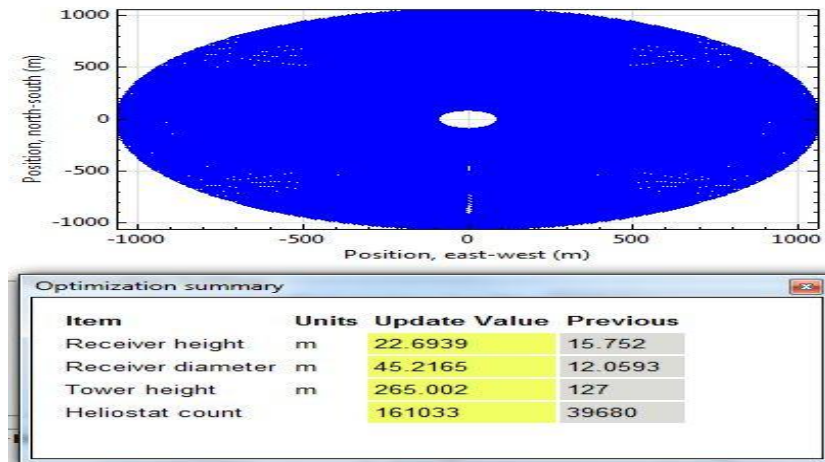


Figure 7.146 Solar Field Geometry and Characteristics of Scenario 2.5

Scenario 2.6: Solar multiple = 16.8

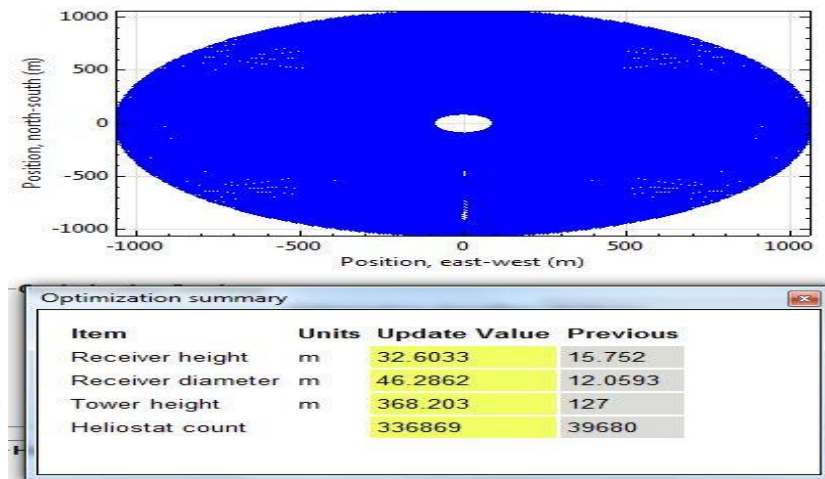


Figure 7.147 Solar Field Geometry and Characteristics of Scenario 2.6

Scenario 2.7: Solar multiple = 21

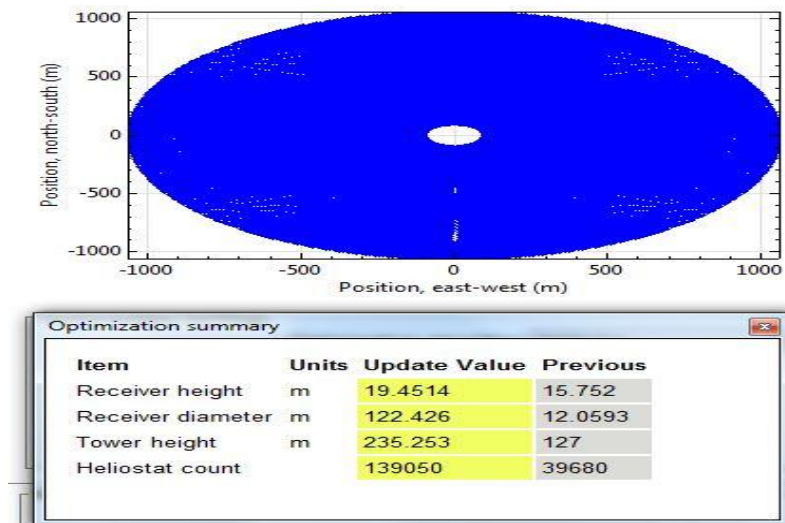


Figure 7.148 Solar Field Geometry and Characteristics of Scenario 2.7

In the case of the solar multiple, the solarfield is relatively light at first and the tower is placed southwards. As we increase the solar multiple price the solar field moves to the center of the area. In the optimal case the tower is at the center and the heliostats are placed with more density around the tower. In cases that follow we have density and the almost same center solar field geometry is kept so that the tower is at the center of the area and the hole around the tower is getting smaller. The surface of the solar field begins from 1,500 m x 800 m, it increases and then it is 1,000 m x 1,500 m and at the final scenario it is 2,000 m x 2,000 m.

The previous values in the tables are the non-optimized values and we would expect to be higher than the optimized values (yellow) but in many cases the optimized values are greater. In case of solar multiple it is obvious that the optimized height of the tower is increased in order to be suitable for the system to be effective, even if we only changed the solar multiple prices, it was necessary for the tower height to change in order to be a realistic case, in our solar multiple cases tower height has reached even 370 m. Another observation of this solar field geometry is that the receiver height does not get over 32 m, it increases as the tower height increases but not analogical, it has its ups and downs, as well as the same happens to the receiver diameter. The number of the heliostats is analogical to the solar multiple price, so the greater the solar multiple is

the more heliostats we have in the solar field, except the last case for solar multiple = 21 where the number of the heliostats falls unpredictably, in comparison with all the other cases where we had an analogical increase in the heliostat's number.

7.4.3 Design Point DNI

Scenario 3.1: Design Point DNI = 475W/m²

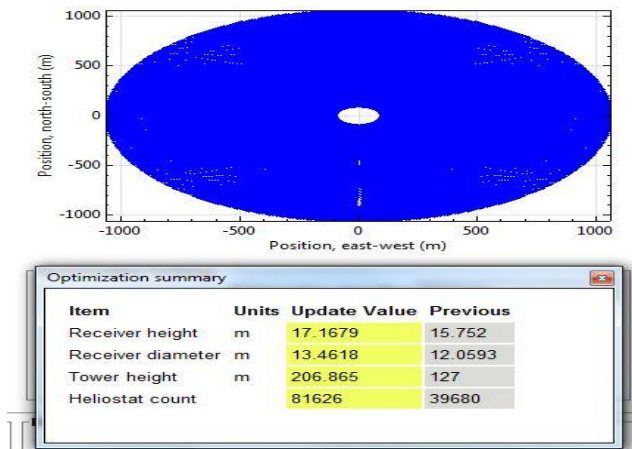


Figure 7.149 Solar Field Geometry and Characteristics of Scenario 3.1

Scenario 3.2: Design Point DNI = 700 W/m²

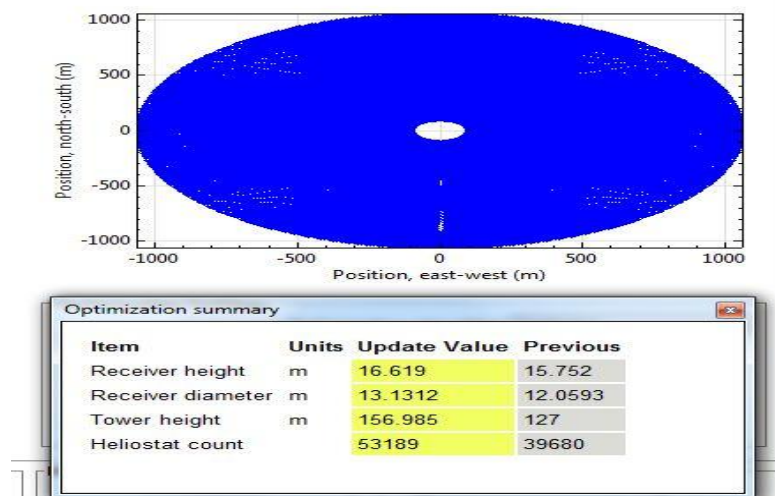


Figure 7.150 Solar Field Geometry and Characteristics of Scenario 3.2

Scenario 3.3: Design Point DNI = 800W/m²

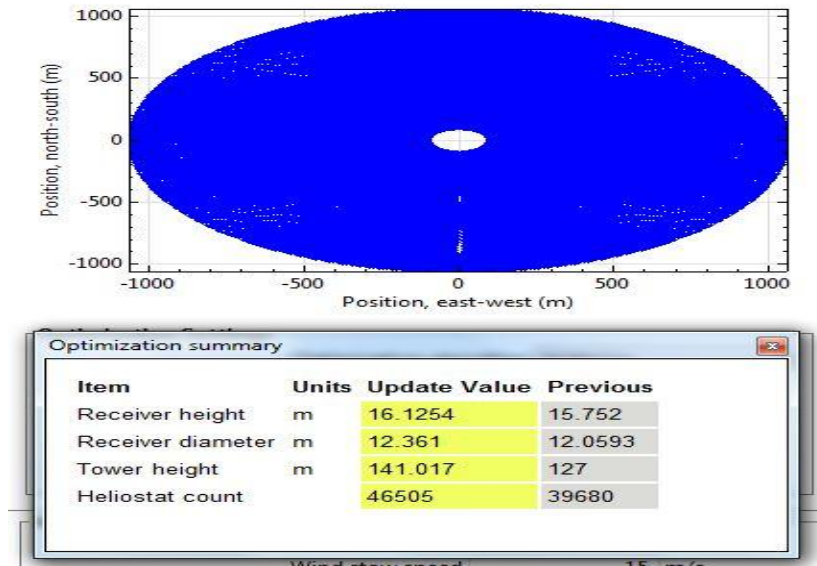


Figure 7.151 Solar Field Geometry and Characteristics of Scenario 3.3

Scenario 3.4: Design Point DNI = 1000 W/m²

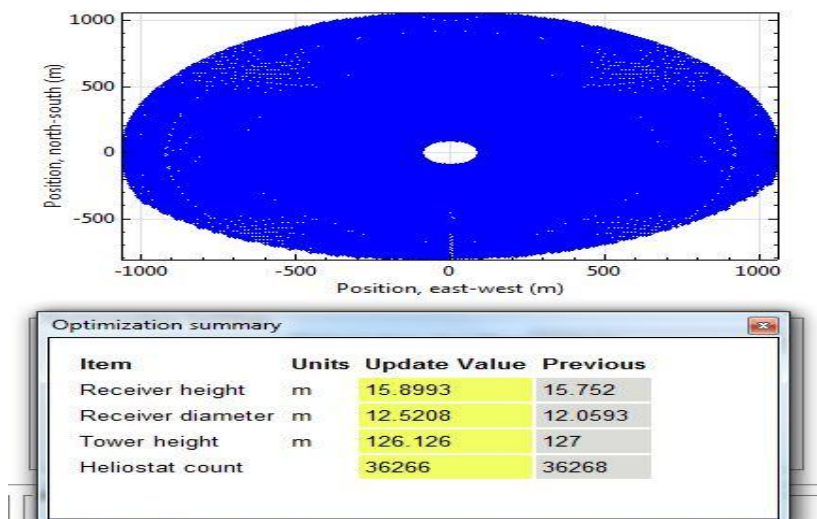


Figure 7.152 Solar Field Geometry and Characteristics of Scenario 3.4

Scenario 3.5: Design Point DNI = 1110 W/m²

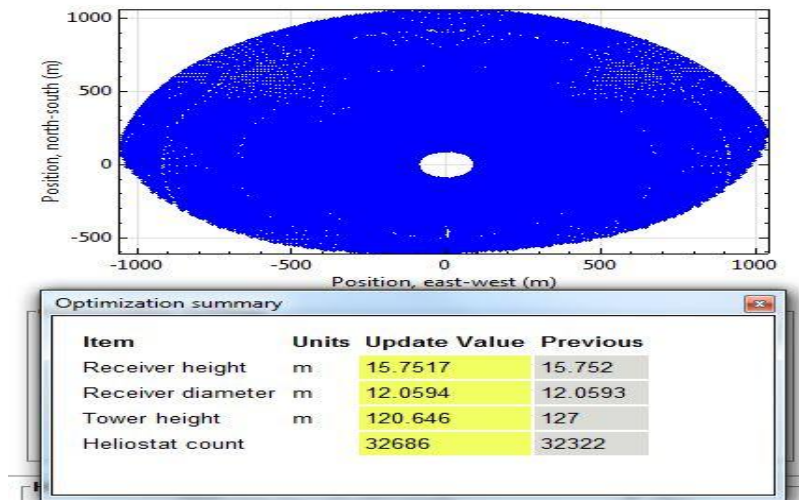


Figure 7.153 Solar Field Geometry and Characteristics of Scenario 3.5

Scenario 3.6: Design Point DNI = 1425 W/m²

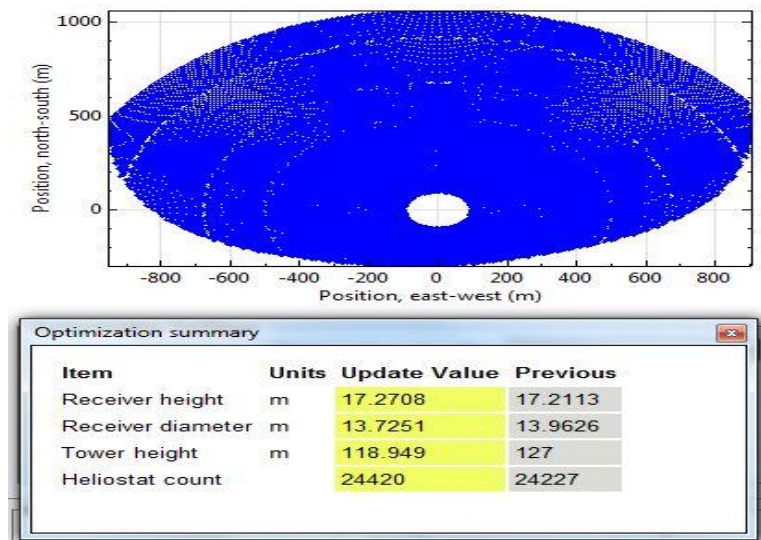


Figure 7.154 Solar Field Geometry and Characteristics of Scenario 3.6

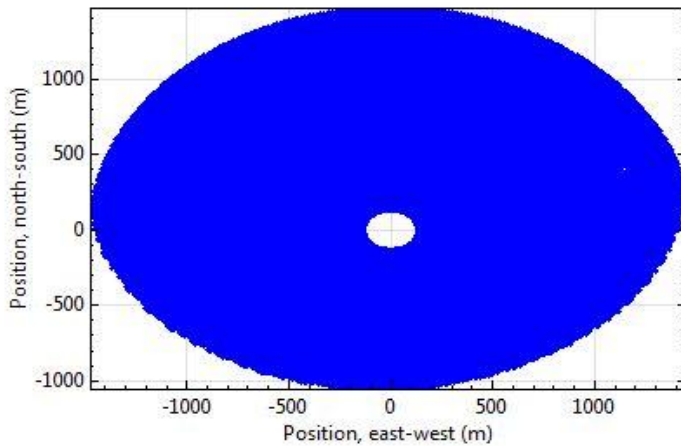
In the case of the Design Point DNI, in the optimal case the tower is at the center and the heliostats are placed with density around the tower. For the other cases that

follow the solar field is relatively like the optimal one in almost all cases, so that the tower is placed at the center of the area and they keep the same high density. At the last cases of Design Point DNI where the Design Point DNI has increased a lot the solar field tends to get a triangular shape at the edges, and it seems to move southwards. In the last case of the highest Design Point DNI price it is obvious that the field has moved a lot of southwards and it has taken a triangular shape at the edges, while the north density is not the same, it has a lighter density there. The surface of the solar field begins from 2,000 m x 2,000 m, it decreases and then it is 2,000 m x 1,600 m and at the final scenario it is 1,800 m x 2,000 m.

The previous values in the tables are the non-optimized values in case of Design Point DNI it is obvious that the optimized values are higher than the no optimized one. As we increase the Design Point DNI we can see that the tower height gets smaller, in order to be suitable for the system to be effective, even if we only changed the Design Point DNI prices, it was necessary for the tower height to change in order to be a realistic case. Another observation of this solar field geometry is that the receiver height does not get over 18 m, it decreases as the Design Point DNI increases but not analogical, it unpredictably increases in the highest Design Point DNI case, as well as the same happens to the receiver diameter. The number of the heliostats decreases as the Design Point DNI increases, so the higher Design Point DNI we have, the less heliostats we have in the solar field.

7.5 Scenario 4 - Optimal Scenario

This scenario includes the optimal prices of tower height, solar multiple and Design Point DNI that result from the previous 21 scenarios analyzed below, so Tower Height= 127 m, Solar Multiple = 2.6 and Design Point DNI= 700 W/m². The results of that optimal scenario are:



Item	Units	Update Value	Previous
Receiver height	m	18.2903	15.752
Receiver diameter	m	14.2357	12.0593
Tower height	m	174.108	127
Heliostat count		66531	39680

Figure 7.155 Solar Field Geometry and Characteristics of Optimal Scenario

Metric	Value
Annual energy (year 1)	155,665,408 kWh
Capacity factor (year 1)	34.1%
Annual Water Usage	56,370 m ³
PPA price (year 1)	62.60 €/kWh
PPA price escalation	1.00 %/year
Levelized PPA price (nominal)	82.68 €/kWh
Levelized PPA price (real)	69.55 €/kWh
Levelized COE (nominal)	76.39 €/kWh
Net present value	\$102,234,160
Internal rate of return (IRR)	11.00 %
Year IRR is achieved	20
IRR at end of project	11.84 %
Net capital cost	\$1,130,605,824
Equity	\$1,130,605,824
Size of debt	\$0

Figure 7.156 CSP 's Performance results as simulated in SAM of Optimal Scenario

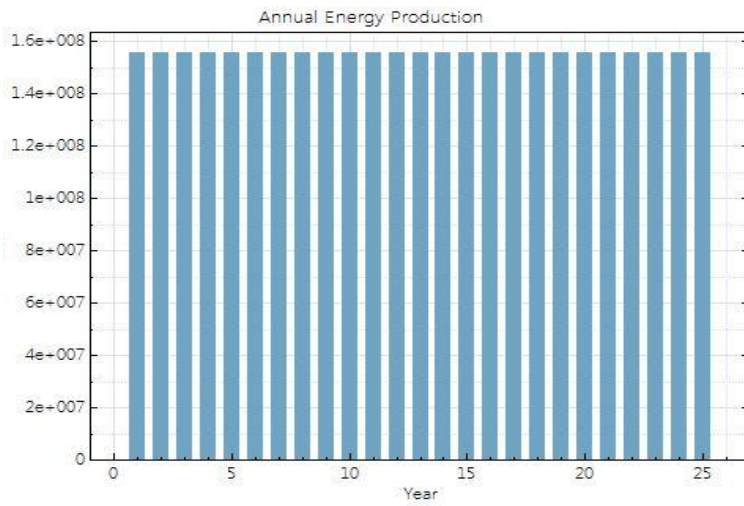


Figure 7.157 CSP's Annual Electricity Production as simulated in SAM of Optimal Scenario

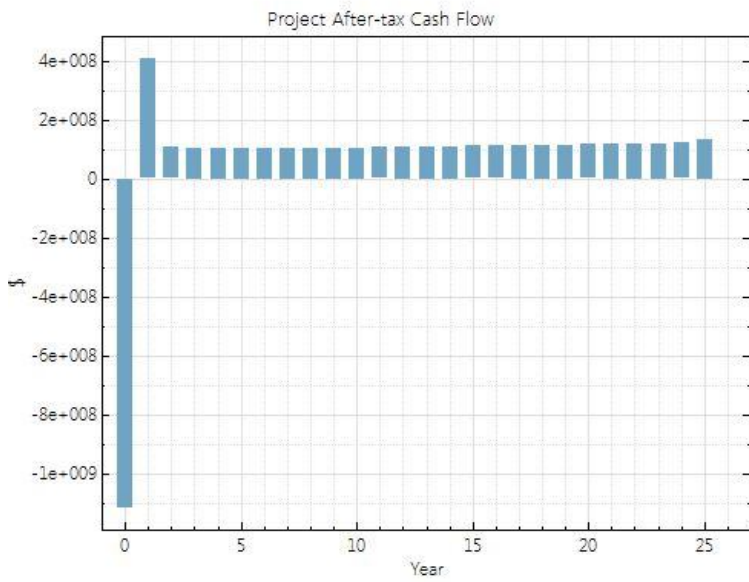


Figure 7.158 CSP 's Cash Flow as simulated in SAM of Optimal Scenario

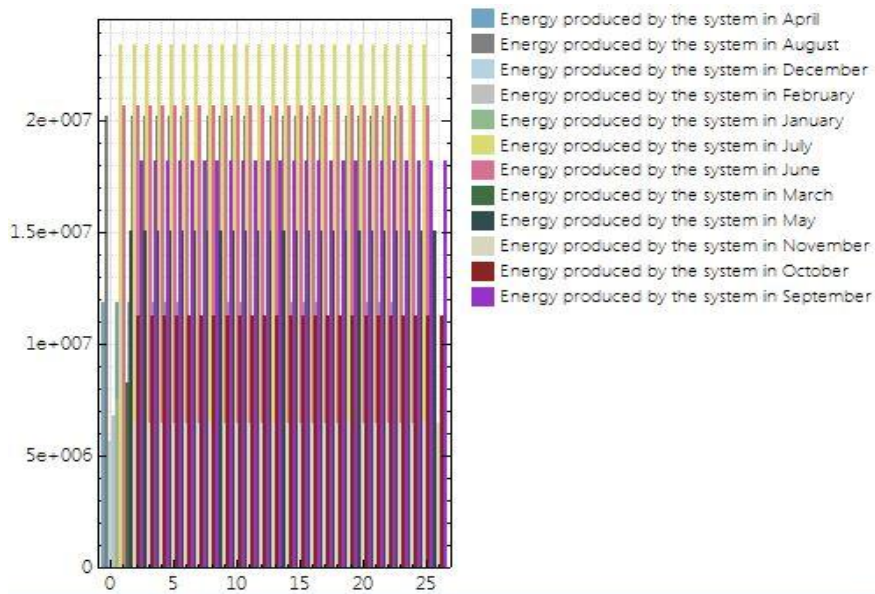


Figure 7.159 CSP 's Energy Production as simulated in SAM of Optimal Scenario

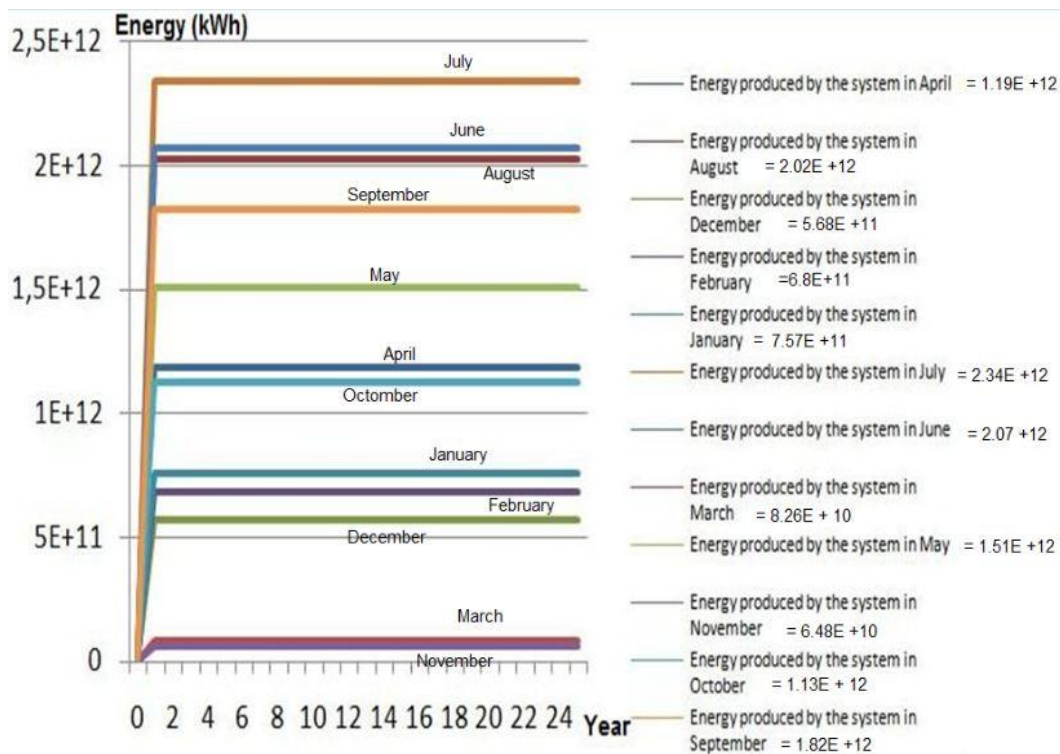


Figure 7.160 CSP 's Energy Production as simulated in SAM of Optimal Scenario

Annual electricity production (year 1) is now calculated to be equal to $P_{el,net}=155,665,408$ kWh, the capacity factor (year 1) is now equal to 34.1% and the annual water use is now equal to $56,370$ m³. Regarding the financial data, about the sales price (PPA price (year 1) = 62.60 \$/kWh) and the increase in the sales price (PPA Escalation = 1% / year), same as the other scenarios. The nominal Levelized PPA price is now equal to 82.68\$/kWh, the real Levelized price is now equal to 69.55 \$/kWh and the Levelized Cost of Energy (LCOE) is now equal to 76.39 \$/kWh. The Net Present Value (NPV) is now \$ 102,234,160 and the IRR (internal rate of return) of the investment is again equal to 11%, we can see that year IRR is again achieved (20) and IRR at the end of the project is again equal to 11.84%. The net capital cost is now equal to \$1,130,605,824, the equity is also equal to \$1,130,605,824 and the size of debt is again equal to \$0.

<i>Optimal Tower Height Scenario</i>	<i>Optimal Solar Multiple Scenario</i>	<i>Optimal Design Point DNI Scenario</i>	<i>Optimal Scenario - Scenario 4</i>
<i>Scenario 1.1 Tower Height=127m</i>	<i>Scenario 2.3 Solar Multiple = 2.6</i>	<i>Scenario 3.2 Design Point DNI= 700W/m²</i>	<i>Tower Height= 127 m, Solar Multiple = 2.6, Design Point DNI= 700W/m²</i>
<i>Annual Energy Production = 121,964,560 kWh</i>	<i>Annual Energy Production = 139,210,688 kWh</i>	<i>Annual Energy Production = 152,287,760 kWh</i>	<i>Annual Energy Production = 155,665,408 kWh</i>
<i>LCOE=83.69 \$/kWh</i>	<i>LCOE=77.36 \$/kWh</i>	<i>LCOE=72.74 \$/kWh</i>	<i>LCOE=76.39 \$/kWh</i>

Table 7.4 Comparison about Annual Energy Production and LCOE of Optimal Scenarios of each category with the most optimal scenario - Scenario 4

In Table 7.4, we can see the comparison between the optimal scenarios of each category with the final optimal Scenario, that uses the optimal values of the optimal

scenarios of each category. It is obvious that the Scenario 4 has the highest Annual Energy Production of all scenarios, while the LCOE price of scenario 4 is lower than scenario 1.1 and scenario 2.3 but higher than scenario 3.2, but it continues to have a good price, it does not have a high deviation from the other LCOE prices. A lower LCOE suggests a more profitable project. This implies lower cost, with more energy production.

Scenario 1.1 Tower Height= 127 m	Scenario 2.3 Solar Multiple = 2.6	Scenario 3.2 Design Point DNI= 700W/m ²	Scenario 4
Figure 7.134 High symmetrical geometry	Figure 7.144 High symmetrical geometry	Figure 7.150 High symmetrical geometry	Figure 7.155 Most symmetrical geometry
Receiver Height = 15.7455 m	Receiver Height = 16.333 m	Receiver Height = 16.619 m	Receiver Height = 18.2903 m
Receiver Diameter = 12.0708 m	Receiver Diameter = 13.2012 m	Receiver Diameter = 13.1312 m	Receiver Diameter = 14.2357 m
Tower Height = 128.17 m	Tower Height = 143.17 m	Tower Height = 156.985 m	Tower Height = 174.108 m
Number of Heliostats = 38,570	Number of Heliostats = 47,820	Number of Heliostats = 53,189	Number of Heliostats = 66,531

Table 7.5 Comparison about Geometry of the solar field and optimized characteristics of Optimal Scenarios of each category with the most optimal scenario - Scenario 4

In the final Scenario, Scenario 4, the geometry of the solar field seems to be symmetrical, the most symmetrical solar field geometry of all it could be said, the receiver height is now optimized at 18.2903 m, higher than the optimized Scenarios, the receiver diameter is now optimized at 14.2357 m, higher than the optimized Scenarios, the tower height is now optimized at 174.108, higher than the optimized Scenarios, and the number of heliostats is now optimized at 66,531, higher than the optimized Scenarios. (Table 7.5)

	<i>Scenario 1.1 Tower Height= 127 m</i>	<i>Scenario 2.3 Solar Multiple = 2.6</i>	<i>Scenario 3.2 Design Point DNI= 700W/m²</i>	<i>Scenario 4</i>
<i>Max Energy Production in July (the most productive month)</i>	<i>2e+007 kWh</i>	<i>2.15e+007 kWh</i>	<i>2.32e+007 kWh</i>	<i>2.35e+007 kWh</i>
<i>Max cash flow during 25 years operation is during 1st year</i>	<i>\$ 3.6e+008</i>	<i>\$ 3.7e+008</i>	<i>\$ 3.8e+008</i>	<i>\$ 4.1e+008</i>
<i>Max Annual Energy Production is same during 25 years</i>	<i>1.2e+008 kWh</i>	<i>1.38e+008 kWh</i>	<i>1.52e+008 kWh</i>	<i>1.56e+008 kWh</i>
	<i>Figure 7.43, Figure 7.44, Figure 7.45</i>	<i>Figure 7.83, Figure 7.84, Figure 7.85</i>	<i>Figure 7.107, Figure 7.108, Figure 7.109</i>	<i>Figure 7.157, Figure 7.158, Figure 7.159</i>

Table 7.6 Comparison about Energy production of Optimal Scenarios of each category with the most optimal scenario - Scenario 4

The month of the maximum Energy production is always July for all Scenarios and the Energy production at Scenario 4 is the highest of all optimal Scenarios, and it is equal to 2.35e+007 kWh. Max cash flow during 25 years operation is during 1st year for all Scenarios, and the highest price is for Scenario 4 and it is equal to \$ 4.1e+008. Max Annual Energy Production is stable during 25 years, the highest price happens at Scenario 4 and it is equal to 1.56e+008 kWh. (Table 7.6)

Parameter	Range	Units
<i>Tower Height</i>	<i>[63.5-480]</i>	<i>[m]</i>
<i>Solar Multiple</i>	<i>[1.05-21]</i>	<i>[-]</i>
<i>Design Point DNI</i>	<i>[475-1475]</i>	<i>[W/m²]</i>

Table 7.7 Decision - Input variables for the optimization.

Parameter	Range	Units
	Solar Field	
<i>Solar Multiple</i>	2.6	<i>[-]</i>
<i>Single Heliostat Mirror Area</i>	14.625	<i>[m²]</i>
<i>Number of Heliostats</i>	66,531	<i>[-]</i>
<i>Solar Field Area</i>	973,015	<i>[m²]</i>
<i>Average Solar Field Efficiency- Attenuation</i>	8.2	<i>[%]</i>
	Receiver / Tower	
<i>Tower Height</i>	174.108	<i>[m]</i>
<i>Receiver Height</i>	18.2903	<i>[m]</i>
<i>Receiver Diameter</i>	14.2357	<i>[m]</i>

	TES (Thermal Energy Storage)	
Storage Size	5	[h]
Energy-Thermal Capacity	748.4	[MWh _{th}]
	Power Block	
Net Power Output	52.0869	[MW]
Gross Power Output	59.87	[MW]
Estimated Gross to Net Conversion Factor	0.87	[-]
Cycle Thermal Efficiency	0.4	[-]
Cycle Thermal Power	149.675	[MW _t]
HTF (Heat Transfer Fluid) Hot Temperature	565	[°C]
HTF Cold Temperature	290	[°C]

Table 7.8 Selected optimal CSP configuration

II Simplified LCOE Calculation

$$\frac{\sum_{t=1}^n \frac{I_t + M_t + F_t}{(1+r)^t}}{\sum_{t=1}^n \frac{E_t}{(1+r)^t}}$$

- I_t = Investment expenditures in year t (including financing)
- M_t = Operations and maintenance expenditures in year t
- F_t = Fuel expenditures in year t
- E_t = Electricity generation in year t
- r = Discount rate
- n = Life of the system

Figure 7.161 LCOE definition

Conclusions

We saw the energy problem worldwide and in Greece and the ways of solving this problem, continue with renewable energy, analyzing some basic categories, with and exploitation of solar energy. We continue with concentrated solar systems that take advantage of solar energy. An analysis of the types of CSP was made and of the thermodynamic cycles they use during their operation. After the available technologies of solar thermal systems were analyzed, we saw that solar power towers is mature new and economically viable technology. We made an analysis of the parts of the system and the mode of operation, we understood the contribution of all these parts to the production of electrical power. References were made to the different technologies they have been researched for parts of the system, such as types of solar receivers as well as the choice of heat transfer fluid, for full exploitation of solar radiation using a thermal storage system or using a backup system for continuous operation of the CSP.

Designing of CSP is a complex and important process, that nowadays is made using software because it would be very difficult to calculate the optimal positions for a few thousand heliostats, as it is impossible to calculate the efficiency of the solar field for any moment. In our case SAM (System Advisor Model by NREL) was used. The methodology for designing of such an installation was developed, and the contribution of all parameters to the station performance was analyzed. The simulation was needed to draw safer conclusions. We saw how important all parts of the system are and the influence of the station's location on the system.

We made 21 Scenarios, keeping constant one factor while changing the rest of the three factors: of the Tower Height, the Solar Multiple and the Design Point DNI, that drove us to the optimal Scenario, choosing the best characteristics every time of each category of Scenarios, so the final Scenario had the optimal characteristics of the examined ones.

The results are positive and CSP seems to be sustainable projects. Future work is to find out where and when a small power plant of this given size could be usefully applied, and to combine CSP with PV. CSP are unique among solar electric technologies in their ability to efficiently store solar energy and dispatch electricity to the grid when needed, even at night or during cloudy days. Solar energy comes directly from sun, it is not only renewable and non-pollutant but also accessible in any part of the world and maintenance costs are low. CSP will be the power source for developing countries.

Bibliography

- [1] Oilprice Source for Oil and Energy News <https://oilprice.com/Energy/Energy-General/Oil-Imports-Have-Energy-Poor-Greece-In-A-Stranglehold.html>
- [2] V. Manieniyam, M.Thambidurai, and R.Selvakumar, Study on Energy Crisis and the Future of Fossil Fuels, Proceedings of SHEE 2009, 11 – 12, Engineering Wing, DDE, Annamalai University Dec 2009
https://www.researchgate.net/publication/267439286_STUDY_ON_ENERGY_CRISIS_AND_THE_FUTURE_OF_FOSSIL_FUELS
- [3] U. Shahzad, University of Nebraska at Lincoln, Global Warming: Causes, Effects and Solutions, August 2015
https://www.researchgate.net/publication/316691239_Global_Warming_Causes_Effects_and_Solutions
- [4] K.A.P.E. «The Greek Energy System ». Ministry of Development, 2009.
- [5] National Energy Planning Committee. "National Energy Planning, road map for 2050", YPEKA 2012.
- [6] European Commission. 'Twice from 20 to 2020'. 2008.
- [7] United Nations. "Kyoto Protocol to the United Nations Framework Convention on Climate Change". U.N., 1998.
- [8] European Commission. "Sustainable Power Generation from Fossil Fuels: Near-Carbon Emissions beyond 2020". 2007.
- [9] Jose Manuel Barroso. «Energy: Europe's priorities ». Presentation to the European Council, 2011.
- [10] S. Kalogirou, International Journal, Renewable Energy, Cyprus University of Technology, Lemesos, Cyprus, 2019 <https://www.journals.elsevier.com/renewable-energy>
- [11] SolarLight Energy Systems <http://www.solarlight.gr/index.jsp?CMCCode=100305&extLang=>
- [12] Mother nature network <https://www.mnn.com/earth-matters/energy/stories/offshore-wind-farms-can-alone-power-all-human-civilization>
- [13] Alternative forms of energy - Geothermy <http://gewthermia.blogspot.com/2013/02/normal-0-false-false-false-el-ja-x-none.html>
- [14] Hydrodynamic Energy <http://www.hellenic-college.gr/works/energy-sources/ydro.htm>
- [15] Advantages of Concentrated Solar Power Technology <http://www.greenissexy.tv/advantages-of-concentrated-solar-power-technology/>
- [16] Ideal-Stirling-Cycle https://www.researchgate.net/figure/P-V-and-T-S-diagrams-of-the-Ideal-Stirling-Cycle_fig1_281590001
- [17] The First Law of Thermodynamics & Cyclic Processes <https://slideplayer.com.br/slide/342945/>

- [18] Rankine Cycle <http://notbukofaprofessor.blogspot.com/2013/07/rankine-cycle.html>
- [19] Ivanpah Solar Electric Generating System <https://newatlas.com/ivanpah-fully-operational/30862/>
- [20] Ivanpah Solar Electric Generating System <https://www.dreambigfilm.com/stories/image-29-ivanpah/>
- [21] Mojave Solar Project <https://inhabitat.com/grand-opening-today-the-mojave-solar-project-is-officially-fully-operational/>
- [22] Solana Solar Power Plant
http://www.abengoa.es/web/en/noticias_y_publicaciones/noticias/historico/2014/10_octubre/abg_20141002-1.html
- [23] Transient System Simulation Tool <http://www.trnsys.com/>
- [24] National Renewable Energy Laboratory <http://www.nrel.gov/csp/solarpilot-download.html>
- [25] National Renewable Energy Laboratory <http://www.nrel.gov/csp/solarpilot.html>
- [26] Homer Energy http://www.homerenergy.com/HOMER_legacy.html
- [27] Skelion <http://www.skelion.com/>
- [28] Easy Solar App <http://easysolar-app.com/en/>
- [29] National Resources Canada <https://www.nrcan.gc.ca/energy/software-tools/7465>
- [30] University of Massachusetts <http://www.umass.edu/windenergy/research/topics/tools/software/hybrid2>
- [31] Viessmann <http://viessmann.solar-software.de/index.php?lang=en>
- [32] Kalkener energy saving solutions <http://kalkener.com/en/>
- [33] DLR Institute of Solar Research <http://freegreenius.dlr.de>
- [34] Software Informer <http://combisun.software.informer.com/>
- [35] Oventrop Online Solar Calculation and Simulation of Solar Thermal Systems <http://oventrop.solar-software.de/system/lang/eng>
- [36] Energy2D Interactive Heat Transfer Simulations <http://energy.concord.org/energy2d/>
- [37] Sandia National Laboratories <http://energy.sandia.gov/energy/renewable-energy/solar-energy/csp-2/csp-codes-and-tools/>
- [38] National Renewable Energy Laboratory - SAM <https://sam.nrel.gov/>
- [39] Genesis Solar Energy Project <http://solarenergyzamearu.blogspot.com/2017/05/genesis-solar-energy-project.html>
- [40] Alex Phocas-Cosmetatos & Konstantinos Kynigalakis Nur Energie Ltd. MINOS Concentrated Solar Power Project June 2017
https://setis.ec.europa.eu/system/files/minos_concentrated_solar_power_project_0.pdf

- [41] Schott Solar CSP <https://www.us.schott.com/csp/english/parabolic-through-technology.html>
- [42] Dynamic Solar Energy Converter System
http://invencomm.com/InvenComm_Englisch/products/system-capsule-servis/
- [43] Linear Fresnel Reflector System <https://shaikmohasin.wordpress.com/2012/08/28/linear-fresnel-reflector-system/>
- [44] CleanLead How Power Tower Works <http://cleanleap.com/2-power-tower/how-power-tower-works>
- [45] Components of Solar Power Plant <http://solarpowerplantkukiriga.blogspot.com/2017/02/components-of-solar-power-plant.html>
- [46] Renewable Technology Gemasolar CSP Seville <https://www.renewable-technology.com/projects/gemasolar-concentrated-solar-power-seville/>
- [47] Energia.gr Production License for Solar Tower from Motor Oil in Crete
<https://www.energia.gr/article/43440/adeia-paragoghs-gia-hliako-pyrigo-apo-thn-motor-oil-sthn-krhth>
- [48] First Concentrated Solar Power (CSP) in Saudi Arabia <https://www.evwind.es/2015/04/02/first-concentrated-solar-power-csp-heliostat-field-in-saudi-arabia/51318>
- [49] cmi Central Tower Receivers for Solar Thermal Electricity <https://www.cmigroupe.com/thermal-solar-receivers>
- [50] University of Kavala Department of Oil and Natural Gas - Solar Power Tower-
<https://docplayer.gr/53602269-Tei-kavalas-tmima-tehnologias-petrelaioy-kai-fysikoy-aerioy-ptyhiaki-ergasia-iliakos-pyrgos-ishyos-ypeythynos-kathigitis-kos-marmanis-dimitrios.html>
- [51] OmarBehar^a AbdallahKhella^b KamalMohammed^a, A review of studies on central receiver solar thermal power plants, July 2013 <https://www.sciencedirect.com/science/article/pii/S1364032113001184>
- [52] Farret, F.A.; Simoes, M.G. *Integration of Alternative Sources of Energy* IEEE Press 2006
- [53] <http://www.powerfromthesun.net/Book/chapter11/chapter11.html>
- [54] Solar Thermal Storage <https://www.mtholyoke.edu/~wang30y/csp/thermal%20storage.html>
- [55] Sapana Deshmukh, P. M. Gadhe and R. J. Yadav, *International Journal of Current Engineering and Technology, Design of Heliostat Field for Small Scale Central Receiver System, 2017*
<https://inpressco.com/wp-content/uploads/2017/06/Paper85363-367.pdf>
- [56] Green Rhino Energy <http://www.greenrhinoenergy.com/solar/radiation/empiricalevidence.php>
- [57] G. Beretta, *International Journal of Environmental Technology and Management: World energy consumption and resources- An outlook for the rest of the century, 2007*
https://www.researchgate.net/publication/228622897_World_energy_consumption_and_resources_An_outlook_for_the_rest_of_the_century
- [58] National Renewable Energy Laboratory - Solar Multiple <https://sam.nrel.gov/content/solar-multiple>

- [59] Basim Belgasim, and Mohamed Elmnafi, *Evaluation of a Solar Parabolic Trough Power Plant under Climate Conditions in Libya*, Mechanical Engineering Department, Benghazi University, Benghazi, Libya, 2014 <http://uob.edu.ly/assets/uploads/pagedownloads/d4057-set2014-e10031.pdf>
- [60] Men Wirz, *Design Point for Predicting Year-Round Performance of Solar Parabolic Trough Concentrator Systems*, 2013 https://www.researchgate.net/publication/267644465_Design_Point_for_Predicting_Year-Round_Performance_of_Solar_Parabolic_Trough_Concentrator_Systems
- [61] Gerhard Weinrebe *Towards Holistic Power Tower System Optimization*, 2014 https://www.researchgate.net/publication/275222785_Towards_Holistic_Power_Tower_System_Optimization
- [62] National Renewable Energy Laboratory *Molten Salt Power Tower Cost Model for the System Advisor Model (SAM)* <https://www.nrel.gov/docs/fy13osti/57625.pdf>
- [63] Basim Belgasim, *Evaluation of a Solar Parabolic Trough Power Plant under Climate Conditions in Libya*, 2014 https://www.researchgate.net/publication/269095678_Evaluation_of_a_Solar_Parabolic_Trough_Power_Plant_under_Climate_Conditions_in_Libya
- [64] *Reasons Why Globalization is a Huge Problem* <https://ourfiniteworld.com/2013/02/22/twelve-reasons-why-globalization-is-a-huge-problem/>
- [65] *Photovoltaic Software* <https://photovoltaic-software.com/solar-thermal-softwares/free-solar-thermal-softwares/cec-fchart>
- [66] *Renewable Energy Solutions Solar thermal energy – Solar COMBI systems* <http://cf.cdn.unwto.org/sites/all/files/docpdf/re26solarthermalenergy-solarcombisystemstaq.pdf>
- [67] *Solo - Tecsol* <https://photovoltaic-software.com/solar-thermal-softwares/free-solar-thermal-softwares/solo-tecsol>
- [68] *ScanTheSun photovoltaic-software* <https://photovoltaic-software.com/solar-thermal-softwares/free-solar-thermal-softwares/scanthesun>
- [69] National Renewable Energy Laboratory. <http://www.nrel.gov>
- [70] C. Turchi & G. Heath. “*Molten Salt Power Tower Cost Model for the System Advisor Model*”. National Renewable Energy Laboratory U.S.A.. 2013.
- [71] P. Kuntz Falcone. “*A Handbook for Solar Central Receiver Design*”. Sandia National Laboratories, Livermore. 1986.
- [72] William B. Stine & Michael Geyer. “*Power from the Sun*”. <http://www.powerfromthesun.net> , 2001.
- [73] G. Kolb. “*Heliostat Cost Reduction Study*”. SANDIA NATIONAL LABORATORIES, SANDIA REPORT SAND 2007-3293. 2007.

- [74] X. Wei. "Optimization Procedure for Design of Heliostat Field Layout of a 1MWe Solar Tower Thermal Power Plant". 2008.
- [75] M. A. Mustafa. "Analytical Study of an Innovated Solar Power Tower (PS10) in Aswan". *International Journal of Energy Engineering* 2012. 2(6). 2012
- [76] Solar Radiation Data. "SoDa" <http://www.soda-is.com>
- [77] SolarPACES. "PS10". <http://www.solarpaces.org/Tasks/Task1/ps10>
- [78] M. Romero Alvarez & Zarza. "Handbook of Energy Efficiency and Renewable Energy: Concentrating Solar Power". CRC Press. 2007.
- [79] X. Wei. "A New Code for the Design and Analysis of the Heliostat Field Layout for Power Tower System". Elsevier, *Solar Energy* Vol. 84. 2010.
- [80] B. L. Kistler. "A User's Manual for DELSOL3: A Computer Code for Calculating the Optical Performance and Optimal System Design for Solar Thermal Central Receiver Plants". Sandia National Laboratories, Livermore. 1986.
- [81] S.J. Bode. "Review of Optical Software for Use in Concentrating Solar Power Systems". Southern African Solar Energy Conference. Stellenbosch, South Africa. 21 – 23 May 2012.
- [82] T. Mukai. "A 1MWe Solar Thermal Electric Power Pilot Plant (Sunshine Project)". Agency of Industrial Science and Technology, MITI. *Solar Energy R&D in the European Community*, Vol.2. 1985.
- [83] X. Wei. "A New Method for the Design of the Heliostat Field Layout for Solar Tower". Elsevier, *Renewable Energy* Vol. 35. 2010.
- [84] Z. Yao. "Modeling and Simulation of the Pioneer 1 MW Solar Thermal Central Receiver System in China". Elsevier, *Renewable Energy* Vol. 34. 2009
- [85] World Energy Consumption Since 1820 in Charts
<https://ourfinitemworld.com/2012/03/12/world-energy-consumption-since-1820-in-charts/>
- [86] A. Kosmetatos. "Rules for the Operation of Solar Thermal Stations in the Island of Greece". NUR-MOH A.E., Workshop of Panhellenic Association of Chemical Engineers. Athens 24/11/2009. [87] P.A.E. «ΑΠΟΦΑΣΗΡ.Α.Ε. ΥΠ' ΑΡΙΘΜ. 469/2013». <http://www.rae.gr>. 2013
- [88] National Renewable Energy Laboratory . <http://www.nrel.gov>
- [89] J. E. Pacheco. "Summary of the Solar Two. Test and Evaluation Program". Sandia National Laboratories. 2000.
- [90] National Renewable Energy Laboratory U.S.A. "System Advisor Model (SAM) Case Study: Gemasolar, Fuentes de Andalucía, Spain". 2013.
- [91] RAE "Evaluation Guide for Electricity Production with Solar Radiation Concentration". Version 1.0. 2010.
- [92] F. Collado. "Quick evaluation of the annual heliostat field efficiency". University of Saragoza. *Solar Energy* Vol. 82 Issue 4. 2008.

- [93] *Torresol Energy*. <http://www.torresolenergy.com>
- [94] *CSP World*. <http://www.csp-world.com>
- [100] Ch. Fardellas, *Technological Education Institute of Crete, School of Department of Mechanical of Engineer "Description and Indicative Study Stainless Station for Electricity Energy Production, 2014*
<http://nefeli.lib.teicrete.gr/browse/stef/mhx/2014/FardellasChristos/attached-document-1410624942-372396-23676/FardellasChristos2014.pdf>
- [101] John P. Holdren *Population and the energy problem, 1991*
<https://link.springer.com/article/10.1007/BF01357916>
- [102] Euan Mearns, *Greek Tragedy, 2015* <http://euanmearns.com/greek-tragedy/>
- [103] *Solar for Energy - Solar Collectors* <http://www.solar-for-energy.com/solar-collectors.html>
- [104] *Energy Informative- Wind Energy* <http://energyinformative.org/windenergy>
- [105] *The Earth Project- Biomass* <http://theearthproject.com/biomass/>
- [106] *Energy Efficiency and Renewable Energy - Dish System CSP Basics*
<https://energy.gov/eere/energybasics/articles/dishengine-system-concentrating-solar-power-basics>
- [107] *The Solar Eclipse - Compact Linear Fresnel Reflector*
<https://scitechfrontiers.wordpress.com/2016/05/22/compact-linear-fresnel-reflector/>
- [108] *Photovoltaic Software Free Photovoltaic Software to Download* <http://photovoltaic-software.com/free.php>
- [109] *Natural Resources Canada- RETScreen* <http://www.nrcan.gc.ca/energy/software-tools/7465>
- [110] *Nur MOH Crete: 38MW Solar Electricity License Granted From Greek Regulatory Agency*
<http://www.prnewswire.co.uk/news-releases/crete-38mw-solar-electricity-license-granted-from-greek-regulatory-agency-156602075.html>
- [111] *SolarPACES Solar Power and Chemical Energy Systems* <http://www.solarpaces.org/country-information/greece>
- [112] *Maximus Project* <http://cspworld.org/cspworldmap/maximus-dish-project>
- [113] *Greek Solar Projects* <http://www.chinagoabroad.com/en/newsletter/greek-projects-in-ner300>
- [114] *Ivanpah solar power plant* <http://www.marketwatch.com/story/could-californias-massive-ivanpah-solar-power-plant-be-forced-to-go-dark-2016-03-16>
- [115] *KRAMER JUNCTION SOLAR ELECTRIC GENERATING STATION, CALIFORNIA*
<http://clui.org/ludb/site/kramer-junction-solar-electric-generating-station>
- [116] *The Most Exciting Solar Projects in the U.S.* <https://www.fastcompany.com/1689125/8-most-exciting-solar-projects-us-updated>

- [117]] Ivanpah solar power plant <https://hdspwsz.wordpress.com/2014/09/04/some-largest-solar-thermal-power-stations/>
- [118] MOJAVE SOLAR PROJECT <http://clui.org/project-page/13231/13242>
- [119] Solana-generating-plant <http://earthtechling.com/tag/solana-generating-plant/>
- [120] Gunther Portfolio Photovoltaics Solar Energy and Energy Policy Solana-generating-plant <http://guntherportfolio.com/2013/01/abengoa-solar-solana-generating-station-sortie/>
- [121] California Energy Commission <http://calenergycommission.blogspot.gr/2014/04/with-flip-of-switch-genesis-solar.html>
- [122] Ministry of Environment and Energy of Greece sanctions for international conventions and protocols (Y.PE.K.A) <http://www.ypeka.gr/Default.aspx?tabid=557>
- [123] Energy.gov- Energy Efficiency and Renewable Energy <https://energy.gov/eere/energybasics/articles/power-tower-system-concentrating-solar-power-basics>
- [124] IRENA - International Renewable Energy Agency, Concentrating Solar Power, Renewable Energy Technologies: Cost Analysis Series, 2012 https://www.irena.org/DocumentDownloads/Publications/RE_Technologies_Cost_Analysis-CSP.pdf
- [125] M. Romero Alvarez & Zarza. Handbook of Energy Efficiency and Renewable Energy: Concentrating Solar Power. CRC Press. 2007.
- [126] GreenTerraFirma -Solar Thermal for Electricity <http://greenterrafirma.com/solar-thermal-for-electricity.html>
- [127] Central Receiver Systems <http://www.powerfromthesun.net/Book/chapter10/chapter10.html>
- [128] "World Energy Consumption". http://en.wikipedia.org/wiki/World_energy_consumption
- [129] K.A.P.E.- Center for Renewable Energy Sources and Savung - <http://www.cres.gr>
- [130] William B. Stine & Michael Geyer. "Power from the Sun". <http://www.powerfromthesun.net> , 2001.
- [131] I. E.Fragiadakis. «Photovoltaic systems". Ziti, 2006.
- [132] Mohd Rizwan Sirajuddin Shaikh, A Review Paper on Electricity Generation from Solar Energy, 2017 https://www.researchgate.net/publication/320226399_A_Review_Paper_on_Electricity_Generation_from_Solar_Energy
- [133] C. Julian Chen. "Physics of Solar Energy". Department of Applied Physics and Applied Mathematics, Columbia University. WILEY. 2001.
- [134] Y. Cengel & M. Boles. "Thermodynamics for Engineers". Volume B, 3rd edition, Tziola, 1998.
- [135] A. Eiffel, A. Mazara, Brayton Cycle-The Ideal Cycle for Gas Turbine Engines https://www.academia.edu/9972055/BRAYTON_CYCLE_THE_IDEAL_CYCLE_FOR_GAS-TURBINE_ENGINES

- [136] Ignatius Djoko Irianto, *Performance Analysis of Rankine Cycle Using Supercritical Steam for Energy Conversion System of RDE*, 2017
https://www.researchgate.net/publication/321669383_PERFORMANCE_ANALYSIS_OF_RANKINE_CYCLE_USING_SUPERCRITICAL_STEAM_FOR_ENERGY_CONVERSION_SYSTEM_OF_RDE
- [137] M. Romero Alvarez & Zarza. "Handbook of Energy Efficiency and Renewable Energy: Concentrating Solar Power". CRC Press. 2007.
- [138] SolarPACES. "Solar Dish Engine ". <http://www.solarpaces.org>
- [139] SolarPACES. "Solar Parabolic Trough". <http://www.solarpaces.org>
- [140] SolarPACES. "Solar Dish Engine ". <http://www.solarpaces.org>
- [141] P. Kuntz Falcone. "A Handbook for Solar Central Receiver Design". Sandia National Laboratories, Livermore. 1986.
- [142] A. Fokas Cosmetatos. "Rules for the Operation of Solar Thermal Stations in the Island of Greece". NUR-MOH A.E., Workshop of Panhellenic Association of Chemical Engineers. Athens 24/11/2009.
- [143] Energy Register. "NUR – MOH A.E." <http://www.energyregister.gr/stathmos-ape/nur-moh-ae->
- [144] A. Strub, J. Gretz, W. Palz. "Thermo-Mechanical Solar Power Plants: Eurelios, the 1MWel Experimental Solar Thermal Electrical Power Plant in the European Community. Final Report of the Construction of Eurelios". Commission of the European Communities. 1984.
- [145] T. Mukai. "A 1MWe Solar Thermal Electric Power Pilot Plant (Sunshine Project)". Agency of Industrial Science and Technology, MITI. Solar Energy R&D in the European Community, Vol.2. 1985.
- [146] Dr. P. Kesselring, C. Selvage. "The IEA/SSPS Solar Thermal Power Plants — Facts and Figures— Final Report of the International Test and Evaluation Team (ITET)". International Energy Agency/Small Solar Power Systems Project. Book of Summaries Vol.4. 1986.
- [147] CSP World. <http://www.csp-world.com>
- [148] A. Munoz Torralbo. "A Spanish 'Power Tower' Solar System – Project CESA-1". ASME, Journal of Solar Energy Engineering Vol 106. 1984.
- [149] Themis (solar power plant) [http://en.wikipedia.org/wiki/Themis_\(solar_power_plant\)](http://en.wikipedia.org/wiki/Themis_(solar_power_plant)) [150] Ivanpah solar power plant <http://www.ivanpahsolar.com>
- [151] BrightSource, Ivanpah, Solar Electric Generating System, 2014
http://www.brightsourceenergy.com/stuff/contentmgr/files/0/3eac1a9fed7f13fe4006aaab8c088277/attachment/ivanpah_white_paper_0414.pdf
- [152] National Renewable Energy Laboratory <http://www.nrel.gov>
- [153] Solar Reserve - Solar energy with itergrated storage <http://www.solarreserve.com/what-wedo/csp-projects/crescent-dunes/>
- [154] Crescent Dunes Solar Energy Project
http://en.wikipedia.org/wiki/Crescent_Dunes_Solar_Energy_Project